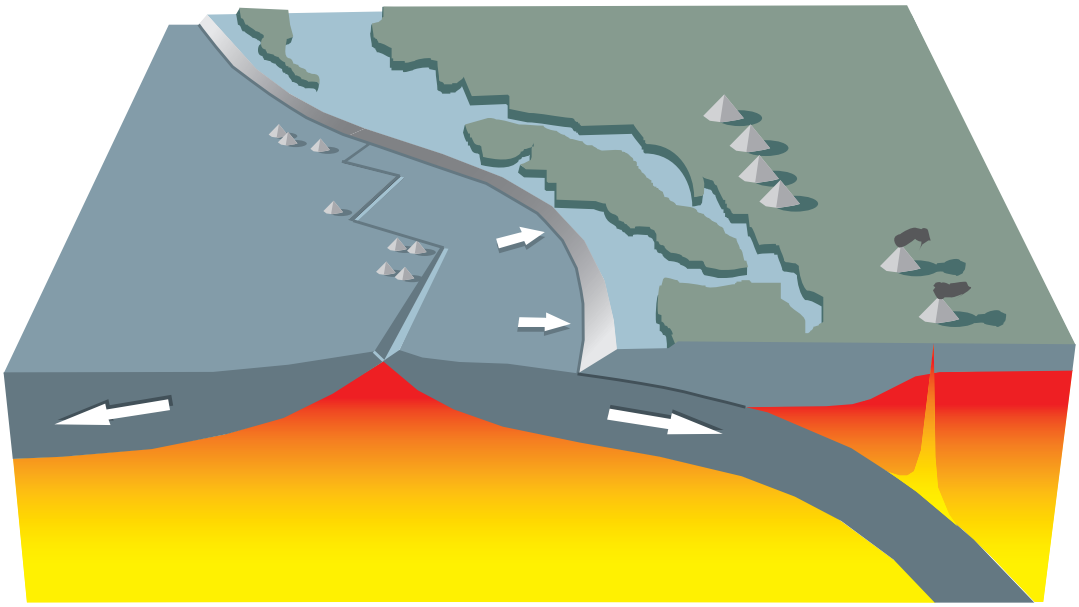

THE CASCADIA SUBDUCTION ZONE AND RELATED SUBDUCTION SYSTEMS

Seismic Structure, Intraslab Earthquakes and Processes, and Earthquake Hazards

Editors: Stephen Kirby, Kelin Wang and Susan Dunlop

U.S. Geological Survey Open-File Report 02–328
Geological Survey of Canada Open File 4350

August 2002

The Cascadia Subduction Zone and Related Subduction Systems—Seismic Structure, Intraslab Earthquakes and Processes, and Earthquake Hazards

Edited by Stephen Kirby[1], Kelin Wang[2], and Susan Dunlop[3]

Released simultaneously as
U.S. GEOLOGICAL SURVEY OPEN-FILE REPORT 02–328 and
GEOLOGICAL SURVEY OF CANADA OPEN FILE 4350

Version 1.0
2002

U.S. DEPARTMENT OF THE INTERIOR
U.S. GEOLOGICAL SURVEY

1 U.S. Geological Survey MS 977, 345 Middlefield Road, Menlo Park, California, 94025, USA
2 Pacific Geoscience Centre, Geological Survey of Canada, PO Box 6000, Sidney, British Columbia, V8L 4B2, Canada
3 Centre for Earth and Ocean Research, University of Victoria, P.O. Box 3055, STN CSC, Victoria, BC, V8W 3P6, Canada

ISBN: 0-607-99675-7

This publication and any updates to it can be found online at:
http://geopubs.wr.usgs.gov/open-file/of02-328/

Preface

The following report is the principal product of an international workshop titled "Intraslab Earthquakes in the Cascadia Subduction System: Science and Hazards" and was sponsored by the U.S. Geological Survey, the Geological Survey of Canada and the University of Victoria. This meeting was held at the University of Victoria's Dunsmuir Lodge, Vancouver Island, British Columbia, Canada on September 18–21, 2000 and brought 46 participants from the U.S., Canada, Latin America and Japan. This gathering was organized to bring together active research investigators in the science of subduction and intraslab earthquake hazards. Special emphasis was given to "warm-slab" subduction systems, i.e., those systems involving young oceanic lithosphere subducting at moderate to slow rates, such as the Cascadia system in the U.S. and Canada, and the Nankai system in Japan. All the speakers and poster presenters provided abstracts of their presentations that were a made available in an abstract volume at the workshop. Most of the authors subsequently provided full articles or extended abstracts for this volume on the topics that they discussed at the workshop. Where updated versions were not provided, the original workshop abstracts have been included. By organizing this workshop and assembling this volume, our aim is to provide a global perspective on the science of warm-slab subduction, to thereby advance our understanding of internal slab processes and to use this understanding to improve appraisals of the hazards associated with large intraslab earthquakes in the Cascadia system. These events have been the most frequent and damaging earthquakes in western Washington State over the last century. As if to underscore this fact, just six months after this workshop was held, the magnitude 6.8 Nisqually earthquake occurred on February 28th, 2001 at a depth of about 55 km in the Juan de Fuca slab beneath the southern Puget Sound region of western Washington. The Governor's Office of the State of Washington estimated damage at more than US$2 billion, making it among the costliest earthquakes in U.S. history.

Table of Contents

Workshop consensus findings and recommendations

Stephen H. Kirby[1], Kelin Wang[2], Workshop Steering Committee (Garry C. Rogers[2], Robert S. Crosson[3], Anne M. Tréhu[4], Chris Goldfinger[4] and Tom M. Brocher[1]) and the workshop participants

1 United States Geological Survey, 345 Middlefield Road, Menlo Park, California, 94025, USA
2 Pacific Geoscience Centre, Geological Survey of Canada, PO Box 6000, Sidney, British Columbia, V8L 4B2, Canada
3 Geophysics Program, University of Washington, PO Box 351650, Seattle, Washington, 98195–1650, USA
4 College of Oceanic and Atmospheric Sciences, Oregon State University, Corvallis, Oregon, 97331–5503, USA
skirby@usgs.gov, wang@pgc.nrcan.gc.ca, rogers@pgc.nrcan.gc.ca, crosson@u.washington.edu, trehu@oce.orst.edu, gold@oce.orst.edu, brocher@usgs.gov

Intraslab earthquake science for Cascadia and related subduction zones: what can we presently agree upon?

Building upon the findings of the oral and poster presentations and the related discussions, we held a plenary session to develop a consensus view of what we could agree upon as to the primary characteristics of warm-slab intraslab earthquakes and what interpretive models are both consistent with these characteristics and suggestive of productive research directions toward understanding their origin. This section summarizes those discussions.

1. Large intraslab earthquakes, by virtue of their frequency of occurrence, locations directly beneath population centers and source characteristics, represent a major earthquake hazard in the Cascadia subduction zone.
2. There are two regions of observed deep seismicity in the Cascadia system: one just north of the Mendocino triple junction and another under the Puget lowlands/Georgia Strait. This heterogeneous distribution probably reflects the stresses and seismic-strain-rate localization connected with the northward collision of the Pacific plate along the Mendocino fracture zone and the stress effects of the geometrical arch in the northern region, respectively. The absence of large, deep intraslab earthquakes beneath western Oregon is probably not due to inadequate sampling during the instrumental seismic era, at least since the late 1950s.
3. Many of the fundamental characteristics of the Cascadia subduction system are shared by numerous other "warm" subduction systems involving young lithosphere descending at slow rates. These characteristics include usually shallow earthquake hypocentral depth ($<100 \pm 25$ km), generally low average dip of the seismic zone ($<20°$), focal mechanisms with in-slab *T* axes, and feeble or absent arc volcanism. Trenches in these settings are also generally muted in relief and often have neutral or reverse curvature.
4. Investigations to date of shallow intraslab earthquake sources worldwide show that they tend to be enriched in high-frequency energy compared to nearby interplate thrust earthquakes of comparable scalar seismic moment. Subduction in some particular warm-slab environments, such as Mexico, Peru and Chile has produced many large ($M \geq 7.0$–8.0) and very destructive slab earthquakes probably in the subducted slab mantle. These events are sometimes exceptionally enriched in high-frequency energy compared to nearby interplate earthquakes, a factor that contributes to their destructiveness. These unusual regions may involve downdip changes in the sign of slab curvature (implied by their flat-slab geometry that occurs in some of those localities). The normal-faulting focal mechanisms of these events are consistent with reverse-curvature flexure in the slab mantle but the physical mechanisms for faulting in such settings are not known.
5. Aftershocks of the largest earthquakes in this class are usually smaller and fewer, and are not known to be damaging. This contrasts with both shallow interplate and forearc earthquakes, and argues for significant differences in the mechanics of faulting.
6. Seismological observations in Cascadia, Nankai (Southwest Japan), the Chilean Andes and the Aleutians indicate that small to intermediate-sized intraslab earthquakes largely occur in a thin low-wavespeed layer identified as subducting crust.
7. Thermo-mineralogical models for warm-slab subduction predict that the metamorphic reactions that lead to dehydration and eclogite formation should occur at depths shallower than 100 km in the oceanic crust. This shallow depth distribution of intraslab earthquakes in many warm slabs suggests that they also reflect the shallow metamorphism of subducted crust predicted by thermo-mineralogical models.
8. Laboratory studies indicate that release of water by

dehydration of hydrous minerals under stress can permit brittle fracture by faulting, even at pressures corresponding to depths greater than a few tens of kilometers, by elevating pore pressure and reducing the frictional resistance to fault sliding, a process termed dehydration embrittlement. Such a process acting inside faults hydrated by water could also permit reactivation of such faults during the heating accompanying slab descent.

9. Simplified theoretical models predict that densification to eclogite of the slab crust by metamorphism should produce internal slab stresses that may be important in driving seismic deformation of the slab. These predicted deviatoric stresses also vary in sign across the subducting crust–mantle boundary and hence can cause sharp spatial variations in focal mechanisms, as is sometimes observed. This phase-change source of slab stress also should act in combination with those associated with regional plate-scale forces, membrane deformation associated with trenches having neutral or reverse curvature, and with slab buoyancy forces.

Summary recommendations of research directions for intraslab earthquake science and hazard appraisal

These recommendations were arrived at based on discussions in three breakout groups and subsequently refined in plenary session and by the Workshop Steering Committee.

Recommendation 1

Largely marine investigations of the incoming structure of the Juan de Fuca plate with normal seafloor spreading and regions of sheared oceanic lithosphere as described by Wilson [this volume].

- Thermal structure: heat flow.
- Seismic wavespeed structure: seismic refraction.
- Identify faults and active faulting in subducting Juan de Fuca plate: ocean bottom seismometer deployments for detecting near-trench earthquakes. Seismic reflection and sonar surveys.
- Improve knowledge of slab motions: refine the Juan de Fuca plate/Oregon Coast microplate and other North America forearc microplate motions using GPS. Integrate with longer-term geophysical and geologic evidence to refine the earlier Cenozoic slab motions.

Possible payoffs include:

- Improved thermal/mineralogical models of slab evolution with descent.
- Identify possible future sources of intraslab earthquakes that can occur by reactivation during dehydration (fault dimensions and orientations).

Recommendation 2

Relocations of intraslab earthquakes using double difference, waveform correlation, three-dimensional wavespeed models and modern teleseismic methods.

- Integrate historical analogue and modern digital teleseismic data using consistent wavespeed models.
- Integrate all analog and digital Pacific Northwest network data with recent three-dimensional wavespeed models.
- Reconcile hypocenters from regional network and teleseismic station data.

Possible payoffs:

- Identify possible subsurface faults and hence fixed earthquake sources.
- Establish subsurface fault dimensions and hence place possible limits on the maximum scalar moments and magnitudes of earthquakes along them.
- Refine slab shape and, with slab motions, refine spatial rates of slab flexural deformation and compare with distribution of slab seismicity moment release rates.
- Discriminate between upper plate and slab events.

Recommendation 3

Modern waveform analysis of pre-digital and historical intraslab earthquakes in Cascadia for source properties (targets: 1939, 1946 (?), 1949, 1965, 1976 slab events).

- Invert waveforms for centroid moment tensor (CMT) M_{ij} (focal mechanism), scalar moment M_o, and moment magnitude M_w. Reconcile with Pacific Northwest network first-motion focal mechanisms.
- Establish source shapes and directivity. Relate source shapes to the geometry of seismogenic zone.
- Invert for radiated energies, E_o. Why does E_o/M_o tend to be high compared with interplate thrust earthquakes?

Possible payoffs:

- Basic improvement of the magnitude estimates for large and damaging slab earthquakes in Cascadia.
- Improved Gutenberg–Richter distribution and seismicity-rate data.
- Improvement in models for slab seismic deformation and deformation rates.
- Better constraints on ground-motion models in relation to the observed strong motions and earthquake effects.

Recommendation 4

Active and passive seismic experiments and associated modeling that image slab wavespeed anomalies (plus forearc structure) and refine slab geometry *vis a vis* intraslab earthquake hypocenters.

- Regional tomography from active sources and earthquakes.
- Reflections off slab interfaces.
- Detection of possible slow, high-frequency phases trapped in a shallow crustal waveguide in the slab.

- Teleseismic tomography and receiver-function analysis (including *S* waves).
- Body-wave conversions from teleseismic sources.
- Attenuation tomography?

Possible payoffs:

- Independent mapping of the spatial limits of the zone of slab seismogenesis based on theoretical relationship between slab mineralogical changes, their effects on wavespeed anomalies and on the release of water triggering slab earthquake faulting.
- Improved absolute hypocenter locations using three-dimensional wavespeed models and hence improved slab geometry and deformation (see recommendation 2).
- Develop a physical basis for the low level of slab seismicity beneath western Oregon, including Portland and its environs.
- Improve strong ground-motion models.
- Investigate possible slab "bank shot" ground motions due to reflection of waves from shallow forearc sources (e.g., along the Seattle fault) reflecting off the slab structure (e.g., effects of Moho reflections on ground motions from the 1989 Loma Prieta earthquake).

Recommendation 5

Develop two- and three-dimensional theoretical models for slab earthquake seismogenesis. Compare slab deformation rates inferred from models with those inferred from observed slab seismic moment release rates and their spatial distribution.

- Slab shape and kinematics, thermal structure, seismic structure and lab findings as inputs.
- Mineralogy and its changes with *P–T* conditions, fluid evolution and its effects on deformation, and deformation state and stress state as outputs.

Possible payoffs:

- Could establish upper bounds on slab earthquake-moment production rates and their spatial distribution.
- Could develop a physical basis for mapping the spatial limits of seismogenesis, including the low level of slab seismicity beneath western Oregon, including Portland and its environs.

Recommendation 6

Followup workshops: proposed workshops, mini-workshops or forums (some that could coincide with SSA or AGU annual meetings).

- Planning for seismic experiments with slab targets (Tacoma SHIPS and Oregon SHIPS; Canadian ocean bottom seismometer and broadband experiments, etc.) March 19–20, 2001, USGS/University of Washington support. Kirby, Brocher and Creager (see recommendation 4 above). Workshop held as planned.
- Historical slab earthquakes in Cascadia, southern Alaska, the Caribbean and in analog foreign subduction systems (see recommendations 2 and 3). Coordinate the efficient collection and processing of seismograms.
- Public forum on slab earthquake hazards, Seattle or Olympia, 2 days. Improve public awareness of slab earthquake hazards, develop partnerships between USGS, universities, state and local government agencies, and support for slab investigations.
- Geological and geodetic expressions of slab earthquakes and slab deformation (uplift or subsidence with respect to sea level, liquifaction, debris flows or debris avalanches off Mount Ranier). University of Washington at Seattle. Include State of Washington representatives. Search for geological information that provides a longer-term record of slab earthquake deformation and effects than the short instrumental era provides.

Possible payoffs:

- Enhanced focus on intraslab earthquakes.
- Cooperative, multidisciplinary and complex projects can be made possible (e.g., SHIPS).

Recommendation 7

International cooperation in countries having analog subduction systems and modern regional seismic networks. Promote exchange of scientists and data.

- Canada: PGC/GSC, UBC, UVic. Rapid data exchange of phase data/waveforms? Cross-border seismic experiments?
- Japan: JAMSTEC, Subduction Dynamics Frontiers Program (focus on Nankai). Planned 2003–2004 ocean bottom seismometer deployment off the northern Cascadia margin. Tohoku University: Tohoku seismology group.
- Mexico: UNAM (Instituto de Geofisica) is developing a hazards program with internal funding for new work.
- Costa Rica: Universidad Nacional de Costa Rica.

Possible payoffs:

- Can leverage information on a greater number of slab earthquakes in similar settings and thereby identify global trends in seismicity rates, ground motions, and seismic effects of slab earthquakes in warm-slab environments.
- Cross-fertilization of ideas and approaches.

References

Wilson, D .S. The Juan de F uca plate and slab: isochron structure and Cenozoic plate motions, in *The Cascadia Subduction Zone and Related Subduction Systems*, edited by S.H. Kirby , K. Wang and S.G. Dunlop, pp. 9–12, U.S. Geological Survey Open-F ile Report 02–328, Geological Survey of Canada Open File 4350, 2002.

Introduction to a global systems approach to Cascadia slab processes and associated earthquake hazards

Steve H. Kirby[1] and Kelin Wang[2]
1 United States Geological Survey, 345 Middlefield Road, Menlo Park, California, 94025, USA
2 Pacific Geoscience Centre, Geological Survey of Canada, PO Box 6000, Sidney, British Columbia, V8L 4B2, Canada
skirby@usgs.gov, wang@pgc.nrcan.gc.ca

Intraslab (Wadati–Benioff zone) earthquakes are often under-appreciated as earthquake hazards. In Latin America, such earthquakes have, in fact, had far greater human impact in the 20th century than great interplate earthquakes. Plate boundary earthquakes may have larger magnitudes but they occur largely offshore. Shallow intraslab earthquakes in the Americas may cause greater hazards because they usually occur inland where population centers tend to be located. Other factors, such as systematically higher energy yields at high frequency [*Choy et al.*, this volume] and the triggering of debris flows and avalanches on steep slopes of nearby orogenic and volcanic mountain belts also may contribute to the larger impacts of intraslab earthquakes.

Intraslab earthquakes present a special challenge for hazard appraisal because the causative faults do not rupture the ground surface, and, unlike plate-boundary earthquakes that occur on a single fault, their moment release represents distributed deformation on many faults. Their depths and localization in the subducting slab mute their expressions on the surface. With a few exceptions, geologic and geodetic observations recording uplift or subsidence and other expressions of subsurface slip have rarely been recognized.

The Cascadia subduction system has repeatedly sustained the effects of large, destructive intraslab shocks in the last century [*Rogers and Crosson*, this volume]. After this workshop was held, the $M=6.8$ Nisqually earthquake occurred on February 28, 2001 at a depth of about 53 to 58 km beneath the southern Puget lowland. This event was within the Wadati–Benioff zone defined by previous slab earthquakes, including five destructive $M>5.5$ events since 1945. All focal mechanism determinations of the 2001 earthquake indicate that it was a normal faulting event and only four small aftershocks, with magnitudes ranging from 1.0 to 4.3, occurred during the year following the main shock. The governor of the State of Washington estimated that the monetary losses connected with this earthquake exceeded US$2 billion. This most recent shock is a reminder that such earthquakes are a recurring expression of an ongoing process of slab deformation in a seismically active belt including the Willamette Valley in western Oregon, the Puget lowland in western Washington, and the Georgia Strait between Vancouver Island and the Canadian mainland.

Recent integrated models for slab thermal structure, mineralogy, slab deformation and seismic activity at intermediate depths have given useful insight into the patterns of earthquake hypocenter distribution and the fine structure of seismic wavespeeds in slabs and forearcs [e.g., *Kirby et al.*, 1996; *Peacock and Wang*, 1999; *Kirby*, 2000]. In particular, these models recognize that earthquakes deeper than about 35 km are unlikely to occur by ordinary brittle fracture and frictional sliding. It is widely believed that deeper earthquakes occur by a process of dehydration embrittlement where internal pore fluid pressure due to water liberated from hydrous minerals reduces the effective normal stresses along faults and permits fracture and frictional sliding to occur provided that the shear stresses are sufficiently high [*Raleigh*, 1967].

More recent investigations of the roles of fluids released from slabs by dehydration suggest that faults created in the ocean basins at mid-ocean ridges and trenches may be reactivated in descending slabs by dehydration embrittlement [*Kirby et al.*, 1996; *Kirby*, 2000].

Not only do metamorphic reactions in mafic oceanic crust liberate water but they also densify the crust by 12 to 15%, ultimately producing eclogite. If the crust does not detach from the underlying stable slab mantle, such large volume changes should cause large internal slab stresses, extensional in the crust and compressional in the underlying mantle [*Kirby et al.*, 1996]. Thus, metamorphism of the oceanic crust should produce both an internal source of slab stresses and a mechanism for stress release by faulting associated with dehydration. The depths at which such metamorphic changes occur depend largely on slab thermal structure. In "warm" slabs (involving young lithosphere or older lithosphere subducting at slow rates) the mafic crust (hydrous and anhydrous) probably densifies to eclogite facies at shallow depths (<100 km) (Figure 1), whereas slab dehydration and eclogite formation in "cold" slabs probably persists to far greater depths

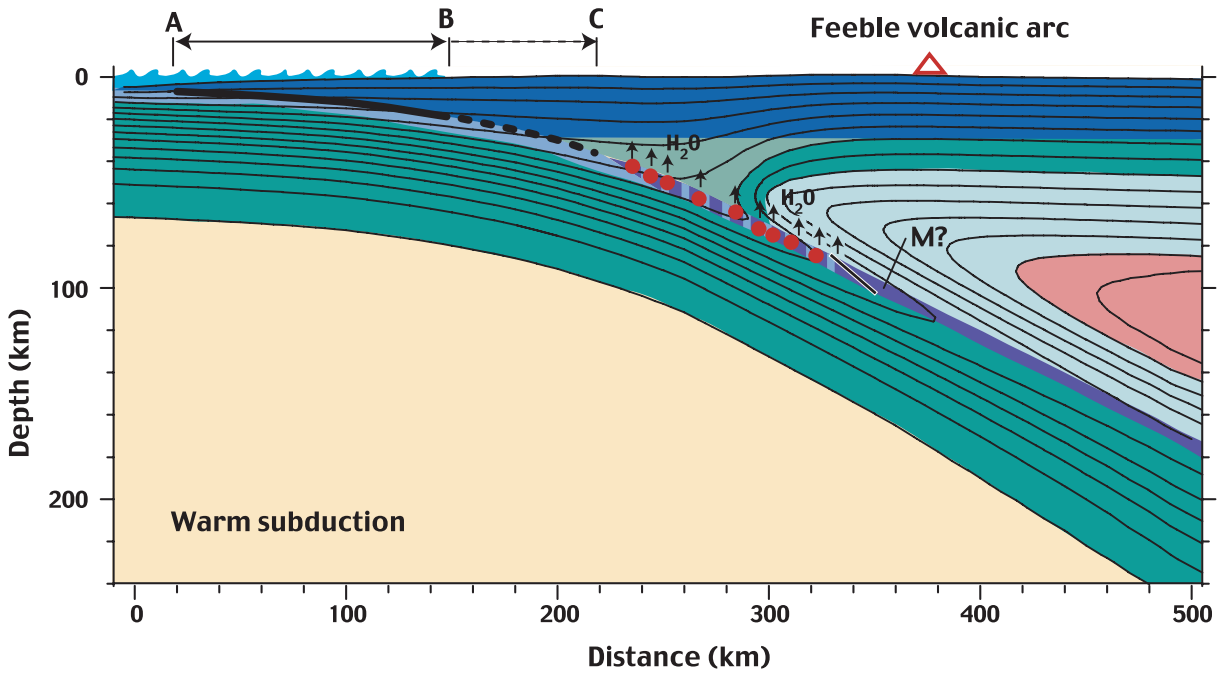

FIGURE 1: Mineralogical structure during warm subduction (after *Kirby* [2000] and based on the models of *Kirby et al.* [1996], *Peacock and Wang* [1999], and P*eacock and Hyndman* [1999]). The crust in the subducting plate is as much as 300 to 500°C warmer than for cold subduction. This hotter thermal structure restricts the region of interplate thrust seismic slip on the plate contact to shallower depths (defined by points A to B or A to C) but generally over a larger area of slip than for cold slabs, producing the potential for very large offshore interplate earthquakes. The release of water stored in crustal minerals at shallow depths of 40 to 90 km is expected to promote shallow metamorphism of normal crustal rocks (blue) to eclogite (purple), and facilitate shallow intraslab earthquakes (red dots) within slabs. Shallow dewatering also is expected to reduce partial melting of the asthenosphere and reduce volcanic vigor. Higher temperatures may also induce slab crustal melting (M?) and produce anomalous magma chemistries for such volcanoes (open red triangle). The contour interval is 100°C, with the surface held at 0°C

(>>100 km) [*Kirby et al.*, 1996; *Peacock and Wang*, 1999]. The seismic deformation associated with such densification is therefore expected to be largest at shallowest depths in warm-slab environments. Its specific seismic expression depends on how it interacts with other sources of stress, such as the forces at triple junctions [*ten Brink*, this volume], slab flexure, interplate coupling (and its variation in the plate-boundary earthquake cycle) [*Taylor et al.*, 1996], membrane deformations accompanying subduction with reverse trench curvature [*Chiao and Creager*, this volume], and slab interactions with the underlying asthenosphere [*Wang et al.*, this volume].

These mineralogical models for warm-slab subduction [*Hacker et al.*, *Peacock et al.* and *McKenna and Blackwell*, all this volume] are broadly consistent with the observed characteristics of warm subduction (shallow intraslab earthquakes, feeble or absent arc volcanism, localized "adakitic" arc lava compositions) compared to cold subduction (earthquakes to much greater depths and "normal" arc volcanism). Moreover, the models are largely consistent with the fine wavespeed structures and focal mechanisms of earthquakes in slabs in relation to the fine structure of the Wadati–Benioff zone. Cascadia is a classic end-member warm-slab environment and displays many of these characteristic features (see papers in the section on other warm-slab subduction systems).

These preliminary models for warm-slab evolution with descent are promising, and hence it follows that a global "top-to-bottom" systems approach to providing constraints on key factors important to seismic hazard appraisal is called for. Our goals guiding this systems approach include improving the constraints on seismicity rates and depth distribution (and how these vary along strike), better estimates of the maximum credible earthquake size, and improvements in the factors that govern model estimates of strong ground motions in the Cascadia subduction system, including the source characteristics of intraslab events and the fine wavespeed and attenuation structure of the slab and forearc. The components of such an approach should therefore include:

1. The state of stress and the thermal, hydrologic, fault and mineralogical structures of the offshore oceanic plates entering the "trench" of the Cascadia system, as deduced from marine geology and geophysics [*Goldfinger et al.*, this volume]. The subducted slab travels northward in the mantle, and this has a first-

order effect on the stress pattern of the offshore plate [*Wang et al.*, 1997] and potentially on intraslab stresses. Knowledge of the heat flow and hydrogeologic regime of the Juan de Fuca (JDF) plate prior to subduction [*Davis et al.*, 1999] is a prerequisite for any understanding of the thermal and metamorphic processes of the plate after subduction. The isochron structure of the exposed and subducted Explorer, Juan de Fuca and Gorda plates [*Wilson*, this volume] is an important constraint on the thermal structure of these plates and slabs.

2. High-resolution redetermination of intraslab earthquake hypocenters in light of improved models of the seismic wavespeed and attenuation structure of the Cascadia slabs and forearc. This work obviously needs to build upon recent seismic tomography based on seismic station data from the Pacific Northwest and GSC networks [*Villasenor et al.*, this volume], and on the observations made during SHIPS [*Trehu et al.* and *Crosson et al.*, this volume]. This element should also include comparisons with seismic structures in other warm slab environments, such as those in Latin America [*Singh et al.* and *Protti*, this volume] and Southwest Japan [*Cummins et al.*, this volume].
3. We also need to exploit the global instrumental record for large intraslab earthquakes in other warm-slab environments, including appraisal of the magnitudes, focal mechanisms, and hypocenter distributions of large intraslab shocks in the pre-digital era. This is necessary in order to overcome the problem of generally low slab seismicity rates of large intraslab earthquakes in Cascadia and to understand the effect of subduction parameters on the variability of intraslab earthquakes in these settings [*Kirby et al.*, this volume].
4. Improvements in our knowledge of the heat transfer, rheology, phase equilibria, and kinetic properties of the oceanic crust and mantle, especially at estimated slab *P–T* conditions. Deformation experiments on hydrous mafic and ultramafic rocks at the *P–T* conditions where the crust in the Cascadia slab is dehydrating under stress are needed in order to test further the dehydration–embrittlement mechanism and to search for other potential faulting mechanisms.
5. Using the above constraints, construct two-dimensional thermo-mechanical models of warm-slab evolution with descent, including theoretical estimates of slab stresses and deformation rates. Extend these models to three dimensions by including knowledge of the reconstructed isochron structure of the subducted parts of the Explorer, Juan de Fuca and Gorda plates, and the along-strike variations of convergence rates and slab dip. These models should give insight into the marked along-strike variations in intraslab seismicity and earthquake hazards in Cascadia.
6. Use the results of these well-constrained numerical models to reduce the uncertainties in the factors noted above that influence the hazard appraisal for intraslab earthquakes.

References

Chiao, L.-Y., and K.C. Creager, Geometry and membrane deformation rate of the subducting Cascadia slab, in *The Cascadia Subduction Zone and Related Subduction Systems*, edited by S.H. Kirby, K. Wang, and S.G. Dunlop, pp. 47–54, U.S. Geological Survey Open-File Report 02–328, Geological Survey of Canada Open File 4350, 2002.

Choy, G.L., J.L. Boatwright, and S.H. Kirby, The radiated seismic energy and apparent stress of interplate and intraslab earthquakes at subduction zone environments: implications for seismic hazard estimation, in *The Cascadia Subduction Zone and Related Subduction Systems*, edited by S.H. Kirby, K. Wang, and S.G. Dunlop, pp. 107–114, U.S. Geological Survey Open-File Report 02–328, Geological Survey of Canada Open File 4350, 2002.

Crosson, R.S., N.P. Symons, K.C. Creager, L.A. Preston, T. Van Wagoner, T.M. Brocher, M.A. Fisher and the SHIPS98 Working Group , Three-dimensional structure of the Cascadia forearc region from SHIPS active experiment and earthquake observations: tomographic inversion provides a high-resolution view into the core of the Cascadia forearc complex, in *The Cascadia Subduction Zone and Related Subduction Systems*, edited by S.H. Kirby, K. Wang, and S.G. Dunlop, p. 33, U.S. Geological Survey Open-File Report 02–328, Geological Survey of Canada Open File 4350, 2002.

Cummins, P.R., Y. Kaneda, and K.C. Hori, Large, intermediate-depth earthquakes in Southwest Japan, in *The Cascadia Subduction Zone and Related Subduction Systems*, edited by S.H. Kirby, K. Wang, and S.G. Dunlop, pp. 99–102, U.S. Geological Survey Open-File Report 02–328, Geological Survey of Canada Open File 4350, 2002.

Davis, E.E., D.S. Chapman, K. Wang, H. Villinger, A.T. Fisher, S.W. Robinson, J. Grigel, D. Pribnow, J. Stein, and K.Becker, Regional heat-flow variations across the sedimented Juan de Fuca ridge eastern flank: constraints on lithospheric cooling and lateral hydrothermal heat transport, *J. Geophys. Res., 104,* 17,675–17,688, 1999.

Goldfinger, C., R.P. Dziak, and C. Fox, Offshore structure of the Juan de Fuca plate from marine seismic and sonar studies, in *The Cascadia Subduction Zone and Related Subduction Systems*, edited by S.H. Kirby, K. Wang, and S.G. Dunlop, pp. 13–16, U.S. Geological Survey Open-File Report 02–328, Geological Survey of Canada Open File 4350, 2002.

Hacker, B.R., G.A. Abers, and S.M. Peacock, Theoretical mineralogy, density, seismic wavespeeds and H_2O

content of the Cascadia subduction zone, with implications for intermediate-depth seismicity and earthquake hazard, in *The Cascadia Subduction Zone and Related Subduction Systems*, edited by S.H. Kirby, K. Wang, and S.G. Dunlop, pp. 133–138, U.S. Geological Survey Open-File Report 02–328, Geological Survey of Canada Open File 4350, 2002.

Kirby, S.H., Taking the temperature of slabs, *Nature*, *403*, 31–34, 2000.

Kirby, S.H., E.R. Engdahl, and R. Denlinger, Intermediate-depth intraslab earthquakes and arc volcanism as physical expressions of crustal and uppermost mantle metamorphism in subducting slabs, in *Subduction: Top to Bottom, Geophysical Monograph 96,* edited by G. Bebout, D. Scholl, S. Kirby, and J. Platt, pp. 195–214, American Geophysical Union, Washington, D.C., 1996.

Kirby, S.H., E.R. Engdahl and A. Villaseñor, Warm-slab subduction as a global process, in *The Cascadia Subduction Zone and Related Subduction Systems*, edited by S.H. Kirby, K. Wang, and S.G. Dunlop, p. 75, U.S. Geological Survey Open-File Report 02–328, Geological Survey of Canada Open File 4350, 2002.

McKenna, J.R., and D.D. Blackwell, Heat sources in the subduction zones: implications for slab seismicity and arc volcanism in *The Cascadia Subduction Zone and Related Subduction Systems*, edited by S.H. Kirby, K. Wang, and S.G. Dunlop, pp. 127–132, U.S. Geological Survey Open-File Report 02–328, Geological Survey of Canada Open File 4350, 2002.

Peacock, S.M., and R. Hyndman, Hydrous minerals in the mantle wedge and the maximum depth of subduction thrust earthquakes, *Geophys. Res. Lett., 26*, 2517–2520, 1999.

Peacock, S.M., and K. Wang, Seismic consequences of warm versus cool subduction metamorphism: examples from Southwest and Northeast Japan*, Science, 286,* 937–939, 1999.

Peacock, S., K. Wang, and A.M. McMahon, Thermal structure and metamorphism of subducting oceanic crust: insight into Cascadia intraslab earthquakes in *The Cascadia Subduction Zone and Related Subduction Systems*, edited by S.H. Kirby, K. Wang, and S.G. Dunlop, pp. 123–126, U.S. Geological Survey Open-File Report 02–328, Geological Survey of Canada Open File 4350, 2002.

Protti, M., Seismicity and seismotectonics of Central America with emphasis on intraslab seismic activity in *The Cascadia Subduction Zone and Related Subduction Systems*, edited by S.H. Kirby, K. Wang, and S.G. Dunlop, pp. 93–98, U.S. Geological Survey Open-File Report 02–328, Geological Survey of Canada Open File 4350, 2002.

Raleigh, C.B., Tectonic implications of serpentinite weakening, *Geophys. J. Royal Astro. Soc., 14,* 113–118, 1967.

Rogers, G.C., and R.S. Crosson, Intraslab earthquakes beneath Georgia Strait/Puget Sounds, in *The Cascadia Subduction Zone and Related Subduction Systems*, edited by S.H. Kirby, K. Wang, and S.G. Dunlop, p. 68, U.S. Geological Survey Open-File Report 02–328, Geological Survey of Canada Open File 4350, 2002.

Singh, S.K., V. Kostoglodov, and J.F. Pacheco, Intraslab earthquakes in the subducting oceanic plates below Mexico, in *The Cascadia Subduction Zone and Related Subduction Systems*, edited by S.H. Kirby, K. Wang, and S.G. Dunlop, pp. 87–92, U.S. Geological Survey Open-File Report 02–328, Geological Survey of Canada Open File 4350, 2002.

Taylor, M.A.J., G. Zheng, and J.R. Rice, Cyclic stressing and seismicity at strongly coupled subduction zones, *J. Geophys. Res., 101,* 8363–8381, 1996.

ten Brink, U.S., Slab deformation at the edge of subduction zones: an example from Cascadia, in *The Cascadia Subduction Zone and Related Subduction Systems*, edited by S.H. Kirby, K. Wang, and S.G. Dunlop, pp. 139–142, U.S. Geological Survey Open-File Report 02–328, Geological Survey of Canada Open File 4350, 2002.

Tréhu, A.M., T.M. Brocher, K.C. Creager, M.A. Fisher, L.A. Preston, G. Spence and the SHIPS98 Working Group, Geometry of the subducting Juan de Fuca plate: new constraints from SHIPS98, in *The Cascadia Subduction Zone and Related Subduction Systems*, edited by S.H. Kirby, K. Wang and S.G. Dunlop, pp. 25–32, U.S. Geological Survey Open-File Report 02–328, Geological Survey of Canada Open File 4350, 2002.

Villaseñor, A., D. Stanley, and H. Benz, Velocity structure of western Washington from local earthquake tomography, in *The Cascadia Subduction Zone and Related Subduction Systems*, edited by S.H. Kirby, K. Wang and S.G. Dunlop, pp. 35–36, U.S. Geological Survey Open-File Report 02–328, Geological Survey of Canada Open File 4350, 2002.

Wang, K., J. He, and E.E. Davis, Transform push, oblique subduction resistance, and intraplate stress of the Juan de Fuca plate, *J. Geophys. Res., 102,* 661–674, 1997.

Wang, K., J. He, E.E. Davis, and C. Goldfinger, Stresses in the Juan de Fuca Plate and the role of mantle resistance to horizontal slab motion, in *The Cascadia Subduction Zone and Related Subduction Systems*, edited by S.H. Kirby, K. Wang, and S.G. Dunlop, p. 143, U.S. Geological Survey Open-File Report 02–328, Geological Survey of Canada Open File 4350, 2002.

Wilson, D.S. The Juan de Fuca plate and slab: isochron structure and Cenozoic plate motions, in *The Cascadia Subduction Zone and Related Subduction Systems*, edited by S.H. Kirby, K. Wang and S.G. Dunlop, pp. 9–12, U.S. Geological Survey Open-File Report 02–328, Geological Survey of Canada Open File 4350, 2002.

The Juan de Fuca plate and slab: Isochron structure and Cenozoic plate motions

Douglas S. Wilson
Department of Geological Sciences, University of California at Santa Barbara, Santa Barbara, California, 93106, USA
wilson@rapa.geol.ucsb.edu

The Juan de Fuca ridge has a long history of complex tectonics, with propagating ridge offsets having been more common than stable transform faults for most of the time since 25 Ma. The spreading rate has been intermediate at about 50–65 mm/yr since about 20 Ma. Several incremental clockwise shifts in the spreading direction during this time have led to reorganization of the propagating rift pattern. The most prominent shift occurred during a Pacific-wide reorganization at 5.9 Ma, when Juan de Fuca–Pacific relative motion changed by 10-15˚and the first stable transform fault segment of the Blanco fracture zone formed. Subsequent propagation has shortened pre-existing ridge segments that became intra-transform spreading centers when their bounding offsets became additional strands of the transform fault system, eventually developing into the four major strands of the modern Blanco transform. The Juan de Fuca plate has not remained rigid as its motion relative to the Pacific plate has evolved.

Since at least 10 Ma, the strike of the Mendocino transform fault has not reoriented to remain parallel to the increasingly clockwise direction of Juan de Fuca–Pacific relative motion. Since at least 3 Ma, the resulting space problem has been accommodated in a diffuse boundary zone east of the southern Gorda ridge commonly (but erroneously) known as the Gorda plate. Prior accommodation may have included a minor component of thrusting along the Mendocino transform. At roughly 4 Ma, the Explorer micro-plate separated from the northern Juan de Fuca plate and the motion of the Explorer plate relative to North America is slow enough that it could be considered to have been captured by the North American plate. The Sovanco transform zone between the Explorer and Pacific plates is either extremely broadly distributed or has migrated north and south numerous times (probably both), and remains poorly understood.

As is the case with other plate pairs in the Pacific, minor changes in plate motion since 3 Ma indicate that 0–0.78 Ma averages may be more indicative of modern motions than 0–3 Ma averages. The recent averages give spreading rates of 55 mm/yr for Endeavour segment and 51 mm/yr for northern Gorda ridge [*Wilson*, 1993].

In a reference frame fixed to North America, convergence of the Juan de Fuca plate has been roughly constant since 20 Ma at the slow to intermediate rate of about 40 mm/yr in a northeasterly direction. Current rates increase northward from about 30 mm/yr at 42˚N to about 45 mm/yr at 49˚N, but rate gradients have varied substantially through time. Recent revisions in the determination of current Pacific–North America relative motion, as well as corrections for possible slight biases in converting magnetic anomaly width to spreading rate, both indicate a convergence direction several degrees counterclockwise from previous determinations. Northward motion of the continental margin relative to rigid North America reduces the obliquity of the convergence direction [*McCaffrey et al.*, 2000].

The age structure of the slab can be extrapolated from offshore isochrons with fairly high confidence. A narrow, young and barely subducting slab attached to the Explorer plate lies under northwestern Vancouver Island. From southern British Columbia to central Oregon the inferred age pattern is very simple, with age increasing eastward, about 12 Ma below the coastline. In this area, structural complexities inherited from shear deformation of young seafloor near the ridge axis are restricted to narrow, northeast-striking zones. Below southern Oregon and northern California, the age pattern is much more complex. A broad area was sheared prior to formation of the Blanco transform at 5.9 Ma and the south edge of the slab has been pervasively sheared as it passed through the Gorda deformation zone over the past several million years. The location of active seismicity at the south end of the slab is fairly well predicted by simple models that treat the corner of the Pacific plate at the Mendocino triple junction as a rigid indentor into the much weaker Juan de Fuca plate, with little or no influence from inherited structures in the slab.

References

Botros, M., and H.P. Johnson, Tectonic evolution of the Explorer-northern Juan de Fuca region from 8 Ma to the present, *J. Geophys. Res., 93*, 10,421–10,437, 1988.

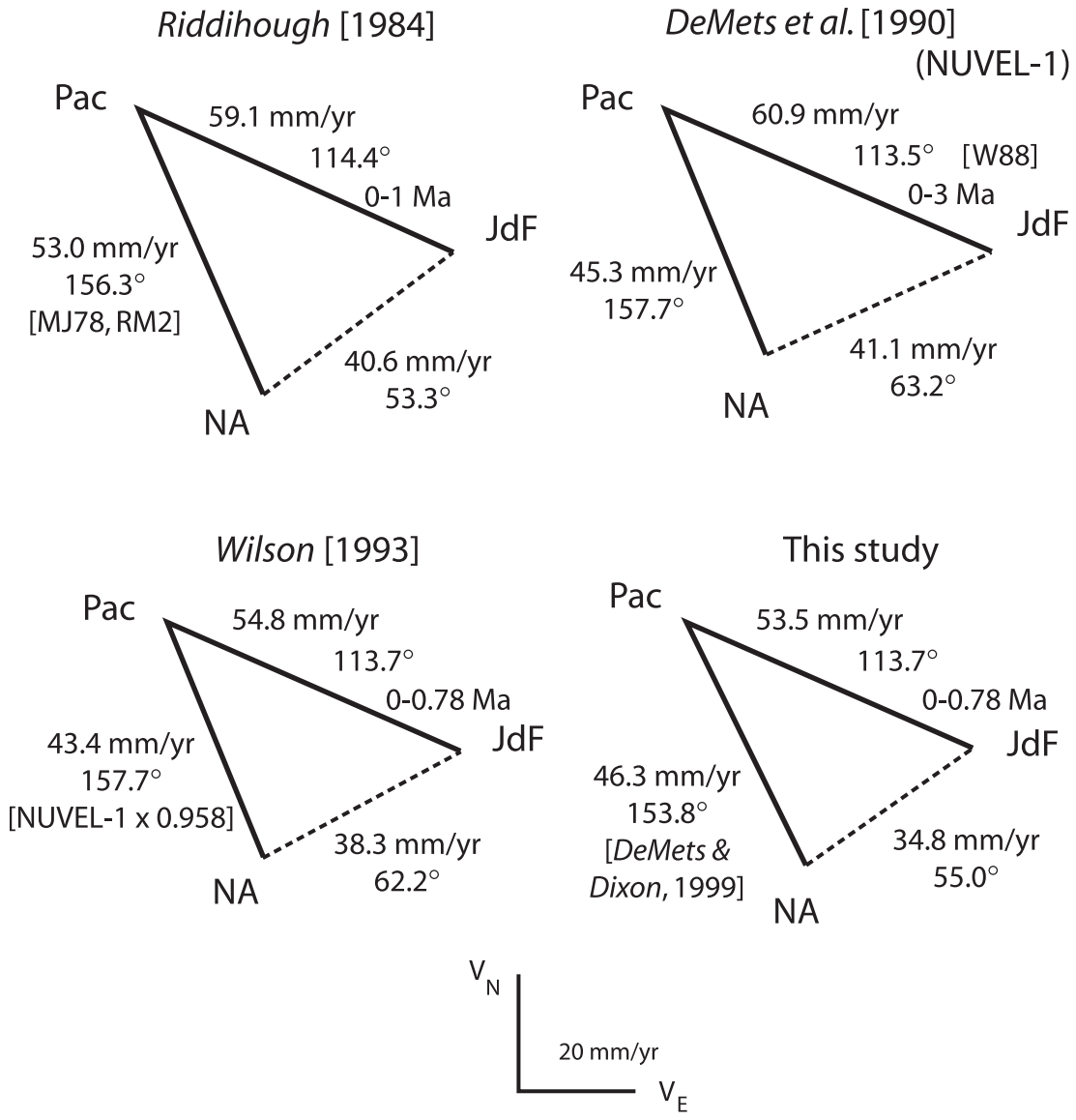

FIGURE 1: History of estimates of convergence velocity between Juan de Fuca and stable North America, calculated for 46°N, 125°W. All estimates are based on vector subtraction of Pacific–North America and Pacific–Juan de Fuca rates. Changes in Pacific–North America rates reflect significant changes in input data, while changes for Juan de Fuca are dominated by time-scale revisions. The current estimate for Juan de Fuca–Pacific includes a small correction based on the assumption that the axial magnetic anomaly is one kilometer wider than the plate motion since the magnetic polarity reversal. Resulting rotation vector for North America–Juan de Fuca is 33.7°N, -115.1°E, 1.257°/Myr. Actual convergence rates on the subduction zone will need a correction for motion of the continental margin relative to stable North America, up to 6–9 mm/yr northward [*McCaffrey et al.*, 2000].

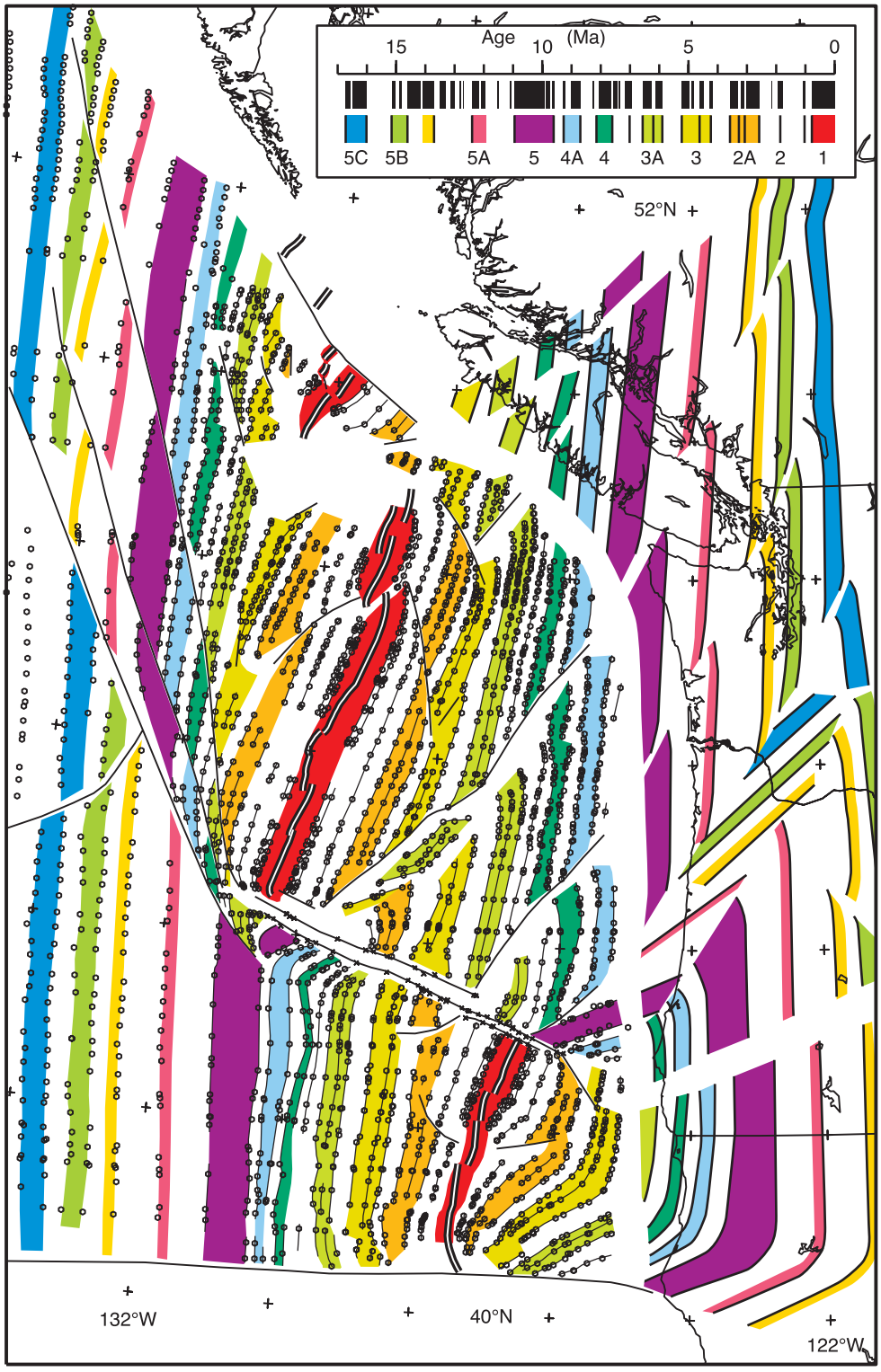

FIGURE 2: Seafloor age map, modified from *Wilson* [1988; 1993], and prediction of slab age, modified from *Wilson* [1988] to include nonrigid plate behavior. No correction for slab dip has been applied. Areas in the slab with north–south isochron strikes should be undeformed; other areas experienced significant shear prior to subduction.

Cowan, D.S., M. Botros, and H.P. Johnson, Bookshelf tectonics: rotated crustal blocks within the Sovanco fracture zone, *Geophys. Res. Lett., 13*, 995–998, 1986.

Denlinger, R.P., A model for large-scale plastic yield of the Gorda deformation zone, *J. Geophys. Res., 97*, 15,415–15,423, 1992.

DeMets, C., and T.H. Dixon, New kinematic models for Pacific–North America motion from 3 Ma to present, I: evidence for steady motions and biases in the NUVEL-1A model, *Geophys. Res. Lett., 26*, 1921–1924.

DeMets, C., R.G. Gordon, D.F. Argus, and S. Stein, Current plate motions, *Geophys. J. Int, 101*, 425–478, 1990.

Embley, R.W., and D.S. Wilson, Morphology of the Blanco transform, northeast Pacific: implications for its tectonic evolution, *Mar. Geophys. Res., 14*, 25–45, 1992.

Hey, R.N., A new class of "pseudofaults" and their bearing on plate tectonics: a propagating rift model, *Earth Planet. Sci. Lett., 37*, 321–325, 1977.

Hey, R.N., and D.S. Wilson, Propagating rift explanation for the tectonic evolution of the northeast Pacific: the pseudomovie, *Earth Planet. Sci. Lett., 58*, 167–188, 1982.

Hyndman, R.D., R.P. Riddihough, and R. Herzer, The Nootka fault zone: a new plate boundary off western Canada, *Geophys. J. R. Astron. Soc., 58*, 667–683, 1979.

Jachens, R.C., and A. Griscom, Three-dimensional geometry of the Gorda plate beneath northern California, *J. Geophys. Res., 88*, 9375–9392, 1983.

Johnson, H.P., J.L. Karsten, J.R. Delaney, E.E. Davis, R.G. Currie, and R.L. Chase, A detailed study of the Cobb offset of the Juan de Fuca ridge: evolution of a propagating rift, *J. Geophys. Res., 88*, 2297–2315, 1983.

Kleinrock, M.C., and R.N. Hey, Migrating transform and lithospheric transfer at the Galapagos 95.5°W propagator, *J. Geophys. Res., 94*, 13,859–13,878, 1989.

McCaffrey, R., and 6 others, Rotation and plate locking at the southern Cascadia subduction zone, *Geophys. Res. Lett., 27*, 3117–3120, 2000.

McKenzie, D., The geometry of propagating rifts, *Earth Planet. Sci. Lett., 77*, 176–186, 1986.

Riddihough, R.P., A model for recent plate interactions off Canada's west coast, *Can. J. Earth Sci., 14*, 384–396, 1977.

Riddihough, R., Recent plate motions of the Juan de Fuca plate system, *J. Geophys. Res., 89*, 6980-6994, 1984.

Silver, E.A., Tectonics of the Mendocino triple junction, *Geol. Soc. Am. Bull., 82*, 2965–2978, 1971.

Vine, F.J., Magnetic anomalies associated with mid-ocean ridges, in *The History of the Earth's Crust*, edited by R.A. Phinney, pp. 73–89, Princeton University Press, Princeton, N. J., 1968.

Wang, K., J. He, and E.E. Davis, Transform push, oblique subduction resistance and intraplate stress of the Juan de Fuca Plate, *J. Geophys. Res., 102*, 661–674, 1997.

Wilson, D.S., A kinematic model for the Gorda deformation zone as a diffuse southern boundary of the Juan de Fuca plate, *J. Geophys. Res., 91*, 10,259–10,269, 1986.

Wilson, D.S., Tectonic hisotry of the Juan de Fuca ridge over the last 40 million years, *J. Geophys. Res., 93*, 11,863–11,876, 1988.

Wilson, D.S., Deformation of the so-called Gorda plate, *J. Geophys. Res., 94*, 3065–3075, 1989.

Wilson, D.S., Kinematics of overlapping rift propagation with cyclic rift failure, *Earth Planet. Sci. Lett., 96*, 384–392, 1990.

Wilson, D.S., Confidence intervals for motion and deformation of the Juan de Fuca plate, *J. Geophys. Res., 98*, 16,053–16,071, 1993.

Wilson, D.S., R.N. Hey, and C. Nishimura, Propagation as a mechanism of reorientation of the Juan de Fuca Ridge, *J. Geophys. Res., 89*, 9215–9225, 1984.

Offshore structure of the Juan de Fuca plate from marine seismic and sonar studies

Chris Goldfinger[1], Robert P. Dziak[2] and Chris Fox[2]
1 College of Oceanic and Atmospheric Sciences, Oregon State University, Corvallis, Oregon, 97331, USA
2 National Oceanic and Atmospheric Administration, Pacific Marine Environmental Laboratory
Hatfield Marine Science Center, Newport, Oregon, 97365, USA
gold@oce.orst.edu, dziak@pmel.noaa.gov, fox@pmel.noaa.gov

Juan de Fuca deformation

Using sidescan sonar, seismic reflection profiles and swath bathymetric data, we have mapped a set of west–northwest trending left-lateral strike-slip faults that deform the Oregon and Washington submarine forearc. Evidence for left-lateral separation includes: offset of accretionary wedge folds, channels and other surficial features; sigmoidal left bending of accretionary wedge folds; and offset of abyssal plain basement and sedimentary units. Five of these faults cross the plate boundary, extending 5–21 km into the Juan de Fuca plate. Using offset of subsurface piercing points and offset of approximately dated submarine channels, we calculate slip rates for these five faults of 5.5 to 8.5 mm/yr. Little or no offset of these faults by the basal thrust of the accretionary wedge is observed. Holocene offset of submarine channels and unconsolidated sediments is observed in sidescan records and directly by submersible [*Goldfinger et al.,* 1997].

We also observe compressional and extensional regions near the ends of the rotating blocks that are consistent with the expected space problems inherent in any block rotation kinematic model. The presence of underlying differential slip on the subducting slab has left a characteristic pattern of accretionary wedge development. The slip of the underlying slab faults results in local apparent variations in plate convergence on the décollement, resulting in variations in rates of growth of overlying accretionary wedge anticlines.

The strike-slip faults are most likely driven by dextral shearing of the subducting slab and propagate upward through the overlying accretionary wedge. Plate coupling forces are insufficient to account for rupture of the slab, and thus independent slab rupture is the best explanation for the presence of these structures [*Goldfinger et al.,* 1997]. Tangential hydrodynamic drag caused by oblique insertion of the slab into the mantle is a possible driving mechanism. Four sinistral faults observed in only the upper plate may be remnant traces of previous basement-driven deformation. Such traces are expected as the slab faults more to the northeast with the Juan de Fuca plate. A model of overall right-lateral simple shear of the submarine forearc is consistent with the observed surface faults, which may be *R′* or antithetic shears to the overall right-shear couple. The major strike-slip faults define elongate blocks that, because of their orientation and sinistral slip direction, must rotate clockwise. We infer that the deformation of the submarine forearc (here defined to include the lower plate) is highly strain-partitioned into arc-normal shortening and arc-parallel strike-slip and translation. The high slip rates of the strike-slip faults, coupled with the lack of offset of these faults as they cross the plate boundary, imply that the seaward accretionary wedge is not moving at the expected convergence rate relative to the subducting plate. We conclude that the accretionary wedge is rotating and translating northward, driven by the tangential component of Juan de Fuca–North American plate convergence. This conclusion is also supported by the lack of offset across the deformation front between large landslide scarps and associated debris packages on the abyssal plain. These slides range in age from 14 ka to 1000 ka, yet the debris and the scarps appear to be largely in their original relative positions [*Goldfinger et al.,* 2000].

Scholz and Campos [1995] proposed a dynamic model of interplate coupling and decoupling at subduction zones that incorporates the hydrodynamic resistance of the motion of the slab through the viscous mantle. In their model, the mantle is considered stationary in a hot spot reference frame. This "sea anchor" force, in a mantle system that is fixed to the hot spot frame, should have trench-parallel and trench-normal components in the case of oblique subduction [*Scholz and Campos,* 1995] (Figure 1). The trench–parallel component of hydrodynamic mantle resistance to subduction is an unbalanced force that sets up a shear couple in the plane of the slab. For Cascadia, the shear couple would be dextral, and antithetic shears should be left-lateral and east–west to northwest trending. We propose that this shear couple may be responsible for the observed transverse rupture of the slab

we have observed in the central Cascadia forearc. Limited slab seismicity is consistent with a model of transverse shearing in the subducting slab. The largest instrumentally recorded earthquake in Cascadia (1949, M_b=7.1; 47.13°N, 122.95°W [*Baker and Langston,* 1987]) occurred in the Puget Sound region in Washington. The focal depth of 54 km places this event in the upper part of the subducting plate [*Baker and Langston,* 1987; *Ludwin et al.,* 1991]. The focal mechanism is strike-slip with a preferred fault plane striking east–west ± 15° (azimuth 255–285°) and has nearly pure left-lateral slip [*Baker and Langston,* 1987]. While this strike-slip mechanism indicates shearing within the Juan de Fuca plate, the fault planes of the 1949 event are not parallel to the convergence direction, negating a possible tear fault origin [*Weaver and Baker,* 1988]. A similar left-lateral strike-slip solution was determined for a small 1981 earthquake (magnitude 3.3) in the upper Juan de Fuca plate on the southern Washington coast (Figure 2) [*Taber and Smith,* 1985; *Weaver and Baker,* 1988]. The Olympia event, and the Washington coast strike-slip event, lie at the eastern end of an east–west linear trend of earthquakes that lie roughly on the projection of one of the basement sinistral faults, the South Nitinat fault, and are near a major east-west reverse fault mapped on the shelf. We suggest that these slab events may have occurred on the downdip part of this known slab structure.

Could these basement-involved faults be reactivated structures in the oceanic basalt? Comparison of the strikes of the oblique faults to the seafloor magnetic anomaly map of *Wilson* [1993] shows that the three Washington faults, with strikes of about 283°, could be reactivated small fracture zones perpendicular to the magnetic anomalies. The Oregon faults strike 292° to 325°, deviating from an orthogonal to the magnetic lineations by 12° to 45°, and thus are unlikely to be related to pre-existing basement structure. We have also considered conjugate shortening of the forearc of the type described by *Lewis et al.* [1988]; however, extensive mapping of margin structures [*Wagner et al.,* 1986; *Clarke,* 1990; this paper] has not identified structures conjugate to the west–northwest faults. We have mapped two major northeast trending structures, one on the slope off northern Oregon and one off central Washington, but both of these are clearly left-lateral tear faults of the accretionary fold-thrust belt.

Implications for plate coupling

In much of the Oregon and northern California forearcs, two domains of fold orientation are separated by a break in topographic slope. The dominant north–northwest to west–northwest trending structural grain of the upper slope and shelf is nearly orthogonal the plate convergence direction, suggesting strong plate coupling. The lower slope, in contrast, consists of margin parallel folds that are more open, and have mixed or seaward vergence directions. The sharp division of structural domains in the mid-continental slope may correspond to the seismic front of *Byrne et al.* [1988]. We speculate that seaward of this boundary, basal shear stress is less than that needed to form structures normal to the maximum principal stress (σ_1), and that a "backstop" effect at or near the slope break (SB) dominates the margin-parallel orientation of the youngest structures [*Goldfinger et al.,* 1992; 1996]. Landward of this boundary, folds that are oblique to the continental margin but close to normal to the inferred plate convergence direction, dominate structural orientations, suggesting strong coupling eastward to the coastal region. We note a longitudinal pattern of deformation along several of the transverse strike-slip faults that we infer is related to this sharp stress transition. We observe strong expression of these faults on the abyssal plain, poor expression on the lower slope, and strong expression on the upper slope and outer shelf. This pattern could result from reduced fault slip across the overpressured and poorly coupled décollement beneath the lower slope. The decrease of deformation from the plain to lower slope is also consistent with a lower plate origin. Rejuvenation of the faults on the upper slope is consistent with progressive dewatering of the wedge and resulting stronger interplate coupling as would be expected for the rearward part of the wedge. The landward widening of individual fault zones is also consistent with fault slip transmitted upward through and eastward thickening accretionary wedge [*Goldfinger et al.,* 1996].

Gorda deformation

Several models have been proposed to explain the curvature and fanning of magnetic lineations. These include a rigid plate rotation model proposed by *Riddihough* [1980] that incorporates three subplates corresponding to the three segments of the Gorda Ridge, driven by faster spreading at the northern end of the ridge (Model A). Another incorporates three subplates and accommodates motion of the faster spreading northern segment with left-lateral slip along northeast trending faults inherited from the Gorda Ridge (Model B) [*Knapp*, 1982]. A third incorporates a series of right-lateral faults to accommodate the faster moving northern block (Model C) [*Bolt et al.,* 1968]. A fourth model uses flexural-slip buckling to account for the curvature of the magnetic lineations and assumes that deformation is widely distributed, mostly along pre-existing weaknesses inherited from the ridge (Model D) [*Silver,* 1971; *Stoddard,* 1987]. This model also utilizes principally left-lateral slip on northeasterly striking faults, and includes a broad northeast-striking shear zone to obviate the need for subduction or obduction at the Mendocino transform [*Wilson,* 1986; 1989].

All of these models can explain, to a first-order, the pattern of the magnetic lineations. However, each also has potential problems, many of which were not appar-

ent when they were developed. For example, the first three do not produce the smoothly curved magnetic lineations that are observed, although prior to the new SeaBeam data it was not known whether or not the smoothness was real or an artifact of the relatively low-resolution magnetic data. This is an important consideration and is further discussed below. Model C is partially supported by GLORIA sidescan sonar data that suggest two right-lateral northwest-trending shear zones in the west-central part of the plate. However, this model is not in good agreement with seismicity data which indicate that the northeast trending nodal planes are preferred [*Silver,* 1971; *Velasco et al.,* 1994]. Model D fits the seismicity data and limited fault mapping, but requires the plate to buckle in a full sinusoid, as for the case of an end-loaded beam, an unlikely elastic state for the hot, thin Gorda lithosphere. The absence of the full waveform is explained by delamination of the lithosphere and accretion of the missing upper crust to the Mendocino Ridge [*Stoddard,* 1987]. Model E fits the seismicity data, the shape of the magnetic lineations, and the evidence for a shear zone in the central part of the Gorda plate, but requires the northern part of the plate to be undeformed and moving entirely with the Juan de Fuca plate. Although instrumental seismicity suggests that the northern Gorda segment is less seismically active at present, evidence of active faulting (discussed below) indicates that this part of the plate is deforming. This model also does not allow convergence at the Mendocino Ridge. Recent submersible observations and dated samples from the Mendocino Ridge, however, suggest that the ridge is constructed principally of Gorda plate material and that the ridge has been raised above sea level during possible obduction events. This is indicated by wave cut platforms with rounded cobbles now on the ridge flanks at ~1800 m depth [*Duncan et al.,* 1994; *Krause et al.,* 1997]. None of the models incorporate dip-slip faulting that is occurring along both the fabric-parallel faults and the pseudofaults, nor are most of them consistent with the faulting we observe in the northern Gorda (except *Stoddard,* [1987]).

New constraints from the 1997 SeaBeam survey

The new SeaBeam bathymetric dataset now available for the Gorda plate provides new constraints on the kinematics of Gorda deformation. Prior to its collection, the deformation was analyzed using magnetic lineations, augmented in some cases by analysis of GLORIA regional sidescan sonar data. A primary observation we can make from the new data is that the pervasive basement ridges present in the Gorda plate, and used in some of the models to constrain kinematics, are smoothly curved and mostly unbroken by strike-slip faulting crossing these lineations (with two exceptions). This observation alone places a strong constraint on models that require significant faulting at angles to them on major structures. Shearing along a multitude of faults, each with slip smaller than the 100 m resolution of the data, is an unlikely but possible alternative that is not resolved with SeaBeam data. In some areas, the basement fabric, while remaining smoothly curved, is also "kinked." Each of these kinks is associated with a basement fold pair oriented parallel to the kink axis. Additionally, basement fabric ridges appear to be drag folded adjacent to pseudofaults that may have been activated as tectonic structures.

On a finer scale, we observe clear evidence for strike-slip separation along these linear curved ridges. The ridges vary considerably in height along strike, and the exposed highs are ubiquitously split and offset in the long direction. Though space permits showing only a few examples, this faulting style is pervasive and can be subdivided into two domains, sinistral separation in the south, and dextral separation in the north, along the same linear features. This surprising result strongly supports a model that is similar to the flexural-slip model first proposed by *Stoddard* in 1987. In effect, the entire Gorda plate appears to be deforming as a huge flexural-slip fold [*Yeats,* 1986] in the horizontal plane. This model well explains the left-lateral slip on the southern "limb" and lesser right-lateral slip on the northern "limb" of the asymmetric syncline. As with a flexural-slip syncline, separation is reduced near the axis and opposing limbs have opposite senses of motion. Younger (in this case more westerly) units have lesser amounts of slip, indicating that this slip has occurred during the post-accretion history of the plate. We can calculate approximate minimum slip-rates for these faults using offsets from the SeaBeam data, where it can be estimated, and the approximate age of the underlying basement as a maximum age of fault motion. This method yields slip rates of 0.5–2 mm/yr for the offsets we have measured thus far. The age of first motion and the slip history of these faults is unknown, adding further though unquantifiable uncertainty to these rates.

The flexural-slip model of Stoddard cannot be correct in a dynamic sense. His model required an elastic flexure and thus must have a complete wavelength. On this basis, he predicted that since a complete wave is not observed, the missing part must have been obducted or subducted along the Mendocino fault. To test this idea, we did a simple line length balancing of the flexural-slip buckle. To a first order, we find that line lengths are equal along basement lineations between the Blanco and Mendocino faults, indicating little or no area of the Gorda plate has been differentially obducted or subducted. In terms of the flexure model, the "missing" material is not missing since dynamic flexure is not required. Obduction may have occurred but line length balancing suggests relatively consistent obduction and or subduction along the ridge.

References

Baker, G.E., and C.A. Langston, Source parameters of the 1949 magnitude 7.1 south Puget Sound, Washington, earthquake as determined from long-period body waves and strong ground motions, *J. Geophys. Res., 77,* 1530–1557, 1987.

Bolt, B.A., C. Lomnitz, and T.V. McEvilly, Seismological evidence on the tectonics of central and northern California and the Mendocino Escarpment, *Bull. Seismol. Soc. Am., 58,* 1725–1767, 1968.

Byrne, D.E., D.M. Davis, and L.R. Sykes, Loci and maximum size of thrust earthquakes and the mechanics of the shallow region of subduction zones, *Tectonics, 7,* 833–857, 1988.

Duncan, R.A., M.R. Fisk, A.G. Carey, D. Lund, L. Douglas, D.S. Wilson, D.C. Krause, R. Stewart, and C.G. Fox, Origin and emergence of Mendocino Ridge, *EOS Trans. AGU, 75,* p. 175, 1994.

Goldfinger, C., L.D. Kulm, R.S. Yeats, B. Appelgate, M. MacKay, and G.F. Moore, Transverse structural trends along the Oregon convergent margin: implications for Cascadia earthquake potential, *Geology, 20,* 141–144, 1992.

Goldfinger, C., L.D. Kulm, R.S. Yeats, C. Hummon, G.J. Huftile, A.R. Niem, and L.C. McNeill, Oblique strike-slip faulting of the Cascadia submarine forearc: the Daisy Bank fault zone off central Oregon, in *Subduction: Top to Bottom*, *Geophys. Monogr. Ser., Vol. 96*, edited by G.E. Bebout et al., pp. 65–74, American Geophysical Union, Washington, D.C., 1996.

Goldfinger, C., L.D. Kulm, R.S. Yeats, L.C. McNeill, and C. Hummon, Oblique strike-slip faulting of the central Cascadia submarine forearc, *J. Geophys. Res., 102,* 8217–8243, 1997.

Goldfinger, C., L.D. Kulm, L.C. McNeill, and P. Watts, Super-scale failure of the southern Oregon Cascadia margin, *Pure and Applied Geophysics, 157,* 1189–1226, 2000.

Knapp, J.S., Seismicity, crustal structure and tectonics near the northern termination of the San Andreas fault, Ph.D Thesis, 343 pp., University of Washington, Seattle, 1982.

Krause, D.C., M.R. Fisk, R.A. Duncan, C.G. Fox, and E. Christofferson, Mendocino Ridge: vertical tectonics through Gorda plate transpression, submitted abstract for the Oceanography Society meeting, May, 1997.

Ludwin, R. S., C.S. Weaver, and R.S. Crosson, Seismicity of Washington and Oregon, in *Neotectonics of North America*, DNAG CSMV-1, edited by D.B. Slemmons, E.R. Engdahl, D. Blackwell, and D. Schwartz, pp. 77–98, Geological Society of America, Boulder, Colorado, 1991.

Riddihough, R.P., Gorda plate motions from magnetic anomaly analysis, *Earth Planet. Sci. Lett., 51,* 163–170, 1980.

Scholz, C., and J. Campos, On the mechanism of seismic decoupling and back arc spreading at subduction zones, *J. Geophys. Res, 100,* 22,103–22,115, 1995.

Silver, E.A., Tectonics of the Mendocino triple junction, *Geol. Soc. Am. Bull., 82,* 2965–2978, 1971.

Stoddard, P.R., A kinematic model for the evolution of the Gorda plate, *J. Geophys. Res., 92,* 11,524–11,532, 1987.

Taber, J. J., Jr., and S.W. Smith, Seismicity and focal mechanisms associated with the subduction of the Juan de Fuca plate beneath the Olympic Peninsula, Washington, *Bull. Seismol. Soc. Am., 75,* 237–249, 1985.

Velasco, A.A., C.J. Ammon, and T. Lay, Recent large earthquakes near Cape Mendocino and in the Gorda plate: Broadband source time functions, fault orientations, and rupture complexities, *J. Geophys. Res., 99,* 711–728, 1994.

Weaver, C.S., and G.E. Baker, Geometry of the Juan de Fuca plate beneath Washington and northern Oregon from seismicity, *Bull. Seismol. Soc. Am., 78,* 264–275, 1988.

Wilson, D.S., A kinematic model for the Gorda deformation zone as a diffuse southern boundary of the Juan de Fuca plate, *J. Geophys. Res., 91,* 10,259–10,269, 1986.

Wilson, D.S., Deformation of the So-Called Gorda Plate, *J. Geophys. Res., 94,* 3065–3075, 1989.

Wilson, D.S., Confidence intervals for motion and deformation of the Juan de Fuca plate, *J. Geophys. Res., 98,* 16,053–16,071, 1993.

Yeats, R.S., Active faults related to folding, in *Active Tectonics,* edited by R.E. Wallace, pp. 63–79,Washington, DC, National Academy Press, 1986.

Cascadia microplate models and within-slab earthquakes

Ray E. Wells[1], Richard J. Blakely[1] and Craig S. Weaver[2]
1 United States Geological Survey, 345 Middlefield Road, Menlo Park, California, 94025, USA
2 United States Geological Survey at University of Washington, Box 351650, Seattle, Washington, 98195, USA
rwells@usgs.gov, blakely@usgs.gov, craig@geophys.washington.edu

Introduction

Intermediate-depth earthquakes (30–90 km) in young, warm slabs like the subducting Juan de Fuca plate may in part be controlled by dehydration reactions and phase changes, which in turn are a function of the age of the plate and convergence rate [*Kirby et al.*, 1996]. Because the Cascadia convergent margin is caught in the dextral shear couple between the much larger Pacific and North American plates, the forearc is rotating clockwise in a broad deformation zone along the plate boundary. Such motion of the forearc can affect the convergence rate and we note that within-slab earthquakes are rare beneath the rotating forearc block. We use a recent kinematic model for Cascadia forearc motion [*Wells et al.*, 1998; *Wells and Simpson*, 2001] to calculate long-term convergence rates with respect to the forearc and discuss possible controls on the distribution of earthquakes in the subducting plate.

Block model and implications for convergence

Wells et al. [1998] calculated a pole of rotation and present-day velocity field for the Cascadia forearc by assuming that paleomagnetically-determined Cenozoic tectonic rotation of the forearc [e.g., *Magill et al.*, 1982] continues today and is linked to contemporary northward migration of the Sierra Nevada block [e.g., *Pezzopane and Weldon*, 1993; *Walcott*, 1993]. In the model, the Cascadia forearc is migrating northward along the coast and breaking up into large, clockwise rotating blocks (Figure 1). Deformation occurs mostly around the margins of a large, relatively aseismic Oregon coastal block (OC), in part composed of thick, accreted oceanic seamount crust (compare Figure 1 with Figure 2b). This 400 km-long block is rotating clockwise with respect to North America about a rotation pole located in the backarc (OC–NA), and thus it rotates over the trench at Cape Blanco and creates an extensional volcanic arc on its trailing edge. Northward motion of the block breaks western Washington into smaller, seismically active blocks and compresses them against the Canadian Coast Mountains restraining bend. Arc-parallel transport of forearc blocks is calculated to be up to 8 mm/yr with respect to stable North America. Shortening appears to be concentrated in Washington, where active east–west-trending thrust faults and folds (e.g. Seattle fault) accommodate north–south shortening.

Predicted long-term block motions are consistent with global positioning system (GPS) velocities observed in the Oregon forearc when elastic deformation due to subduction is taken into account. The GPS velocity field in the forearc has largely been explained as the sum of two processes [*Kahzaradze et al.*, 1999; *Savage et al.*, 2000; *McCaffrey et al.*, 2000; *Wells and Simpson*, 2001]: 1) elastic deformation above the locked Cascadia subduction zone (also constrained independently by heat flow, seismic profiling and vertical deformation, *Hyndman and Wang*, [1995], *Flück et al.* [1997]); and 2) the paleomagnetically and geologically constrained long term clockwise rotation of an Oregon forearc microplate in response to oblique subduction, basin–range extension and Pacific–North America dextral shear [*Wells et al.*, 1998].

Rotation of the Oregon forearc significantly affects Juan de Fuca plate (JDF) convergence rates (Figure 3, Table 1). In a North America-fixed reference frame, convergence velocities are highly oblique and decrease from about 40 mm/yr off Vancouver Island to 28 mm/yr near the Mendocino triple junction (JDF-NA pole of *DeMets and Dixon*, [1999]). However, adding clockwise rotation of the Oregon forearc increases the convergence rate south of Cape Blanco (up to 35 mm/yr) and decreases it northward (down to 29 mm/yr off the mouth of the Columbia River). The northern limit of the "convergence low" is constrained by the presumed northern limit of the rigid OC block. Northwest Washington and Vancouver Island are not part of the rotating block, so faster convergence is calculated there because we assume it to be kinematically more like North America than coastal Oregon.

Although there are large uncertainties in the OC–NA pole, and convergence is quite sensitive to the pole location (compare results of *Wells et al.*, [1998]), a similar result is obtained from the well-constrained GPS-derived pole of *McCaffrey et al.* [2000]). Given these caveats, convergence rates off central and northern Oregon are about 16% lower on average, and more than 25% lower than

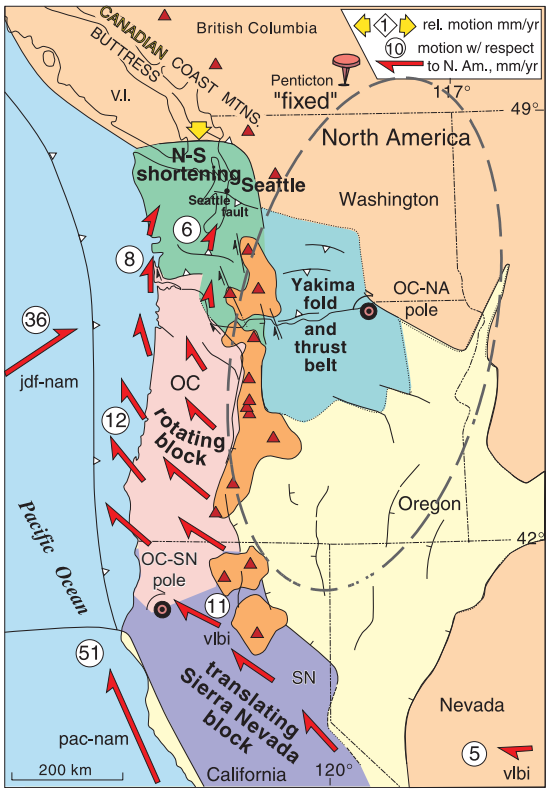

FIGURE 1: Velocity field for Oregon forearc microplate calculated from OC–NA pole (from *Wells and Simpson*, [2001], modified from *Wells et al.*, [1998]). Oregon block (OC) rotating at Neogene paleomagnetic rate is linked to Sierra Nevada (SN) block moving at vlbi rate by Euler pole (OC–SN) in Klamath Mountains. Extensional arc forms along trailing edge of Oregon forearc block which absorbs Sierra Nevada displacement by rotating over trench. North end of Oregon block deforms Washington forearc against Canadian re-entrant in the margin, causing north–south compression, uplift, thrust faulting and forearc earthquakes. Rates from very long baseline interferometry (vlbi), paleoseismology (ps), and magmatic spreading (m).

the maximum convergence along the northern and southern Cascadia subduction zone. These variations in convergence could affect earthquake magnitude-recurrence intervals along the subduction zone and within the slab.

Seismicity and volcanism

Great subduction zone earthquakes have occurred repeatedly along the plate boundary in the recent geologic past [e.g., *Atwater and Hemphill-Haley*, 1997], but the subduction zone is presently seismically quiet. Paleoseismic evidence indicates that the entire plate boundary has ruptured in the past, although geodetic evidence suggests that the width of the plate boundary locked zone may be much narrower off Oregon. The thick mafic core of the rotating Oregon block [*Tréhu et al.*, 1994] has the lowest uplift rate along the coast [*Mitchell et al.*, 1994; *Hyndman and Wang*, 1995], and the inferred narrow locked zone is entirely offshore, apparently following the western limit of the accreted Siletzia mafic terrane. Outboard of the Siletz terrane, sediments of the Eocene to Quaternary accretionary wedge and marginal basin complex comprise the geodetically and thermally defined locked zone along the plate boundary megathrust [*Hyndman and Wang*, 1995]. *McNeill et al.* [1998; 2000] and *Wells et al.* [2000] have suggested that the accretionary-marginal basin complex is subdivided by a variety of oblique, upper plate folds and faults that may in part be related to large-scale seismic segmentation of the subduction zone. The Oregon segment, which is characterized by a narrow locked zone and our calculated slower convergence rates, coincides with the region of low crustal and slab seismicity and may indicate lower strains inboard of the narrow locked zone. Slower inferred convergence rates (~30 mm/yr) in central Cascadia are still consistent with 500 year great earthquake recurrence intervals, assuming 15 m average slip per event is typical, as was calculated from the 1700 AD tsunami waveforms [*Satake and Wang*, 2000].

Contemporary seismicity in Cascadia is concentrated in western Washington, Vancouver Island and northern California (Figure 2). The crustal earthquakes and active faults outline a western Oregon region that has very low rates of seismicity and internal deformation. Although internal deformation rates are low, paleomagnetic rotation rates are high, consistent with its rotation as a large, semi-rigid block, as discussed above. Focal mechanisms in the forearc indicate north–south compression and are consistent with north–south shortening against the Canadian Coast Mountains re-entrant.

On the trailing edge of the rotating Oregon forearc block, the extensional Cascade arc accommodates some of the westward motion through magmatism and normal faulting (Figure 2). The extensional arc ends near the latitude of the calculated pole of rotation and the sparse arc volcanoes to the north rest on a folded and uplifted basement (Figure 2c). Compared to some other circum-Pacific arcs, Cascade volcanic production rates are modest [*Sherrod and Smith*, 1990]. The arc is producing two major end member primitive basalts which reflect variable input of slab volatile component and mantle sources: 1) Low potassium olivine tholeiite (LKOT), which indicates hot dry melting of depleted upper mantle; and 2) more fluid-rich calc-alkaline basalt (CAB; *Bacon et al.*, [1997]; *Conrey et al.*, [1997]). LKOT dry melts are associated with rifting and are common in the basin and range and in the extensional arc as far north as Mount St. Helens [*Conrey et al.*, 1997]. These magma types and modest volumes are consistent with subduction of a young, warm slab [*Kirby et al.*, 1996], but it is worth noting that the largest slab earthquakes occur north of Mount St. Helens and the LKOT-bearing

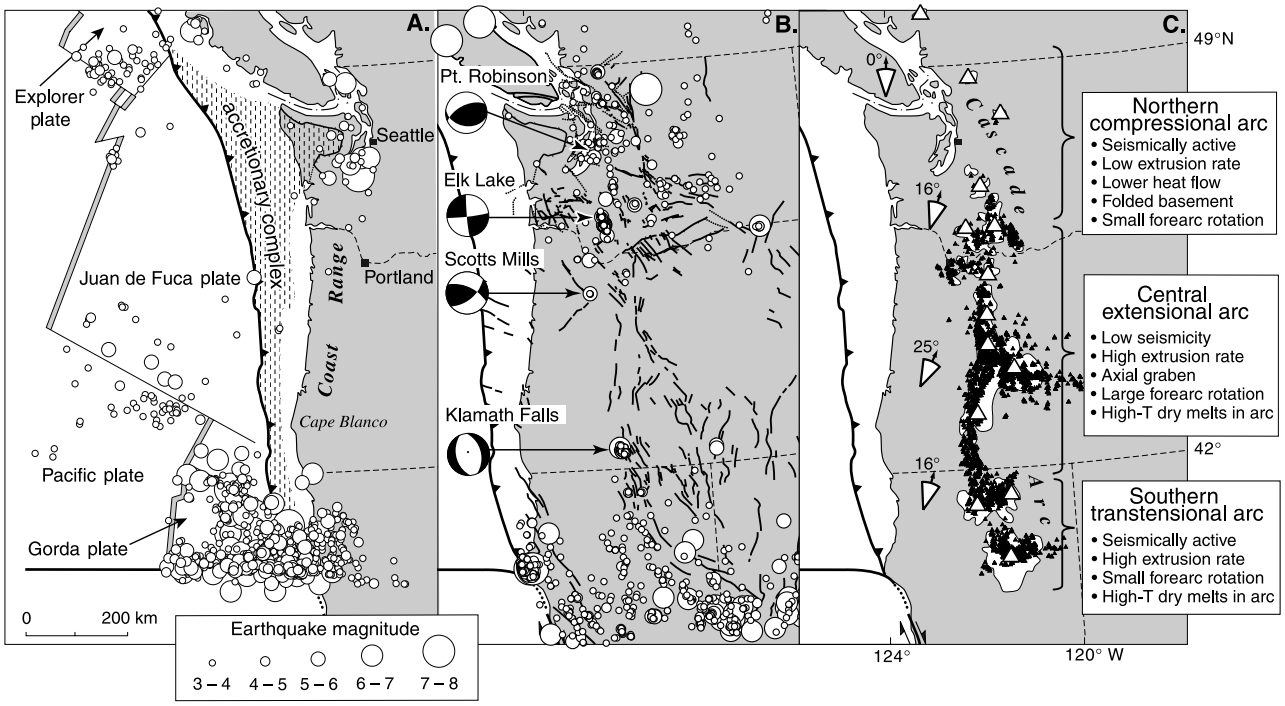

FIGURE 2: Cascadia earthquakes, faults, volcanoes and Neogene forearc rotation. A) lower plate seismicity; B) upper plate seismicity, recent focal mechanisms (M_w>5), and late Cenozoic faults; C) Quaternary arc volcanism (white), major volcanoes (open triangles), post-five Ma volcanic vents (filled triangles) and post-15 Ma forearc rotations with uncertainties (arrows).

extensional arc segment. On the other hand, the California rifted arc segment is associated with abundant Wadati–Benioff zone seismicity.

The distribution of in-slab earthquakes generally follows that of upper plate earthquakes in the forearc; they are concentrated in the Puget Lowland, are rare beneath Oregon and become most abundant in the Gorda "plate" near the Mendocino triple junction (MTJ) (Figure 2). *Kirby et al.* [1996] and *Rogers* [this volume] argue that the co-location of upper and lower plate earthquakes is the result of fluid flow into the upper plate from dehydration reactions in the subducting plate. Some of the earthquakes in the lower plate beneath Washington appear to line up along gravity gradients presumed to be caused by structures in the upper plate (Figure 4). Although slab earthquakes and those in the upper plate have similar distributions, the stress regimes for the two populations are quite different [*Ma et al.*, 1996]. Earthquakes in western Washington and in the MTJ area have *T*-axes that lie within the slab and are consistent with a slab-pull force, in addition to local stresses due to bending of the slab and transformation of basalt crust to eclogite. *Ma et al.* [1996] show that *T*-axes follow the arch in the plate beneath Puget Sound, with focal mechanisms that are consistent with bending of the arch. In general, within-slab earthquakes appear to be concentrated in areas where strain is concentrated in the bending slab and near the Mendocino and JDF/Explorer/NA triple junctions.

Why are there few in-slab earthquakes beneath Oregon? The paucity of intermediate-depth earthquakes beneath southwest Washington and western Oregon is puzzling (Figure 4). If dehydration reactions and phase changes are major constituents in triggering intermediate-depth earthquakes, one might expect earthquakes beneath Oregon as well. However, our calculated 20% southward decrease in convergence between 47° and 46°N coincides with the drop off in within-slab seismicity (Figure 4) but it is not clear if this modest decrease could affect the seismic behavior of the slab. Perhaps it is warm enough to promote greater aseismic deformation.

Alternatively, the lack of slab seismicity beneath Oregon may indicate a low stress environment in the subducting plate. One important difference between Washington and Oregon is the depth to which the subducting slab can be recognized beneath the continent. Beneath Washington, the slab can be imaged to a depth of about 500 km by teleseismic methods, but no deep slab under Oregon is recognizable below about 150 km [*Rasmussen and Humphreys*, 1989]. If no deep slab exists beneath Oregon, then resulting slab-pull forces would be low. Lower slab-pull, coupled with lower forces along the narrow locked zone offshore, may produce lower stresses in the Juan de Fuca plate beneath the Oregon

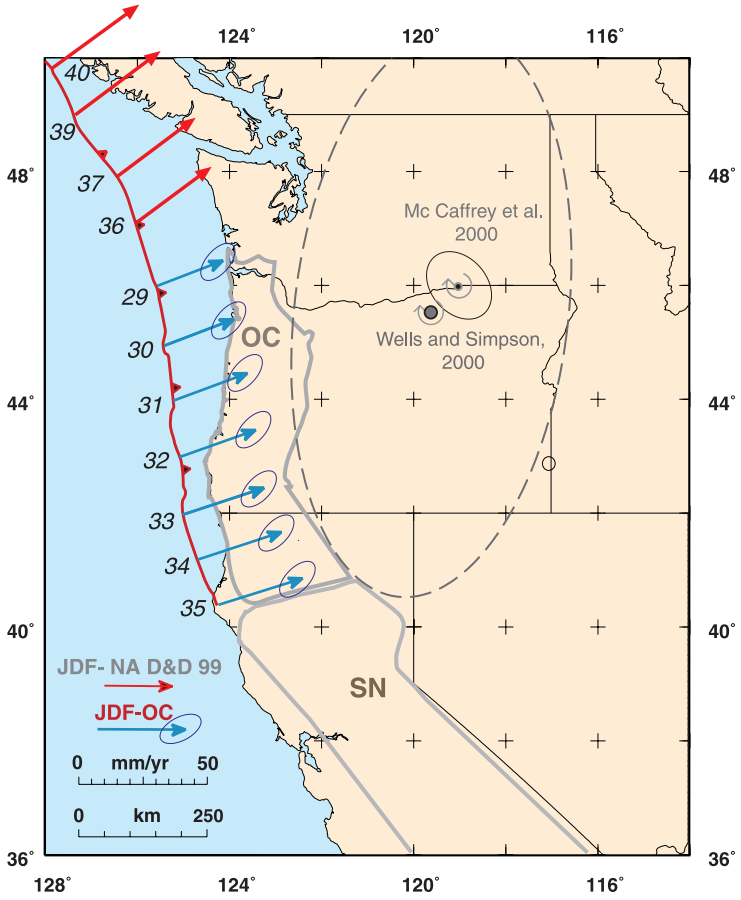

FIGURE 3: Cascadia convergence velocities with respect to the forearc. North of 47°N, calculated from the JDF–NA pole of *DeMets and Dixon* [1999]; south of 47°N, from the JDF–OC pole of *Wells and Simpson* [2001]. Note that convergence rate is low offshore of Oregon.

TABLE 1: Convergence velocities of the Juan de Fuca plate (JDF) with respect to North America (NA) and Oregon Coastal block (OC).

Site (Lat ° N/Lon ° W)	JDF-NA (DD99) Az ° E	JDF-NA (DD99) rate mm/yr	JDF-OC (WS00) Az ° E	JDF-OC (WS00) rate mm/yr
40/125			72.7	**35.0**
41/125	45.6	28.7	72.1	**34.0**
42/125	47.6	29.8	71.6	**33.0**
43/125	49.4	30.9	71.0	**32.0**
44/125	51.1	32	70.3	**31.0**
45/125	52.7	33.1	69.6	**29.9**
46/125.5	52.1	34.9	69.2	**28.8**
47/126	53.5	**36**	68.7	27.6
48/126	54.8	**37.2**	67.9	26.6
49/127	54.2	**38.9**	67.7	25.2
50/127	53.5	**40.5**	66.7	24.2

Note: DD 99 is pole of DeMets and Dixon (1999); WS00 is pole of Wells and Simpson, [2001]; bold rates are used in this paper.

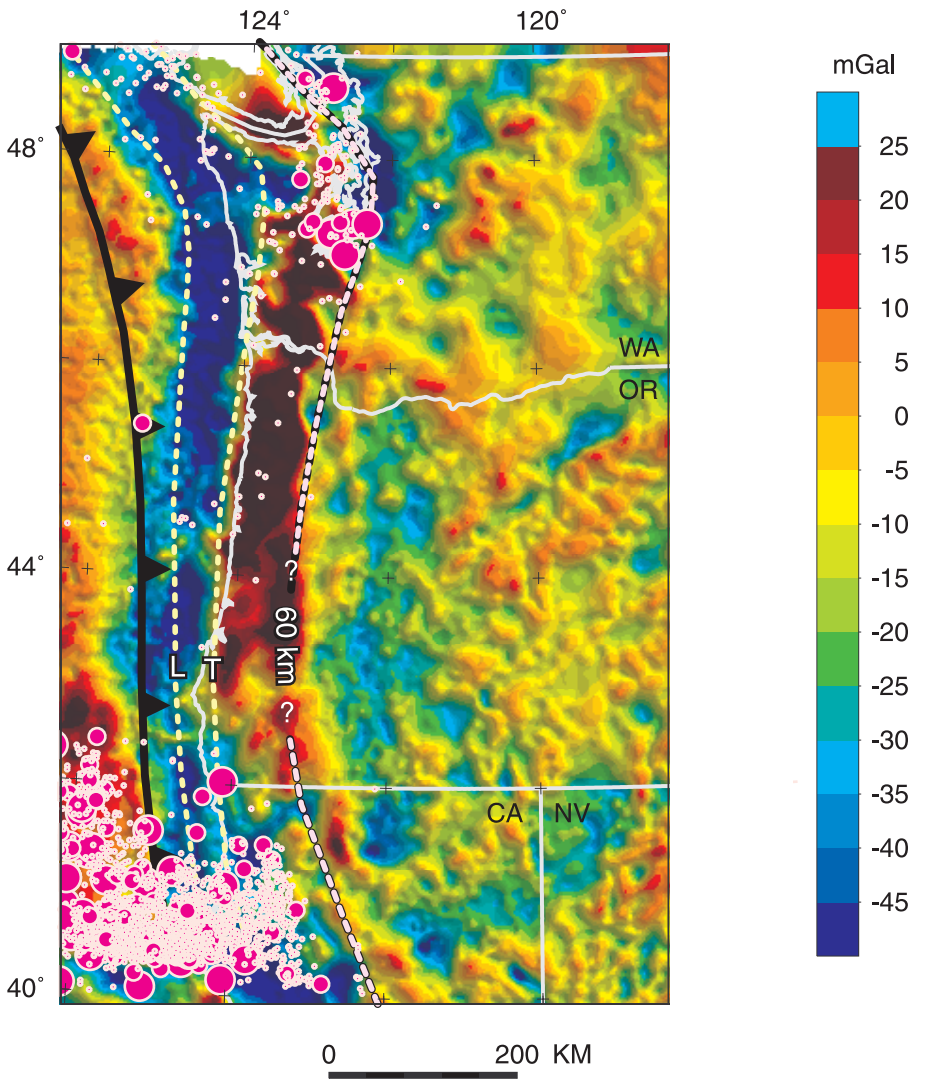

FIGURE 4: Earthquakes within the Juan de Fuca plate (*M* ≥ 2; *Yelin et al.,* [1994]*, Weaver and Meagher*, unpub compilation) plotted on isostatic residual gravity [*Blakely and Jachens*, 1990], along with downdip limit of locked zone and transition zone (450°C) from *Oleskevich et al*. [1999]. Sixty km depth contour on Wadati–Benioff zone seismicity modified from *Ludwin* (http://www.geophys.washington.edu/SEIS/PNSN/INFO_GENERAL/platecontours.html) and *Shedlock and Weaver* [1991], and including the most recent *M*=2.6 slab earthquake 63 km beneath Salem, Oregon (http://www.geophys.washington.edu/SEIS/EQ_Special/WEBDIR_00123001530o/welcome.html).

forearc and thus few within-slab earthquakes. If the deep slab is missing beneath Oregon, it implies a condition that may have existed for a considerable period of time. Long-term variations in slab-pull and within-slab seismicity along strike may have implications for deformation history in the forearc that could be explored and tested. If subsidence of the Puget–Willamette lowland is related to phase changes and geometry of the slab at depth, then variations in subsidence history along strike could be used to infer the long-term distribution of slab earthquakes [*Rogers*, this volume; *Engebretson and Kirby*, 1995]. The number of within-slab earthquakes and thickness of post-mid Miocene Puget–Willamette basin fill both decrease southward from Puget Sound [*Yeats et al.*, 1996] and terminate at Eugene. This is approximately at the same latitude as the northward termination of the basin and range and suggests a possible long-term relationship between back arc extension, the rotating forearc and the lack of slab seismicity beneath Oregon.

Summary

Within-slab earthquakes in Cascadia are generally consistent with tectonic stresses expected from slab-pull, basalt–eclogite phase changes, triple junction deforma-

tion and slab bending beneath the Olympic arch. The lack of within-slab earthquakes beneath Oregon coincides with the rotating Oregon forearc, which is inferred to reduce the subduction rate offshore by 15–25%. This may advance dehydration rea ctions and reduce slab seismicity, although the lack of slab-pull beneath Oregon is also a possible cause. Dehydration reactions and phase changes may be important constituents in causing intermediate-depth earthquakes, but the overall pattern of within-slab earthquakes in Cascadia suggests that tectonic stresses may also be a necessary condition of their occurrence. Additional work is needed to addresss the possible relationship between lowland physiography, within-slab earthquakes, rotation of western Oregon and the inferred lack of a deep slab beneath Oregon.

References

Atwater, B.F., and E. Hemphill-Haley, *Recurrence Intervals for Great Earthquakes of the Past 3,500 Years at Northeastern Willapa Bay, Washington*, 108 pp., United States Geological Survey Professional Paper P 1576, 1997.

Bacon, C.R., P.E. Bruggman, R.L. Christiansen, M.A. Clynne, J. Donnely-Nolan, and W. Hildreth, Primitive magmas at five Cascade volcanic fields: melts from hot, heterogeneous sub-arc mantle, *Canadian Mineralogist*, *35*, 397–424, 1997.

Blakely, R.J., and R.C. Jachens, Volcanism, isostatic residual gravity and regional tectonic setting of the Cascade volcanic province, *J. Geophys. Res.*, *95*, 19,439–19,451, 1990.

Conrey, R.M., D.R. Sherrod, P.R. Hooper, and D.A Swanson, Diverse primitive magmas in the Cascade arc: northern Oregon and southern Washington, *Canadian Mineralogist*, *35*, 367–396, 1997.

DeMets, C., and T.H. Dixon, New kinematic models for Pacific–North America motion from 3 Ma to present, I: Evidence for steady motion and biases in the NUVEL-1A model, *Geophys. Res. Lett., 26*, 1921–1924, 1999.

Engebretson, D.C., and S.H. Kirby, Localized intraslab earthquakes and associated forearc basin subsidence in the Juan de Fuca subduction zone: subsidence mechanisms and earthquake hazard implications, *EOS Supplement Fall Abstracts*, p. 85, 1995.

Flück, P., R.D. Hyndman, and K. Wang, Three-dimensional dislocation model for great earthquakes of the Cascadia subduction zone, *J. Geophys. Res.*, *102*, 20,539–20,550, 1997.

Hyndman, R.D., and K. Wang, The rupture zone of Cascadia great earthquakes from current deformation and the thermal regime, *J. Geophys. Res., 100*, 22,133–22,154, 1995.

Kirby, S.H., E.R. Engdahl, and R. Denlinger, Intermediate-depth intraslab earthquakes and arc volcanism as physical expressions of crustal and uppermost mantle metamorphism in subducting slabs, in *Subduction: Top to Bottom, Geophysical Monograph 96*, edited by G. Bebout, D. Scholl, S. Kirby and J. Platt, pp.195–214, American Geophysical Union, Washington, D.C., 1996.

Khazaradze, G., A. Qamar, and H. Dragert, Tectonic deformation in western Washington from continuous GPS measurements, *Geophys. Res. Lett.*, *26*, 3153–3156, 1999.

Ma, L., R. Crosson, and R. Ludwin, Western Washington focal mechanisms and their relationship to regional tectonic stress, in *United States Geological Survey Professional Paper 1560*, pp. 257–284, 1996.

Magill, J.R., R.E. Wells, R.W. Simpson, and A.V. Cox, Post-12 m.y. rotation of southwest Washington, *J. Geophys. Res.*, *87*, 3761–3776, 1982.

McCaffrey, R., M.D. Long, C. Goldfinger, P.C. Zwick, J.L. Nabelek, C.K. Johnson, and C. Smith, Rotation and plate locking along the southern Cascadia subduction zone, *Geophys. Res. Lett., 27*, 3117–3120, 2000.

McNeill, L.C., C. Goldfinger, R.S. Yeats, and L.D. Kulm, The effects of upper plate deformation on records of prehistoric Cascadia subduction zone earthquakes in *Coastal Tectonics, Geological Society of London Special Publication 146*, edited by Stewart and Vita-Finzi, pp. 321–342, 1998.

McNeill, L.C., C. Goldfinger, L.D. Kulm, R.S. Yeats, Tectonics of the Neogene Cascadia forearc basin: investigations of a deformed late Miocene unconformity, *Geol. Soc. Amer. Bull.*, *112*, 1209–1224, 2000.

Mitchell, C.E., P. Vincent, R.J. Weldon II, and M.A Richards, Present-day vertical deformation of the Cascadia margin, Pacific Northwest, *J. Geophys. Res., 99*, 12,257–12,277, 1994.

Oleskevich, D.A., R.D. Hyndman, and K. Wang, The updip and down-dip limits to great subduction earthquakes: thermal and structural models of Cascadia, south Alaska, Southwest Japan and Chile, *J. Geophys. Res., 104*, 14,965–14,992, 1999.

Pezzopane, S.K., R.J. Weldon II, Tectonic role of active faulting in central Oregon, *Tectonics*, *12*, 1140–1169, 1993.

Rasmussen, J. and E. Humphreys, Tomographic image of the Juan de Fuca plate beneath Washington and Western Oregon using teleseismic *P*-wave travel times, *Geophys. Res. Lett., 15*, 1417–1420, 1989.

Rogers, C., The role of phase changes in the development of forearc basins, in *The Cascadia Subduction Zone and Related Subduction Systems*, edited by S.H. Kirby, K. Wang, and S.G. Dunlop, p. 147, U.S. Geological Survey Open-File Report 02–328, Geological Survey of Canada Open File 4350, 2002.

Satake, K., and K. Wang, Co-seismic fault slip and seismic moment of the Cascadia earthquake estimated

from Japanese tsunami observations, in *Great Cascadia Earthquake Tricentennial, Summary and Abstracts, Oregon Dept. of Geology and Mineral Industries Special Paper 33*, pp. 110–111, 2000.

Savage, J.C., J.L. Svarc, W.H. Prescott, and M.H. Murray, Deformation across the forearc of the Cascadia subduction zone at Cape Blanco, Oregon, *J. Geophys. Res., 105*, 3095–3102, 2000.

Shedlock, K.M., and C.S. Weaver, C. S., *Program for earthquake hazards assessment in the Pacific Northwest*, 29 pp., U. S. Geological Survey Circular Report C1067, 1991.

Sherrod, D.R., and J.G. Smith, Quaternary extrusion rates of the Cascade Range, northwestern United States and southern British Columbia, *J. Geophys. Res., 95*, 19,465–19,474, 1990.

Trehu, A.M., I. Asudeh, T.M. Brocher, J. Leutgert, W.D. Mooney, J.N. Nabelekand, and Y. Nakamura, Crustal architecture of the Cascadia fore arc, *Science, 265*, 237–243, 1994.

Walcott, D., Neogene kinematics of western North America, *Tectonics*, *12*, 326–333, 1993.

Wells, R.E., C.S. Weaver, and R.J. Blakely, Forearc migration in Cascadia and its neotectonic significance, *Geology, 26*, 759–762, 1998.

Wells, R.E. and R.W. Simpson, Microplate motion of the Cascadia forearc and implications for subduction deformation, *Earth, Planets, Space*, *53*, 275–283, 2001.

Wells, R.E., R.J. Blakely, and Y. Sugiyama, Forearc basins and co-seismic slip in great subduction zone earthquakes, *Supplement to EOS, Transactions of the American Geophysical Union, 81*, p. 907, 2000.

Yeats, R.S., E.P. Graven, K.S. Werner, C. Goldfinger, and T.A. Popowski, Tectonics of the Willamette Valley, Oregon, in *United States Geological Survey Professional Paper 1560*, pp. 183–222, 1996.

Yelin, T.S., A.C. Tarr, J.A. Michael, and C.S. Weaver, *Washington and Oregon earthquake history and hazards*, 11 pp., U. S. Geological Survey Open-File Report 94–226B, 1994.

Geometry of the subducting Juan de Fuca plate: New constraints from SHIPS98

Anne M. Tréhu[1], Tom M. Brocher[2], Kenneth C. Creager[3], Mike A. Fisher[2], Leiph A. Preston[3], George Spence[4] and the SHIPS98 Working Group

1 College of Oceanic and Atmospheric Sciences, Oregon State University, Corvallis, Oregon, 97331–5503, USA
2 United States Geological Survey, 345 Middlefield Road, Menlo Park, Caifornia, 94025, USA
3 Earth and Space Sciences, Box 351650, University of Washington, Seattle, Washington, 98195, USA
4 Earth and Ocean Sciences, University of Victoria, PO Box 3055, Victoria, British Columbia, V8W 3P6, Canada
trehu@oce.orst.edu, brocher@usgs.gov, kcc@geophys.washington.edu, mfisher@usgs.gov, prestola@u.washington.edu, gspence@uvic.ca

ABSTRACT

We have processed seismic reflection profiles acquired in the Strait of Juan de Fuca, inverted travel times of first arrivals from onshore recordings of the offshore shots to determine the velocity of the upper crust in this region and inverted the travel times of first and secondary arrivals that undershoot the central core of the Olympic Mountains. The seismic reflection profiles show a pattern of crustal reflectivity similar to that recorded beneath Vancouver Island. Inversion of first arrivals, interpreted to be diving waves through the upper and mid-crust indicate a 5–7 km-deep linear, northwest-trending basin beneath the southwestern shore of the Strait and uplift of the basement Crescent terrane rocks beneath the northwestern shore. Velocities beneath the central Olympic Peninsula at 15–25 km depth show strong lateral variation, with higher velocities underlying the surface exposures of the Crescent terrane and lower velocities at these depths beneath the Olympic core rocks. Inversion of secondary seismic arrivals interpreted to be reflections from the base of the crust of the subducted Juan de Fuca plate indicate that the Moho is at a depth of about 34 km beneath the western Strait of Juan de Fuca and dips about 7° to the east, reaching a depth of about 46 km beneath the eastern boundary of Olympic National Park. Correlating these results with results of previous experiments on Vancouver Island and in southwestern Washington confirm earlier interpretations of an arch in the subducted slab beneath the Olympic peninsula but indicate that the arch is asymmetric and less pronounced than previously thought. We attribute both the northwest-trending folding of the Crescent terrane and the asymmetry in the shape of the subducting slab to resistance to the northward motion of the Paleocene-age Cascadia forearc terrane by the thick lithosphere of the pre-Tertiary terranes of British Columbia.

Introduction

In March 1998, as part of the USGS-sponsored SHIPS (Seismic Hazards Investigations of Puget Sound) project [*Fisher et al.*, 1999; *Brocher et al.*, 1999], the R/V Thompson towed a 2.4 km-long, 96 channel digital seismic streamer and a 13 gun, 79.3 liter (4838 in^3) airgun array through the waterways of the Puget Basin, Strait of Juan de Fuca and Strait of Georgia (Figure 1). During the early part of the survey (lines 1–4), before deploying the streamer, it was able to fire a 16 airgun, 110.3 liter (6730 in^3) array at a 40 second interval. The airgun shots were also recorded on 273 REFTEK seismometers (Figure 1) and on 15 ocean-bottom seismometers. Because they were far from sources of cultural noise, many stations on the Olympic Peninsula recorded clear direct arrivals (Pg) and secondary arrivals interpreted to be reflections from the base of the crust of the Juan de Fuca plate (PmP) from shots in the Strait of Juan de Fuca, Puget Sound and the Hood Canal (Figure 2). Using these data, we have developed a preliminary model for the shape of the subducting plate beneath the Olympic Peninsula and for the overlying crust beneath the Strait of Juan de Fuca and Olympic core.

Multi-channel seismic data

The multi-channel seismic data from line 7 (labeled JDF1 and JDF2 in Figure 1) were processed through brute stack stage (i.e. the data were edited to remove bad traces, sorted, band pass filtered and stacked using a simple velocity function). The primary objective of this analysis was to determine the pattern of lower crustal reflectivity. Because of the relatively low frequency of arrivals from the lower crust and the insensitivity of these deep arrivals to velocity for the limited aperture of the streamer, this simple analysis is adequate to meet our primary objective of imaging lower crustal reflectivity. More detailed

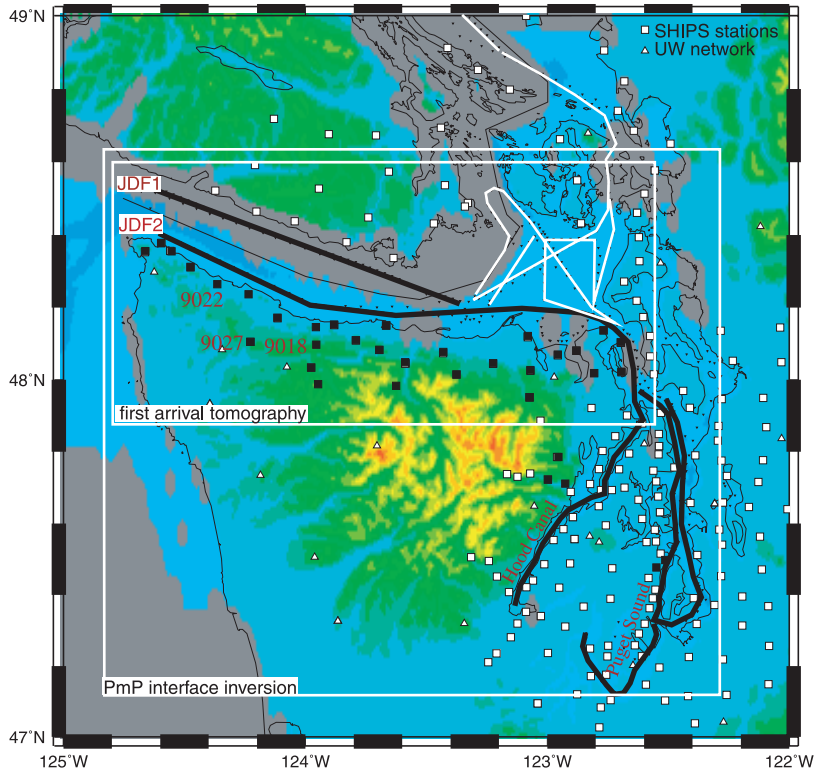

FIGURE 1: Topographic map of the Olympic Peninsula and Puget Basin showing the locations of mulit-channel seismic profiles (lines), temporary REFTEK seismometers (squares) and University of Washington network stations (triangles). Lines and REFTEKs used to date in our analysis are shown in black. The boxes show the regions included in the first arrival and wide-angle tomography presented here. These regions overlap and complement analyses done by other participants in SHIPS. Stations for which data are shown in Figure 2 are labeled.

velocity and static analysis is needed to determine shallow crustal structure. The results of the brute stack for JDF1 are shown in Figure 3a. On both profiles, a subhorizontal, two-second wide band of high reflectivity is observed at a two-way travel time of 7–9 seconds beneath the Strait west of ~123.6°W. Adopting the LITHOPROBE terminology, these reflections are labeled "E" in Figure 3. Beneath this band of reflections, a second reflection is intermittently observed, corresponding to the LITHOPROBE "F" reflection (Figure 3b). East of 123.6°W, the "E" reflections dip east. The wide-angle analysis discussed below indicates that the "F" reflection comes from a boundary 3–6 km above the Moho of the subducted Juan de Fuca plate crust. This boundary may be the top of the subducted oceanic crust, as previously interpreted for the LITHOPROBE data [*Hyndman et al.*, 1990]. The geologic nature of the "E" reflection zone remains controversial [*Calvert*, 1996].

Onshore/offshore REFTEK/airgun data

To image the geometry of the subducted plate beneath the core of the Olympic Mountains, we first correct the travel time observations for effects of upper crustal structure beneath Puget Sound, the Hood Canal and the Strait of Juan de Fuca by replacing the upper ten km beneath each shot by material with a velocity of 5.5 km/s. We then invert the corrected data for the three-dimensional velocity structure and Moho position beneath the Olympic Peninsula. This two-step approach permits us to use a small grid spacing to model the large effects on observed travel time of shallow basin structure and a relatively sparse grid to model the velocity and Moho structure beneath the Olympic Peninsula. The corrections in step 1 are based on a three-dimensional model for Puget Sound from *Brocher et al.* [2001] and our new model, presented below, for the Strait of Juan de Fuca.

Inversion of first arrivals for velocity structure beneath the Strait of Juan de Fuca

First arrivals from shots on line 4 (coincident with line 7, but shot with a larger volume airgun) recorded on stations deployed along the northern Olympic Peninsula were inverted to obtain velocities in a volume with one kilometer grid spacing using code developed by John Hole [*Hole*, 1992]. Several horizontal slices through the resulting model are shown in Figure 4. Only model cells constrained by data are shown. The starting model was a one-dimensional model with velocity increasing with

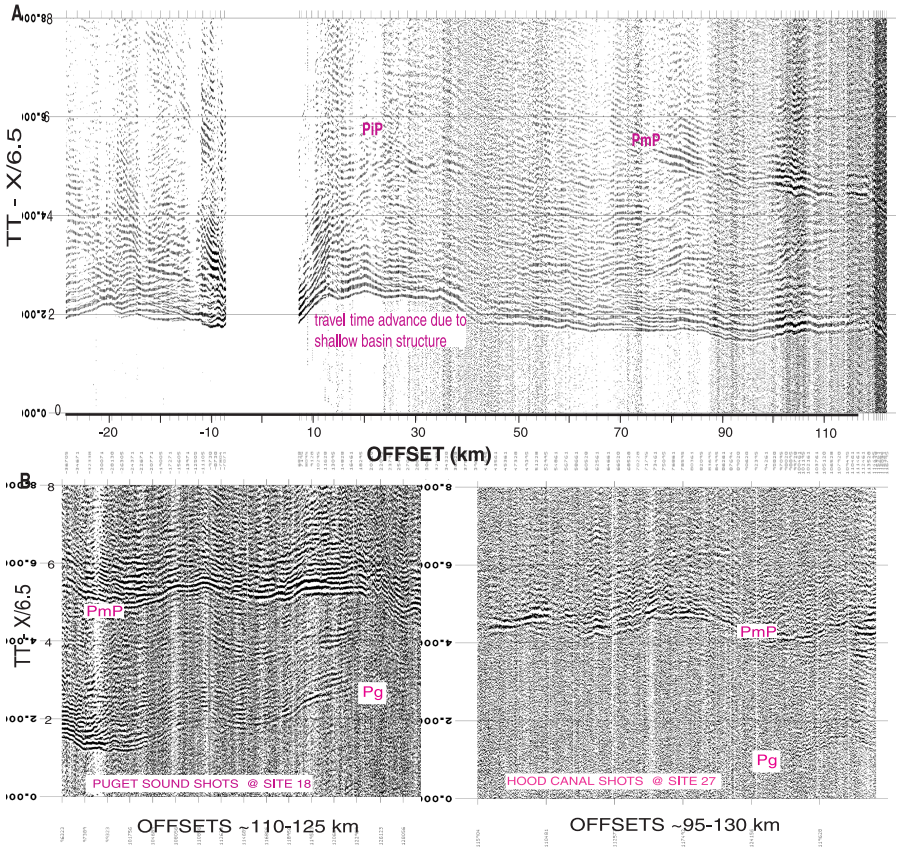

FIGURE 2: A) Data from JDF2 recorded at station 9022. Note wide-angle reflection interpreted as PmP, shallow reflections at nearer offset (PiP) and a 0.5 second travel time delay due to the Clallum basin. B) Examples of record sections recorded on the northern Olympic Peninsula from shots in Puget Sound and the Hood Canal. Note the strong amplitude of secondary arrivals. Comparison of the travel time and offset of these arrivals with the arrival interpreted as PmP in Figure A suggests that these are also PmP.

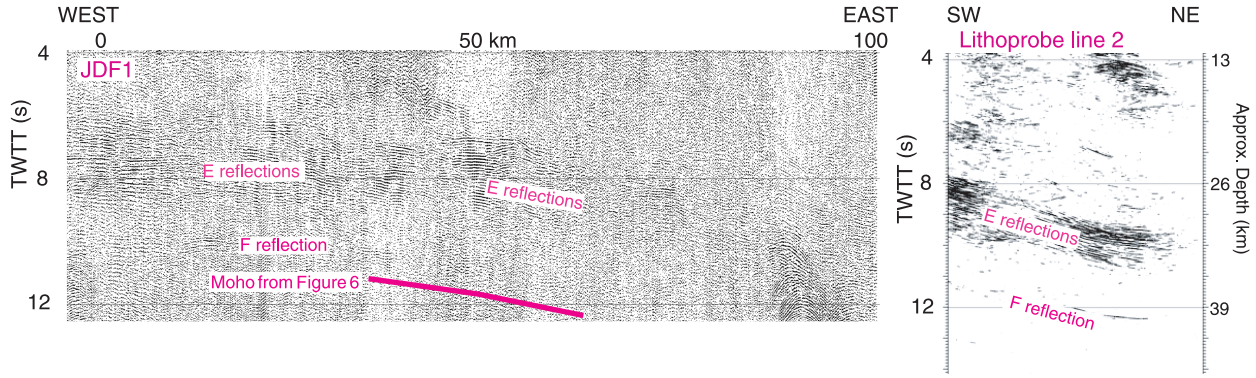

FIGURE 3: Multi-channel seismic line JDF1 and LITHOPROBE line 2. "E" and "F" reflections on JDF1 are interpreted to be the same as the similarly named events in the LITHOPROBE data. The location of LITHOPROBE line 2 is shown in Figure 7 (LP2). Figure is from the on-line LITHOPROBE atlas (http://www.litho.ucalgary.ca/atlas/atlas.html). Velocity modeling suggests that 6.5 is a reasonable velocity for converting two-way travel time to depth. Correlation with the Moho depths shown in Figure 6 suggests that the "F" reflection is ~6 kilometers above Moho, suggesting that it is the top of the crust of the subducting plate and probably the plate boundary.

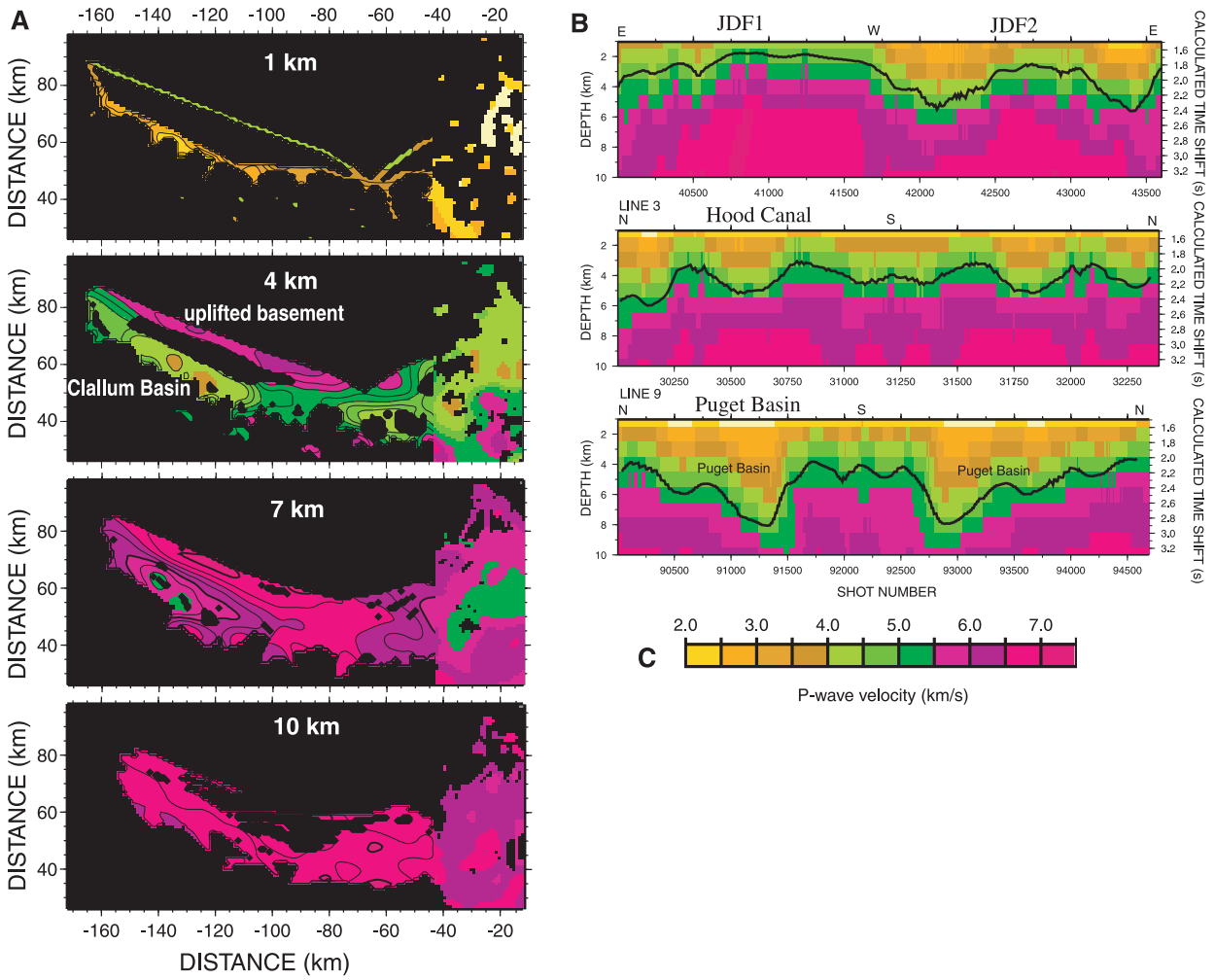

FIGURE 4: A) Three-dimensional inversion of first arrivals from shots in the Strait of Juan de Fuca recorded on stations along the northern Olympic Peninsula. *Rms* travel time misfit of the initial one-dimensional velocity model was 0.49 seconds; misfit was decreased to 0.08 seconds after 11 iterations. B) Velocity in the upper ten km along each line of shots used in the three-dimensional Olympic Peninsula lower crust and PmP inversions. For the Strait of Juan de Fuca, the model of 4a was used. For the Hood Canal and Puget Sound, the model of *Brocher et al.* [2001] was used. The vertical travel time beneath each shot to a depth of ten km is also shown. C) Velocity scale for 4a and 4b.

depth and a root-mean-squared (*rms*) misfit between observed and calculated travel times of 0.56 seconds. The model converged smoothly in 11 iterations to a model with an *rms* misfit of 0.08 seconds, similar to the picking uncertainty. Tests with several significantly different initial models indicated that the final model is not sensitive to the starting model. Because of the high velocities at relatively shallow depth, few rays penetrate beneath 15-km depth, even with offsets as great as 110 km.

East of km 40, the model of *Brocher et al.* [2001] has been "patched" into our model because it includes data from shots along short profiles in the eastern Strait of Juan de Fuca (Figure 1). The good match between the two models where they overlap validates the SHIPS working group approach of having various groups working on different subsets of the data to address specific scientific problems. Eventually, all data will be merged to generate a regional "super-model". Figure 4b shows the vertical velocity in the upper ten km beneath each shot for the Strait of Juan de Fuca (line 4), Hood Canal (line 3) and Puget Sound (line 9), and the corresponding vertical travel time through the model. These times were used to correct the observed travel times to replace the upper ten km beneath the shots with material with a constant velocity of 5.5 km/s.

Low velocities in the upper crust along JDF2 west of km 100 indicate the presence of a linear, northwest-trending basin that is not present beneath the northern line. This basin is known as the Clallam basin where it extends on land on the Olympic Peninsula. We interpret

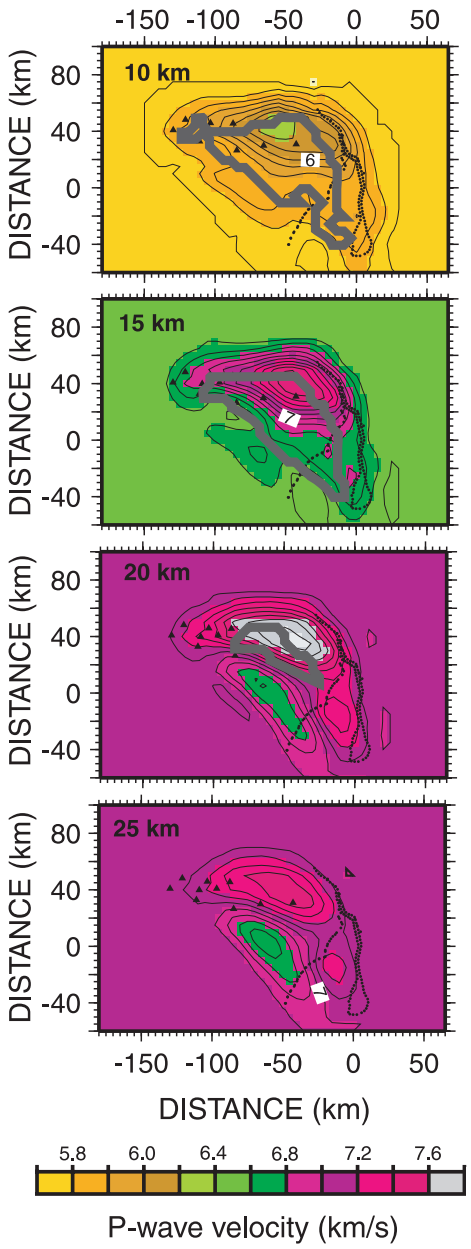

FIGURE 5: Inversion of first arrivals from shots in the Hood Canal and Puget Sound (small black dots) recorded at sites along the northern Olympic Peninsula (black triangles). Initial model had velocity 5.5 km/s from -5 to 10 km depth, 6.5 km/s at 15 km, and 7.0 km/s for depth >20 km. The model converged after nine iterations. *Rms* travel time misfit of the initial model was 1.04 seconds, decreasing to 0.16 seconds for the model shown here. Contours are shown at 0.1 km/s intervals. Velocities in each layer are only constrained within the thick gray line. Note the pronounced lateral contrast in velocity at 15 and 20 km depth, where velocities beneath the Crescent terrane are 1 km/s greater than those beneath the Olympic core. This is consistent with the anomaly at this depth obtained by *Crosson et al.* [2002] using earthquake data and a different subset of the SHIPS data. With the smoothing parameters used for this inversion, the anomaly extends to 30 km, beneath which the velocity is constant at 7.0 km/s.

this basin to be the result of warping of the Siletz/Crescent terrane along a west–northwest-trending axis, perhaps in response to compression generated by northward migration of the Tertiary forearc relative to the pre-Tertiary terranes of southwestern Canada. The basin beneath the eastern Strait of Juan de Fuca, known as the Port Townsend basin, is discussed by *Brocher et al.* [2001].

Inversion of first arrivals for mid-crustal velocity structure beneath the Olympics

Because the first arrivals recorded from shots in the Hood Canal and Puget Sound, corrected for the model of Figure 4, show clear evidence for additional lateral variation in velocity structure, we inverted these arrivals for the velocity structure of the mid-crust beneath the Olympic Mountains using a five kilometer grid within the box outlined in Figure 1 for the PmP inversion. The results are shown in Figure 5. The 1 km/s lateral variation in velocity at mid-crustal depth is similar to that obtained by *Crosson et al.* [this volume] at this depth in a more comprehensive regional model based on earthquake and SHIPS data (but not yet including the source/receiver pairs used here). Because it is based on data from the same shot/receiver pairs for which PmP arrivals that undershoot the Olympics were observed, the model of Figure 5 provides a useful starting model for the Moho interface inversion while waiting until the final "master model" incorporating all SHIPS is complete. The effect of ignoring this mid-crustal lateral velocity variation is discussed below.

Inversion of PmP wide-angle reflection times for Moho depth beneath the Olympics

Figure 6 shows our working three-dimensional model for the Moho of the subducting Juan de Fuca plate, determined using the interface inversion technique of *Zelt et al.* [1996] as provided by J. Hole. Reflection times were calculated by ray tracing through the model of Figure 5 after application of the correction for shallow structure discussed above.

The model indicates that the Moho is at 34–36 km depth beneath the western Strait of Juan de Fuca, dipping ~7° to the east–southeast. Because the "F" reflection on lines JDF1 and JDF2 falls at a depth of ~30 km, this result supports the LITHOPROBE interpretation that the "F" reflection is not the Moho and may be the top of the subducted ocean crust (and probably the plate boundary). The apparent east–southeast dip of the Moho is not inconsistent with the apparently sub-horizontal "E" and "F" reflections beneath the western Strait of Juan de Fuca since the portion of the subducted plate imaged by the common-midpoint data and that imaged by the PmP wide-angle reflections are not coincident. Moreover, the LITHOPROBE data indicate that the "F" reflection generally dips somewhat more steeply than the better-de-

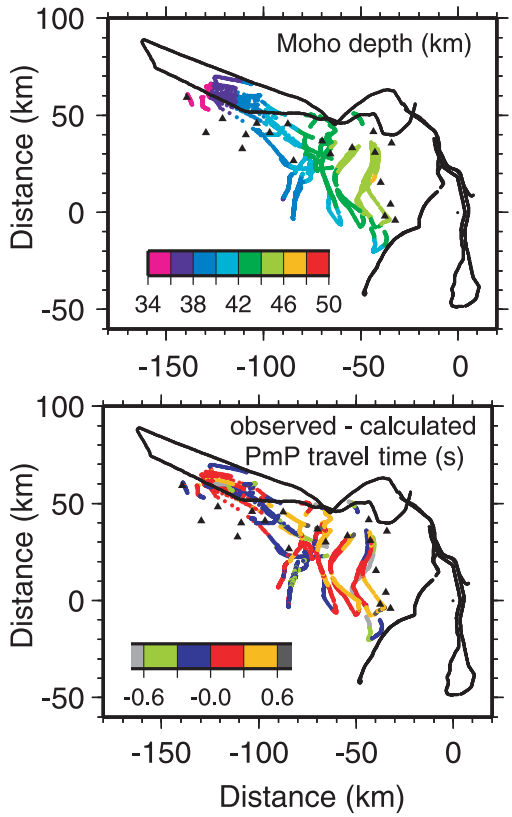

FIGURE 6: Inversion of PmP arrival times to determine the depth to the Moho of the subducted Juan de Fuca plate. Travel times, corrected as described in Figure 4, were calculated through the velocity model of Figure 5. Upper figure shows the depth to Moho after five iterations. *Rms* travel time misfit is 0.30 seconds, compared to an *rms* travel time misfit of 0.86 seconds for the initial model, which was a horizontal surface at 45 kilometers depth. Lower panel shows the observed/calculated travel times. Positive and negative residuals are distributed over the entire surface.

fined "E" reflection. Our model for the depth and dip of Moho is also generally consistent with the model of *Creager et al.* [this volume] derived using a different modeling approach and a different subset of the data.

The shape of the Moho obtained via inversion of PmP travel times is quite sensitive to the starting model. Ignoring the lateral velocity variation shown in Figure 5, and assuming a mid-crustal velocity that increases only with depth, leads to a solution that has considerable curvature and an *rms* misfit of 0.36 seconds.

The inversion results are also quite sensitive to which secondary arrivals are included in the solution. Initially, we included all secondary arrivals observed from shots in the Hood Canal into stations on the northern Olympic Peninsula. Including these arrivals, however, results in a best fit solution that also has considerable curvature and a large *rms* misfit of 0.56 seconds. Re-examination of the data indicated that some arrival time picks from shots in the Hood Canal to stations near Port Angeles were incompatible with picks from these shots to stations further west. The origin of these incompatible arrivals remains enigmatic. Unlike other SHIPS observations reported by *Creager* [2002], the travel times of these particular arrivals do not appear to be consistent with a simple planar interface parallel to and shallower than the Moho, suggesting additional, more complex lateral heterogeneity in the lower crust beneath the Olympics.

Comparison to other data

Figure 7 shows the results of the Moho model, converted to depth to the plate boundary by assuming a constant thickness of the Juan de Fuca plate crust of six kilometers and assuming that the plate boundary is at the top of the Juan de Fuca plate crust. Normalization to either the plate boundary or the base of the crust of the subducting plate is necessary for comparing reflection data (LITHOPROBE data from Vancouver Island), which are more sensitive to the former, to wide-aperture data [*Parsons et al.*, 1998; this study], which are more sensitive to the latter. Extension of the contours south of the *Parsons et al.* [1998] profile is constrained by the results of *Trehu et al.* [1994] and *Gerdom et al.* [2000]. This comparison confirms that the dip of the subducting plate is relatively shallow beneath the Olympic Peninsula. The dip of 7–8° beneath the Olympics is similar to the dip of the subducting plate beneath the continental shelf throughout the Cascadia, but significantly less than the dip of 11–15° determined beneath the Coast Ranges to the south from northern California to southwestern Washington or the dip of ~20° determined beneath Vancouver Island [e.g. *Hyndman et al.*, 1990; *Trehu et al.*, 1994; 1995; *Parsons et al.*, 1998; *Clowes*, this volume; *Gerdom et al.*, 2000. These results support earlier inferences of an arch beneath the Olympics but suggest that the arch is less pronounced than previously thought and that it is asymmetric. We speculate that both the steeper dip of the plate beneath Vancouver Island and the northwest-trending folding of the Crescent terrane beneath the Strait of Juan de Fuca may be due to the interaction between the subducting plate and the thicker, stronger lithosphere beneath the pre-Tertiary terranes of British Columbia.

Figure 7 also shows the epicenters of large, damaging lower plate earthquakes in this region, including the January, 2001 Nisqually event. All of these events appear to have hypocenters 6–8 km below the inferred plate boundary, or 0–2 km below the Moho of the subducting oceanic plate. Given uncertainties in hypocenteral parameters and in the velocity model, we cannot determine conclusively whether these events initiated in the uppermost mantle or at the base of the crust of the subducted plate. We expect that the answer to this question, which is important for understanding the physical processes causing these events, will be obtained

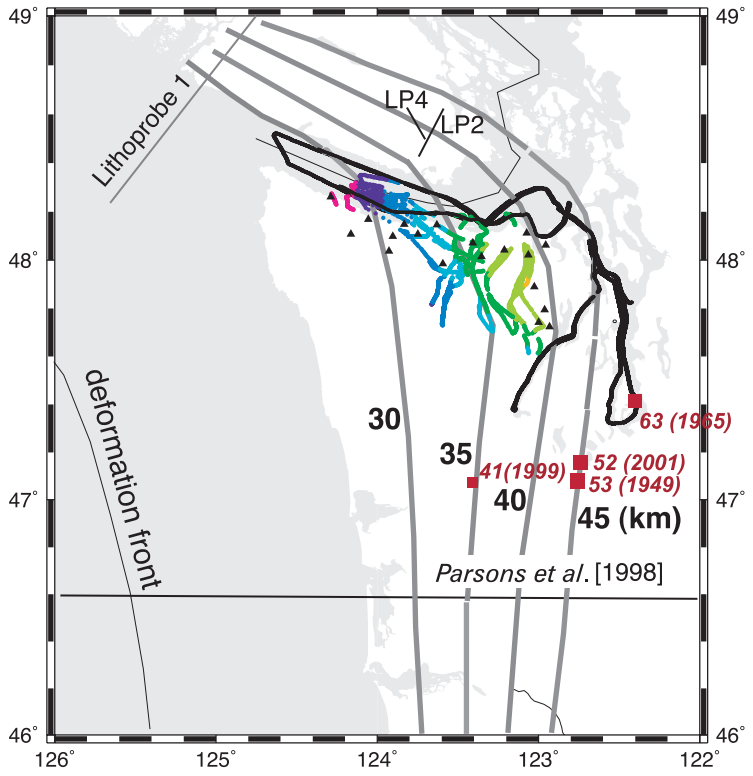

FIGURE 7: Contours of depth to the top of the subducting plate, assuming that the plate boundary is six kilometers above Moho. Contours are constrained by LITHOPROBE data in British Columbia and by the results of *Parsons et al.* [1998] and *Tréhu et al.* [1994] in southwestern Washington. The results confirm earlier reports of an arch in the subducting plate beneath the Olympic Peninsula, but suggest that the arch is asymetric. Also shown as red squares are the epicenters of historic, damaging lower plate earthquakes, including the Nisqually earthquake of January, 2001. Numbers next to the squares indicate hypocentral depth and the year of occurrence. All hypocenters are 6–8 km beneath the inferred plate boundary near the Moho of the subducting Juan de Fuca plate.

through more detailed analysis of the Nisqually event.

Acknowledgements

We thank the many individuals who helped survey station sites and deploy instruments. We also thank the many landowners that graciously offered us access to their land. This work was funded by the United States Geological Survey through grants 1434HQ98GR00041 and 99HQGR0071 to Oregon State University.

References

Brocher, T.M., and 18 others, *Wide-angle Seismic Recordings from the 1998 Seismic Hazards Investigation of Puget Sound (SHIPS), Western Washington and British Columbia*, 110 pp., U.S.Geological Survey Open-File Report 99–314, 1999.

Brocher, T.M., T. Parsons, R.J. Blakely, N.I. Christensen, M.A. Fisher, R.E. Wells, and the SHIPS working group, Upper crustal structure in the Puget lowland, Washington: results from the 1998 seismic hazards investigation in Puget Sound, *Jour. Geophys. Res.,106*, 13,541–13,564, 2001.

Calvert, A.J., Seismic reflection constraints on imbrication and underplating of the northern Cascadia convergent margin, *Canadian Jour. Of Earth Sci., 33*, 1294–1307, 1996.

Clowes, R.M., Crustal structure of northern Juan de Fuca plate and Cascadia subduction zone—new results, old data, in *The Cascadia Subduction Zone and Related Subduction Systems*, edited by S.H. Kirby, K. Wang, and S.G. Dunlop, pp. 55–58, U.S. Geological Survey Open-File Report 02–328, Geological Survey of Canada Open File 4350, 2002.

Creager, K.C., L.A. Preston, R.S. Crosson, T. Van Wagoner, A.M. Tréhu, and the SHIPS98 working group, Three-dimensional reflection image of the subducting Juan de Fuca Plate, in *The Cascadia Subduction Zone and Related Subduction Systems*, edited by S.H. Kirby, K. Wang, and S.G. Dunlop, pp. 37–42, U.S. Geological Survey Open-File Report 02–328, Geological Survey of Canada Open File 4350, 2002.

Crosson, R.S., N.P. Symons, K.C. Creager, L.A. Preston, T. Van Wagoner, T.M. Brocher, M.A. Fisher, and the SHIPS98 Working Group, Three-dimensional struc-

ture of the Cascadia forearc region from SHIPS active experiment and earthquake observations: tomographic inversion provides a high-resolution view into the core of the Cascadia forearc complex, in *The Cascadia Subduction Zone and Related Subduction Systems*, edited by S.H. Kirby, K. Wang, and S.G. Dunlop, p. 33, U.S. Geological Survey Open-File Report 02–328, Geological Survey of Canada Open File 4350, 2002.

Fisher, M.A., T.M. Brocher, R.D. Hyndman, A. M. Tréhu, C.S. Weaver, K.C. Creager, R.S. Crosson, T. Parsons, A.K. Cooper, D. Mosher, G. Spence, B.C. Zelt, P.T. Hammer, U. ten Brink, T.L. Pratt, K.C. Miller, J.R. Childs, G.R. Cochrane, S. Chopra, and R. Walia, Seismic survey probes urban earthquake hazards in Pacific Northwest, *EOS, Trans. Am. Geophys. Un., 80*, 13–17, 1999.

Gerdom, M., A.M. Tréhu, E.R. Flueh, and D. Klaeschen, The continental margin off Oregon from seismic investigations, *Tectonophysics*, *329*, 79–97, 2000.

Hole, J.S., Nonlinear, high-resolution, three-dimensional seismic travel time tomography, *J. Geophys. Res., 97*, 6553–6562, 1992.

Hyndman, R.D., C.J. Yorath, R.M. Clowes, and E.E. Davis, The northern Cascadia subduction zone at Vancouver Island: seismic structure and tectonic history, *Can. J. Earth Sci., 27*, 313–329, 1990.

Parsons, T., A.M. Tréhu, J.H. Luetgert, F. Kilbride, K. Miller, R.E. Wells, M.A. Fisher, N.I. Christensen, U. ten Brink, E. Flueh, and W.D. Mooney, A new view into the Cascadia subduction zone and volcanic arc: implications for earthquake hazards along the Washington margin, *Geology, 26*, 199–202, 1998.

Tréhu, A.M., I. Asudeh, T.M. Brocher, J. Luetgert, W.D. Mooney, J.L. Nabelek, and Y. Nakamura, Crustal architecture of the Cascadia forearc, *Science, 265*, 237–243, 1994.

Tréhu, A.M., and the Mendocino Working Group, Pulling the rug out from under California: seismic images of the Mendocino triple junction region, *EOS, Trans. Am. Geophys. Un, 76*, 369–381, 1995.

Zelt, B.C., R.M. Ellis, R.M. Clowes, and J.A. Hole, Inversion of three-dimensional wide-angle seismic data from the southwestern Canadian Cordillera, *J. Geophys. Res., 101*, 8503–8530, 1996.

Three-dimensional structure of the Cascadia forearc region from SHIPS active experiment and earthquake observations: Tomographic inversion provides a high-resolution view into the core of the Cascadia forearc complex

Robert S. Crosson[1], Neill P. Symons[2], Kenneth C. Creager[1], Leiph A. Preston[1], T. Van Wagoner[1], Thomas M. Brocher[3], Michael A. Fisher[3] and the SHIPS98 Working Group

1 Department of Earth and Space Sciences, University of Washington, Seattle, Washington, 98195–1650, USA
2 Sandia National Laboratories, Box 58000, Albuquerque, New Mexico, 87111, USA
3 United States Geological Survey, 345 Middlefield Road, Menlo Park, California, 94025, USA
crosson@u.washington.edu, npsymon@sandia.gov, kcc@geophys.washington.edu, prestola@u.washington.edu, tvan@geophys.washington.edu, brocher@andreas.wr.usgs.gov, mfisher@octopus.wr.usgs.gov

Phase I of SHIPS (Seismic Hazards in Puget Sound) was a large-scale airgun deployment in the inland waterways of western Washington State and western British Columbia. The coincidence of SHIPS travel time data in the Puget Sound region with earthquake arrival time data from the Pacific Northwest Seismograph Network has allowed us to carry out high-resolution joint active source and earthquake travel time inversion (tomography) for *P* wave velocity structure to depths of approximately 60 km over a portion of the Cascadia forearc margin. A total of about 70,000 *P* wave arrival observations were used in our initial effort; approximately 1000 earthquakes comprise 45% of the total number of *P* wave observations. Excellent constraint of the shallow structure by SHIPS data allows greatly improved resolution of the deep structure through earthquake observations, compared to inversion using earthquake data alone. The three-dimensional velocity model fits both airgun and earthquake picks to approximately 0.1 second root-mean-squared (*rms*) overall. Simple variance reduction from a best fitting one-dimensional model to our preferred three-dimensional model exceeds 90%.

After inversion, earthquake hypocenters migrate in general to slightly shallower depths relative to depths computed with a best fitting one-dimensional starting model. Increasing the average velocity of the one-dimensional model could bring the one-dimensional and three-dimensional depths into closer agreement; however, because of very significant three-dimensional effects, such a model may still not provide a satisfactory one-dimensional average earth model. Earthquakes in the Wadati–Benioff zone are moved an average of about three kilometers shallower but generally maintain the average dip of the zone (about 14°). The scatter of Wadati–Benioff zone earthquakes about a plane is also reduced by a factor of about two in standard deviation in going from one-dimensional to three-dimensional models.

Mafic Crescent/Siletz volcanic rocks form the basement of the Puget basin region with *P* wave velocity exceeding 7 km/s at 20 km depth. In the central Puget basin, Crescent/Siletz is in turn underlain at a depth of about 30 km by lenses of lower-velocity, subducted accretionary prism rocks which are gradational with rocks of the Olympic core further to the west. This suggests that the Olympic core rocks are mechanically emplaced by subduction beneath the Crescent/Siletz eastward of the Olympic Mountains, producing a local low velocity zone in the deep crust beneath the Puget basin (although in the conventional sense "crust" may be ill-defined in this region). The *P* wave velocity reversal produced by this emplacement process is typically about 0.5 km/s. The relationship between Olympic core rocks and the Crescent/Siletz terrane is consistent with models of "unroofing" of the Olympic core [e.g., *Brandon et al.*, 1998].

References

Brandon, M.T., M.K. Roden-Tice, and J.I. Garver, Late Cenozoic exhumation of the Cascadia accretionary wedge in the Olympic Mountains, northwest Washington State, *GAS Bulletin, 110*, 985–1009, 1998.

Velocity structure of western Washington from local earthquake tomography

Antonio Villaseñor, D. Stanley and Harley Benz
United States Geological Survey, MS 966, Denver Federal Center, Denver, Colorado, 80225, USA
antonio@gldvisitor.cr.usgs.gov, benz@usgs.gov

Accurate assessment of seismic hazards in Washington, especially the heavily populated Puget Sound region, requires insights into the complex crustal and upper mantle structure and associated seismicity. Numerous geophysical studies have used seismic refraction and reflection data [*Tréhu et al.*, 1995; *Johnson et al*., 1996], seismic tomography [*Michaelson and Weaver*, 1986; *Rasmussen and Humphreys*, 1988; *Bostock and VanDecar*, 1995], magnetotelluric soundings [*Stanley et al*., 1992], and gravity and magnetic modeling [*Finn*, 1990] to understand crust and upper mantle development in the Pacific Northwest due to subduction of the Juan de Fuca plate beneath the western margin of North America. The geometry of the subducting Juan de Fuca plate has been demonstrated to be complex [*Crosson and Owen*, 1987] and better definition of this geometry is a prerequisite for understanding tectonic interactions between the subducting plate and the overlying continental plate and intraslab earthquakes. The combination of an accurate three-dimensional velocity model for the crust and upper mantle beneath Washington combined with other geophysical data such as gravity, magnetic, and electromagnetic sounding data, provides new constraints on the lithology and distribution of key geologic units that control seismic energy release. In this talk, we describe new three-dimensional *P*- and *S*-wave velocity models of the crust and upper mantle beneath Washington and use the results to interpret the structural framework under which earthquakes occur in western Washington.

The three-dimensional *P*- and *S*-wave velocity models interpreted in this study were determined by inversion of local earthquake arrival time data from the Pacific Northwest Seismic Network (PNSN) earthquake catalog using a technique developed by *Benz et al*. [1996]. Travel times are calculated by extrapolation of the Eikonal equation in a finite difference grid. The three-dimensional velocity structure is determined by solving for perturbation to the velocity model using a linear inverse formulation that is solved with a large, sparse matrix solver (LSQR) with smoothing constraints. The study region is a 280 km east–west by 344 km north–south area centered on Puget Sound, which is subdivided into 8 x 8 x 2 km (2-km-vertical) constant velocity cells. In addition, the model extends from four kilometers above sea level to 80 km depth. A finer 1 x 1 x 1 km grid is used to calculate the travel times with errors less than ± 0.05 seconds. Velocities in the finer grid are determined by interpolation from the coarser inversion grid. From 36,565 earthquakes in the PNSN catalog in the time interval from 1970–1996, 3431 well-recorded events were selected for the inversion process. This resulted in 61,906 source-station pairs to 87 seismic stations in western Washington. These events also provided 16,972 *S*-wave arrival times that were inverted to obtain a three-dimensional *S*-wave velocity model using the same grid as the *P*-wave inversion.

Results show a complicated arch structure under the Olympic Peninsula and Puget Sound region, and high-velocity mafic complexes in the middle to lower crust in western Washington that appear to control the distribution of crustal seismicity. The main mafic rock unit imaged in the crust is the Eocene-age Crescent Formation, a sequence of basalt flows that forms the basement beneath much of western Washington. In addition, a deeper high-velocity section of the mid-crust under Puget Sound is interpreted as either imbricated, pre-Eocene oceanic crust, or an advancing mantle wedge that generated the Crescent Formation. The Juan de Fuca plate may be partially coupled to the overlying, rigid mafic units. Thick, low-velocity accretionary sedimentary rocks in the Olympic Peninsula contrast with the high-velocity Crescent Formation units, which form the backstop for tectonic thickening of the sedimentary rocks. Northwest-trending, strike-slip zones in the Cascades volcanic belt and step-overs between these slip zones appear to also be controlled by the geometry of the Crescent Formation. In general, relatively slow lower-crustal velocities occur beneath the Cascades, possibly due to thermal effects and/or a depleted crust.

High-resolution velocity models of the crust and subducting Juan de Fuca plate in western Washington provide detailed images of the subducting plate and several important crustal features. A previously interpreted arch in the Juan de Fuca plate has been mapped in more detail. Mafic blocks composed of Crescent Formation

and possibly an underlying section of pre-Eocene mafic rocks, stand out in the velocity model, especially in contrast to thick low-velocity sedimentary rocks in the Olympic Peninsula and in the Seattle basin. The occurrence of a thick mafic wedge above the subducting Juan de Fuca plate may control seismicity patterns in the Puget Sound region due to enhanced stress transfer through the rigid mafic rocks. Regions of high stress within the mafic rocks may be detectable with V_p/V_s ratios, although further analysis and detailed modeling is required. We interpret crustal blocks as being forced northeast around the arch in the Juan de Fuca plate. Northeast shear stresses from the subduction direction are expressed in crustal focal mechanisms in southwest Washington. The development of the velocity model has allowed us to accurately relocate most of the earthquake database for western Washington, with the result that seismicity patterns can be more completely understood.

References

Benz, H.M., B.A. Chouet, P.B. Dawson, J.C. Lahr, R.A. Page, and J.A. Hole, Three-dimensional P and S wave velocity structure of Redoubt Volcano, Alaska, *J. Geophys. Res., 101*, 8111–8128, 1996.

Bostock, M.G., and J.C. VanDecar, Upper mantle structure of the northern Cascadia subduction zone, *Can. J. Earth Sci., 32*, 1–12, 1994.

Crosson, R.S., and T.J. Owens, Slab geometry of the Cascadia subduction zone beneath Washington from earthquake hypocenters and teleseismic converted waves, *Geophys. Res. Lett., 14*, 824–827, 1987.

Finn, C., Geophysical constraints on Washington convergent margin structure, *J. Geophys. Res., 95*, B12, 19,533–19,546, 1990.

Johnson, S.Y., C.J. Potter, J.M. Armentrout, J.J. Miller, C.A. Finn, and C.S. Weaver, The southern Whidbey Island fault and active structure in the Puget lowland, Washington, *Geol. Soc. Am. Bull., 108*, 334–354, 1996.

Michaelson, C.A., and C.S. Weaver, Upper mantle-structure from teleseismic *P* arrivals in Washington and northern Oregon, *J. Geophys. Res., 91*, 2077–2094, 1986.

Rasmussen, J., and G. Humphreys, Tomographic image of the Juan de Fuca plate beneath Washington and western Oregon using teleseismic *P*-wave travel times, *Geophys. Res. Lett., 15*, 1417–1420, 1988.

Stanley, W.D., W.J. William, G. Latham, and K. Westhusing, The southern Washington Cascades conductor—a previously unrecognized thick sedimentary sequence? *Am. Assoc. Petrol. Geol. Bull., 76*, 1569–1585, 1992.

Tréhu, A.M., G. Lin, Maxwell, and C. Goldfinger, A seismic reflection profile across the Cascadia subduction zone offshore central Oregon: new constraints on methane distribution and crustal structure, *J. Geophys. Res., 100*, 15,101–15,116, 1995.

Three-dimensional reflection image of the subducting Juan de Fuca plate

Kenneth C. Creager[1], Leiph A. Preston[1], Robert S. Crosson[1], T. Van Wagoner[1], Anne M. Tréhu[2] and the SHIPS98 Working Group

1 Department of Earth and Space Sciences, University of Washington, Seattle, Washington, 98195–1650, USA
2 College of Oceanic and Atmospheric Sciences, Oregon State University, Corvallis, Oregon, 97330, USA
kcc@ess.washington.edu, prestola@u.washington.edu, bob@geophys.washington.edu, tvan@geophys.washington.edu, trehu@oce.orst.edu

The dynamics and environment under which intraslab earthquakes occur have been debated during the past several decades. Earthquake nucleation dynamics proposed for the shallow crust, involving brittle fracture when shear stresses overcome normal stresses, are difficult to extend to the high lithostatic pressures encountered in subduction zones. A process known as transformational faulting has been invoked to explain catastrophic faulting of ice at high confining pressure as ice undergoes a phase transition to ice II [*Kirby,* 1987]. The olivine to spinel phase transition exhibits similar behavior in the laboratory, offering a reasonable explanation for deep earthquakes [e.g., *Green and Burnley*, 1989; *Houston and Green*, 1995; *Kirby*, 1995; *Kirby et al.*, 1991]. An important phase transformation in the shallowest 100 km of subduction zones is the transition of the basalt in the subducting oceanic crust to eclogite. Dehydration embrittlement, faulting associated with the release of fluids as a result of this phase transition, provides an especially attractive explanation for these earthquakes [*Kirby*, 1995]. The depth range over which this reaction proceeds is strongly temperature dependent because the equilibrium mineral assemblages depend strongly on the temperature [*Peacock and Wang*, 1999] and because the transition may be thermally inhibited in a cold, fast moving slab [*Kirby*, 1995]. For example, the oceanic crust of the Pacific plate subducting under northeast Japan is very old and fast moving. Earthquakes apparently in the subducted crust occur to depths as great as 100 km, as well as in a more active zone clearly within the mantle part of the subducted plate that extends deeper. In contrast, the Philippine Sea plate subducting below southwest Japan is young and slow, and contains shallow Wadati–Benioff seismicity down to only 60 km. Geotherms calculated by thermal modeling of these two subduction zones can explain the first order differences in observed seismicity in terms of basalt to eclogite phase transitions in equilibrium [*Peacock and Wang*, 1999].

An obvious test of the hypothesis that earthquakes are associated with the basalt to eclogite phase transition is to determine whether the earthquakes occur within the subducted crust or the subducted mantle. For example, do the earthquakes occur above or below seismic reflectors associated with the subducted oceanic crust-mantle boundary, or with the interplate interface? *P*–to–*S* and *S*–to–*P* conversions from local earthquakes to seismometers in northern Honshu, Japan show convincing evidence for a strong discontinuity at the upper edge of the seismicity, probably associated with the interplate interface [e.g., *Hasegawa et al.*, 1978; *Matsuzawa et al.*, 1990; *Zhao et al.*, 1997]. They infer that earthquakes occur within both the crustal and mantle portions of the old subducted Pacific plate.

In contrast, the width of the Cascadia seismogenic zone is much narrower, perhaps as narrow as five kilometers. Our goal is to determine the relative position of intraslab earthquakes to reflector surfaces estimated using data from the 1998 active-source Wet SHIPS experiment [*Fisher et al.*, 1999]. We observe strong secondary arrivals (Figure 1) with mid-points under a broad area of the northern Olympic Peninsula (Figure 2). The amplitudes and polarities of reflected arrivals vary systematically over spatial scales as short as one to two kilometers (Figure 1). Beyond offsets of 80 km, the reflected arrivals are typically larger than direct arrivals. We picked approximately 500 travel times from stacks of reflected arrivals after applying a low-pass filter at 14 Hz. Using three-dimensional ray tracing through a three-dimensional tomography model obtained from SHIPS and earthquake first arrival data [*Crosson et al.*, 1999], we determine the locus of all point scatterers which would correspond to an observed travel time for a given source and receiver. This defines an approximately ellipsoidal surface from which a ray could reflect and produce the observed travel time. For coherent arrivals, a reflector must be locally tangent to this ellipsoid. We invert for a smooth reflective surface that optimally is tangent to each of the data ellipsoids.

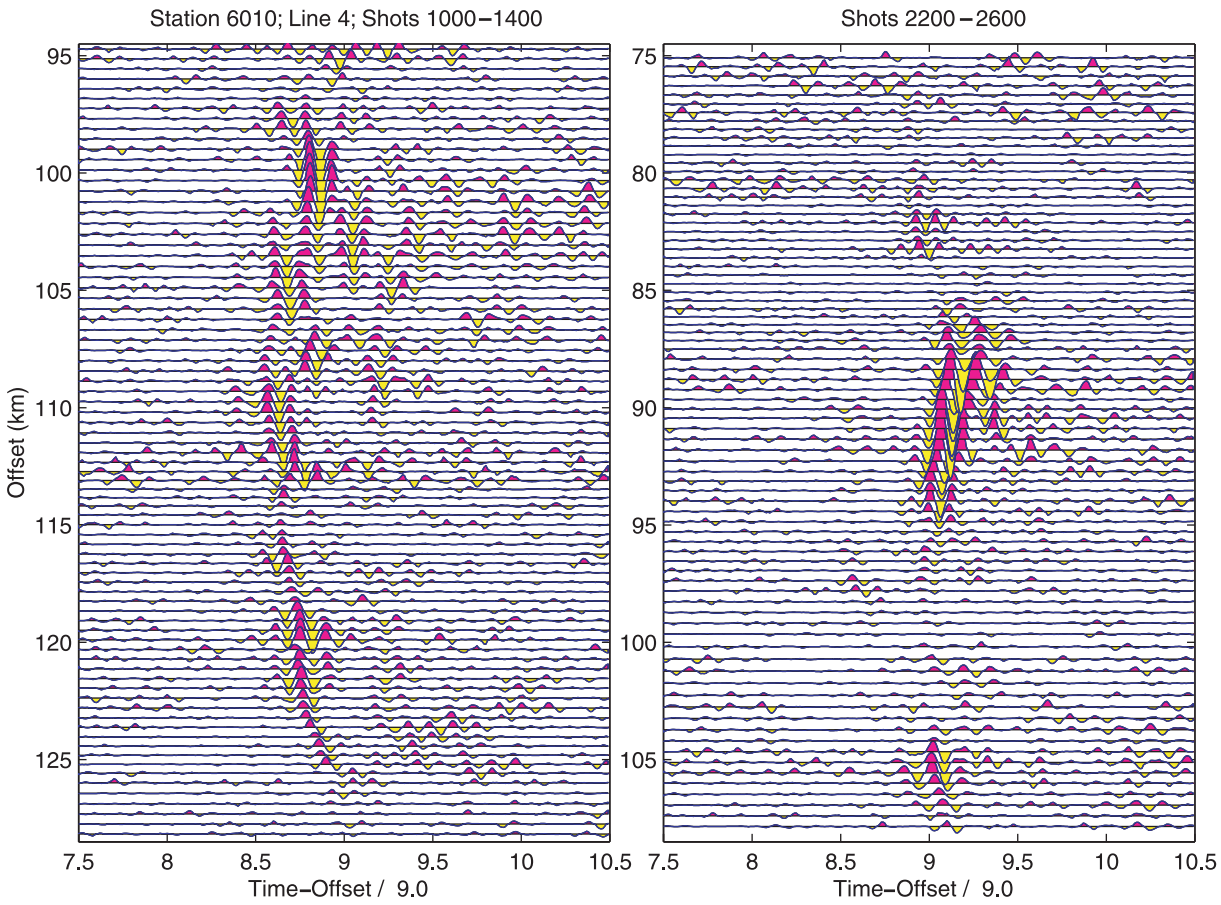

FIGURE 1: Record sections from station 6010 (triangle in Figure 2 at 123˚W, 47.7ºN) from shots (red pluses in Figure 2) reduced at 9 km/s showing examples of the phases that are inferred to reflect off the subducted slab. The first arrivals are off the left of the sections. Raw seismograms are low-pass filtered with a corner at 14 Hz. Each trace in this figure represents a phase-weighted stack [*Schimmel and Paulssen*, 1997] of five adjacent, non-overlapping seismograms. Midpoints for each stack shift by 250 m. Note the rapid spatial variation in the amplitude, apparent velocity, first motion and general character of the reflected arrivals.

The optimal reflector is approximately 30 km deep under the central Olympics, dipping about 13° to the east, reaching a depth of about 60 km under Puget Sound (Figures 2 and 3). Earthquakes that have been relocated as part of the three-dimensional tomographic inversion [*Van Wagoner et al.*, 2000] define a planar surface that is parallel to and consistently above this reflector (Figures 2 and 3). Note that earthquakes in this area move consistently up by a few kilometers, relative to the standard Pacific Northwest Seismic Network (PNSN) catalog hypocenters, as a result of correcting for the inferred three-dimensional velocities of this area. We interpret the reflector as the Moho of the subducting slab. Thus, these earthquakes occur completely within the subducting oceanic crust.

We also image a weaker reflector, more geographically localized, which lies parallel to and just above the seismicity, about seven kilometers above the deep reflector (Figure 4). Our preliminary interpretation is that this reflector is associated with the interplate boundary.

The two major sources of error that affect uncertainties in the geometry of these reflectors are picking errors and errors associated with the velocity model. Picking errors are estimated to be less than 0.1 second for most of the data; errors of this size will not effect our primary conclusions. However, velocity model errors could be quite large where sampling is poor. The shallowest structures under the Strait of Juan de Fuca are poorly sampled in our current three-dimensional model. Perturbing the model in the upper ten kilometers of this region by up to ± 30% and reinverting, the lower reflector surface moved up by as much as ten kilometers in the westernmost quarter of our study region. However, the remaining eastern three-quarters of our area was unaffected and remained beneath the seismicity. Below a depth of 20 km, the estimated model variance increases. We perturb this region uniformly by as much as ± 3%. Reinverting, we observed the surface to move vertically by

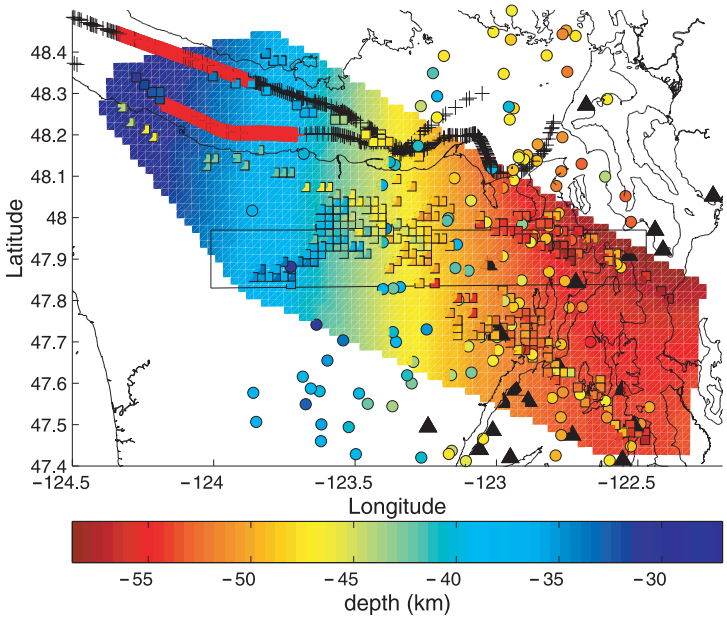

FIGURE 2: Map view of the inferred reflector geometry (color shading), stations with observed reflectors (triangles), shots (plusses, red for shots recorded in Figure 1), relocated earthquakes (circles), and three-dimensional migrated reflection points (squares). Depths of the reflector surface, earthquakes and migrated reflection points are given by the color bar.

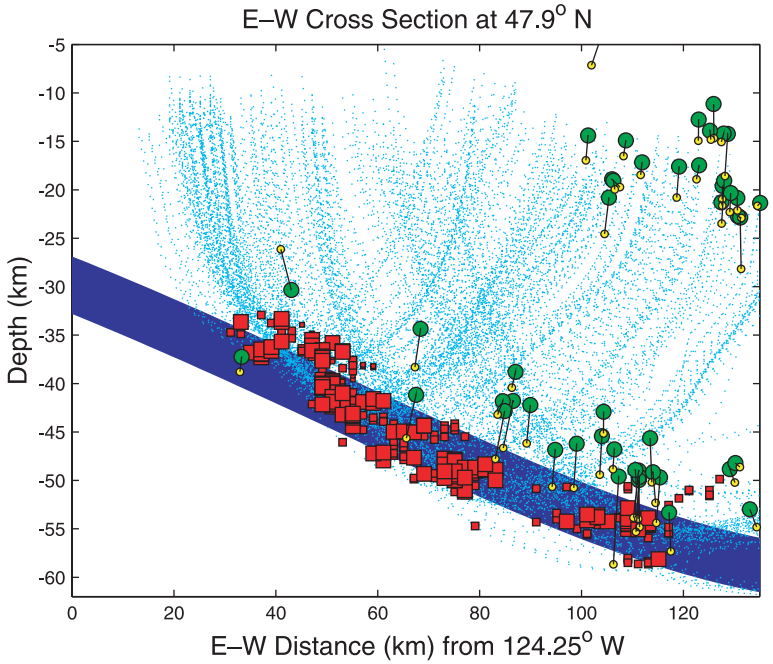

FIGURE 3: Cross section of volume within the black box of Figure 2 showing standard Pacific Northwest Seismic Network (PNSN) earthquake locations (small yellow circles), hypocenters relocated using the three-dimensional velocity model (large green circles) and the migrated reflection points (squares). Larger squares represent higher quality picks. Cross sections of the data ellipsoids (see text) are also shown as dotted blue lines. The reflector surface (thick blue line) optimally fits both the reflection points and the slope of the data ellipsoids at the migrated reflection points.

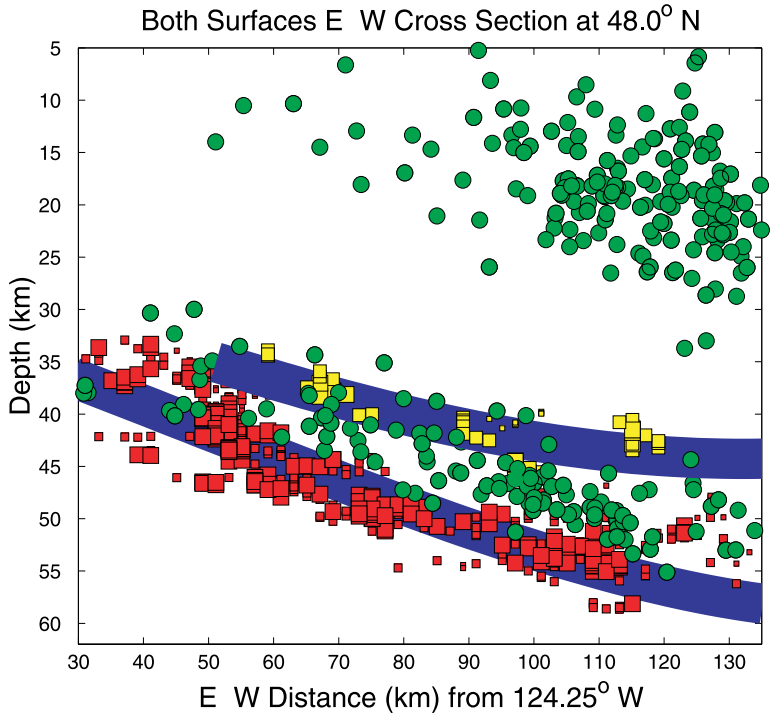

FIGURE 4: Cross sectional view containing all data collapsed along the north–south direction showing both the upper and lower reflector surfaces. See caption for Figure 3 for an explanation of symbols.

up to five kilometers with slight changes in slope. Again, the lower surface remained beneath the seismicity. We conclude that the lower reflector is indeed beneath the seismicity despite uncertainties in the velocity model.

Our observations indicate that the intraplate seismicity under the northern part of the Olympic Peninsula is completely confined to the crust of the subducting Juan de Fuca slab, consistent with the dehydration embrittlement hypothesis [*Kirby*, 1995].

Bounce point locations associated with rapid spatial amplitude variations, like those seen in Figure 1 shots 2200-2600, correlate well with each other indicating that these "bright spots" are associated with slab structure and are perhaps a consequence of the partial transformation of basalt to eclogite. We have not yet been able to rigorously determine polarities for the two reflector surfaces, but the data appear to be of sufficient quality to provide this information. Preliminary analysis of data with clear polarities demonstrate that, like the amplitudes, polarities can also coherently and clearly change over short spatial scales, suggesting the Moho reflector is not a simple interface. The focal mechanisms of Wadati–Benioff zone earthquakes in this region are quite variable but are most consistent with in-plane tension. This is consistent with the stresses in the slab associated with the 15% decrease in volume from the basalt to eclogite phase transition. As the crustal part of the subducting plate shrinks it imposes an in-plane compressive stress on the subducting mantle, which in turn resists shrinking thus putting the subducted crust in in-plane tension.

References

Crosson, R.S., K.C. Creager, N.P. Symons, T. Van Wagoner, Y. Xu, L.A. Preston, T.M. Brocher, T. Parsons, M.A. Fisher, T.L. Pratt, C. Weaver, U.S. ten Brink, K. Miller, A. Trehu, R. Hyndman, and G. Spence, High-resolution 3-D regional P wave velocity tomography of the Puget basin region from SHIPS first-arrival data, *EOS, 80 (46),* F763, 1999.

Fisher, M.A., T.M. Brocher, R.D. Hyndman, A.M. Trehu, C.S. Weaver, K.C. Creager, R.S. Crosson, T. Parsons, A.K. Cooper, D. Mosher, G. Spence, B.C. Zelt, P.T. Hammer, U. ten Brink, T.L. Pratt, K.C. Miller, J.R. Childs, G.R. Cochrane, S. Chopra, and R. Walia, Seismic survey probes urban earthquake hazards in Pacific Northwest, *EOS, Trans. AGU, 80 (2)*, 13–17, 1999.

Green, H.W., II, and P.C. Burnley, A new self-organizing mechanism for deep-focus earthquakes, *Nature, 341,* 733–737, 1989.

Hasegawa, A., N. Umino, and A. Takagi, Double planed deep seismic zone and upper mantle structure in the northeastern Japan arc, *Geophys. J. R. Astron. Soc., 54*, 281–296, 1978.

Houston, H., and H.W. Green, II, The mechanics of deep earthquakes, *Ann. Rev. Earth Planet. Sci., 23*, 169–213, 1995.

Kirby, S.H., Localized polymorphic phase transformations in high-pressure faults and applications to the physical mechanism of deep earthquakes, *J. Geophys. Res., 92*, 13,789–13,800, 1987.

Kirby, S.H., Intraslab earthquakes and phase changes in subducting lithosphere, *Rev. Geophys., Suppl., U.S. National Report to IUGG 1991–1994*, 287–297, 1995.

Kirby, S.H., W.B. Durham, and L.A. Stern, Mantle phase changes and deep-earthquake faulting in subducting lithosphere, *Science, 252*, 216–225, 1991.

Matsuzawa, T., T. Kono, A. Hasegawa, and A. Takagi, Subducting plate boundary beneath the northeastern Japan arc estimated from SP converted waves, *Tectonophysics, 181*, 123–133, 1990.

Peacock, S.M., and K. Wang, Seismic consequences of warm versus cool subduction metamorphism: examples from southwest and northeast Japan, *Science, 286*, 937–939, 1999.

Schimmel, M., and H. Paulssen, Noise reduction and detection of weak, coherent signals through phase-weighted stacks, *Geophys. J. Int., 130*, 497–505, 1997.

Van Wagoner, T.M., R.S. Crosson, K.C. Creager, L.A. Preston, N.P. Symons, T.M. Brocher, T. Parsons, T.L. Pratt, C. Weaver, A. Trehu, and M.A. Fisher, 3-D structure of the Cascadia forearc region from tomographic inversion of SHIPS active experiment and earthquake observations, *EOS, 81 (22)*, WP125, 2000.

Zhao, D., T. Matsuzawa, and A. Hasegawa, Morphology of the subducting slab boundary in the northeastern Japan arc, *Phys. Earth Planet. Int., 102*, 89–104, 1997.

Modeling post-critical Moho reflections from intraslab earthquakes in the Cascadia subduction zone

Jeff Shragge[1], Michael Bostock[1] and Garry C. Rogers[2]
1 Earth and Ocean Sciences, The University of British Columbia, Vancouver, British Columbia, V6T 1Z4, Canada
2 Pacific Geoscience Centre, Geological Survey of Canada, PO Box 6000, Sidney, British Columbia, V8L 4B2, Canada
shragge@geop.ubc.ca, bostock@geop.ubc.ca, rogers@pgc.nrcan.gc.ca

Ten years ago, *Cohee et al*. [1991] undertook a study to predict ground response of the Seattle Basin and Puget Sound lowlands to a megathrust earthquake in Cascadia. Their modeling suggested that the response at distances beyond 75 km from the rupture could be dominated by waves post-critically reflected from the oceanic Moho. Wavefield radiation from intraslab earthquakes may be similarly affected by post-critical Moho reflections. It is therefore important to investigate this potential contribution to intraslab earthquake hazard for major population centres in the Pacific Northwest.

To examine this phenomenon and its importance in southwestern British Columbia, we present two-dimensional pseudo-spectral synthetic seismogram computations for a model of the Cascadia subduction zone. Large-scale velocity and density structure are obtained from LITHOPROBE seismic studies on southern Vancouver Island [*Drew and Clowes,* 1990], gravity anomaly modeling [*Riddihough,* 1979], and Wadati–Benioff seismicity compiled by the GSC (see Figure 1). The modeling includes both *P–SV* and *SH* propagation, and the effect of source directivity for intraslab earthquakes within and below the oceanic crust. This permits us to examine the characteristics of post-critical reflections from the oceanic Moho for a variety of source locations and mechanisms.

To illustrate the potential hazard of post-critical reflections from the dipping oceanic Moho, three displacement seismogram sections for an intraslab event located beneath the accretionary sedimentary prism complex offshore of Vancouver Island are presented in Figures 2–4 (*Uz*, *Ux*, and *Uy* components respectively). Post-critical reflections are highly visible at distances corresponding to the British Columbia lower mainland between 160 and 250 km in epicentral distance (Figure 1) for both *P–SV* (Figures 2 and 3) and *SH* (Figure 4) propagation. Note that in the case of *SH* propagation the amplitude of the post-critical reflection at 190 km in epicentral distance is comparable to that of the direct *S*-wave arrival at 50 km. Similar behavior is observed for *P–SV* although results are generally dependent on the chosen source mechanism.

References

Cohee, B.P., P.G. Somerville, and N.A. Abrahamson, Simulated ground motions for hypothesized M_w=8 subduction earthquakes in Washington and Oregon, *Seism. Soc. Am. Bull., 81,* 28–56, 1991.

Drew, J.J., and R.M. Clowes, A re-interpretation of the seismic structure across the active subduction zone of western Canada, in *Studies of Laterally Heterogeneous Structures Using Seismic Refraction and Reflection Data,* edited by A. G. Green, Geol. Surv. Can. Paper 89–13, 115–132, 1990.

Riddihough, R.P., Gravity and structure of an active margin—British Columbia and Washington, *Can. J. Earth Sci., 16,* 350–363, 1979.

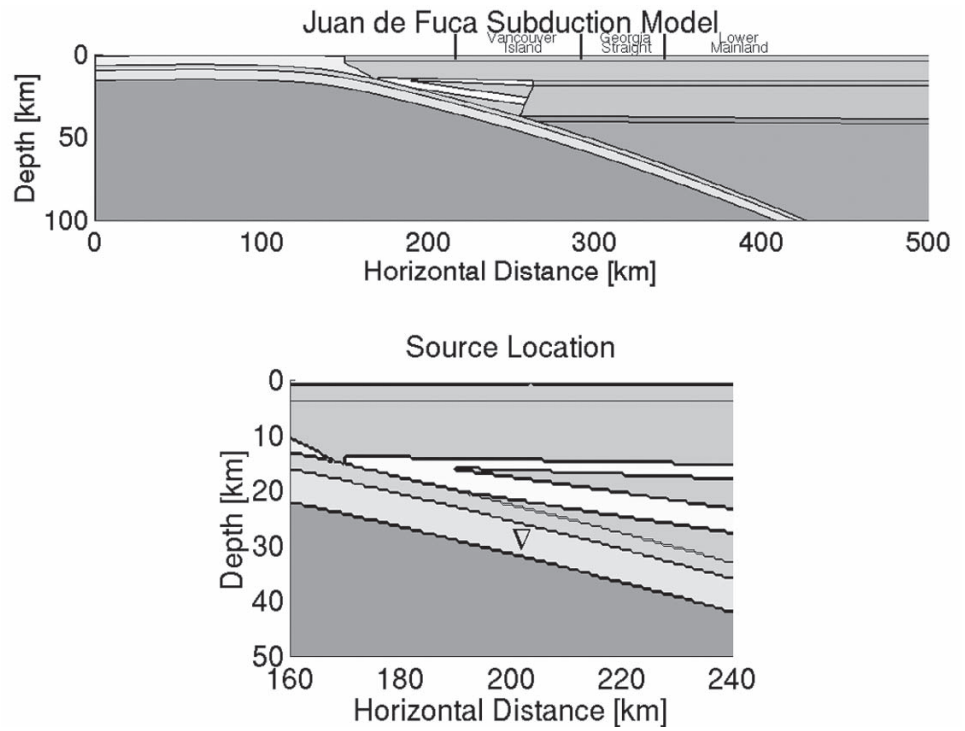

FIGURE 1: Top: model of Cascadia subduction zone beneath southwestern British Columbia after *Drew and Clowes* [1990]. Bottom: location of intraslab earthquake source.

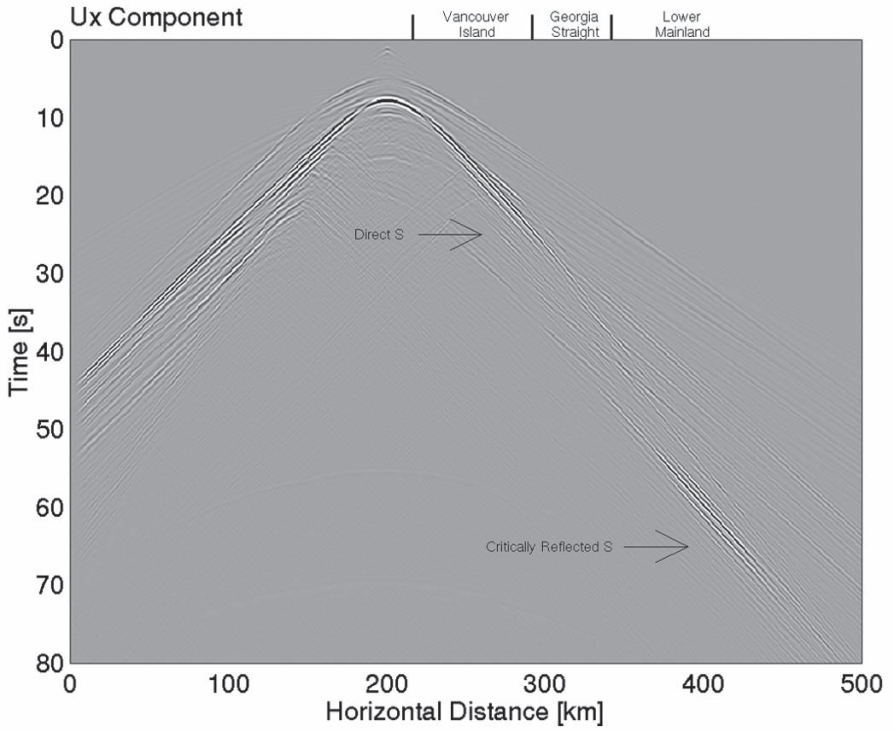

FIGURE 2: Vertical component of displacement (*Uz*) for model configuration in Figure 1. The source consists of a summation of point double couples to yield an extended double couple line source oriented along the dip of the slab.

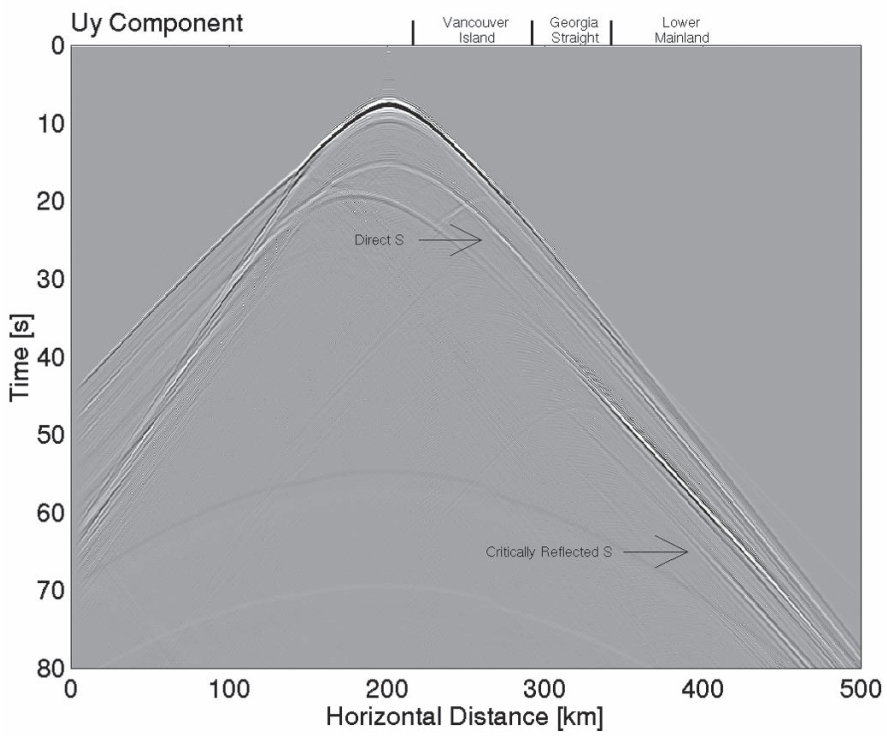

FIGURE 3: Radial component of displacement (*Ux*) for model configuration in Figure 1. The source consists of a summation of point double couples to yield an extended double couple line source oriented along the dip of the slab.

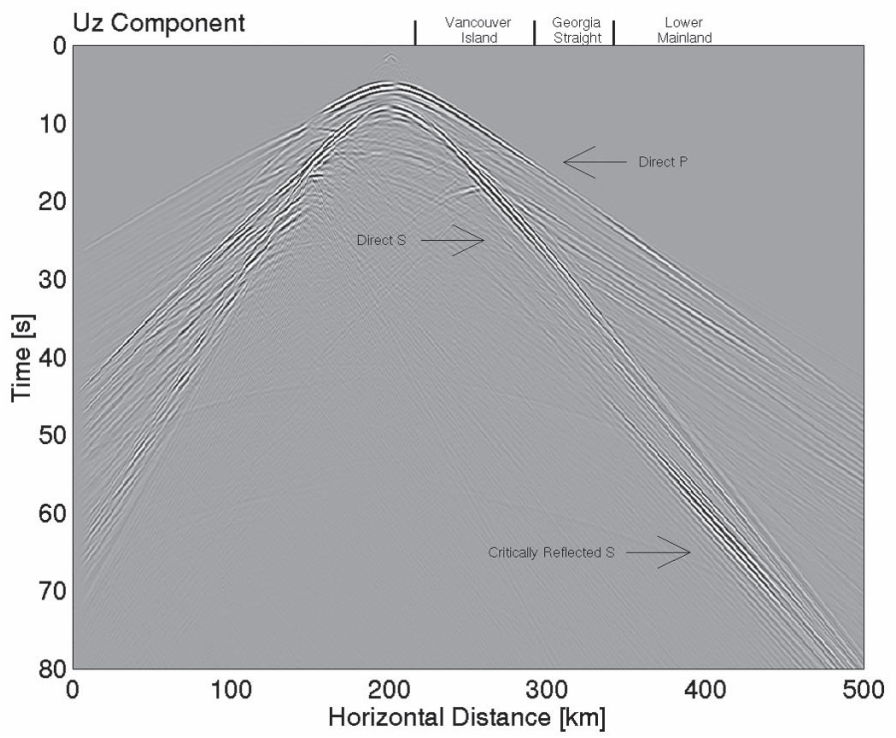

FIGURE 4 : Transverse component of displacement (*Uy*) for model configuration in Figure 1. The source consists of a summation of point rotations to yield an extended couple oriented parallel to the strike of the slab.

Geometry and membrane deformation rate of the subducting Cascadia slab

Ling-Yun Chiao[1] and Kenneth C. Creager[2]
1 Institute of Oceanography, National Taiwan University, Taipei, Taiwan, R.O.C.
2 Department of Earth and Space Sciences, University of Washington, Seattle, Washington, 98195–1650, USA
chiao@ccms.ntu.edu.tw, kcc@ess.washington.edu

ABSTRACT

The Juan de Fuca plate subducts along the west coast of North America along a plate boundary that extends some 1000 km from northern California to Vancouver Island. In map view, the plate boundary is nearly straight along its northern and southern regions, but exhibits a 35° change in orientation offshore from northern Washington State. Landward from this bend is an arch in the shape of the subducting plate, a concentration in Wadati–Benioff seismicity and an anomalously thick Miocene accretionary prism that makes up the two kilometer-high Olympic Mountains. We speculate that all three are related, directly or indirectly, to the fact that the Cascadia slab is subducting into a concave, oceanward corner which creates a geometric space problem analogous to pleats in a tablecloth hanging off the corner of a table. To test this hypothesis, we develop a theory of steady state, incompressible three-dimensional fluid flow that is asymptotically valid for a thin slab with high linear (or non-linear) viscosity relative to the surrounding fluid. Flow in this simple model is constrained by kinematic boundary conditions rather than buoyancy forces. Fixing the slab geometry to the same trench-normal profile along the entire subduction zone, we invert for the flow field that minimizes the dissipation power of the system and find that strain rates, characterized by along-strike compression, are concentrated along the west coast of Washington, reaching values of $2x10^{-16}$ s^{-1}. In a second experiment, we constrain the same 20° dip along the northern and southern edges of the subducting plate and find that the optimal slab geometry contains an arch in a location similar to the seismologically observed arch, and that the root-mean square of the strain rates are reduced by a factor of five. Thus, if these strain rates are accommodated by intraplate earthquakes, this arching model provides a geometry that allows a five-fold reduction in seismic moment release rates. The predicted strain rates are consistent with the observed moment release rate associated with one $M_w=7$ and several $M_w>6$ earthquakes per century in the Olympic Mountain/Puget Sound region, and a much lower rate to the north and south. Predicted strain rates associated with slab bending and unbending are generally smaller than the predicted membrane strain rates. The anomalously thick accretionary prism associated with the Olympic Mountains can be explained by the critical taper theory as being caused by the shallow dip of the slab along the arch.

Introduction

The trend of the deformation front demarking the boundary between the North American and Juan de Fuca plates bends by 35° from a north–south trajectory off Oregon and Washington to N 35°W off Vancouver Island (Figure 1). Landward of this bend, the subducting oceanic plate has a shallow 10° dip to a depth of about 50 km [e.g., *Crosson and Owens*, 1987; *Weaver and Baker*, 1988; *Creager et al.* and *Tréhu et al.*, this volume], whereas the dip under Vancouver Island to the north is steeper (~18°) [*Davis and Hyndman*, 1989; *Cassidy and Ellis*, 1993]. The slab dip to the south underneath Oregon is less well resolved. However, a few small earthquakes that are inferred to be slab events in Oregon suggest a steeper dip in this region as well. The shallow dipping region represents an arch-like structure with an east–west trending axis under the Olympic Mountains and Puget Sound (Figure 1). Support for this arching structure comes from the analysis of receiver functions (*P*-to-*S*-wave conversions off the subducting plate) [*Crosson and Owens*, 1987; *Owens et al.*, 1988; *Cassidy and Ellis*, 1993]. Tomographic images [*Rasmussen and Humphreys*, 1988; *VanDecar*, 1991; *Bostock and VanDecar*, 1995] also indicate that after passing beneath the Puget Sound region, the slab goes to a steeper ~55° dip.

The arch structure has been attributed to a space problem [e.g., *Rogers*, 1984; *Crosson and Owens*, 1987], which can be visualized by considering the analogy between the subducting plate and a tablecloth hanging over the corner of a table. The tablecloth has folds as it hangs over the corner. The extra material can be accommodated either by along-arc compression, or by geometric buckling or arching. The primary purpose of this paper

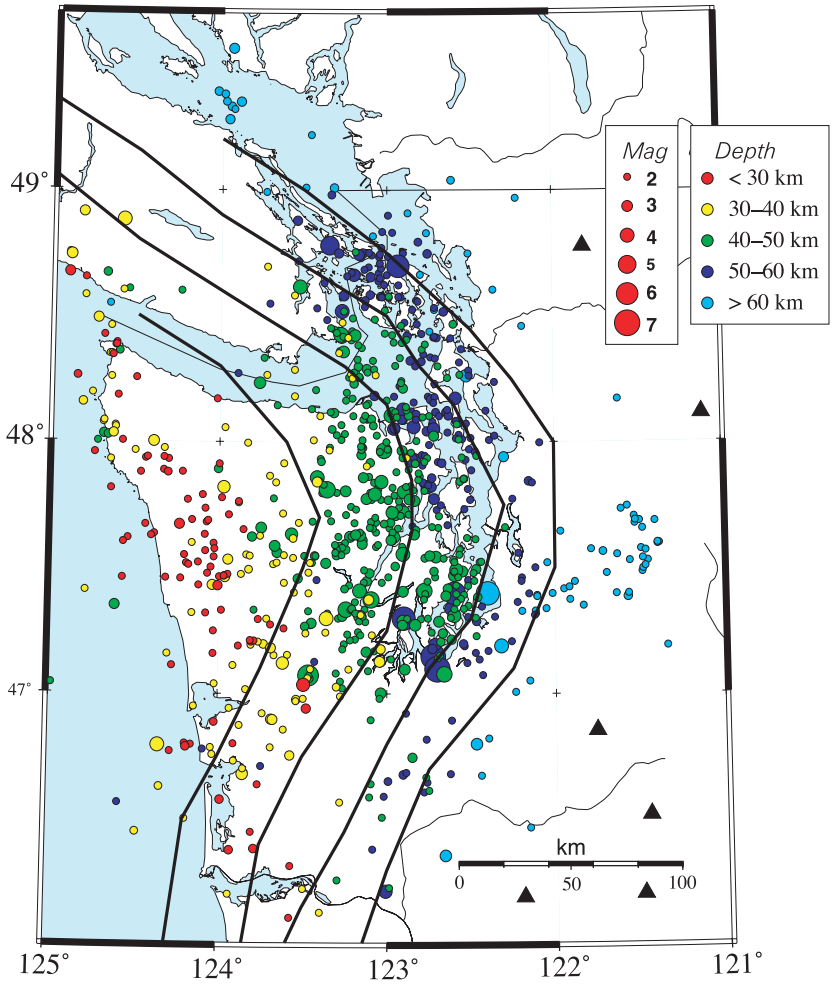

FIGURE 1: Lambert projection of earthquakes (circles) inferred to be within the subducting Cascadia plate, slab depth contours (thick lines) showing the arch structure inferred by *Crosson and Owens* [1987], and active volcanoes (triangles). Earthquake magnitudes and depths are indicated by the scale. Earthquakes with magnitudes exceeding 2 are from the Pacific Northwest Seismic Network and the Pacific Geoscience Centre Network. Older, large earthquakes are also shown.

is to analyze the possible relationships among this bend in the trench, the shape and internal deformation of the subducted plate, the spatial distribution of deep seismicity, and the location of the Olympic Mountains.

The well-located microseismicity inferred to be in the down-going plate, recorded by the Pacific Northwest Seismic Network (PNSN) and the Pacific Geoscience Centre (PGC) during the past three decades, as well as large earthquakes during the twentieth century (Table 1), are concentrated in the vicinity of the Puget Sound basin (Figure 1). There are markedly fewer events south of Olympia, Washington and even fewer south of Portland, Oregon. Perhaps even more striking is the variation in strain rate inferred from this seismicity. From 47.1° to 48.8°N (Olympia to Victoria, British Columbia), several magnitude 5.5 to 7 earthquakes are well documented whereas to the north and south the largest known deep earthquake is a magnitude 3.7. Using standard magnitude to seismic moment scaling [*Hanks and Kanamori*, 1979], it appears that the seismic moment release rate (which is proportional to strain rate) within these latitudes is five orders of magnitude greater than that outside.

Nearly all other subduction zones, which are characterized by an oceanward concave bend in the axis of the trench, also exhibit an arching structure with anomalously shallow dip landward of the bend. Examples include the Pacific plate subducting under Alaska *[Page et al.*, 1989] and the Kamchatka, Kuril, Japan, Izu–Bonin trench system which, taken as a whole, has an oceanward-concave curvature. The Japan slab, at the center, exhibits a shallow 30° dip, while the dips under Izu–Bonin to the south and Kamchatka to the north are 90° and 50° respectively. On a smaller scale, arc–arc junctions such as the Hokkaido corner, the corner between Honshu and Izu–Bonin, and the New Britain–Solomon corner all exhibit pronounced arches [*Yamaoka et al.*, 1986; *Yamaoka*

and Fukao, 1987; *Chiao*, 1991] in the upper few hundred kilometers. A counter example is the Bolivia orocline which currently has an anomalously steep dip landward of a bend in the trench [*Creager et al.*, 1995].

The Olympic Mountains are part of an Eocene to Miocene highly deformed sedimentary and meta-sedimentary accretionary complex which is bounded to the north and east by the horseshoe shaped Eocene Crescent basalts. This highly anomalous, subaerial accretionary wedge is confined to less than 100 km along the arc, but extends nearly 200 km from the deformation front. This unusual geometry has been attributed to the shallower slab dip beneath the Olympic Peninsula [*Davis and Hyndman*, 1989; *Brandon and Calderwood*, 1990; *Brandon et al.*, 1998] as described in more detail below.

In order to understand these relations among slab geometry and internal deformation, membrane strains (or strain rates) associated with slab flow have been analyzed using physical models [*Yamaoka et al.*, 1986; *Yamaoka and Fukao*, 1987], analytic solutions to very simple geometries [*Bevis*, 1986; *Bevis*, 1988] and numerical analyses [*Burbach and Frohlich*, 1986; *Chiao*, 1991; *Creager and Boyd*, 1991; *Creager et al.*, 1995]. Deformation in plate interiors, as observed by seismic activity, is generally very low. However, the Gorda plate is a counter example in which high levels of seismicity occur throughout the interior of the plate. These large in-plane strain rates are forced by geometric constraints imposed by the much older and stronger Pacific plate [*Denlinger*, 1992]. Similarly, large in-plane or membrane strain rates are required by the geometry of subduction. In this paper, we extend the methods developed by *Creager and Boyd* [1991] and *Chiao* [1991] to analyze the membrane and bending strain rates in the Cascadia subduction zone. We explore, not only the orientation and amount of the strain rate required of a given slab geometry, but also determine the geometry that is most compatible with a given trench configuration and other geometric boundary conditions.

Kinematic modeling of in-plane deformation rate

We postulate that the arching structure, the concentration of intraslab earthquakes along the arch axes, and the anomalously thick accretionary prism located above the arch are all linked directly or indirectly to the bend in the trench. The essence of our approach is to consider solutions to the three-dimensional fluid flow problem that are asymptotically valid in the vicinity of a smooth surface defining the slabs cold thermal core. We assume that: 1) the effective viscosity of the fluid is high near this surface and decreases rapidly away from it; 2) no flow crosses this surface; 3) the flow is steady state; and 4) incompressible. First, we provide arguments to justify and motivate these assumptions and then show how they can be used to reduce the essence of a fully three-dimensional flow problem to a calculation in two-dimensions on the 'slab surface' which is valid both on the surface and in the vicinity of the surface. See *Chiao* [1991] for details.

The rheology of subducting slabs and the surrounding mantle is not well constrained. However, most mechanisms associated with steady state flow are observed in the laboratory to depend exponentially on homologous temperature (absolute temperature divided by the solidus) [e.g., *Carter*, 1976]. *Creager and Boyd* [1991] estimate the homologous temperatures along the Aleutian subduction zone by dividing thermal models by the pressure dependent solidus of a dry peridotite [*Takahashi and Kushiro*, 1983]. They estimate very low values of homologous temperature (<0.4) in the seismogenic parts of the slab, comparable to the homologous temperatures predicted for the seismogenic parts of the oceanic lithosphere prior to subduction. This suggests that the effective viscosity in the cold core of slabs is orders of magnitude greater than in the surrounding asthenosphere (see also *Davies* [1999]). The thickness of the stiff part of the subducted plate is thus expected to be comparable to the mechanical thickness of the oceanic lithosphere, which for young oceanic plates is 10–20 km [*McNutt*, 1984]. It appears reasonable to treat the slab as a thin sheet given that its lateral dimensions are in the order of 1000 km. A consequence of a large contrast in effective viscosity is that large-scale shear strain rates parallel to the slab surface will occur preferentially in the weaker fluid. We assume that within the cold core of the slab, there is no shear-strain rate parallel to the slab. This is analogous to the Kirchhoff's Hypothesis in studying the deformation of elastic shells [e.g., *Calladine*, 1983].

Consider a three-dimensional, incompressible, steady-state flow field $v(x)$. The symmetric part of the gradient of the particle velocities is the deformation rate tensor field $D(x)$. Consider a smooth, curved surface that describes the slab geometry and assume that the slab flow does not cross this surface. A mathematically convenient way to impose Kirchhoff's Hypothesis is to construct the local projection operator ($P = I - n \otimes n$) [e.g. *Parlett*, 1980] which projects vectors onto the slab surface if n is the unit vector locally normal the surface, $n \otimes n$ is a dyadic (outer) product, and I is the identity tensor. Operating on D by P from both sides, $D^{pp} = P\,D\,P^T$ annihilates shear parallel to the slab as well as compression or extension in the slab normal direction [*Chiao*, 1991], while not modifying the in-plane part of the deformation rate. To comply with the assumption that the fluid is incompressible, while maintaining Kirchhoff's Hypothesis, we define

$$D^{in} = D^{pp} - tr(D^{pp})\, n \otimes n$$

where tr is the trace (sum of diagonals). D^{in} is then the strain-rate tensor describing the membrane deformation rate and the thickening (or thinning) of the thin viscous

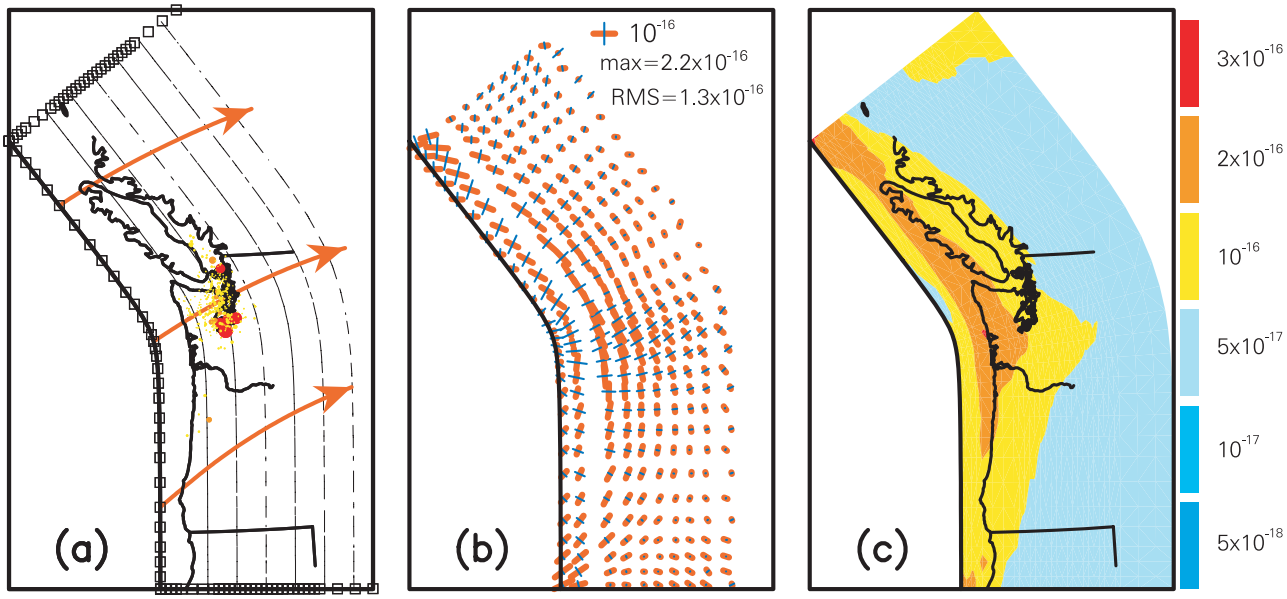

FIGURE 2: Flow field inversion of the constant-dip experiment with a Newtonian rheology. a) Depth contours, at 30 km intervals, showing the fixed geometry of the subducting plate, earthquakes, and three of the inferred particle paths. b) Principal axes of calculated membrane strain rates (bold red bars show compression and thin blue line segments show extension). Length is proportional to the value of the strain rate as shown by the scale. c) Spatial distribution of effective strain rate. Root mean square of the effective strain rate over the entire area of the subducted plate is 1.3×10^{-16} s^{-1} .

slab. It represents the deformation of a flow field that satisfies Kirchhoff's Hypothesis and incompressibility. Furthermore, these two approximations allow us to uniquely evaluate all nine components of the deformation rate tensor within the high viscosity part of the fluid from knowledge of the flow field in the plane of the slab. In other words, within the high-viscosity region of the slab, D asymptotically approaches D^{in} as the viscosity contrast increases and the slab thickness decreases.

The effective strain rate (γ) within the slab is defined by:

$$\gamma^2 = 1/2\ D_{ij}\ D_{ij} \approx 1/2\ D^{in}_{ij}\ D^{in}_{ij} \qquad (1)$$
$$= 1/2\ [D^{pp}_{ij}\ D^{pp}_{ij} + \mathrm{tr}(D^{pp})^2\ ]$$

Suppose the slab has a power-low viscous rheology [eg., *Ranalli*, 1987] in which D is proportional to the n^{th} power of the deviatoric stress: $D_{ij} = B^{-n}\ (1/2\ \tau_{kl}\ \tau_{kl})^{n-1}\ \tau_{ij}$, where τ_{kl} is the deviatoric stress tensor. B depends on temperature and is much larger in the cold slab than outside. The dissipation power of the entire flow within the region of high viscosity equals the thickness, H, of this region times the surface integral over the entire slab of half the stress deviator contracted with the strain rate tensor [*Chiao*, 1991]:

$$I = H \int 1/2\ \tau_{ij}\ D_{ij}\ dA = H\ B \int \gamma^{1+1/n}\ dA \qquad (2)$$

In summary, given a slab geometry and a continuous flow field following that surface, we calculate the deformation rate tensor and the dissipation power (2) associated with the flow field in the high viscosity region near the slab. The goal is to use this forward formulation to solve the inverse problem of determining the slab geometry and the flow field that minimizes the dissipation power. In this simplified formulation, the flow is driven by boundary conditions rather than buoyancy forces. We specify the flow along a spherical shell corresponding to the pure rotation of the oceanic lithosphere prior to subduction and force the slab to remain at the earth's surface until it reaches a predefined trench location. We then specify part or all of the slab geometry and invert for the flow field that minimizes the dissipation power. According to equation (2), a Newtonian rheology ($n=1$) corresponds to minimizing the L^2 norm of the effective strain rate, while a power-law rheology with $n=\infty$ corresponds to minimizing the L^1 norm. We consider solutions in these two end-member rheologies.

Results

Constant dip geometry, Newtonian rheology

In our first experiment, we fix the geometry to have a dip of 20° along the entire trench. To go from a dip of 0 at the trench to 20°, we determine the geometry that minimizes the integral of the change of curvature [*Chiao*, 1991], which minimizes the total bending strain rates. The boundary condition is that, prior to entering the trench, the flow field satisfies the relative plate motions on a sphere described by the Euler pole at (29.11°N, -112.72°E) and an angular velocity of 1.05° per million

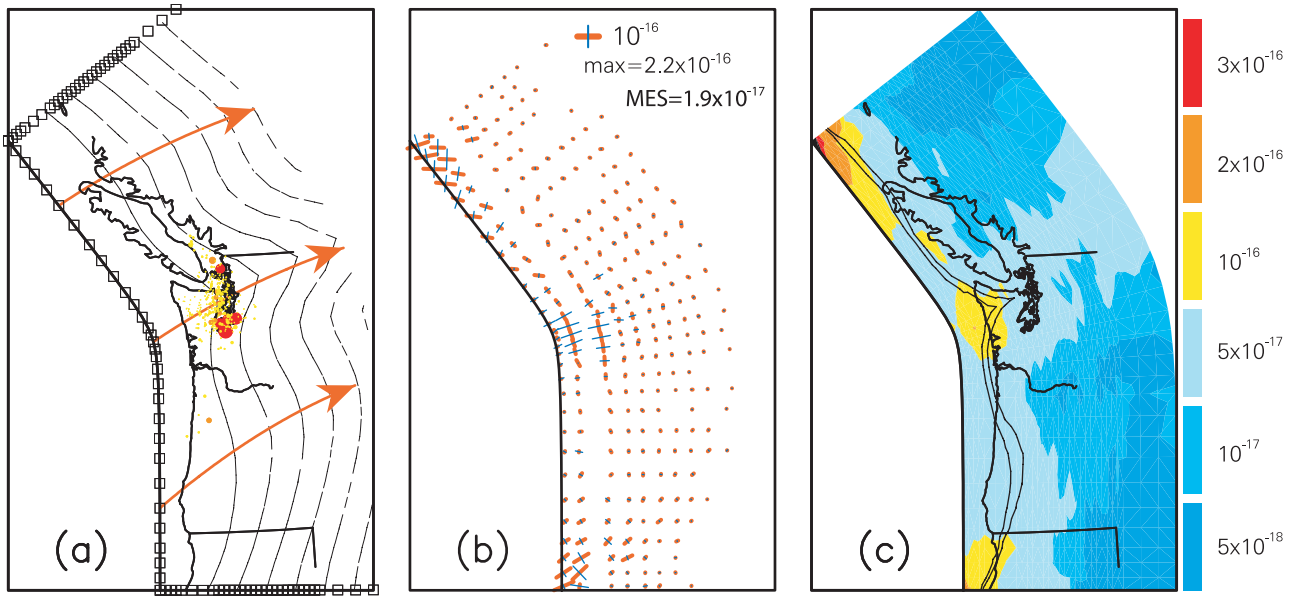

FIGURE 3: The variable-dip experiment showing results of the full inversion involving both the flow field and the slab geometry (see captions for Figure 2) for a power-law rheology ($n=10^6$). The 10° and 12° iso-dip contours of the slab dip shown in panel c), come onshore under the Olympic Mountains, providing a possible explanation for the existence and location of this thick accretionary prism as explained in the text. The mean effective strain rate (MES) for power-law rheology is 2×10^{-17} s^{-1}.

years [*Nishimura et al.*, 1984]. Using a finite element formulation, we invert for the flow field $v(x)$ on the slab surface that minimizes the dissipation power (2) and satisfies the given slab geometry and boundary condition (Figure 2). From this flow field, we calculate the strain-rate tensor and display its principal axes, their corresponding magnitudes, and the effective strain rate, γ (Figure 2). The bend of the trench clearly imposes a smoothly varying along-arc compression which reaches values as high as 2×10^{-16} s^{-1}. This integrates along particle paths to strains of several percent. The root-mean square of the effective strain rate is 1.3×10^{-16} s^{-1}.

Arch geometry, Newtonian rheology

Next we relax the geometric boundary conditions such that the geometry is imposed only along the trench (and oceanward of the trench) and along two cross sections at the northern and southern edges of the slab. These cross sections are the same as in the constant dip model. Now both the geometry of the slab surface and the flow field within this surface are allowed to vary to find the minimum deformation-rate solution. The root-mean square of the effective strain rate is reduced by a factor of five relative to the constant dip model.

Arch geometry, power-law rheology

In a third experiment, we use the same boundary conditions, but consider a power-law rheology with a very large exponent ($n=10^5$). The resulting best slab geometry is nearly identical to the solution for the linear rheology so we show only the result for the power-law rheology (Figure 3). The main difference is that the power-law rheology causes a concentration of the region of high effective strain rate and a higher contrast relative to background values. The resulting slab geometry exhibits a pronounced arch (Figure 3a), much like that previously estimated (Figure 1) from seismicity and the analysis of receiver functions [*Crosson and Owens*, 1987].

Furthermore, the 10° and 12° slab-dip isolines (Figure 3c) outline the geographic location of the Olympic Mountains. These mountains are highly anomalous in that they represent an extremely thick subaerial accretionary prism, with an along-strike extent of less than 100 km and a trench normal extent of nearly 200 km. One explanation for these mountains is that the geometric bend in the trench produces a geometric space problem that can be accommodated by large compressional strain rates within the plane of the slab (Figure 2) or geometric arching (Figure 3). The observed slab geometry (Figure 1) suggests that the minimum global energy solution is to allow arching. An important consequence of the arching is the anomalously shallow slab dip (<10° for 200 km landward of the deformation front). The critical taper theory, invoked to explain the deformation and mechanics of accretionary prisms [e.g. *Davis et al.*, 1983; *Davis and Hyndman*, 1989], suggests that for a wide range of rheological parameters, a slab dip of less than 11° produces a positive slope to the top of the wedge, such that the topography of the earth's surface will go up landward of the trench. In contrast, once the slab dip increases past

TABLE 1: Large 20th century earthquakes inferred to be in the subducting Cascadia slab.

Date	Latitude (°N)	Longitude (°E)	Depth (km)	Magnitude	Seismic moment (Newton-m)
01/11/09	48.7	-122.8	75	6.0	
11/13/39	47.4	-122.6	60	6.2	
02/15/46	47.3	-122.9	60	6.2	
04/13/49	47.1	-122.7	54	7.1	1.5×10^{19} [*Baker and Langston*, 1987]
04/29/65	47.4	-122.3	59	6.5	1.4×10^{19} [*Langston and Blum*, 1977]

11°, the wedge will decrease in elevation. Indeed, the predicted location of the 11° dip isoline (Figure 3) shows a clear triangular area that extends inland in the Olympic Peninsula region, imitating the distribution of the Crescent basalt backstop and the locus of the thick accretionary wedge material.

Bevis [1988] derived a simple formula to relate the seismic moment release and the average strain rate for intraslab earthquakes:

$$\dot{\varepsilon} = \frac{\Sigma M}{2\mu WLHt}$$

where $\dot{\varepsilon}$ is the average effective strain rate, μ is the rigidity, ΣM is the total seismic moment release summed over a time period *t*, *and W, L, and H* are along-strike width, downdip length and slab thickness. Assuming $\mu = 7 \times 10^{10}$ Newtons/m^2, $W = 200$ km, $L = 200$ km, $H = 10$ km, and $t = 100$ years for the Cascadia slab, we calculate a strain rate of 2×10^{-16} s^{-1} in excellent agreement with the peak calculated membrane strain rates (Figure 2). Note that over 99% of the summed moment release comes from the five events in Table 1.

The bending strain rate, averaged across the thickness (*H*) of a plate is $V (d\kappa/ds) H/4$ [*Chiao*, 1991] where *V* is the velocity of the subducting plate and $d\kappa/ds$ is the rate of change of the curvature of the plate with respect to position along particle paths. In keeping with the philosophy of the membrane strain rate calculations, we calculate slab cross sections that produce the minimum integrated dissipation power associated with bending strain rates and find that the bending strain rates must reach values of at least 10^{-16}s^{-1} to reach a slab dip of 20°, so the predicted bending strain rates are slightly smaller than the membrane strain rates, but in some places may be more important.

Discussion

Our formulation is kinematic. We have not included important dynamics such as gravitational buoyancy that drives the subduction process. Instead, we observe the slab geometry, which presumably is a result of the dynamics and impose that geometry as a boundary condition. We also do not explicitly incorporate bending deformation, though our two-dimensional calculations suggest that maximum strain rates associated with bending are comparable in magnitude to the membrane deformation rates. It is possible that most of the bending deformation occurs just below the seismicity cutoff through ductile creep mechanisms allowed in these warmer portions of the slab. Also, the basalt–eclogite phase transition causes a volume reduction of about 15% in the subducted oceanic crust. This undoubtedly has an important effect on slab deformation that has not been incorporated in our calculations. We also assume a steady state flow, even though it is clear that the geometry of subduction has changed during the past 20 Ma as the Oregon coast ranges have rotated clockwise to exaggerate the bend in the deformation front.

Even though our calculations do not provide a complete formulation of the dynamics of the Cascadia subduction zone, they provide a method to quantify the space problem imposed by a subduction zone with a concave oceanward trench. We show that an arch structure is an efficient way to accommodate the space problem and reduce the in-plane deformation by a factor of five. Indeed, it is observed that nearly all subduction zones with concave oceanward trenches exhibit similar pronounced arches in slab geometry. The shallow slab dip offers an explanation for the anomalously thick subaerial accretionary prism associated with the Olympic Mountains. In addition, the space problem is most severe landward of the bend in the deformation front, providing a plausible explanation of the high level of earthquake moment release rates in the Puget Sound region relative to regions to the north and south. Finally, the predicted membrane strain rates are the same size as the strain rate inferred by summing the seismic moments of slab earthquakes.

References

Baker, G.E., and C.A. Langston, Source parameters of the 1949 Magnitude 7.1 south Puget Sound, Washington, earthquake as determined from long-period body waves and strong ground motions, *Bull. Seismol. Soc. Amer., 77*, 1530–1557, 1987.

Bevis, M., The curvature of Wadati–Benioff zones and the torsional rigidity of subducting plates, *Nature, 323*, 52–53, 1986.

Bevis, M., Seismic slip and downdip strain rates in Wadati–Benioff zones, *Science, 240*, 1317–1319, 1988.

Bostock, M.G., and J.C. VanDecar, Upper mantle structure of the northern Cascadia subduction zone, *Can. J. Earth Sci., 31*, 1–12, 1995.

Brandon, M.T., and A.R. Calderwood, High-pressure metamorphism and uplift of the Olympic subduction complex, *Geology, 18*, 1252–1255, 1990.

Brandon, M.T., M.K. Roden-Tice, and J.I. Garver, Late Cenozoic exhumation of the Cascadia accretionary wedge in the Olympic Mountains, northwest Washington State, *GAS Bulletin, 110*, 985–1009, 1998.

Burbach, G.V., and C. Frohlich, Intermediate and deep seismicity and lateral structure of subducted lithosphere in the circum-Pacific region, *Rev. Geophys. Space Phys, 24*, 833–874, 1986.

Calladine, C.R., *Theory of Shell Structures*, 763 pp., Cambridge Univ. Press, Cambridge, 1983.

Carter, N.L., Steady state flow of rocks, *Rev. Geophys. Space Phys, 13 (3)*, 301–360, 1976.

Cassidy, J.F., and R.M. Ellis, *S* wave velocity structure of the northern Cascadia subduction zone, *J. Geophys. Res., 98*, 4407–4421, 1993.

Chiao, L.-Y., Membrane deformation rate and geometry of subducting slabs, PhD thesis, University of Washington, Seattle, 1991.

Creager, K.C., and T.M. Boyd, The geometry of Aleutian subduction: three-dimensional kinematic flow model, *J. Geophys. Res., 96*, 2293–2307, 1991.

Creager, K.C., L.A. Preston, R.S. Crosson, T. Van Wagoner, A.M. Tréhu, and the SHIPS98 working group, Three-dimensional reflection image of the subducting Juan de Fuca Plate, in *The Cascadia Subduction Zone and Related Subduction Systems*, edited by S.H. Kirby, K. Wang, and S.G. Dunlop, pp. 37–42, U.S. Geological Survey Open-File Report 02–328, Geological Survey of Canada Open File 4350, 2002.

Creager, K.C., J.P. Winchester, L.-Y. Chiao, and E.R. Engdahl, Membrane strain rates in the subducting plate beneath South America, *Geophys. Res. Lett., 22*, 2321–2324, 1995.

Crosson, R.S., and T.J. Owens, Slab geometry of the Cascadia subduction zone beneath Washington from earthquake hypocenters and teleseismic converted waves, *Geophys. Res. Lett., 14*, 824–827, 1987.

Davies, G.F., *Dynamic Earth: Plates, Plumes and Mantle Convection*, 458 pp., Cambridge University Press, Cambridge, 1999.

Davis, D., J. Suppe, and F.A. Dahlen, Mechanics of fold-and-thrust belts and accretionary wedges, *J. Geophys. Res., 88*, 1153–1172, 1983.

Davis, E.E., and R.D. Hyndman, Accretion and recent deformation of sediments along the northern Cascadia subduction zone, *Geo. Soc. Amer. Bull., 101*, 1465–1480, 1989.

Denlinger, R.P., A model for large-scale plastic yield of the Gorda deformation zone, *J. Geophys. Res., 97*, 15,415–15,423, 1992.

Hanks, T.C., and H. Kanamori, A moment magnitude scale, *J. Geophys. Res., 85*, 2348-2350, 1979.

Langston, C.A., and D.E. Blum, The April 29, 1965, Puget Sound earthquake and the crustal and upper mantle structure of western Washington, *Bull. Seismol. Soc. Amer., 67*, 693–711, 1977.

McNutt, M.K., Lithospheric flexure and thermal anomalies, *J. Geophys. Res., 89*, 11,180–11,194, 1984.

Nishimura, C., D.S. Wilson, and R.N. Hey, Pole of rotation analysis of present-day Juan de Fuca plate motion, *J. Geophys. Res., 89*, 10,283–10,290, 1984.

Owens, T.J., R.S. Crosson, and M.A. Hendrickson, Constraints on the subduction geometry beneath western Washington from broadband teleseismic waveform modeling, *Bull. Seismol. Soc. Amer., 78 (3)*, 1319–1334, 1988.

Page, R.A., C.D. Stephens, and J.C. Lahr, Seismicity of the Wrangell and Aleutian Wadati–Benioff zones and the North American plate along the trans-Alaska crustal transect, Chugach Mountains and Copper River Basin, southern Alaska, *J. Geophys. Res., 94*, 16,059–16,082, 1989.

Parlett, B.N., *The Symmetric Eigenvalue Problem*, 348 pp., Prentice-Hall, Englewood Cliffs, N. J., 1980.

Rasmussen, J., and E. Humphreys, Tomographic image of the Juan de Fuca plate beneath Washington and western Oregon using teleseismic *P*-wave travel times, *Geophys. Res. Lett., 15*, 1417–1420, 1988.

Ranalli, G., *Rheology of the Earth: Deformation and Flow Processes in Geophysics and Geodynamics*, 366 pp., Allen and Unwin Inc., Winchester, Massachusetts, 1987.

Rogers, G.C., Seismotectonics of British Columbia, PhD thesis, University of British Columbia, Vancouver, 1984.

Takahashi, E., and I. Kushiro, Melting of a dry peridotite at high pressure and basalt magma genesis, *Am. Mineralogist, 68*, 859–879, 1983.

Tréhu, A.M., T.M. Brocher, K.C. Creager, M.A. Fisher, L.A. Preston, G. Spence and the SHIPS98 Working Group, Geometry of the subducting Juan de Fuca plate: new constraints from SHIPS98, in *The Cascadia Subduc-*

tion Zone and Related Subduction Systems, edited by S.H. Kirby, K. Wang and S.G. Dunlop, pp. 25–32, U.S. Geological Survey Open-File Report 02–328, Geological Survey of Canada Open File 4350, 2002.

VanDecar, J.C., Upper-mantle structure of the Cascadia subduction zone from non-linear teleseismic inversion, PhD thesis, University of Washington, Seattle, 1991.

Weaver, C.S., and G.E. Baker, Geometry of the Juan de Fuca plate beneath Washington and northern Oregon from seismicity, *Bull. Seismol. Soc. Amer., 78*, 264–275, 1988.

Yamaoka, K., and Y. Fukao, Why do island arcs form cusps at their junctions?, *Geology, 15*, 34–36, 1987.

Yamaoka, K., Y. Fukao, and M. Kumazawa, Spherical shell tectonics: effects of sphericity and inextensibility on the geometry of the descending lithosphere, *Rev. Geophys., 24*, 27–55, 1986.

Crustal structure of the northern Juan de Fuca plate and Cascadia subduction zone—new results, old data

Ron M. Clowes
Earth and Ocean Sciences, The University of British Columbia, 6339 Stores Road, Vancouver, V6T 1Z4, Canada
clowes@lithoprobe.ubc.ca

Background

In 1980, the Vancouver Island Seismic Project (VISP 80; *Ellis et al*. [1983]) recorded a series of marine and onshore–offshore seismic refraction/wide-angle reflection (R/WAR) profiles on the Juan de Fuca plate and Vancouver Island. Most of the results from this experiment have been published. However, interpretation of crustal structure for the Juan de Fuca plate along profile VISP II (Figure 1), while completed for a decade, has never been published. The results are highly unusual, indicating a thickness of the oceanic plate, exclusive of sediments, in excess of ten kilometers near ocean bottom seismograph (OBS) 4 but just over seven kilometers near OBS 1.

In 1989, the Reflection-refraction Experiment–Cascadia Accretionary Prism (RECAP'89) was a "piggyback" experiment in which The University of British Columbia (UBC) deployed seismographs on Vancouver Island to record airgun shots fired along a series of profiles during an offshore multi-channel reflection survey acquired by the GSC in support of the Ocean Drilling Program [*Spence et al.,* 1991]. *Wang* [1997] has interpreted data from two lines, 89–03/02 and 89–09, recorded at sites 2A–B and 4A–B, respectively (Figure 1); however, the results have never been published. The crustal velocity structure models provide the only well-constrained interpretation of seismic velocities for the region underlying the continental shelf and slope, and thus have significance for accurate determination of earthquake hypocenters offshore.

Crustal velocity structure of northern Juan de Fuca plate

The VISP II refraction profile was recorded on three OBSs deployed at the ends and middle of a 110 km line oriented parallel to the margin on the ocean basin of the Juan de Fuca plate (Figure 1). An airgun source at 0.5 km spacing and explosive charges at ~2.5 km spacings were fired into the OBSs. A 3.5 kHz sounding profile and a single-channel reflection profile were acquired along the line to provide water depths, structure of the sediments and basement topography. Data from both the airgun and explosive sources were rich in direct, converted and multiple reflected refracted phases, as observed from vertical and horizontal component geophones and the hydrophone channel. From these phases, three one-dimensional velocity models were interpreted; these were interpolated to a two-dimensional starting model. Iterative forward modelling of travel times and amplitudes, using a two-dimensional, ray-theory-based synthetic seismogram program, RAYAMP, was used to interpret the final velocity structure model for line VISP II (Figure 2).

Two significant features of the VISP II model (Figure 2) are: 1) the large increase in oceanic crustal thickness, from ~7.5 km in the southern part of the model to ~10.5 km in the northern part, this increase being due almost entirely to the high velocity wedge (*hvw*) and the underlying low velocity layer (*lvl*) included in layer 3B; and 2) the decrease in velocity in the uppermost mantle in the northern half of the model, this being required by travel times of clear *Pn* phases recorded on the three OBSs.

Figure 3 is a map of the thickness of oceanic crust for northern Juan de Fuca and Explorer plates compiled from VISP II and other refraction interpretations and from multi-channel seismic reflection travel times, converted to depths using 6.5 km/s, for data on which oceanic Moho could be readily identified. The pronounced increase of >3 km in crustal thickness of the Juan de Fuca plate near the Nootka transform fault zone is the most prominent feature. An enigma is the lack of a corresponding anomaly in the free air gravity field. The position of the thickened crust may have relevance for the hypothesis that the Explorer plate is in the process of being dismembered and a new Pacific–North American plate boundary is being established [*Rohr and Furlong,* 1995], because the southern end of the latter coincides approximately with the thickened crust. An alternative or additional explanation for the thickened crust may be asymmetric magma accretion associated with the outside corner of the Juan de Fuca Ridge–Sovanco transform junction, similar to results from recent studies of the Mid-Atlantic Ridge [*Allerton et al.,* 2000].

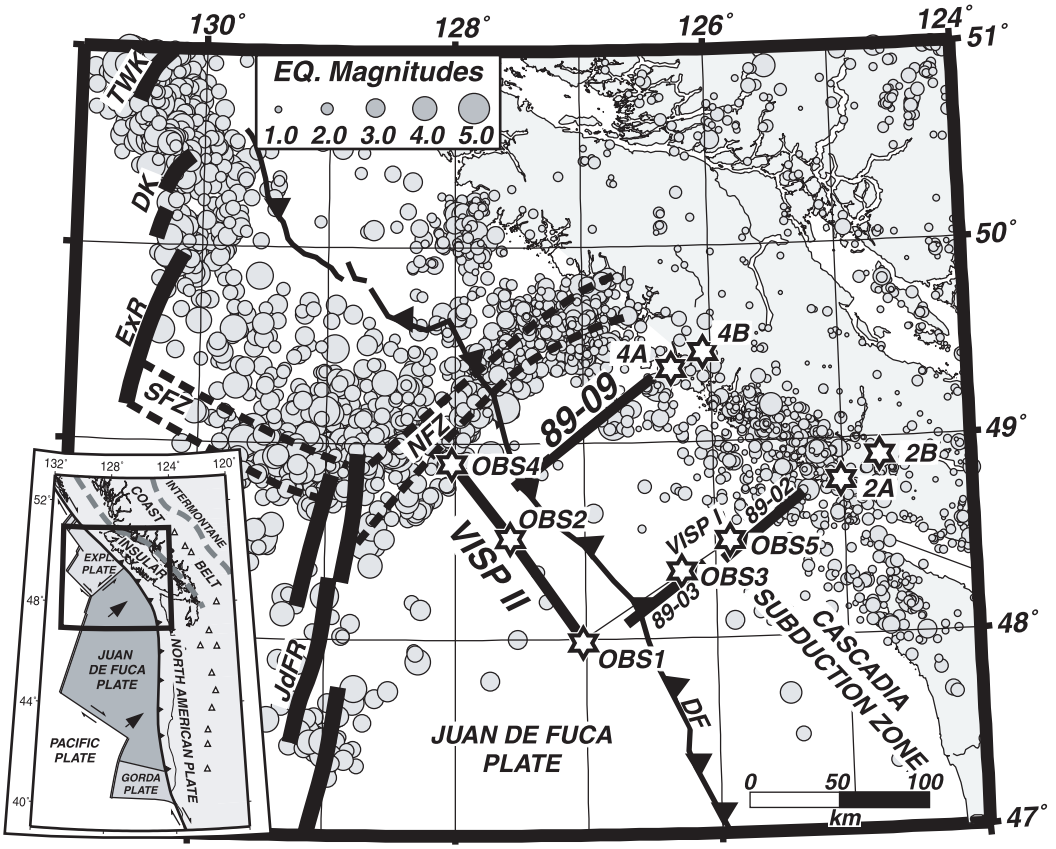

FIGURE 1: Location of seismic refraction/wide-angle reflection studies discusssed in this contribution on a seismicity map of Vancouver Island and the offshore region. New results are presented for the Vancouver Island Seismic Project (VISP) II (Figure 2) from ocean bottom seismographs (OBS) 1, 2 and 4 on the northern Juan de Fuca plate; VISP I (OBSs 1, 3 and 5) has been published. Also, new results are presented for the northern Cascadia subduction zone: airgun reflection lines 89–03/89–02 recorded at land stations 2A and 2B and line 89–09 recorded at land stations 4A and 4B (Figure 4). DF, deformation front; DK, Dellwood Knolls; ExR, Explorer Ridge; JdFR, Juan de Fuca Ridge; NFZ, Nootka fault zone; SFZ, Sovanco fracture zone; TWK, Tuzo Wilson Knolls. Inset shows location of main map area within the Juan de Fuca plate system.

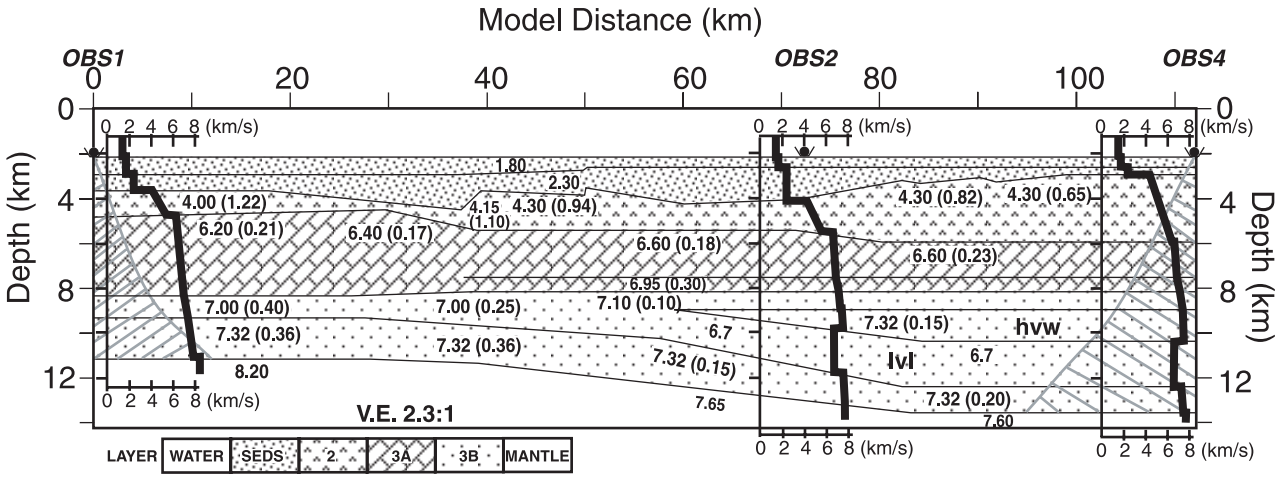

FIGURE 2: VISP II velocity structure model with primary oceanic crustal layers identified. Velocities (km/s) at the top of layers and the velocity gradients (km/s/km) in the layers (numbers in parentheses) are shown on the model. Velocity-depth profiles at the position of each ocean bottom seismograph (OBS) are superimposed. Grey lined region is not constrained by the data.

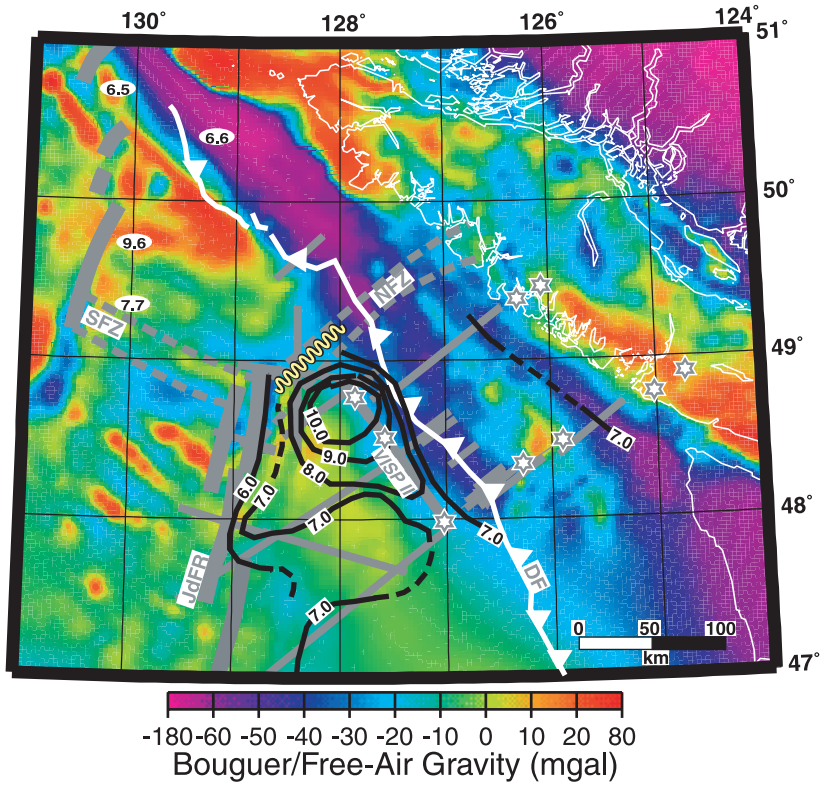

FIGURE 3: Contours (heavy black lines) and point determinations (numbers in white ellipses) of thicknesses of the oceanic plates in kilometers from Vancouver Island Seismic Project (VISP) II and other refraction and reflection lines (thin grey lines) in the offshore region superimposed on a free air/Bouguer gravity anomaly map. Thick and dashed grey lines outline tectonic elements, with same abbreviations as Figure 1. Wiggly line in the Nootka fault zone (NFZ) indicates a possible vertical offset in crustal thickness.

Crustal velocity structure of the Cascadia subduction zone

For RECAP'89, four continuous recording seismographs at eight land sites on the west coast of Vancouver Island acquired good quality data from airgun sources fired at 50 m intervals along four offshore mulit-channel seismic (MCS) reflection lines; two of these lines recorded at four stations have been interpreted (Figure 1). Four principal phases—refractions through the upper continental crust, reflections from the top of the oceanic crust and the Moho, and refractions through the oceanic mantle—were identified. An iterative combination of two-dimensional travel time inversion and amplitude forward modeling was used to interpret crust and upper mantle *P*-wave velocity structure.

Figure 4 shows the final velocity structure model for line 89–09; that for 89–02/03 is similar in general, but has differences in detail. Velocities for the accretionary wedge and Pacific Rim terrane are well constrained; they increase landward and with depth. The crust of the subducting Juan de Fuca plate is defined well by the wide-angle reflection data; along 89–09, the top of the plate is ~2 km shallower than that along 89–02/03 below the ocean basin, and 3–4 km shallower below the continental slope. Whereas profile 89–02/03 required a substantial down plate increase in velocity, this feature was not required for 89–09. For both profiles, average oceanic upper mantle velocities of ~8.0 km/s were determined, although some unusual lateral variations were interpreted; these must be viewed with caution due to relatively poor resolution in this part of the model. These results are the first velocity models for the region below the continental shelf and slope that are well constrained by turning and reflected ray paths in that region. Given that most earthquakes in southwestern Canada occur offshore (Figure 1) but are located primarily from stations located on land, an improved velocity structure for the region between the hypocenters and the stations should lead to more reliable earthquake locations.

Acknowledgements

W.R. Hugh White of Toronto, Ontario, now retired and formerly with Centennial College in Toronto, carried out a detailed interpretation of the VISP II profile during and following a one-year study leave period at the University of British Columbia in 1981–82. Carl Wang, now working in the petroleum industry in Calgary, Alberta,

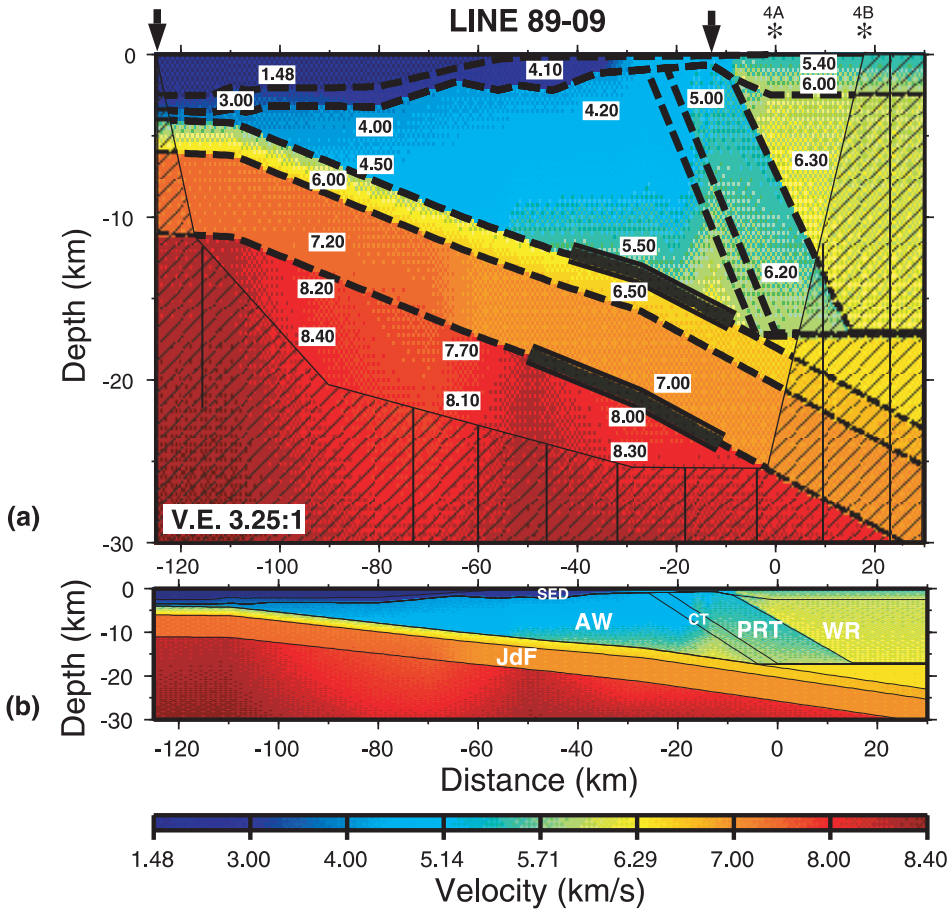

FIGURE 4: a) Velocity structure model for profile 89–09: airgun shots at 50 meter intervals between arrows at top of model were recorded at stations 4A and 4B. Numbers within model represent *P*-wave velocities in km/s at those positions. Dashed lines are boundaries for model layers or blocks; heavy solid lines are boundaries from which wide-angle reflections were observed. b) Velocity structure model with 1:1 representation. SED, sedimentary layer; AW, accreted wedge; CT, Crescent terrane; PRT, Pacific Rim terrane; WR, Wrangellia; JdF, Juan de Fuca plate.

carried out interpretation of profiles 89–02/03 and 89–09 for his M.Sc. at the University of British Columbia.

References

Allerton, S., J. Escartin, and R.C. Searle, Extremely asymmetric magmatic accretion of oceanic crust at the ends of slow-spreading ridge segments, *Geology, 28,* 179–182, 2000.

Ellis, R.M., G.D. Spence, R.M. Clowes, and 13 others, The Vancouver Island seismic project: a COCRUST onshore–offshore study at a convergent margin, *Can. J. Earth Sci., 20,* 719–741, 1983.

Rohr, K.M.M., and K.P. Furlong, Ephemeral plate tectonics at the Queen Charlotte triple junction, *Geology,* 23**,** 1035–1038, 1995.

Spence, G.D., R.D. Hyndman, S. Lanton, C.J. Yorath, and E.E. Davis, Multi-channel seismic reflection profiles across the Vancouver Island continental shelf and slope, *Geological Survey of Canada, Open File 2391,* 1991.

Wang, C.X., Structure of the Cascadia subduction zone off Vancouver Island: new evidence from seismic refraction data, M.Sc. thesis, University of British Columbia, Vancouver, 1997.

Seismic reflection imaging of the Cascadia plate boundary offshore Vancouver Island

Andrew Calvert
Department of Earth Sciences, Simon Fraser University, Burnaby, British Columbia, V5A 1S6, Canada
acalvert@sfu.ca

Two seismic reflection surveys have been shot over the continental slope and shelf of the convergent margin offshore Vancouver Island, in 1985 and 1989 (Figure 1). The 1989 survey, which is shown here and discussed more fully by *Calvert* [1996], was shot using a tuned airgun array with a total volume of 128 l (7820 in^3), and recorded by a 144 channel hydrophone streamer with a 25 m group interval and 3600 m far offset. The 50 m shot point separation provided 36 fold data. The recording parameters for the earlier 1985 survey are similar to those used in the 1989 survey, with the exception that a 120-channel streamer was then employed. The processing sequences applied to the data from both surveys are essentially similar, consisting of amplitude recovery, designature, *F–K* filter, predictive deconvolution to suppress multiples, velocity analysis, normal moveout correction, and stack. A post-stack predictive deconvolution was also applied in order to suppress water-bottom reverberations. A constant velocity migration using a value of 1500 ms^{-1} was applied to each line to focus waterborne coherent noise that contaminates a number of the profiles; the noise appears in the unmigrated data as broad hyperbolae at late record times. A dynamic amplitude equalization was then applied to reduce the amplitude of the focussed coherent noise relative to the rest of the profile and followed by a residual migration.

Both vintages of seismic data image structural boundaries in both the sedimentary prism and two accreted terranes. The subduction décollement, which separates the oceanic crust of the descending Juan de Fuca plate from the overlying continental units, is observed intermittently on the seismic profiles from the area (Figure 2). At the base of the continental slope, thrust faults within the incoming sedimentary section sole out close to the top of the igneous oceanic crust, suggesting that the subduction décollement occurs close to the top of the igneous crust even though it cannot be identified directly [*Davis and Hyndman, 1989*]. The top of the oceanic crust seaward of the continental slope is marked by a high amplitude two-cycle reflection. However, beneath the continental slope this reflection evolves into the broader (in time) zone of reflectivity that characterizes the plate boundary beneath the continental shelf [*Calvert and Clowes, 1990*]. The amplitude of the seismic reflection from the plate boundary appears to vary in both dip and strike directions. The variation normal to the margin is mainly attributable to the difficulty in obtaining a consistent image of the plate boundary beneath the strong lateral variations in seismic velocity caused by the rugged topography at the top of the accretionary wedge. However, amplitude variations parallel to the margin, particularly beneath the volcanic Crescent terrane, where near-surface conditions change slowly, may well be attributable to changes in physical properties at the plate boundary. Close to southern Vancouver Island, the plate boundary reflection splits in two: the upper high-amplitude reflection package continues into the broad band of '*E*' reflectivity identified beneath Vancouver Island; and the lower weaker, short duration reflection marks the top of the descending oceanic plate. This splitting of the plate boundary reflection is interpreted to occur at the seaward edge of a slab of mafic material underplated to southern Vancouver Island and is not observed further north (Figure 3).

References

Calvert, A.J., and R.M. Clowes, Deep, high amplitude reflections from a shear zone above the subducting Juan de Fuca plate, *Geology*, 18, 1091–1094, 1990.

Calvert, A.J., Seismic reflection constraints on imbrication and underplating of the northern Cascadia convergent margin, *Can. J. Earth Sci.*, 33, 1294–1307, 1996.

Davis, E.E., and R.D. Hyndman, Accretion and recent deformation of sediments along the northern Cascadia subduction zone, *Bull. Geol. Soc. Am.*, 101, 1465–1480, 1989.

Dehler, S.A., and R.M. Clowes, Integrated geophysical modelling of terranes and other structural features along the western Canadian margin, *Can. J. Earth Sci.*, 29, 1492–1508, 1992,

Hyndman, R.D., C.J. Yorath, R.M. Clowes, and E.E. Davis, The northern Cascadia subduction zone at Vancouver Island: seismic structure and tectonic history, *Can. J. Earth Sci.*, 27, 313–329, 1990.

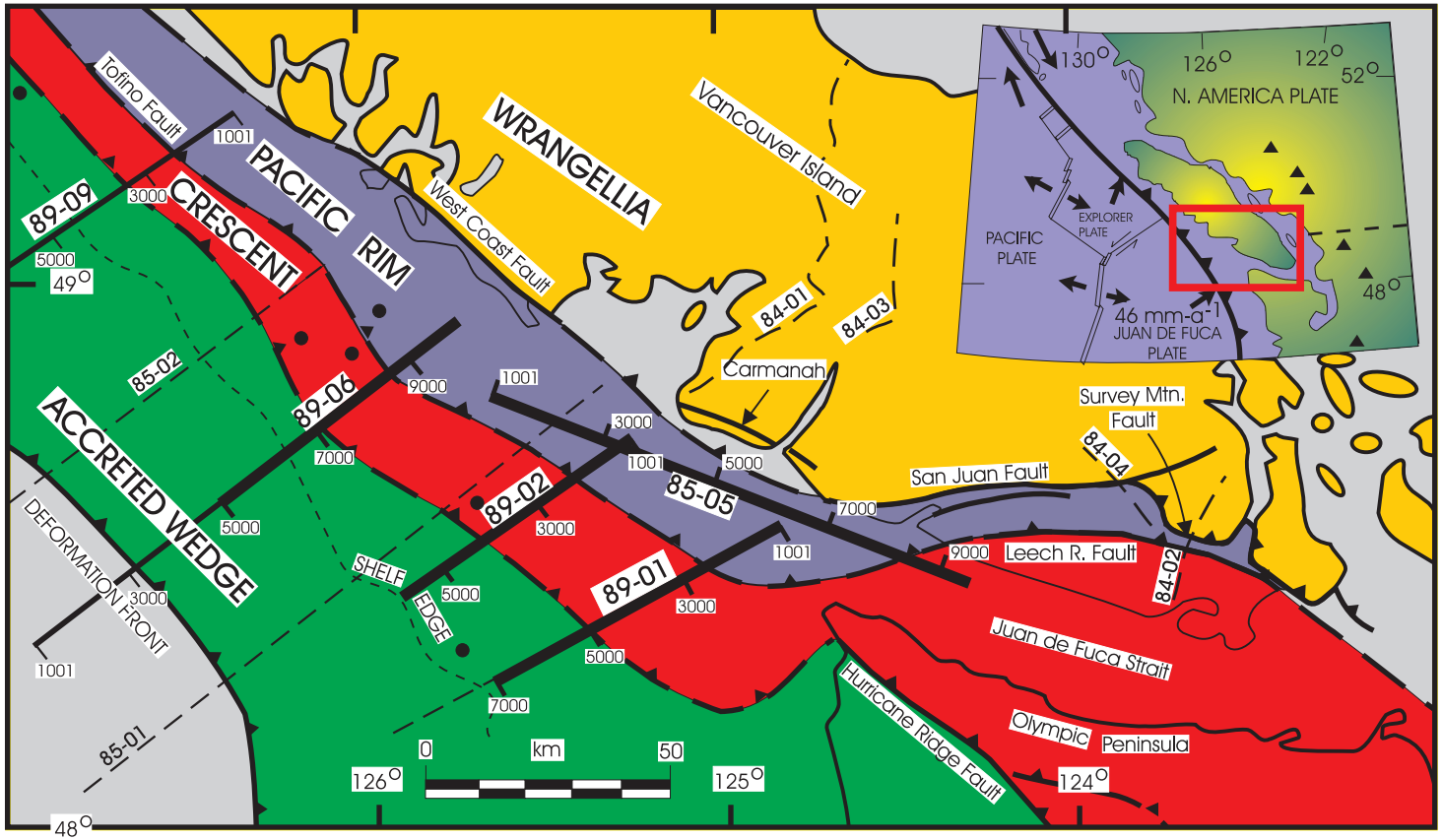

FIGURE 1: Location of the major terranes beneath the Tofino basin in the southern part of the Canadian convergent margin (after *Hyndman et al.* [1990] and *Dehler and Clowes* [1992]). Offshore, the terrane boundaries are defined by magnetic data and the indicated seismic lines; onshore, geological mapping and potential field data are the primary constraints. The location of the multi-channel seismic lines which extend over the continental shelf are shown. CMP numbers are annotated to lines shown here.

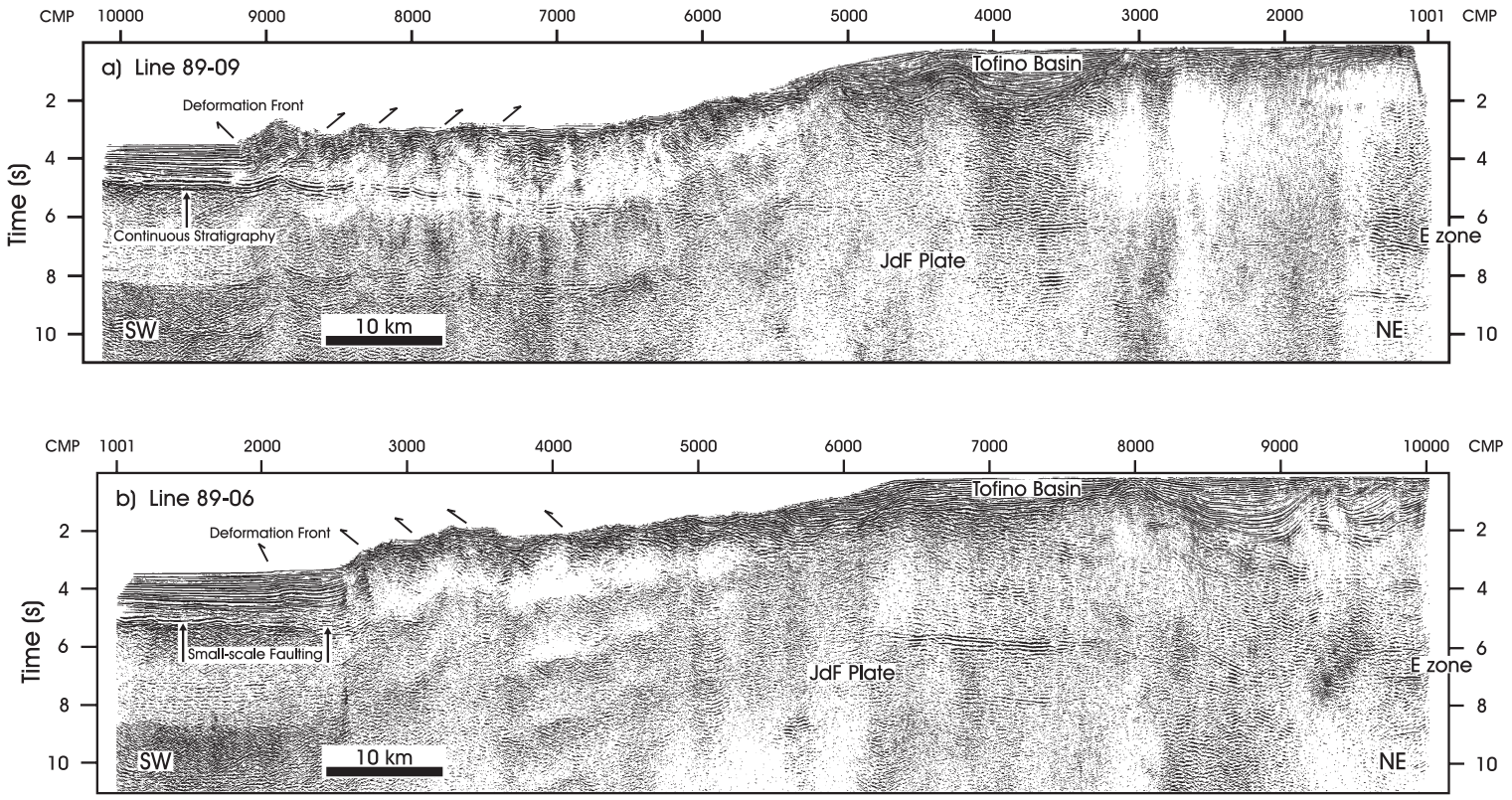

FIGURE 2: a) Line 89–09. b) Line 89–06. Both seismic profiles are displayed after migration with a velocity of 1500 ms^{-1} to focus water-borne coherent noise. The undeformed stratigraphy above the igneous oceanic crust can be seen at the seaward end of both profiles. High amplitude reflections arising in accreted sediments just above the subducting igneous crust can be followed beneath the continental slope on line 89–09 where the incoming sediments are deformed and incorporated into the accretionary wedge. In contrast, strong reflections from the top of the subducting crust do not extend seaward of the continental shelf on line 89-06. Arrows indicate the approximate position and orientation of some thrusts in the sedimentary prism. Both seismic lines are displayed with no time-varying gain in order to permit an approximate comparison of the reflection amplitudes. The changing water depth, the presence of multiple reflections, and lateral velocity variations arising from deformation of wedge and slope sediments prevent detailed interpretation of the seismic data beneath the continental slope.

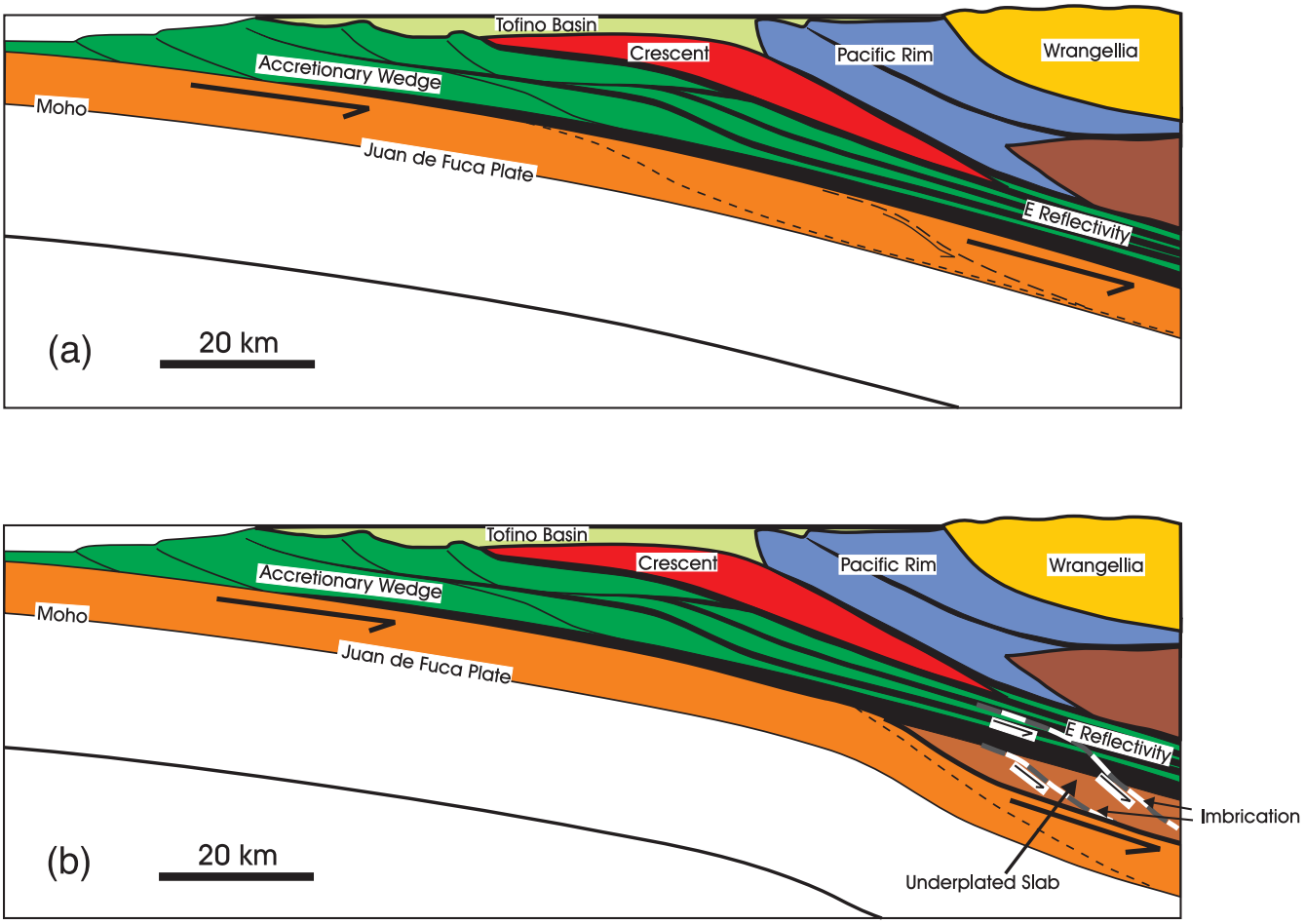

FIGURE 3: Cartoon showing a generalized interpretation of the main features observed in the offshore reflection profiles normal to the margin, and a possible model for formation of the zone of *E* reflectivity. Vertical exaggeration is approximately 1:1. a) Following accretion of the Crescent and Pacific Rim terranes, subduction continued for some time with the subduction décollement lying at the top of the subducting igneous crust. As a result, underthrust sediments were sheared at the interplate décollement forming the *E* reflections. Some time later, the subduction thrust stepped down into the igneous oceanic crust, possibly as a result of reactivation of a pre-existing fault. b) A slab, originally from the downgoing plate, was underplated to the base of the overlying continent. Continuing subduction resulted in some deformation and shortening of the overlying slab and parts of the *E* region. A number of earthquakes presently occur within the downgoing slab beneath the west coast of Vancouver Island. They may be the result of deformation in the subducting slab as it is thrust beneath the underplated region.

An image of the Cascadia subduction zone across central Oregon

Stephane Rondenay and Michael G. Bostock
Earth and Ocean Sciences, The University of British Columbia, 6339 Stores Road, Vancouver, V6T 1Z4, Canada
rondenay@emma.geo.brown.edu, bostock@geop.ubc.ca

Between May 1993 and April 1994, researchers from Oregon State University deployed an array of broadband, three-component seismometers across central Oregon [*Li*, 1996]. The array recorded 32 high-quality teleseisms from a total of approximately 70 receiver locations spaced at five kilometer intervals and occupied at various times during the recording period. Conventional, receiver-function processing of the data set by *Li* [1996] and *Li and Nabelek* [1999] identified free-surface multiples as the most prominent signal from the subducting slab. However, because of the effect of moveout from dipping structure, only forward modeling of individual events was performed.

We have developed a method of formally inverting the teleseismic *P*-wave coda recorded on dense arrays of receivers for underlying, two-dimensional elastic structure. The method accommodates both forward scattering of the incident wavefield and the back-scattering response created by free-surface multiples. Recordings from multiple earthquakes can, moreover, be inverted simultaneously. We have applied this method to the Oregon data set. We image the two principal structural features inferred by *Li* [1996], notably: 1) the appearance of a prominent continental Moho some 150 km from the coast line near 40 km depth; and 2) the low-velocity oceanic crust of the Juan de Fuca plate dipping at 10° beneath North America. In addition, however, we image a disruption in the signature of subducted oceanic crust which commences approximately 50 km from the coastline, and which appears to coincide with an increase in dip of the down-going plate. This disruption coincides with the appearance of enhanced mantle conductivity imaged in an earlier magnetotelluric (MT) experiment (EMSLAB, e.g. *Wannamaker et al.,* [1989]) along the same profile.

The coincidence of seismic and MT anomalies is consistent with an interpretation involving dehydration reactions in the subducted crust occurring near 30 km depth. Following *Hyndman* [1988], we infer that low velocities above the oceanic plate manifest the upward expulsion of hydrous fluids and their entrapment by an impermeable interface. This interface may represent the locus of rehydration reactions producing an effective seal or it may be structurally controlled. Similar interpretations of geophysical data from the northern Cascadia subduction zone and central Andes strongly suggest that hydration reactions in the oceanic crust may play an important role in controlling the physical properties in the overlying wedge.

References

Hyndman, R.D., Dipping seismic reflectors, electrically conductive zones, and trapped water in the crust over a subducting plate, *J. Geophys. Res., 93,* 13,391–13,405, 1988.

Li, X.-Q., Deconvolving orbital surface waves for the source duration of large earthquakes and modeling the receiver function for the earth structure beneath a broadband seismometer array in the Cascadia subduction zone, Ph.D. Thesis, Oregon State University, Corvallis, Oregon, 1996.

Li, X.-Q., and J.L. Nabelek, Deconvolution of teleseismic body waves for enhancing structure beneath a seismometer array, *Bull. Seismol. Soc. Am., 89,* 190–201, 1999.

Wannamaker, P.E., J.R. Booker, A.G. Jones, A.D. Chave, J.H. Filloux, H.S. Waff, and L.K. Law, Resistivity cross section through the Juan de Fuca subduction system and its tectonic implications, *J. Geophys. Res., 94,* 14,127–14,144, 1989.

Intraslab earthquakes beneath Georgia Strait/Puget Sound

Garry C. Rogers[1] and Robert S. Crosson[2]
1 Pacific Geoscience Centre, Geological Survey of Canada, PO Box 6000, Sidney, British Columbia, V8L 4B2, Canada
2 Geophysics Program, University of Washington, PO Box 351650, Seattle, Washington, 98195–1650, USA
rogers@pgc.nrcan.gc.ca, crosson@u.washington.edu

Observations of earthquakes in the northern half of the Cascadia subduction zone can be divided into three time periods: pre-instrumental from about 1850 and 1899, early instrumental from about 1900 to 1969, and modern instrumental from about 1970 to present. The micro-earthquake pattern revealed in the modern instrumental period, shows most of the seismicity in the slab to be in the 40 to 60 km depth range beneath southern Georgia Strait and Puget Sound (Figure 1). Some very small events extend to maximum depths of about 90 km. The seismicity maps out a gentle arch in the subducted plate opposite the change in orientation of the coastline. The main concentration is in a band paralleling the coastline and decreasing in intensity to the north and to the south. Focal mechanisms are variable amongst the small events but most of the larger events have a downdip tension axis in common.

Most of the larger events (Table 1; Figure 2) occurred in the early instrumental period from 1900 to 1970. Locations are teleseismic in the early part of that period but improve with time as the number of seismographs in the region increases and timing becomes more accurate. Depth control is poor for many events in this period, but the low intensities in the epicentral region or lack of aftershocks suggest that some events belong to the deeper inslab suite of events. The locations of the larger ($M>5$) events occur in the region of the modern day concentration of micro-earthquakes beneath southern Georgia Strait and Puget Sound. The two largest events in 1965 ($M_w=6.7$) and 1949 ($M_w=6.8$) occurred near the south end of the modern micro-earthquake concentration.

In the pre-instrumental period from about 1850 to 1899, it appears there were no events greater than magnitude 6.5. The population was sparse during the early part of this period, but for a few widely felt earthquakes, the lack of aftershocks or low intensities in the epicentral region suggest that they were subcrustal in-slab events.

Recent reviews of various aspects of seismicity in the region have been published in the Decade of North American Geology (DNAG) volumes [*Ludwin et al.,* 1991; *Rogers and Horner,* 1991] and in papers contributed to volumes published by the USGS [*Ma et al.,* 1996] and the GSC [*Rogers,* 1998]. These papers include discussions on in-slab seismicity and a complete listing of publications.

References

Ludwin, R.S., C.S. Weaver, and R.S. Crosson, Seismicity of Washington and Oregon, in *Neotectonics of North America, Decade Map Volume 1,* edited by D.B. Slemmons, E.R. Engdahl, M.D. Zoback and D. Blackwell, pp. 77–98, The Geological Society of America, Boulder, Colorado, 1991.

Ma, L., R.S. Crosson, and R. Ludwin, Western Washington earthquake focal mechanisms and their relationship to regional tectonic stress, in *Assessing earthquake hazard and reducing risk in the Pacific Northwest, United States Geological Survey Professional Paper 1560, v.1,* edited by A.M. Rogers, T.J. Walsh, W.J. Kockelman and G.R. Priest, pp. 257–283, 1996.

Rogers, G.C., Earthquakes and earthquake hazard in the Vancouver area, in *Geology and Natural Hazards of the Fraser River Delta, British Columbia, Geological Survey of Canada, Bulletin 525,* edited by J.J. Clague, J.L. Luternauer and D.C. Mosher, pp. 17–25, Geological Survey of Canada, 1998.

Rogers, G.C. and R.B. Horner, An overview of western Canadian seismicity, in *Neotectonics of North America, Decade Map Volume 1,* edited by D.B. Slemmons, E.R. Engdahl, M.D. Zoback and D. Blackwell, pp. 127–130, The Geological Society of America, Boulder, Colorado, 1991.

TABLE 1: Larger known or suspected in-slab earthquakes beneath Georgia Strait and Puget Sound.

Date (yr/mon./day)	Time (hr/min./sec.)	Latitude	Longitude	Depth[1] (km)	Magnitude[2]	Source
1909 01 11	2349	48.7	-122.8	DEEP	6.0	no aftershocks, low I
1920 01 24	0710 0.0	48.6	-123.0	DEEP	5.5	no aftershocks
1939 11 13	0745 53.0	47.4	-122.6	DEEP	6.2	no aftershocks, low I
1943 11 29	0143	48.4	-122.9	DEEP	4.8	no aftershocks
1946 02 15	0314 50.0	47.3	-122.9	DEEP	6.4	UW publication
1949 04 13	1955 41.0	47.13	-122.95	54	6.9	publications
1960 09 10	1506 33.6	47.68	-123.18	60	4.9	PGC
1965 04 29	1528 43.6	47.4	-122.3	63	6.7	publications
1965 10 23	1628 3.0	47.5	-122.4	DEEP	4.8	ISC 64 km
1969 02 14	0833 36.0	48.94	-123.07	52	4.3	PGC/ISC
1976 05 16	0835 15.1	48.80	-123.35	60	5.4	PGC
1976 09 08	0821 2.0	47.38	-123.08	48	4.6	NEIC
1978 08 19	0151 18.8	48.64	-123.58	52	4.3	PGC
1983 08 28	1247 48.0	47.93	-122.85	51	4.1	UW
1989 03 05	0642 0.6	47.81	-123.36	46	4.6	UW
1989 06 18	2038 37.3	47.41	-122.78	45	4.1	UW
1999 07 03	0143 29.0	47.10	-123.50	41	5.7	UW

1. If there is a number in the depth column, it has been calculated by the agency in the last column or has been the object of a published study. The word DEEP means it has been assigned to the deep suite for the reason listed in the last column.
2. Magnitude values are M_w when known.

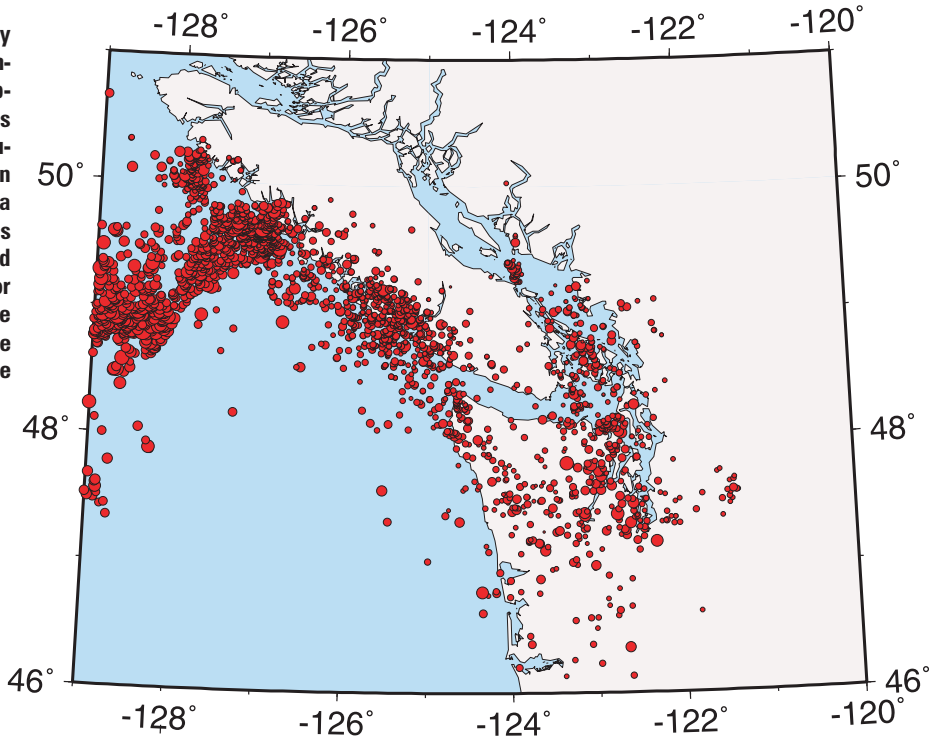

FIGURE 1: Fifteen years of seismicity within the oceanic plate. At the northernmost end of active Cascadia subduction, a band of seismicity exists beneath the west coast of Vancouver Island and another concentration exists beneath southern Georgia Strait and Puget Sound. Circle size is related to earthquake magnitude and ranges from magnitude about zero for the smallest circles to an offshore event of magnitude 6.3. Data from the Geological Survey of Canada and the University of Washington.

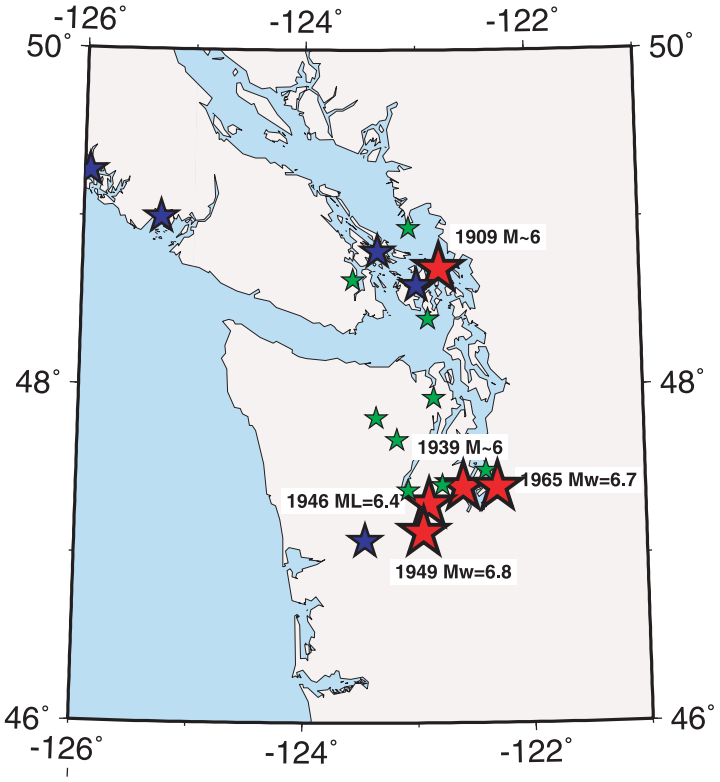

FIGURE 2: Larger earthquakes within the subducting plate. Green stars are magnitude 4 and greater (complete from 1951). Blue stars are 5 and greater (complete from 1899). Red stars are magnitude 6 and greater events, complete from about 1865.

Precise relocations of slab seismicity in the northern Cascadia subduction zone

John F. Cassidy[1] and Felix Waldhauser[2]
1 Pacific Geoscience Centre, Geological Survey of Canada, PO Box 6000, Sidney, British Columbia, V8L 4B2, Canada
2 United States Geological Survey, 345 Middlefield Road, Menlo Park, California, 94025, USA
cassidy@pgc.nrcan.gc.ca, felix@usgs.gov

ABSTRACT

The Gulf Islands region of southwest British Columbia is an ideal location to study, in detail, slab seismicity of the subducting Juan de Fuca plate. Here, there is abundant slab seismicity, a relatively dense network of seismograph stations to obtain accurate hypocenters and some recently deployed three-component broadband stations to constrain the velocity structure. We have relocated slab seismicity near 50–60 km depth in the Gulf Island region using a "double difference" earthquake relocation algorithm designed to provide high-resolution relative hypocenter locations over large distances. The precise relative locations obtained for an initial test set of 27 deep earthquakes in a narrow corridor near Saturna Island, B.C., indicates that most of the slab seismicity here is in a three to four kilometer-thick region dipping at 20° to the northeast. There is some suggestion of a deeper parallel band of seismicity (7–9 km) below the top of the upper band that may be located in the upper mantle of the Juan de Fuca plate.

Introduction

The Cascadia subduction zone is a seismically active region (Figure 1) with three distinct types of earthquakes [*Rogers*, 1998]: those in the continental crust (black dots in Figure 1); those in the subducting oceanic plate (red dots in Figure 1); and megathrust earthquakes that occur on the megathrust fault between the oceanic and continental plates. Of the three types, those that occur within the oceanic plate ("in-slab earthquakes", see Figure 2) pose the greatest hazard to the major cities in the region. The processes that cause these earthquakes and that limit their maximum size and spatial distribution are not well-understood.

We applied a new, high-resolution "double-difference" earthquake location algorithm (Figure 3) of *Waldhauser and Ellsworth* [2000] to obtain precise relative hypocentral locations for deep earthquakes (Figure 2) over distances of up to 40–60 km near Saturna Island, B.C. This is an ideal location to examine deep seismicity as there is a relatively dense seismograph network (Figure 2) that can be used to obtain accurate earthquake hypocenters and for utilizing waveform cross-correlation techniques, as well as a recently deployed three-component broadband station that can be used for structural studies. This allows us to examine the relationship between the structure and well-resolved seismicity of the subducting slab. In this study, we report on the results obtained using the double-difference technique with catalog data only, for test sets of up to 27 deep earthquakes.

Data and analysis method

For these tests we selected deep earthquakes (>40 km) that lie within a 20-km wide corridor about 70 km long, centered near the Saturna Island seismic station (SNB, Figure 4). The initial locations (Figure 4) are taken from the Canadian Earthquake Epicentre File and were determined using standard location methods, with *P*- and *S*-wave arrival times from regional stations.

In the double-difference earthquake relocation scheme, *P*- and *S*-wave differential travel times for all possible pairs of events are minimized. Solid and open circles represent trial hypocenters that are linked to neighboring events by cross-correlation (solid lines) or catalog data (dashed lines). For two events, *i* and *j,* the initial locations (open circles) and corresponding slowness vectors *s* with respect to two stations, *k* and *l*, are shown. Ray paths from the sources to the stations are shown. Thick arrows (Δx) indicate the relocation vector for events *i* and *j* obtained from the full set of equations. Dt is the travel time difference between the events *i* and *j* observed at stations *k* and *l*, respectively. For details of the method, see *Waldhauser and Ellsworth* [2000].

Results and summary

The initial earthquake locations (Figure 4) show a band of seismicity as much as 10–15 km thick, dipping to the northeast.

Applying the double-difference earthquake location scheme to these deep earthquakes in the vicinity of Saturna Island, we find that the band of seismicity

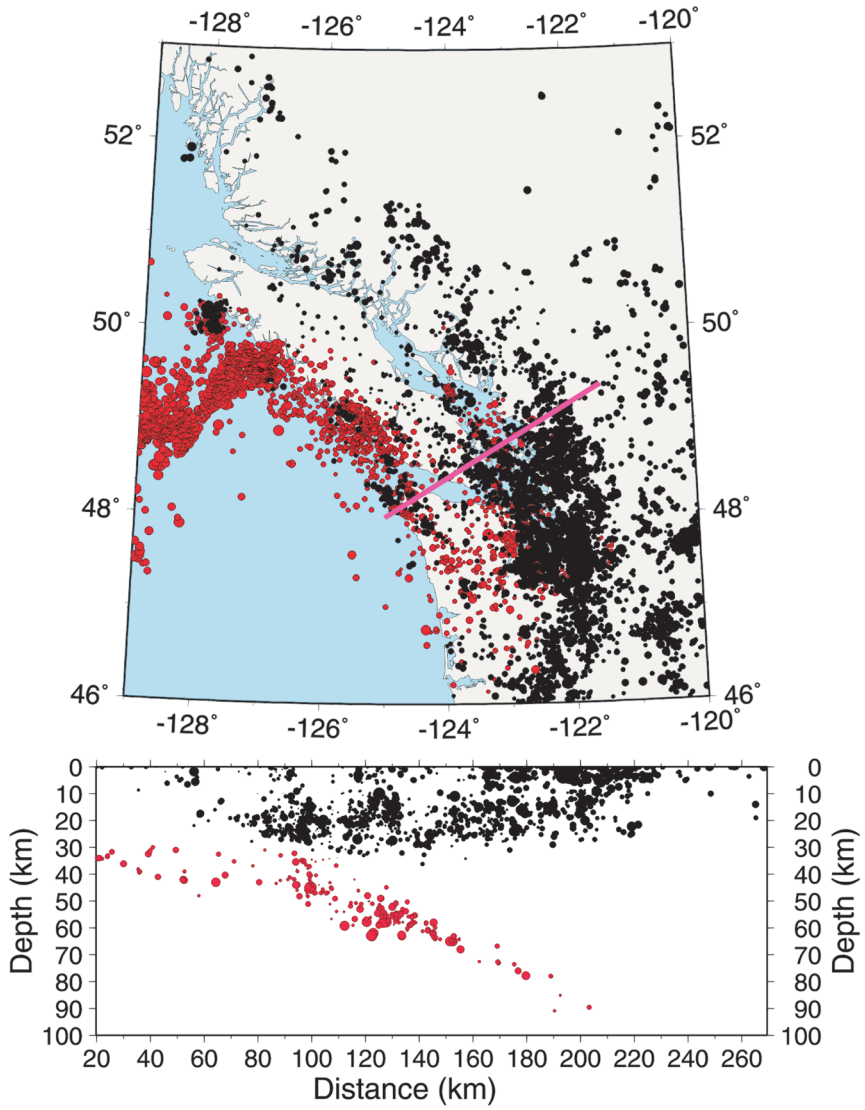

FIGURE 1: Cascadia seismicity during the period 1985–1999. Red dots indicate earthquakes within the oceanic plate, black dots are earthquakes within the continental plate. Earthquake magnitudes range from 0 to 5.5. Cross section shows seismicity along a 50 km-wide corridor centered on the line A–B.

narrows considerably, to become less than about five kilometers thick and dipping at 20° to the northeast (Figure 5). There is the suggestion of two bands of seismicity, separated by approximately five kilometers. It is noteworthy that the location of the upper band corresponds with the low-velocity zone interpreted as the oceanic crust beneath the Pacific Geoscience Centre (PGC) [*Cassidy*, 1995]. This would suggest that the lower band may fall within the uppermost mantle of the subducting Juan de Fuca plate. Tests using various subsets of the data, for example, the subset of events that lie within the 20 km x 30 km rectangular region shown in Figure 5, show these relative hypocentral locations to be robust.

Acknowledgements

We thank Taimi Mulder for her assistance in collecting the catalog data and Richard Franklin for his assistance with figure preparation. Many diagrams were generated using Generic Mapping Tools (GMS) [*Wessell and Smith*, 1995].

References

Cassidy, J.F., A comparison of the receiver structure beneath stations of the Canadian National Seismograph Network, *Can. J. Earth Sci., 32*, 938–951, 1995.

Rogers, G.C., Earthquakes and earthquake hazard in the Vancouver area, in *Geology and Natural Hazards of*

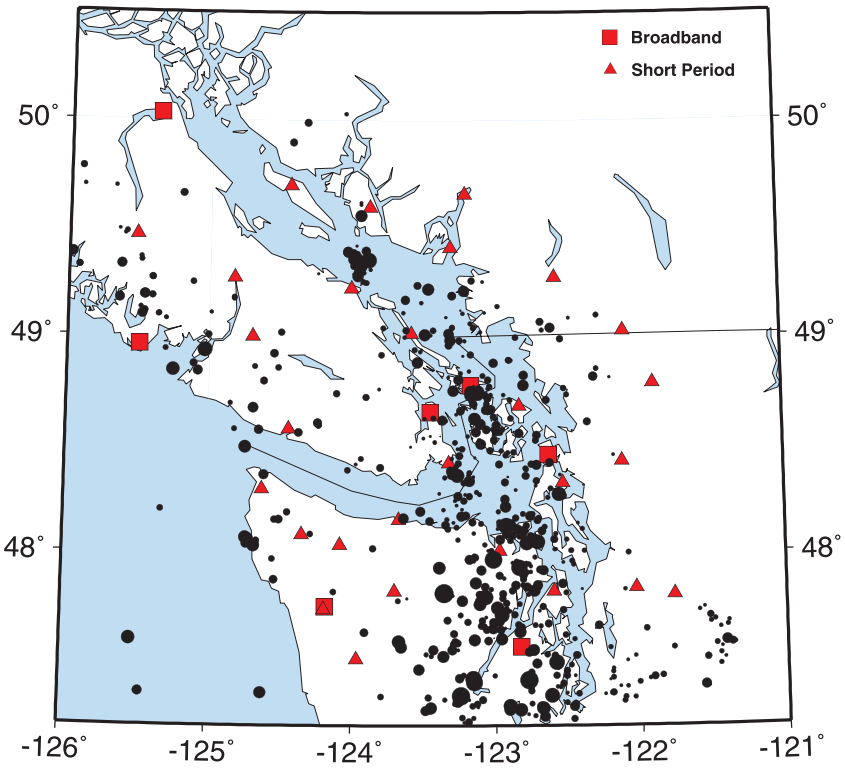

FIGURE 2: Location of seismograph stations (squares are three-component broadband, triangles represent short-period vertical) and the location of deep (>40 km depth) slab seismicity. Magnitudes range from 0 to 4.5.

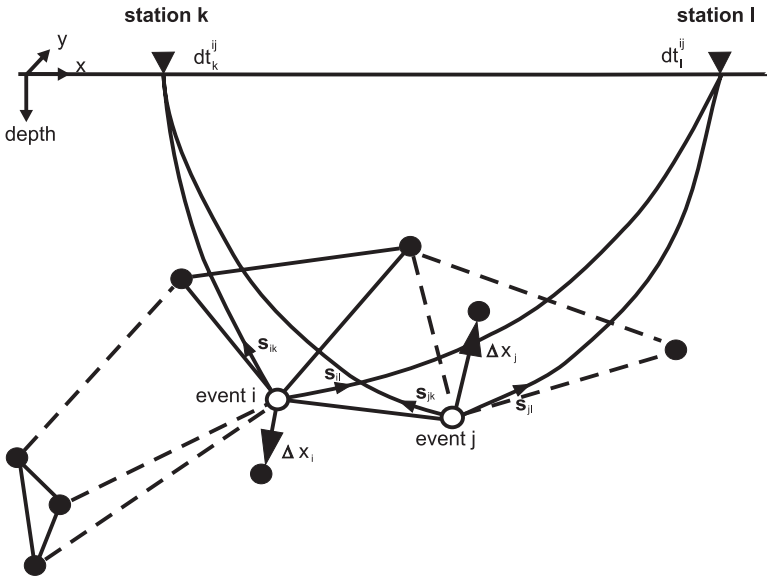

FIGURE 3: Illustration of the double-difference earthquake relocation technique (from *Waldhauser and Ellsworth* [2000]). Solid and open circles represent trial hypocenters that are linked to neighboring events by cross-correlation (solid lines) or catalog data (dashed lines). For two events, *i* and *j*, the initial locations (open circles) and corresponding slowness vectors *s* with respect to two stations, *k* and *l*, are shown. Ray paths from hypocenters to the stations are shown. Thick arrows (x) indicate the relocation vector for events *i* and *j*. *Dt* is the travel-time difference between the events *i* and *j* observed at stations *k* and *l*, respectively.

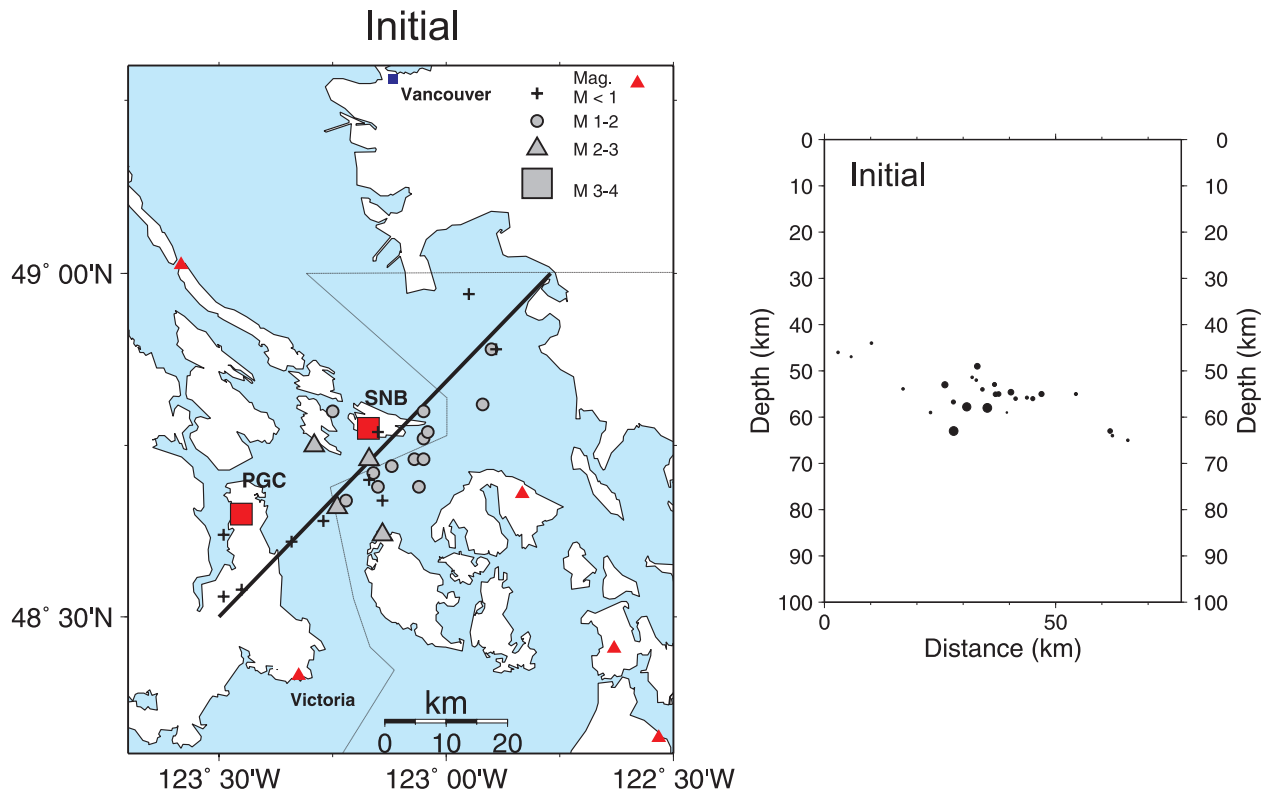

FIGURE 4: Initial locations of earthquake hypocenters in the vicinity of Saturna Island (SNB) shown in both map view (top) and cross section (bottom) along line shown.

the Fraser River Delta, British Columbia, Geological Survey of Canada Bulletin 525, edited by J.J. Clague, J.L. Luternauer, and D.C. Mosher, pp. 17–25, Geological Survey of Canada, 1998.

Waldhauser, F., and W.L. Ellsworth, A double-difference earthquake location algorithm: method and application in the Northern Hayward Fault, California, *Bull. Seism. Soc. Am.*, *90*, 1353–1368, 2000.

Wessell, P., and W.H.F. Smith, New version of the Generic Mapping Tools released, *EOS Trans.*, *76*, 329, 1995.

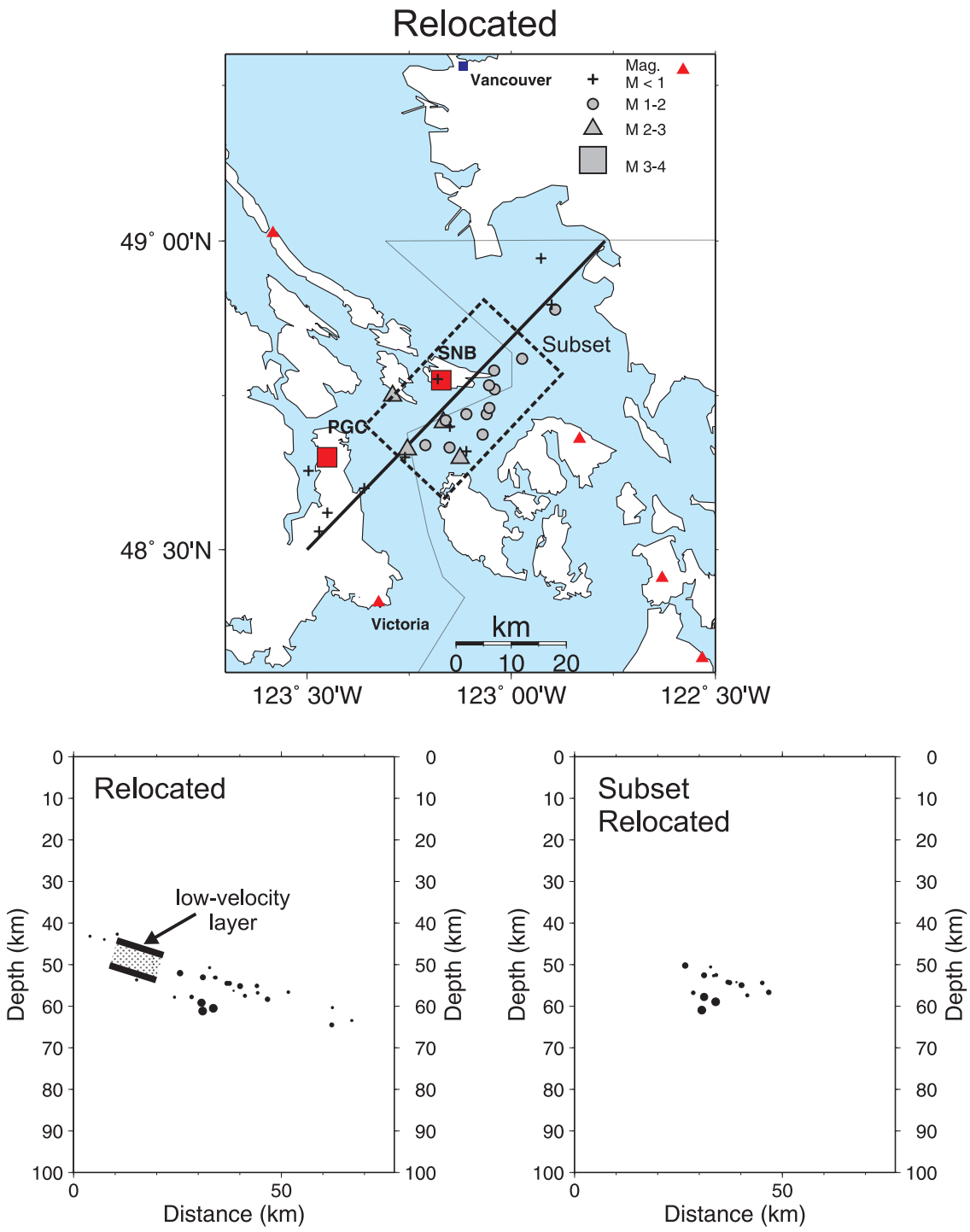

FIGURE 5: Relocated earthquake hypocenters near SNB (Saturna Island). Cross sections show results for all events (lower left) and a subset of events (lower right) closest to SNB (only the earthquakes within box shown on the map). The low-velocity layer was interpreted [*Cassidy*, 1995] as the oceanic crust beneath the seismic station PGC (Pacific Geoscience Centre).

Large earthquakes under our feet and deep beneath the Puget lowland and Georgia Strait: How often do they occur, how big can they get and what are their likely effects?

Stephen H. Kirby[1], Kenneth C. Creager[2] and Leiph A. Preston[2]
1 United States Geological Survey, 345 Middlefield Road, Menlo Park, California, 94025, USA
1 Department of Earth and Space Sciences, University of Washington, Seattle, Washington, 98195–1650, USA
skirby@usgs.gov, kcc@geophys.washington.edu, prestola@u.washington.edu

Several large deep earthquakes have occurred in the last 60 years beneath the Puget lowland in the urban corridor between Olympia, Washington and Vancouver, B.C., and they represent the most destructive type of seismic event in western Washington State in this century. They occur inside the Juan de Fuca plate subducting beneath the North America plate at depths of 40 to 80 km. While smaller than the big, shallow plate-boundary earthquakes, deep shocks occur much more frequently, are closer to population centers and tend to be more destructive for a given magnitude than plate-boundary events. This presentation describes some of the effects of large deep earthquakes in the western hemisphere in the 20th century and some recent ideas of how to estimate better their maximum magnitudes, how often they occur, and what their effects might be.

In-slab seismicity at the north end of Cascadia

Garry C. Rogers[1,2], Alison L. Bird[1], John F. Cassidy[1,2], Taimi L. Mulder[1], Maiclaire K. Bolton[2] and John P. Ristau[2]
1 Pacific Geoscience Centre, Geological Survey of Canada, PO Box 6000, Sidney, British Columbia, V8L 4B2, Canada
2 Earth and Ocean Sciences, University of Victoria, PO Box 3055, Victoria, British Columbia, V8W 3P6, Canada
rogers@pgc.nrcan.gc.ca, bird@pgc.nrcan.gc.ca, cassidy@pgc.nrcan.gc.ca, mulder@pgc.nrcan.gc.ca, bolton@pgc.nrcan.gc.ca, ristau@pgc.nrcan.gc.ca

The in-slab seismicity in the Canadian portion of the Cascadia subduction zone differs from that to the south in northern Washington State in two principal ways. First, there is a very active band of seismicity along the coast in the 25 to 35 km depth range where the angle of the subducting plate goes from horizontal to a dip of about 20°. Second, the deeper seismicity in the 40 to 60 km range that dominates below Puget Sound, gradually tapers off as the age of the plate being subducted becomes younger with the change in orientation of the coastline from north–south along Washington and Oregon to northwest–southeast along British Columbia. The focal mechanisms of the deeper suite are a mixture of strike-slip and normal faulting events with downdip tension events predominating. Focal mechanisms beneath the coast have a very confusing pattern and contain strike-slip, normal and thrust events with a wide variation in the orientation of both *P* and *T* axis. No low-angle thrust events have been detected that would be consistent with movement of the Cascasdia subduction fault. The largest events in both the coastal region and the deeper events beneath southern Georgia Strait have been in the magnitude 5 to 6 range compared to larger events at the south end of Puget Sound.

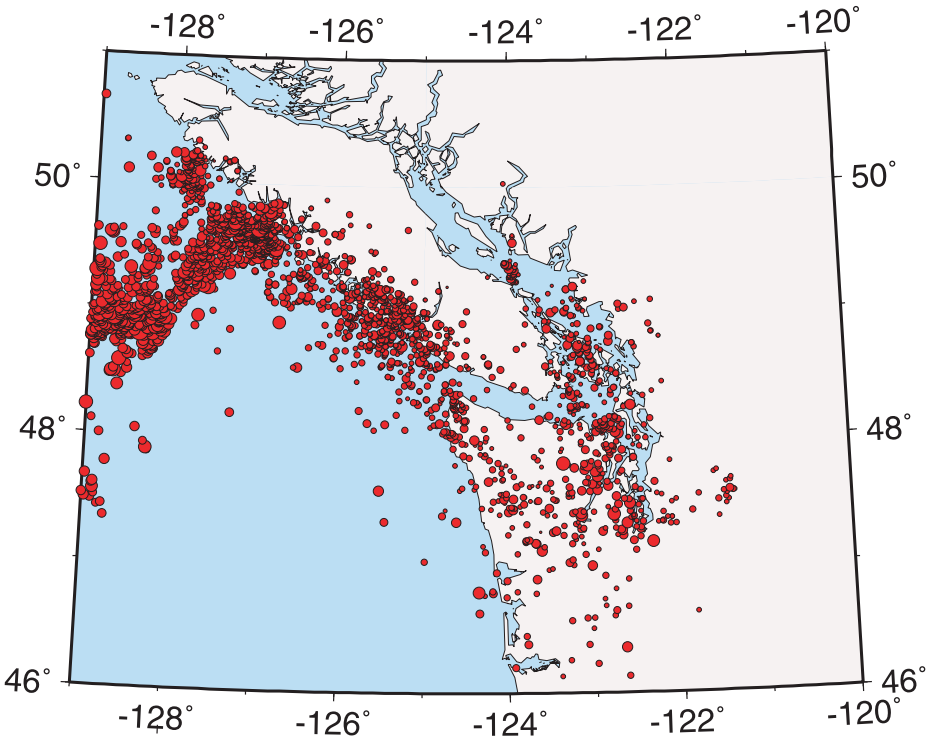

FIGURE 1: Fifteen years of seismicity within the oceanic plate. At the northernmost end of active Cascadia subduction, a band of seismicity exists beneath the west coast of Vancouver Island and another concentration exists beneath southern Georgia Strait and Puget Sound. Circle size is related to earthquake magnitude and ranges from magnitude about zero for the smallest circles to an offshore event of magnitude 6.3. Data from the Geological Survey of Canada and the University of Washington.

Warm-slab subduction as a global process

Stephen H. Kirby[1], E. Robert Engdahl[2] and Antonio Villaseñor[2]
1 United States Geological Survey, 345 Middlefield Road, Menlo Park, California, 94025, USA
2 Department of Physics, University of Colorado at Boulder, Boulder, Colorado, 80309, USA
skirby@usgs.gov, engdahl@lemond.colorado.edu, antonio@gldvisitor.cr.usgs.gov

The Cascadia subduction zone is a prime example of "warm-slab" subduction. As with many such subduction zones, the intraslab seismicity rate is low even though sizable and damaging slab earthquakes can occur in them. This argues for a global approach to estimating seismic hazards in these settings, and for investigations of modern and historical slab events and how seismic moment release rates per trench length vary with slab input parameters. We have identified 28 subduction zone settings that have warm-slab characteristics (Table 1). These common features [*Kirby et al.,* 1996] include: a) hypocentral depths that are largely shallow for intraslab events (<100 to 125 km depth); b) shallow dip of the Wadati–Benioff zone; c) feeble or absent volcanic arc [*Simkin and Siebert,* 1984]; and d) the occasional occurrence of unusual lava compositions thought to represent melting of eclogitic slab crust [*Defant and Drummond,* 1990].

Most of the subduction zone settings in Table 1 involve slow convergence rates, young plate age entering the trench or low slab dip or some combination of these attributes. These factors reduce the temperature contrast between the slab and the surrounding mantle. Slow convergence rates may occur where the overall relative plate motions are slow (<20 mm/a, such as the Makran and South Shetland margins), where plate motions are very oblique over a relatively straight trench (e.g., northwestern New Guinea), or where trench normals become very oblique to plate motions near the ends of subduction zones (e.g., the northern and southern Lesser Antilles, the South Scotia arcs, and the western Aleutians). Examples of warm-slab environments where young lithosphere is subducting include subduction zones where midocean spreading ridges are just offshore (e.g., the Rivera subduction zone, the southeast segment of the Cocos system in Costa Rica, and the northwest part of the Cocos system in Mexico) or where a young fossil backarc spreading system is being subducted (e.g., the Nankai/Shikoku system in Japan and the central Luzon segment of the northern Philippine system). Most of the systems of Table 1 also have shallow average dips where they are known (δ<15–20°), including the avolcanic segments of the classic flat-slab subduction in Peru and northern Chile.

The plate tectonics settings of these slab segments are consistent with the contrast between their minimum slab temperatures and the surrounding mantle being low. This contrast is roughly proportional to the slab thermal parameter [*Kirby et al.,* 1991], given by:

$$\phi = AV \cdot \cos\theta \cdot \sin\delta = AV_n \cdot \sin\delta = AV_z$$

f: A measure of slab "coldness" and is proportional to the depth, *Z*, that v-shaped isotherms are advected downward inside slabs. It has units of length.
A: Age of the plate at the trench
V: Speed of relative plate motion
V_n: Plate convergence speed
V_z: Slab vertical descent rate
q: Obliquity angle of plate motion to the trench normal
d: Slab dip angle

Most of the "warm-slab" subduction zones in Table 1 have thermal parameters less than about 500 km whereas most subduction zones have thermal parameters exceeding 1000 km [*Kirby et al.,* 1996].

Cascadia being placed in this "warm-slab" category is important for earthquake hazard appraisal for several potential reasons that stem from inferences drawn from recent models of "warm-slab" subduction [*Kirby et al.,* 1996; *Peacock and Wang,* 1999; *Peacock et al.*, this volume; *Kirby,* 2000]. Dehydration of the subducting crust and densification to eclogite are expected to take place at shallow depths (40–90 km) under the North American plate forearc, an expectation consistent with the fine seismic wavespeed structure of the Nankai/ Shikoku system [*Hori et al.,* 1985]. This shallow metamorphism means that the forearc has an abundant deep source of slab fluids that may be important in the mechanics of upper plate forearc earthquakes that occur in abundance above the intraslab events. Second, shallow liberation of fluids from the slab should permit slab seismogenic faulting by dehydration embrittlement should slab stresses be adequate. Dehydration embrittlement is a mechanism of unstable faulting in which the pore pressures generated by dewatering of hydrous phases reduced the effective pressures or normal stresses that tend to suppress brittle fracture and frictional sliding [*Raleigh,* 1967]. This mechanism of high-pressure faulting is a leading candidate for seismogenic faulting at depths greater than a

TABLE 1: Examples of "warm-slabs"*.

1.	Nankai/Shokoku (Philippine#): SW Japan	Y^, Sh^
2.	Cascadia (Juan de Fuca): WA, OR, BC	Y, Sh
3.	Southern Mexico (Rivera)	Y
4.	Southern Mexico (Cocos)	Y, Sh (Flat slab)
5.	Southeast Costa Rica (Cocos)	Y, Sh
6.	Northern Panama (Caribbean)	Sh, Sl^
7.	Northern Colombia (Caribbean)	Sl
8.	Northwest Colombia (Nazca)	Y
9.	Peru (Nazca)	Sh (Flat slab)
10.	Northern Chile & Argentina (Nazca)	Sh (Flat slab)
11.	Southern Chile (Nazca)	Y
12.	Tierra del Fuego (Antarctica)	Y, Sh, Sl
13.	South Shetlands (Antarctica)	Y, Sh, Sl
14.	S. Scotia, N & S Sectors (South America)	Sl
15.	New Zealand, Fiordland (Australia)	Y, Sl
16.	Western New Guinea (Caroline)	Sl
17.	Yap and Palau (Caroline)	Sl
18.	South Marianas (Pacific)	Sl
19.	Luzon (Eurasia, Borneo Microplate)	Y
20.	Western Aleutians (Pacific)	Sl
21.	Gulf of Alaska (Pacific)	Sh
22.	Wrangell (Pacific)	Sh, Sl
23.	Andaman/Nicobar (Indian)	Y, Sl
24.	Makran (Arabian)	Sh, Sl
25.	Cyprus/South Turkey (African)	Sl
26.	Hellenic (African)	Sl
27.	Calabrian (African)	Sl
28.	Lesser Antilles, N & S ends (N & S American)	Sl

**Collision zones not included.*
 # Slab provenance plate indicated in parentheses.
Y^ = young plate subducting (<20 Ma).
Sh^ = shallow dip of the seismic zone (d <15 to 20°).
Sl^ = slow convergence (<20 mm/a) either due to slow plate motions or very oblique subduction.

few tens of kilometers. Third, densification of the subducted crust should be a major cause of slab deformation and hence, shallow slab seismicity. Thus warm-slab subduction can focus seismic activity at shallow depths beneath the physiographically low ground in the urban corridor from the Georgia Straight and the Willamette Valley. This places the cultural geography of humans in intersection with the geography of earthquakes in Cascadia.

References

Defant, M.J., and M.S. Drummond, Derivation of some modern arc magmas by melting of young subducted lithosphere, *Nature, 347,* 662–665, 1990.

Hori, S., H. Inoue, Y. Fukao, and M. Ukawa, Seismic detection of the untransformed "basaltic" oceanic crust subducting into the mantle, *Geophys. J. R. Astron. Soc., 83,* 169–197, 1985.

Kirby, S.H., Invited news and views article: taking the temperature of slabs, *Nature, 403,* 31-34, 2000.

Kirby, S.H., W.B. Durham, and L.A. Stern, Mantle phase changes and deep earthquake faulting in subducting lithosphere, *Science, 252,* 216–225, 1991.

Kirby, S.H., E.R. Engdahl, and R. Denlinger, Intermediate-intraslab earthquakes and arc volcanism as physical expressions of crustal and uppermost mantle metamorphism in subducting slabs, in *Subduction: Top to Bottom, Geophysical Monograph 96,* Bebout, edited by G., D. Scholl, S. Kirby and J. Platt, pp. 195–214, American Geophysical Union, Washington, D.C., 1996.

Peacock, S., and K. Wang, Seismic consequences of warm versus cool subduction metamorphism: examples from southwest and northeast Japan *Science, 286,* 937–939, 1999.

Peacock, S., K. Wang, and A.M. McMahon, Thermal structure and metamorphism of subducting oceanic crust: insight into Cascadia intraslab earthquakes in *The Cascadia Subduction Zone and Related Subduction Systems*, edited by S.H. Kirby, K. Wang, and S.G. Dunlop, pp. 123–126, U.S. Geological Survey Open-File Report 02–328, Geological Survey of Canada Open File 4350, 2002.

Raleigh, C.B., Tectonic implications of serpentinite weakening, *Geophys. J. R. Astron. Soc., 14,* 113–118, 1967.

Simkin, T., and L. Siebert, Explosive eruptions in space and time: durations, intervals, and a comparison of the world's active volcanic belts, in *Explosive Volcanism: Inception, Evolution, and Hazards,* edited by Panel on Explosive Volcanism, pp. 110–121, National Academy Press, Washington, D.C., 1984.

The structure and intraslab seismicity of the Philippine Sea plate in Southwest Japan

Yoshiyuki Kaneda, Phil R. Cummins and Kouichi Uhira
Frontier Research Program for Subduction Dynamics, JAMSTEC
2–15 Natsushima-cho, Yokosuka,237–0061, Japan
kaneday@jamstec.go.jp, cummins@jamstec.go.jp

Tectonic setting of the Nankai Trough

The Nankai Trough in Southwest Japan is a convergent plate boundary where the Philippine Sea plate (PSP) is subducting beneath Southwest Japan at rate of about 4.5 cm/yr (Figure 1). Great megathrust earthquakes occur along this subduction zone with a recurrence interval of 100–200 years [*Ando,* 1975]. Hence, it is an area of great concern in terms of seismic risk.

The age of the subducting PSP varies considerably along strike in the Nankai Trough, because of the subduction of a fossil spreading ridge which began 15 Ma. As a result the age of the PSP currently entering the Nankai Trough subduction zone is thought to vary from about 15 Ma near the axis of the fossil spreading ridge to about 30 Ma in the Suruga Trough and off northern Kyushu.

A well-developed accretionary complex is present in the Nankai Trough, composed of off-scraped and underplated trough fill turbidites and hemipelagic sediments. This accretionary prism is over 100 km wide and 7 km deep [*Kodaira et al.,* 1999] and its landward extremity abuts another, older accretionary complex known as the Shimanto belt.

Seismic surveys and constraints on slab structure

After the 1995 Kobe earthquake, a number of research initiatives aimed at earthquake disaster mitigation were established in Japan. One of these was the Frontier Research Program for Subduction Dynamics (Frontier) established at the Japan Marine Science and Technology Center (JAMSTEC), with the goal of studying subduction-zone earthquakes. With this goal in mind, Frontier began a vigorous program of marine seismic surveys, part of which concentrated on the Nankai Trough.

Several of the ocean bottom seismometer (OBS) survey lines shot in the Nankai Trough are illustrated in Figure 1. These were run in combination with multi-channel seismic surveys to provide constraints on structure down to about 30 km depth. The results of these surveys are illustrated in Figure 2, where cross sections from the easternmost survey to the westernmost are arranged from top to bottom. As can be seen from the figure, there is considerable along-strike variation in structure. The accretionary prism thickens considerably in the central part of the Nankai Trough (KR9704), while contact between the island arc crust and the subducting plate covers a wider downdip segment of the plate boundary in the western (KR9806) and eastern (KR9810) cross sections.

We have used the results of our surveys as well as those of other research groups in Japan to construct a model of the plate boundary in the Nankai Trough, as illustrated in Figure 3. All the survey lines used to construct the model are illustrated. At shallow depth the model was constrained to agree with these survey lines, while at deeper depth the shape of the plate boundary was constrained to follow that of the intraslab seismicity [*Nakamura et al.,* 1997]. The contours of the resulting plate boundary model (Figure 3) show substantial contortion of the plate. Dip is shallow in the central part of the Nankai Trough but is steeper to the east and west.

Intraslab seismicity of the Philippine Sea plate

We have used seismic source mechanism determinations of the Japanese Meteorological Agency (JMA) to study the intraslab seismicity of the PSP. These data include earthquakes occurring throughout Japan during the years 1926–1997. For those earthquakes in Southwest Japan, we used the plate boundary model described above to separate those events which occurred in the upper plate from those which occurred in the subducting PSP. Known interplate thrust events were omitted, as were some events which occurred so close to the plate boundary that they could not be unambiguously assigned to either the upper or the lower plate.

Earthquakes occurring in the island arc forearc of Southwest Japan are shown in the upper part of Figure 4. These are predominantly strike-slip events with *P* axes oriented east–west to northwest–southeast. These are thought to reflect a forearc stress field that is close to margin parallel [e.g., *Seno,* 1999], and *Wang and He* [1999] have shown that this suggests a very weak

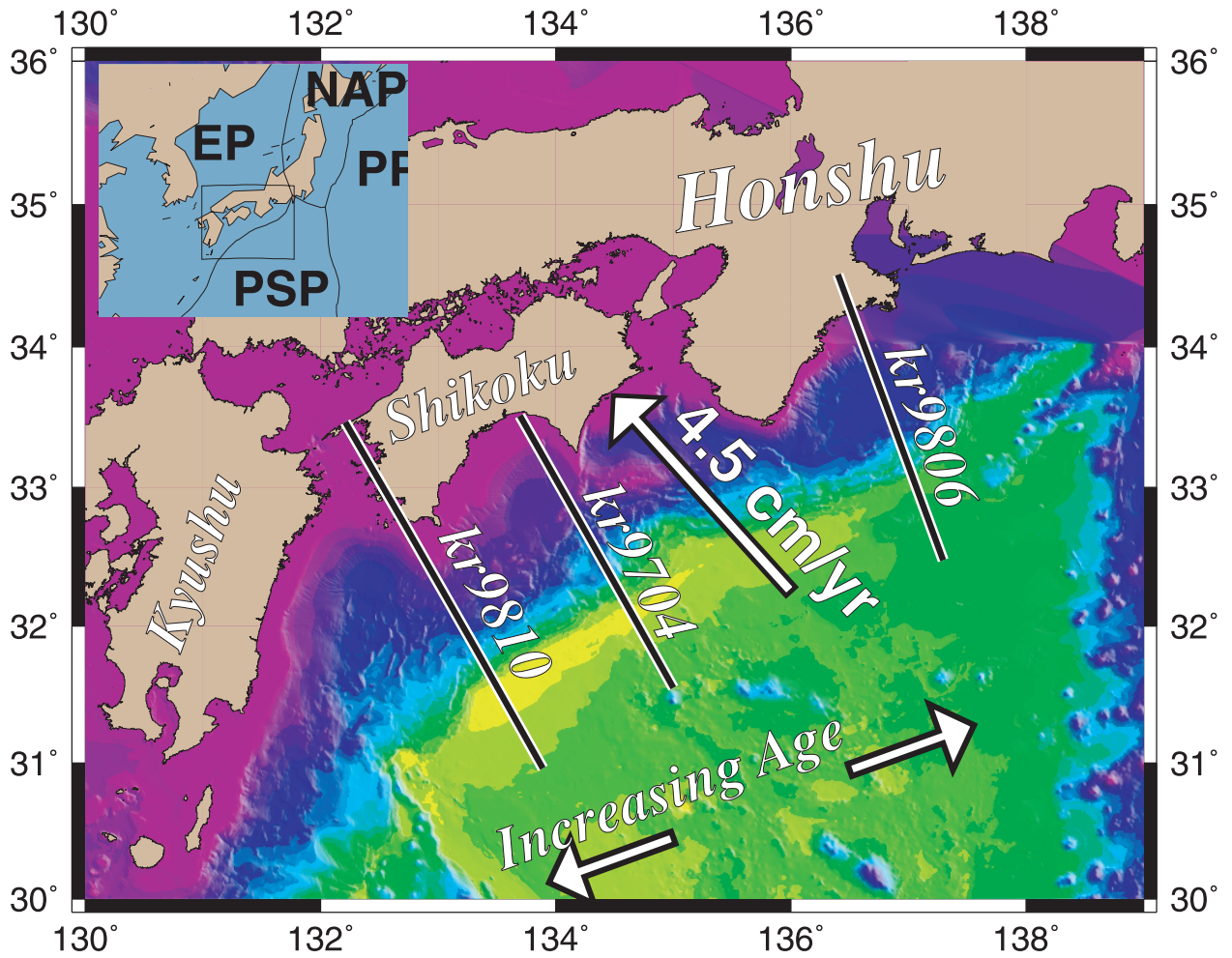

FIGURE 1: Tectonics and seismic survey lines in the Nankai Trough. The survey lines of three JAMSTEC ocean bottom seismometer experiments are indicated, along with plate convergence rate and direction, and the age variation of the Philippine Sea plate.

megathrust in the Nankai Trough.

The intraslab events, shown in the bottom part of Figure 4, span a range of depths whose along-strike maximum increases with the age of the subducting plate: beneath northern Kyushu seismicity extends to 160 km depth, and beneath the Tokai region to 90–100 km depth, while beneath Shikoku the seismicity only extends to 60 km maximum depth. These depths correlate roughly with the maximum depth at which hydrous phases in the subducting plate remain stable [*Peacock and Wang*, 1999], and are thus consistent with the dehydration embrittlement model for intraslab earthquakes [*Kirby et. al,* 1996].

The pattern of focal mechanisms of PSP intraslab earthquakes is complicated but in general follows the contortions of the subducting plate, as suggested by *Imagawa et al*. [1985].

Conclusions

Recent seismic survey results in the Nankai Trough, in combination with seismicity data, have revealed detailed structure of the highly contorted Philippine Sea plate subducting beneath Southwest Japan. This has facilitated the discrimination of intraslab from upper plate earthquakes in order to study the intraslab seismicity of the PSP. This maximum depth of seismicity has a pattern consistent with that expected from dehydration embrittlement of the PSP and the along-strike age variation of the subducting PSP.

Considerations of seismic risk in the Nankai Trough generally focus on the great megathrust earthquakes which repeatedly occur there. All of the recent intraslab seismic activity is associated with relatively small earthquakes which have caused little damage. Early in this century, however, a few large intraslab earthquakes occurred which caused considerable damage and some

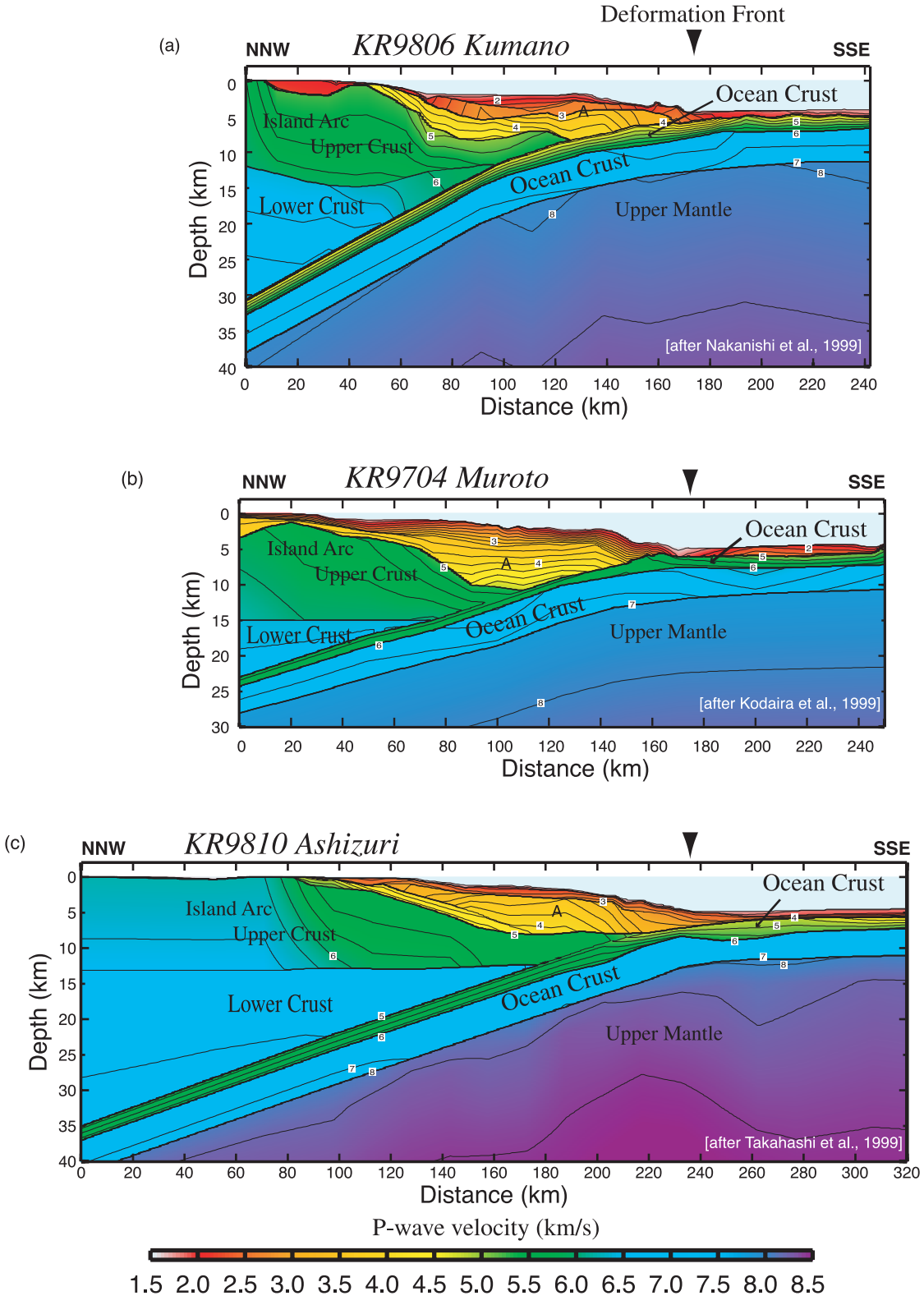

FIGURE 2: Three cross sectional models of seismic velocity structure, corresponding to each of the survey lines in Figure 1. Note the changes in plate boundary dip, and area of contact between the island arc crust and the subducting oceanic plate.

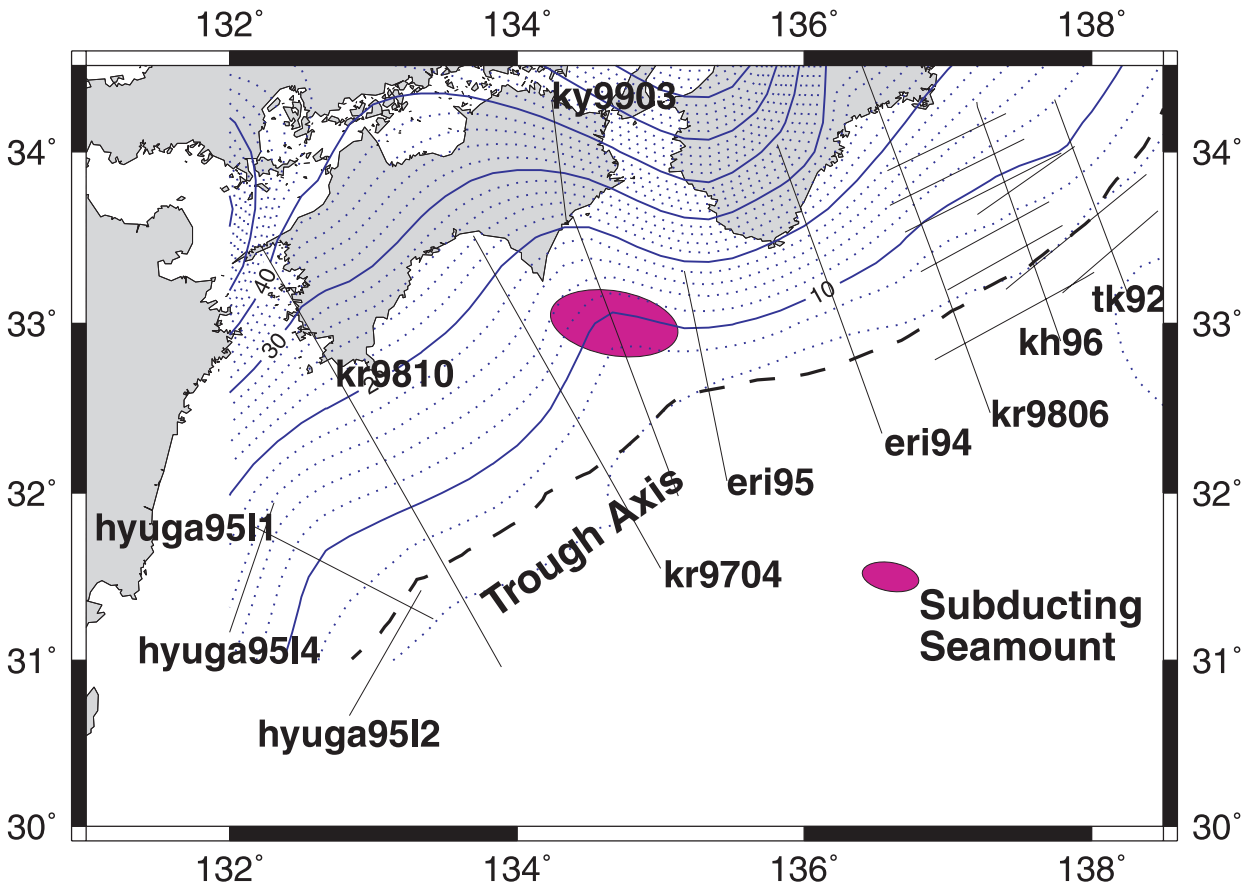

FIGURE 3: A model for the depth to the top of the subducting Philippine Sea plate based on seismic survey results (JAMSTEC and non-JAMSTEC) and seismicity data.

loss of life. What little information is available concerning these earthquakes will be presented in this talk and in a companion poster session.

References

Ando, M., Source mechanisms and tectonic significance of historical earthquakes along the Nankai Trough, Japan, *Tectonophyics, 27,* 119–140, 1975.

Kirby, S., E.R. Engdahl, and R. Denlinger, Intermediate-depth intraslab earthquakes and arc volcanism as physical expressions of crustal and uppermost mantle metamorphism in subducting slabs, in *Subduction: Top to Bottom,* edited by G.E. Bebout et al., pp. 195–214, American Geophysical Union, Washington, D.C., 1996.

Kodaira, S., N. Takahashi, J. Park, K. Mochizuki, M. Shinohara, and S. Kimura, The western Nankai Trough seismogenic zone: results from wide-angle ocean-bottom seismographic survey, *J. Geophys. Res., 105,* 5887–5905, 1999.

Imagawa, K., K. Hirahara, and T. Mikumo, Source mechanisms of subcrustal and upper mantle earthquakes around the northeastern Kyushu Region, southwestern Japan, and their tectonic implications, *J. Phys. Earth, 33,* 257–277, 1985.

Nakamura, M., H. Watanabe, T. Konomi, S. Kimura, and K. Miura, Characteristics activities of subcrustal earthquakes along the outer zone of southwestern Japan, *Ann. Disas. Prev. Res. Inst., Kyoto U., 40,* 1–21, 1997.

Peacock, S., and K. Wang, Seismic consequences of warm versus cool subduction metamorphism: examples from Southwest and Northeast Japan, *Science, 286,* 937–939, 1999.

Seno, T., Synthesis of regional stress fields of the Japanese islands, *The Island Arc, 8,* 66–79, 1999.

Wang, K., and J. He, Mechanics of low-stress forearcs: Nankai and Cascadia, *J. Geophys. Res., 104,* 15,191–15,205, 1999.

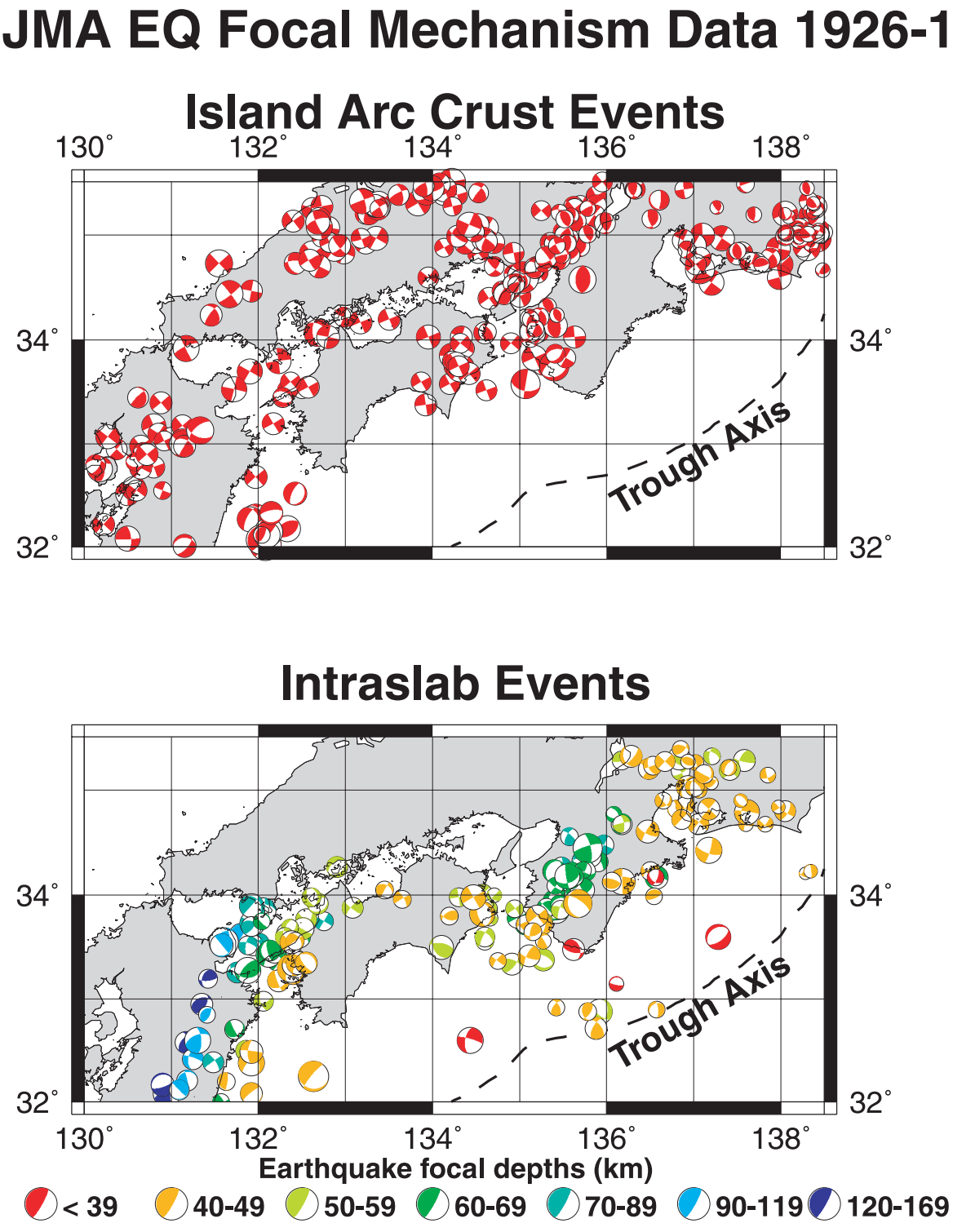

FIGURE 4: Japanese Meteorological Agency earthquake source mechanism solutions. The model from Figure 3 has been used to separate this into a) earthquakes in the island arc crust and b) intraslab earthquakes.

Intraslab earthquakes in the subducting oceanic plates below Mexico

Shri K. Singh, Vladimir Kostoglodov and J. F. Pacheco
Instituto de Geofísica, UNAM, CU, 04510 Mexico, DF, MEXICO
krishna@ollin.igeofcu.unam.mx, vladimir@ollin.igeofcu.unam.mx

Introduction

Moderate and large intraslab earthquakes in the subducted Cocos plate below Mexico are relatively frequent. For example, four of the seven large ($M_w \geq 6.9$) earthquakes which occurred in Mexico between 1995 and 1999 were intraslab earthquakes. Two of these four earthquakes also caused damage and deaths in towns near the epicentral region. Historically, some of the intraslab earthquakes have devastated cities and towns located in the Mexican altiplano. Recent intraslab earthquakes have been well recorded by local and regional seismographs and accelerographs. The analysis of these data, along with previous results, has improved our knowledge of the Benioff zone, source process of intraslab earthquakes, and expected ground motions from such events. In this overview of seismic investigations of intraslab earthquakes in Mexico, we will limit ourselves to the region between Tehuantepec in the southeast and Jalisco in the northwest (94°–105.5°W). The region is characterized by subduction of young slab (age less than about 16 ma).

Plate tectonic framework and intraslab earthquakes

Figure 1 summarizes the plate tectonic framework of the region. The figure gives age [*Kostoglodov and Bandy*, 1995] and relative plate convergence rate at the trench according to NUVEL 1A model [*DeMets et al.,* 1994], epicenters and focal mechanisms of all well-located intraslab events, isodepth contour of the Benioff zone [*Singh and Mortera*, 1991; *Pardo and Suárez*, 1995], and the location of active volcanoes. The earthquakes shown in the figure are based on a catalog of intraslab events ($H \geq 35$ km) which we have compiled from different sources. This catalog contains all intraslab events for which focal mechanism is available. It is probably complete for $M_w \geq 6.0$ since 1963, and for $M_w \geq 5.4$ since 1976, a period for which Harvard centroid-moment tensor (CMT) solutions are available. Table 1 lists the largest earthquakes ($M \geq 6.9$) from this catalog. Figure 1 also illustrates the geometry of the Benioff zone along selected sections [modified from *Singh and Mortera*, 1991; *Suárez et al.*, 1990; *Singh and Pardo*, 1993; *Pardo and Suárez*, 1995; *Kostoglodov et al.*, 1996]. From the figure, it may be noted that the epicenters of the intraslab earthquakes cease before reaching the volcanic front, and there is a significant along-strike variation of the geometry of the Benioff zone and intraslab seismicity. In Jalisco, where the Rivera plate subducts below Mexico with a relatively low convergence rate (NUVEL 1A), the Benioff zone has a usual shape with a dip angle of ~45° [*Bandy et al.*, 1999] (not shown in Figure 1). However, intraslab events apparently do not exceed $M_w = 5.0$ there and our catalog contains no such event. In Michoacan–Guerrero and in Guerrero segments, the subducted Cocos plate bends with a small dip, unbends becoming subhorizontal and reaching a depth about 50 km at a distance of about 250 km from the trench. Subduction becomes normal in the Tehuantepec segment.

Source parameters of recent intraslab earthquakes

Until recently it was thought that large intraslab events below Mexico occurred downdip from the strongly coupled part of the interface at $D > 150$ km. The great Oaxaca earthquake of January 15, 1931 ($M = 7.8$), a normal-faulting intraslab event which caused great destruction to the City and the State of Oaxaca, seemed to be an exception since it was located only 65 km from the coast [*Singh et al.*, 1985]. Recent earthquakes, however, suggest that large intraslab events, which occur below or close to the downdip edge of the coupled plate interface, may be more frequent than previously thought. For example the earthquakes of January 11, 1997 ($M_w = 7.1$) occurred just below the rupture area of the shallow-thrust Michoacan earthquake of September 19, 1985 ($M_w = 8.0$) [*Mikumo et al.*, 1999]. Similarly, the intraslab Oaxaca earthquake of September 30, 1999 ($M_w = 7.4$) occurred just below the coast, near the downdip edge of the aftershock area of the November 29, 1978 ($M_w = 7.7$) thrust event [*Singh et al.*, 2000a]. Near-source and regional records of these two earthquakes have been inverted to map slip history on the fault. Both events show a strong directivity along the strike, which parallels the coast, with a downdip component and relatively small slip near the hypocenter.

TABLE 1: Large intraslab earthquakes of Mexico with known focal mechanism.

Date	Time	Latitude °N	Longitude °E	Depth (km)	M	Strike	Dip	Rake
19310115	1:50:40	16.340	-96.870	40	7.8	270	56	-90
19370726	3:47:13	18.450	-96.080	85	7.3	313	70	-95
19640706	7:22:13	18.215	-100.480	55	7.2	296	38	-63
19730828	9:50:41	18.250	-96.550	82	7.3	326	50	-76
19801024	14:53:35	18.030	-98.270	65	7.1	311	26	-66
19970111	20:28:26	18.340	-102.580	34	7.1	175	18	-28
19990615	20:42:04	18.130	-97.540	61	6.9	309	40	-83
19990930	16:31:13	16.030	-96.960	40	7.4	102	42	-103

During the 1997 event, the rupture initiated at a depth of 34 km, with most of the slip confined in the depth range of 30–50 km [*M. Santoyo*, pers. comm., 2000]. The 1999 rupture initiated at a depth of 40 km and most of the slip occurred within the depth range of 35–52 km [*Hernandez et al.*, 2000]. Since the plate interface in the region lies at a depth of 15–20 km, we conclude that these two events occurred in the oceanic mantle of the subducted Cocos plate.

Aftershocks from intraslab earthquakes

Aftershock activity following intraslab earthquakes in Mexico is very low. For example, only one aftershock with $M_w \geq 5.4$ is reported for the 1997 event, while none at this magnitude level occurred following the two large earthquakes of 1999 listed in Table 1. Although a quantitative comparison is not available at present, at the smaller magnitude level there is considerable variation in the number of aftershocks from one shock to another. For instance, the earthquake of 1973 (M_w=7.0, H=82 km) was followed by few aftershocks. The earthquake of 1980 (M_w=7.0, H=65 km) gave rise to a large number of aftershocks. About 900 aftershocks were recorded by a portable seismic network within nine days after the mainshock. Of these, 300 events could be located [*Yamamoto et al.*, 1984]. The June 15, 1999 earthquake (M_w=6.9, H=61 km) generated 33 aftershocks ($2.3 \leq M \leq 3.7$) within seven days. The 1999 earthquake (M_w= 7.1, H=34 km) produced far fewer aftershocks than the September 30, 1999 earthquake (M_w=7.4, H=40 km). To a first approximation, the number of aftershocks seems to decrease with depth.

Relationship between intraslab and interplate earthquakes

For the Mexican subduction zone, *Lay et al*. [1989] reported that the large, shallow thrust events were preceded by tensional downdip intraslab events, in accordance with the general worldwide pattern, but a decrease in the tensional events following the rupture of the interface was not clear from the available data. *Singh et al*. [2000b] have analyzed intraplate events which occurred in the subducting Cocos plate below northwest Guerrero and Michoacan since 1964 ($M_w \geq 5.4$) and their possible relationship with a sequence of four large/great shallow, thrust earthquakes ($7.3 \leq M_w \leq 8.0$) which ruptured the entire plate interface along this part of the coast during 1979–1985 (a length of ~210 km). This sequence provides an excellent opportunity to study temporal evolution of intraslab seismicity during about 15 years before and after the stress release caused by rupture of the plate interface. The results are in agreement with the model involving locking and unlocking of the coupled plate interface. A detailed study of the earthquake of 1997 (M_w=7.1) also shows that it occurred in the region of maximum coseismic stress increase caused by the 1985 thrust earthquake [*Mikumo et al.*, 1999]. Recent numerical modeling by *Gardi et al*. [2000] demonstrates that the peculiar geometry of the Benioff zone in the region strongly affects the state of intraslab stress and, hence, the pattern of seismicity.

There is also evidence that in Mexico some large, downdip, tensional earthquakes follow shallow thrust earthquakes rather than precede it. For example, the 1931 earthquake of Oaxaca (M=7.8), a normal faulting, downdip intraplate slab occurred after four thrust events ($7.4 \leq M \leq 7.8$) ruptured the plate interface in the region in 1928 [*Singh et al.*, 1985].

Some damaging intraslab events

If Mexico City, with its abnormal soil characteristics and large population, is excluded from the statistics, then the damage and the loss of lives from interplate and intraslab events in Mexico may be about equal, even though the former type of earthquakes is more frequent than the latter type. Some highly damaging intraslab earthquakes: the earthquake of 1858 (M~7.7) which caused severe damage to towns in Michoacan, including the City of

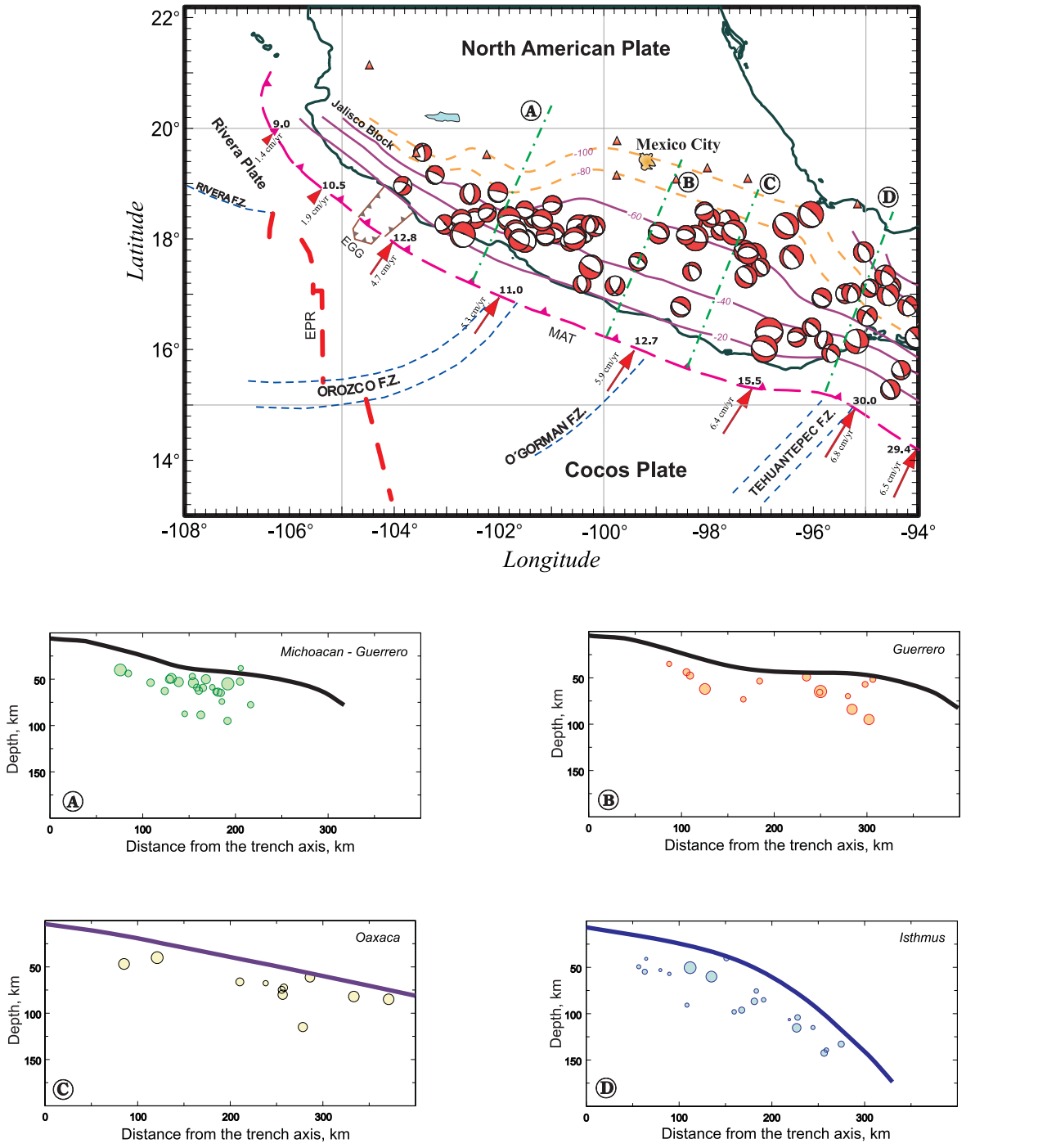

FIGURE 1: Tectonic map of the region. Triangles indicate active volcanoes. All intraslab earthquakes with known focal mechanism are shown. Relative plate convergence rates are given near arrows along the trench. The numbers above the arrow heads indicate the age (Myr) of the oceanic lithosphere at the trench. Isodepth contours are shown by continuous lines when well defined by seismicity and by dashed lines when inferred. Hypocenters of intraslab earthquakes projected on sections A to D are shown on the four graphs.

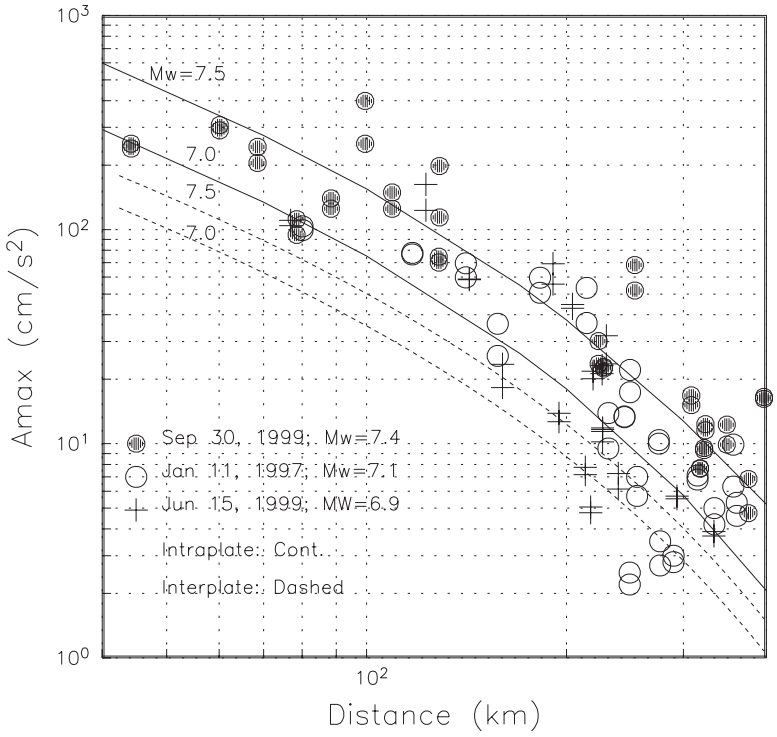

FIGURE 2: The peak horizontal acceleration (*Amax*) data versus hypocentral distance *R* for the last three large intraslab earthquakes of Mexico (Table 1). Also shown are expected *Amax* values, based on regression analysis, for M_w=7.5 and 7.0 earthquakes; continuous lines: intraslab earthquakes, dashed lines: interplate events.

Morelia and Mexico City; the 1931 earthquake which caused major destruction in the State and City of Oaxaca; the Orizaba and Huajuapan de Leon earthquakes of 1973 and 1980; and the 1999 earthquake of Tehuacan which caused unexpectedly large damage to colonial structure in the City of Puebla. Part of the reason for large damage during intraslab earthquakes is the high population density in the Mexican altiplano.

Ground motion from intraslab earthquakes

A comparison of intensities during intraslab and interplate earthquakes in Mexico suggest that the ground motions, and hence the stress drop, involved in the former type of earthquakes is higher than in the latter type. Extensive recordings from recent intraslab events permits regression analysis of different ground motion parameters. Based on hard-site, strong-motion recordings of ten intraslab earthquakes ($5.4 \leq M_w \leq 7.4$; $40 \leq H \leq 65$ km; $R \leq 400$ km) we obtain the following preliminary relation between horizontal *Amax* (in gal), M_w, and hypocentral distance *R* (in kilometers):

$$\log Amax = -0.148 + 0.623\, M_w - \log R - 0.0032\, R$$

The corresponding relation for interplate Mexican earthquake is [*Ordaz et al.*, 1989]:

$$\log Amax = 1.76 + 0.300\, M_w - \log R - 0.0031\, R$$

Note that the preliminary regression suggests a larger dependence of *Amax* on M_w for intraslab events than for interplate events. Figure 2 shows predicted *Amax* for M_w=7.0 and 7.5 for intraslab and interplate earthquakes. The expected *Amax* for an intraslab M_w=7.5 event is four to five times greater than the corresponding value for an interplate event. This difference decreases for M_w=7.0. The figure also shows recorded *Amax* data during the earthquakes of January 11, 1997 (M_w=7.1), June 15, 1999 (M_w=6.9) and September 30, 1999 (M_w=7.4). The large scatter in the data is partially due to the directivity of the sources, which has not been accounted for in the regression.

Research needs

- A reliable catalog for realistic estimation of seismic hazard. It is possible to improve the source parameters of moderate and large intraslab events between 1906 and 1963 by analyzing seismograms and bulletins.
- A denser seismic network to detect small, intraslab events to better define the intraslab seismicity, and the geometry and the extent of the Benioff zone. How close to Mexico City and other important cities in the Mexican altiplano can large intraslab earthquakes occur?

- A model to explain along-strike variation of the Benioff zone and the intraslab seismicity, and the cause of large intraslab earthquakes which occur just below the coupled plate interface at a depth of about 40 km.
- A resolution of the controversy regarding the origin of the volcanism in Mexico (see, e.g., *Verma*, [1999] and the references therein). Is there a direct association between volcanism and subduction? Or is volcanism related to past and present rifting and faulting?

References

Bandy W., V. Kostoglodov, A. Hurtado-Díaz,and M. Mena, Structure of the southern Jalisco subduction zone as inferred from seismicity and gravity, *Geofisica Internacional, 38*, 127–136, 1999.

DeMets, C., R.G. Gordon, D.F. Argus, and S. Stein, Effects of recent revisions to the geomagnetic reversal time scale on estimates of current plate motions, *Geophys. Res. Lett.*, *21*, 2191–2194, 1994.

Gardi, A., M. Cocco, A.M. Negredo, R. Sabadini, and S.K. Singh, Dynamic modeling of the subduction zone of central Mexico*, Geophys. J. Int.*, *143*, 809–820, 2000.

Hernandez, B., N.M. Shapiro, S.K. Singh, J.F. Pacheco, F. Cotton, M. Campillo, A. Iglesias, V. Cruz, J. M. Gomez, and L. Alcántara, Rupture history of September 30, 1999 intraplate earthquake of Oaxaca, Mexico (M_w=7.5) from inversion of strong-motion data in the frequency domain, *Geophys. Res. Lett.*, *28*, 363–366, 2001.

Kostoglodov, V., and W. Bandy, Seismotectonic constraints on the convergence rate between the Rivera and North American plates, *J. Geophys. Res.*, *100*, 17,977–17,989, 1995.

Kostoglodov, V., W. Bandy, J. Domínguez and M. Mena, Gravity and seismicity over the Guerrero seismic gap, Mexico*, Geophys. Res. Lett., 23*, 3385–3388, 1996.

Lay. T., L. Astiz, H. Kanamori, and D.H. Christensen, Temporal variation of large intraplate earthquakes in coupled subduction zones, *Phys. Earth Planet. Interiors*, *54*, 258–312, 1989.

Mikumo, T., S.K. Singh, and M. Santoyo, A possible stress interaction between large thrust and normal faulting earthquakes in the Mexican subduction zone, *Bull. Seism. Soc. Am., 89*, 1418–1427, 1999.

Ordaz, M., J.M. Jara, and S.K. Singh, Riesgo sísmico y espectros de diseño en el estado de Guerrero, Mem. VIII Congreso Nac. de Ingeniería Sísmica, Acapulco, Mexico, D40–D56, 1989.

Pardo, M., and G. Suárez, Shape of the subducted Rivera and Cocos plates in southern Mexico: seismic and tectonic implications, *J. Geophys. Res., 100*, 12,357–12,373, 1995.

Singh, S.K., and F. Mortera, Source-time functions of large Mexican subduction earthquakes, morphology of the Benioff zone and the extent of the Guerrero gap, *J. Geophys. Res.* 96, 21,487–21,502, 1991.

Singh, S.K., G. Suárez, and T. Domínguez, The great Oaxaca earthquake of 15 January 1931: lithosphere normal faulting in the subducted Cocos plate, *Nature, 317*, 56–58, 1985.

Singh, S.K. and M. Pardo, Geometry of the Benioff zone and the state of stress in the overriding plate in central Mexico, *Geophys. Res. Lett., 20,* 1483–1486, 1993.

Singh, S.K., M. Ordaz, J.F. Pacheco, R. Quaas, L. Alcántara, S. Alcocer, C. Gutierrez, R. Meli, and E. Ovando, A preliminary report on the Tehuacán, México earthquake of June 15, 1999 (M_w=7.0), *Seism. Res. Lett., 70*, 489–504, 1999.

Singh, S.K., J. Pacheco, T. Mikumo, and V. Kostoglodov, Intraplate earthquakes in central México and their relationship with large/great intraplate earthquakes, *Seism. Res. Lett., 71*, 239, 2000a.

Singh, S.K., M. Ordaz, L. Alcántara, N. Shapiro, V. Kostoglodov, J.F. Pacheco, S. Alcocer, C. Gutierrez, R. Quaas, T. Mikumo, S. Alcocer, and E. Ovando, The Oaxaca earthquake of 30 September 1999 (M_w=7.5): a normal-faulting event in the subducted Cocos plate, *Seism. Res. Lett., 70*, 489–504, 2000b.

Suárez, G., T. Monfret, G. Wittlinger, and C. David, Geometry of subduction and the depth of the seismogenic zone in the Guerrero gap*, Nature, 345*, 336–338, 1990.

Verma, S.P., Geochemistry of evolved magmas and their relationship to subduction-unrelated mafic volcanism at the volcanic front of the central Mexican volcanic belt, *J. Volcanol. Geotherm. Res., 93*, 151–171, 1999.

Yamamoto, J., Z. Jimenéz, and R. Mota, El temblor de Huajuapan de Leon, Oaxaca, México, del 24 de Octubre de 1980). *Geofis. Internacional, 23*, 83–110, 1984.

Seismicity and seismotectonics of Central America with emphasis on intraslab seismic activity

Marino Protti
Observatorio Vulcanológico y Sismológico de Costa Rica, Universidad Nacional, Costa Rica
jprotti@una.ac.cr

Introduction

Although no large (M_w>7.5) intraslab earthquakes have ever been recorded under the Central American arc, small and moderate-size intermediate depth events are frequent in this region. These events provide the key information needed to map the geometry of the Wadati–Benioff zone and have given important insights for the understanding of tectonic processes at this subduction zone. In Central America, and especially under Nicaragua and Costa Rica, it has been possible to obtain, in great detail, the geometry of the subducted slab and to make correlations with the structure and genesis of the subducting Cocos plate.

Tectonic setting of Central America

Central America is located on the western margin of the Caribbean plate (Figure 1). Here, the Cocos plate subducts beneath the Caribbean plate along the Middle America trench at a rate between 70 and 95 mm/year from Guatemala to southern Costa Rica, respectively (computed from *DeMets et al*. [1990]). The northern boundary between the Caribbean and the North American plate, in Central America, is the Chixoy–Polochic–Motagua fault system.

The subduction of young, warm lithosphere, together with the collision of the Cocos Ridge in southern Costa Rica, produced the fracturing of the southwestern part of the Caribbean plate and the formation of a microplate, the Panama block. This microplate includes the southeast portion of Costa Rica and all of Panama. The northern boundary between the Panama block and the Caribbean plate is a convergent margin, the Panama thrust belt, that extends from the Caribbean coast of Colombia to south of Limón, Costa Rica [*Silver et al.*, 1990]. Although a trench has not yet developed, this convergent margin produces large underthrust earthquakes and moderate size intermediate-depth seismic activity. In Costa Rica, the boundary between the Caribbean plate and the Panama block consists of a diffuse left-lateral shear zone from Limón to the middle American trench.

South of the border between Costa Rica and Panama is the Panama fracture zone. This right-lateral transform fault is the plate boundary between the Cocos and Nazca plates.

Seismicity of Central America

Seismically, Central America is a very active region with sources of different genesis and depths. Shallow events (Z<30 km) occur: a) associated with the subduction of the Cocos plate under the Caribbean plate and Panama block; b) along the Chixoy–Polochic–Motagua fault system; c) along the Panama fracture zone; d) as intraplate faulting of the Panama block and the Cocos and Caribbean plates; e) as interplate activity between the Caribbean plate and the Panama block, both along the Panama thrust belt and along a shear zone across central Costa Rica; and f) associated with the volcanic arc.

Intermediate-depth earthquakes in Central America occur as internal deformation of both the subducted Cocos plate under the Caribbean plate and Panama block, and the subducted Caribbean plate under the Panama block, in northern Panama. The maximum depth of intraslab earthquakes along the middle America trench decreases from near 300 km under the border between Guatemala and El Salvador, to around 50 km in southern Costa Rica.

Intermediate-depth seismicity of Central America

The intermediate-depth seismic activity in Central America shows a very steeply dipping slab under Guatemala, El Salvador and Nicaragua. Under northern Costa Rica the angle begins to shallow and the seismic slab disappears in southern Costa Rica.

Protti [1991] relocated all intraslab seismic activity recorded by the Costa Rica Volcanological and Seismological Observatory (OVSICORI) under Costa Rica from 1984 to 1989 and constructed first-motion focal mechanisms for individual events, and composite focal mechanisms for clusters of events. He found that vertical to subvertical *P* axes dominate at depths below 75 km and vertical to subvertical *T* axes dominate at greater depths.

An analysis of *P* and *T* axes of intermediate-depth seismicity recorded under Central America in the Harvard

FIGURE 1: Tectonic setting of Central America.

catalog was later made by *Guendel and Protti,* [1998]. They grouped the intraslab seismicity in three depth intervals (50–75 km, 75–100 km and >100 km) for two regional areas: under Guatemala–El Salvador and under Nicaragua–Costa Rica. In general, no major differences exist in the orientation of the *P* axes nor in focal mechanisms for these regions and depth intervals (Figure 2). The only important feature found in this study is the bimodal distribution in the orientation of *P* axes for events with focal depths between 75 and 100 km under Guatemala–El Salvador.

Geometry of the Wadati–Benioff zone under Nicaragua and Costa Rica, and its correlation with the age of the subducted Cocos plate

The intermediate-depth seismicity under central Costa Rica reveals a tear on the subducted Cocos plate (the Quesada sharp contortion of *Protti et al.* [1995]) which is recognizable below 70 km (Figure 3). To the northwest, the Cocos plate dips at 80° and seismicity reaches depths of 220 km beneath the Nicaragua border to 135 km at the tear. To the southeast, the Cocos plate dips at 60° and the seismicity does not exceed 125 km [*Protti et al.*, 1995]. The projection of the tear to the trench coincides with an abrupt change in the bathymetry of the Cocos plate along a northeast alignment (the rough/smooth boundary of *Hey* [1977]). This bathymetry change marks the boundary between lithosphere of the Cocos plate created along the East Pacific Rise and that created along the Galapagos spreading centre (Figure 4). The northeast extension of the rough/smooth boundary, which becomes the Quesada sharp contortion after subducting, was interpreted as a relic of the original transform fault along which the Farallon plate broke into Cocos and Nazca plates. It is the contrast in age, and therefore density, which produces the tear at this boundary. The first seismic event with a clear tear focal mechanism occurred on March 7, 1992, precisely where the Quesada sharp contortion begins to manifest. This earthquake, the Naranjo earthquake, had a magnitude M_w=6.6 and a focal depth of 78 km. No important damage was reported from this event; only falling objects.

FIGURE 2: Rose diagrams of the horizontal projection of *P* axes and triangular representation of focal mechanisms for intermediate-depth events under Central America from the Harvard catalog.

Also in central Costa Rica, and almost parallel to the 84°W of longitude, exists another abrupt change in age of the subducting Cocos plate. This age contrast occurs due to the subduction of the transform fault that offsets the Costa Rica rift to the west from the Ecuador rift to the east. The subduction of this feature produces the abrupt termination, to the east, of intraslab seismicity. There, the subducting slab may be so young and warm, that its deformation is mainly plastic. Also, the buoyancy and very low angle of subduction inferred for this youngest segment do not permit the penetration of the slab into lower levels of the asthenosphere, inhibiting the internal phase changes in the slab that have been suggested as a cause of intraslab seismicity.

Potential seismic hazard from intermediate-depth earthquakes in Central America

Because of the relatively large trench-arc distance in Guatemala, El Salvador and Nicaragua, together with the very steep angle of the slab, most of the intermediate-depth events occur either offshore or under the Pacific coast of these countries. Given the depth and the relatively few cities or towns along the Pacific coast of these countries, the potential seismic hazard from intermediate-depth earthquakes in that region is very low.

On the other hand, since under northern Costa Rica the angle of the slab begins to shallow and the trench-arc gap is smaller, intermediate-depth earthquakes tend to have epicentres not only shallower than in the rest of Central America, but right under important concentrations of population and infrastructure, increasing the seismic risk from this kind of activity in Costa Rica. Nevertheless, no large (M_w>7.0) intermediate earthquake has been recorded under Costa Rica.

The largest intermediate-depth event recorded in the Harvard catalog for Central America occurred on June 19, 1982 52 km off El Salvador and had a magnitude M_w=7.3. An earthquake with magnitude M=7.0 and 80 km deep occurred under central Costa Rica on November 19, 1948. Although global catalogs locate this event where no seismic slab has been identified with local data, damage reports locate it further west right where the

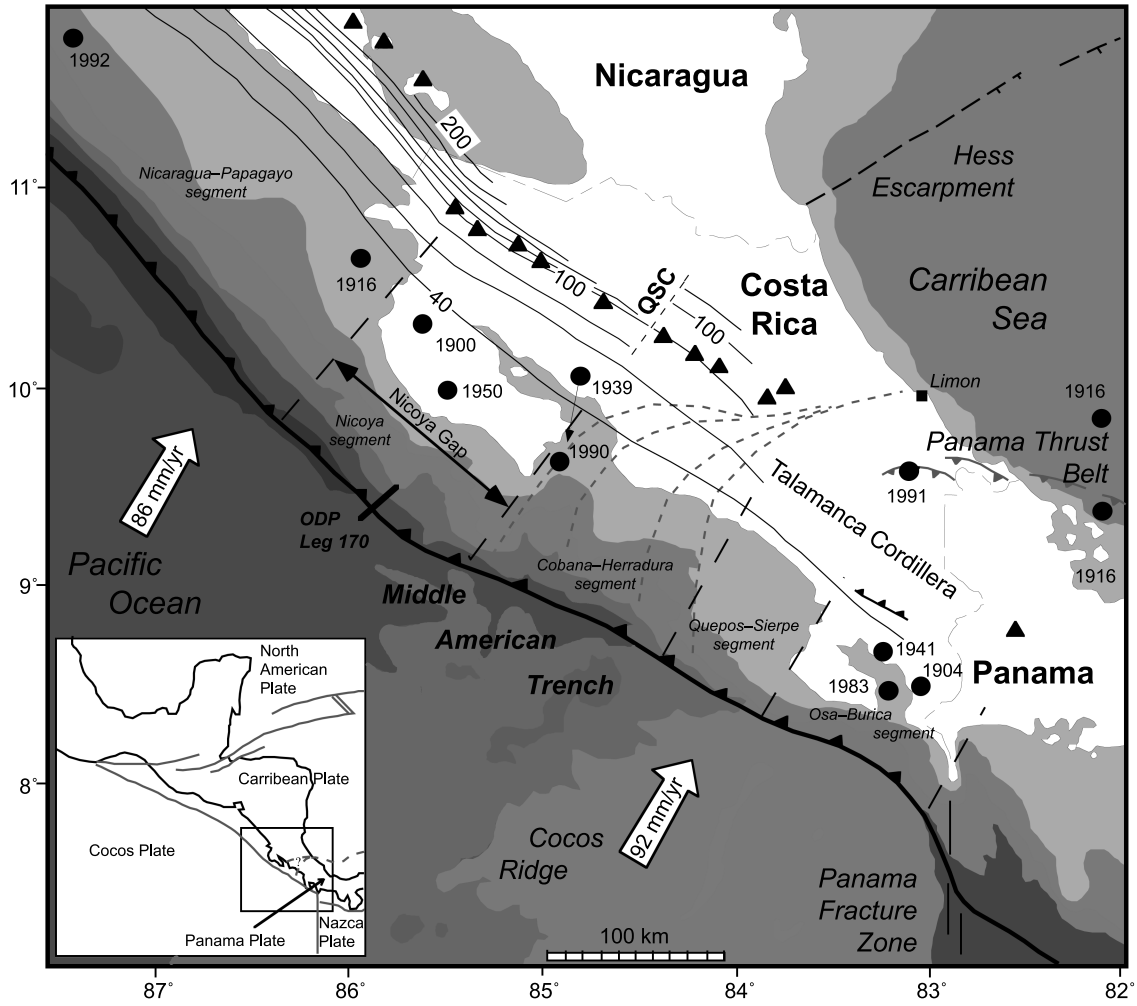

FIGURE 3: Tectonic setting of southern Central America and geometry of the Wadati–Benioff zone (from *Protti et al*., [1995]). Isodepth contours are at 20 km intervals, from 40 km. Filled tringles are active volcanoes and filled circles are the location of large (*M*>7.0) earthquakes that occurred in the 20th centrury. QSC marks the projection of the Quesada sharp contortion.

seismic slab suddenly disappears. The other largest intermediate-depth event under Costa Rica was the Naranjo, 1992, M_w=6.5 event, coincidentally at another major segmentation of the seismic slab.

Future work

Two small projects are suggested here to contribute to the understanding of intraslab events under Central America. First, take the angles of the *P* and *T* axes obtained by *Protti* [1991] from intermediate-depth focal mechanisms and add the projection of the slab dip to them to set them within the slab frame. This will give a better idea of the stress regime within the subducted plate. This should also be done for all intermediate events contained in the Harvard catalog under Central America.

Second, compare the waveforms from the 1948 and the 1992 earthquakes in central Costa Rica, as recorded by the same stations and instruments to learn about their relative locations, size and tectonic implications.

Postscript

A large (M_w=7.7), intermediate-depth (60 km) earthquake occurred off El Salvador on January 13th, 2001, at 17:33 UTC. Despite its large magnitude and the fact that it was felt all over the Central American isthmus, from southern Guatemala to western Panama, the damage produced by this earthquake was relatively small. As mentioned above, the large trench-arc gap, the steep dip angle of the slab, the long hypocentral distance to large cities and the path of the seismic waves through the mantle wedge, contributed to the attenuation of the radiated energy. The El Salvador January 13th, 2001 earthquake had a normal focal mechanism but when the nodal planes are placed within the slab frame, the

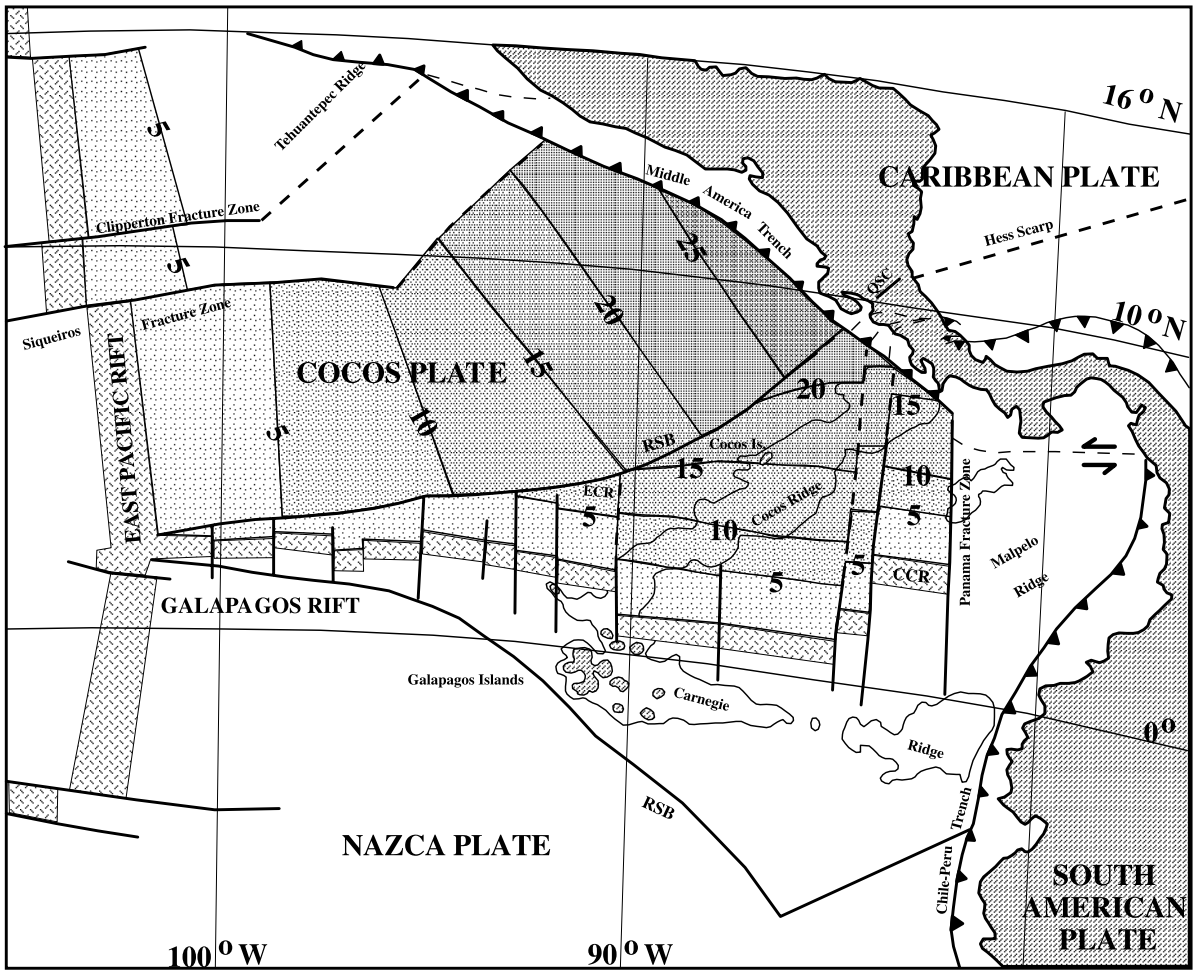

FIGURE 4: Age distribution of the Cocos plate (in Ma). RSB: rough/smooth boundary; QSC: Quesada sharp contortion; CRR and ECR are the Costa Rica and Ecuador rifts, respectively.

slip vector reflects compression within the slab resulting in reverse faulting. There were only nine aftershocks with magnitude above 5.0 in the following eight months and the largest one reached only M_w=6.1. All these aftershocks occurred in a depth range from 55 to 75 km, indicating an elastic thickness of 20 km for the slab and they clustered on less than 80 km along the trench. Considering the large magnitude of this earthquake and the relatively small rupture area, evidenced by the aftershocks, the El Salvador earthquake had a very large stress drop, consistent with intraplate events.

References

DeMets, C., R.G. Gordon, D.F. Argus, and S. Stein, Current plate motions, *Geophys. J. Int., 101*, 425–478, 1990.

Guendel, F., and M. Protti, Sismicidad y sismotectónica de America Central, *Física de la Tierra, 10*, 19–51, 1998.

Hey, R.N. Tectonic evolution of the Cocos–Nazca spreading center, *Geol. Soc. Am. Bull., 88*, 1404–1420, 1977.

Protti, M., Correlation between the age of the subducting Cocos plate and the geometry of the Wadati–Benioff zone under Nicaragua and Costa Rica, M.sc. dissertation, 66 pp., University of California, Santa Cruz, 1991.

Protti, M., F. Güendel, and K. McNally, Correlation between the age of the subducting Cocos plate and the geometry of the Wadati–Benioff zone under Nicaragua and Costa Rica, in *Geologic and Tectonic Development of the Caribbean Plate Boundary in Southern Central America: Boulder, Colorado,* edited by P. Mann, P., Geological Society of America Special Paper *295*, 309–326, 1995.

Silver, E.A., D.L. Reed, J.E. Tagudin, and D.J. Heil, Implications of the north and south Panama thrust belt for the origin of the Panama orocline, *Tectonics, 9*, 261–281, 1990.

Large, intermediate-depth earthquakes in Southwest Japan

Phil R. Cummins, Yoshiyuki Kaneda and Takane Hori
Frontier Research Program for Subduction Dynamics, JAMSTEC
2–15 Natsushima-cho, Yokosuka, 237–0061, Japan
cummins@jamstec.go.jp, kaneday@jamstec.go.jp, horit@jamstec.go.jp

Introduction

The subduction of the Philippine Sea plate beneath Southwest Japan leads to the repeated occurrence of great megathrust earthquakes there, which are the focus of a concerted earthquake disaster mitigation and prediction effort. As shown by the 1995 Kobe earthquake, the seismic risk associated with crustal earthquakes is also substantial. There is, however, less discussion of the earthquake risk associated with intermediate-depth earthquakes within the subducting slab. This is probably due to the fact that almost all of the recent intraslab seismicity has been associated with earthquakes less than $M=6.5$.

There were, however, two large intraslab earthquakes which occurred in Southwest Japan in the very first part of the 20th century. Three earthquakes of moderate size ($M= 6.6–6.8$) occurred in 1952, 1968 and 1983. These earthquakes are listed in Table 1 and the available information on them is reviewed in more detail below. (Much of the information about damage and casualties is from *Usami*, [1987]).

1905 Geiyo earthquake

This earthquake occurred beneath the Seto Inland Sea near Hiroshima and was felt as far away as 600 km. Eleven people were killed, 177 injured, and around 500 buildings were damaged or destroyed.

Japanese sources place the hypocenter at 40–50 km depth, but *Gutenberg and Richter* [1954] and sources based on their table report a depth of 100 km. The latter is almost certainly in error, as suggested not only by the intensity pattern but also by observed vertical surface displacement as large as -4 cm.

There were a number of aftershocks, but none located with sufficient precision to define the fault plane. As far as we know, no focal mechanism for this earthquake has been obtained, but analysis of surface deformation is suggestive of normal faulting with strike south–southeast. Recently, seismograms from various types of Omori seismometers have been discovered at the Earthquake Research Institute in Tokyo but their analysis is complicated by poor knowledge of the instrument characteristics [*Miyakawa et al.,* 1998].

1909 Hyuganada earthquake

The 1909 Hyuganada earthquake occurred beneath northern Kyushu and was felt as far away as 635 km. Despite its size, the great depth must have mitigated its effects sufficiently that there were no deaths, but at least five people were injured and a number of buildings damaged or destroyed.

Although this earthquake appears in a number of lists of significant earthquakes, we have as yet found no more detailed study. Its focal mechanism, as far as we have been able to ascertain, is completely unknown. There appear to have been no reported aftershocks.

1952 Yoshino earthquake

This earthquake occurred near the city of Nara in central Japan. It was felt as far away as 650 km, killed nine people, injured 136, and damaged or destroyed about 350 buildings. There were only four reported aftershocks.

Remarkably, despite the extensive destruction caused by this earthquake, we have been unable to find any detailed study of its source mechanism. There is a Japan Meteorological Agency (JMA) solution, however, which is shown in Figure 1. We think surface deformation data should exist, however, and hope to present these data at the workshop.

1968 Bungo Strait earthquake

This earthquake occurred beneath the Bungo Strait separating Kyushu and Shikoku. It was felt as far away as 500 km, injured 22 people, and damaged or destroyed eight buildings.

Because this earthquake occurred after the establishment of the World Wide Standardized Seismographic Network (WWSSN), an extensive analysis of its source mechanism was possible [*Shiono and Mikumo,* 1975]. A substantial number of aftershocks were reported, defining a fault plane of about 20 x 20 km, with a strike of about 20°E of N and a dip of 72°. The sense of faulting was normal, with rupture initiating near the base of the fault and propagating upward. Three centimeters of subsidence was observed near the epicenter that is consistent with this source mechanism.

TABLE 1

Earthquake	Origin	Time	Lat	Lon	Depth	Mag	Deaths	Injuries	Damage*	Aftershocks
Geiyo (U)	1905/06/02	05:39:07.?	34.1	132.5	40-100	7.2	22	177	500	several
Hyuganada (U)	1909/11/10	06:13:??.?	32.3	131.1	150	7.9	0	5	10+	?
Yoshino (JMA)	1952/07/17	16:09:51.5	34.45	135.78	60	6.8	9	136	350	4
Bungo (SM)	1968/08/05	16:17:06.0	33.30	132.38	40	6.6	0	23	8	
Kunisaki (IHM)	1983/08/25	21:23:34.3	33.55	131.60	116	6.8	0	1	light	
Hyuganada (JMA)	1987/03/18	12:36:29.0	31.97	132.06	48	6.6	0	6	light	?

** Approximate total no. damaged buildings as reported by Usami [1996].*

1983 Kunisaki earthquake

This earthquake occurred beneath northern Shikoku and, probably due to its depth, caused only one reported injury and some light damage. Only a small number of aftershocks were reported, but because this earthquake occurred in (or almost in) the era of digital seismology, an extensive study of the main shock is available [*Imagawa et al.,* 1985]. Assuming a 10 x 5 km fault plane based on the limited number of aftershocks, they obtained an average slip of 3.3 m, with rupture begining at the base of the fault and propagating upwards. Unlike the other earthquakes discussed above, the mechanism appears to be a high-angle thrust, but the horizontal projection of the *T* axis is oriented along the strike of the subducting plate.

Conclusions

Recent intermediate-depth earthquakes in Southwest Japan have been at most moderate in size, and this together with their depth, has led to the impression that the seismic risk associated with such earthquakes is small. However, very early in the century two quite large intermediate-depth earthquakes occurred, so it seems that the recent activity may give a misleading impression. Certainly an event similar to the 1905 Geiyo earthquake occurring today would cause extensive damage and loss of life.

It is not clear whether all the events listed here are really intraslab events. *Shiono and Mikumo* [1975] and *Imagawa et al.* [1985] characterize the 1968 and 1983 events respectively as occurring above the subducting slab. Using our recently constructed model of the Philippine Sea plate boundary, however, we find that the 1968 event does lie within the slab and think this is very likely true for the 1983 event as well (see Figure 1). Thus, it seems likely that all of the events considered here are intraslab events and moreover, are probably consistent with the dehydration embrittlement model of *Kirby et al.* [1996].

References

Gutenberg, B. and C.F. Richter, *Seismicity of the Earth and Associated Phenomena,* Princeton Univ. Press, Princeton, N.J., 310 pp., 1954.

Imagawa, K., K. Hirahara, and T. Mikumo, Source mechanisms of subcrustal and upper mantle earthquakes around the northeastern Kyushu region, southwestern Japan, and their tectonic implications, *J. Phys. Earth, 33,* 257–277, 1985.

Kirby, S., E.R. Engdahl, and R. Denlinger, Intermediate-depth intraslab earthquakes and arc volcanism as physical expressions of crustal and uppermost mantle metamorphism in subducting slabs, in *Subduction: Top to Bottom*, G.E. Bebout et al., Eds., American Geophysical Union, Washington, D.C., pp. 195–214, 1996.

Miyagawa, K., I. Nakanishi, K. Miura, and S. Tanaka, The 1905 Geiyo earthquake (M=7.3) recorded by the Omori seismometers and the digitization of the records, *Zishin, 51,* 113–121, 1998.

Shiono, K. and T. Mikumo, Tectonic implications of subcrustal normal faulting earthquakes in the western Shikoku region, Japan, *J. Phys. Earth, 23,* 257–278, 1975.

Usami, T., *Descriptive catalog of damaging earthquakes in Japan,* University of Tokyo Press, Tokyo, 1987.

Utsu, T., A catalog of large earthquakes ($M \geq 6$) and damaging earthquakes in Japan for the years 1885–1925, in *Historical Seismograms and Earthquakes of the World*, W.H.K. Lee et al., eds., Academic Press, San Diego, pp. 150–161, 1987.

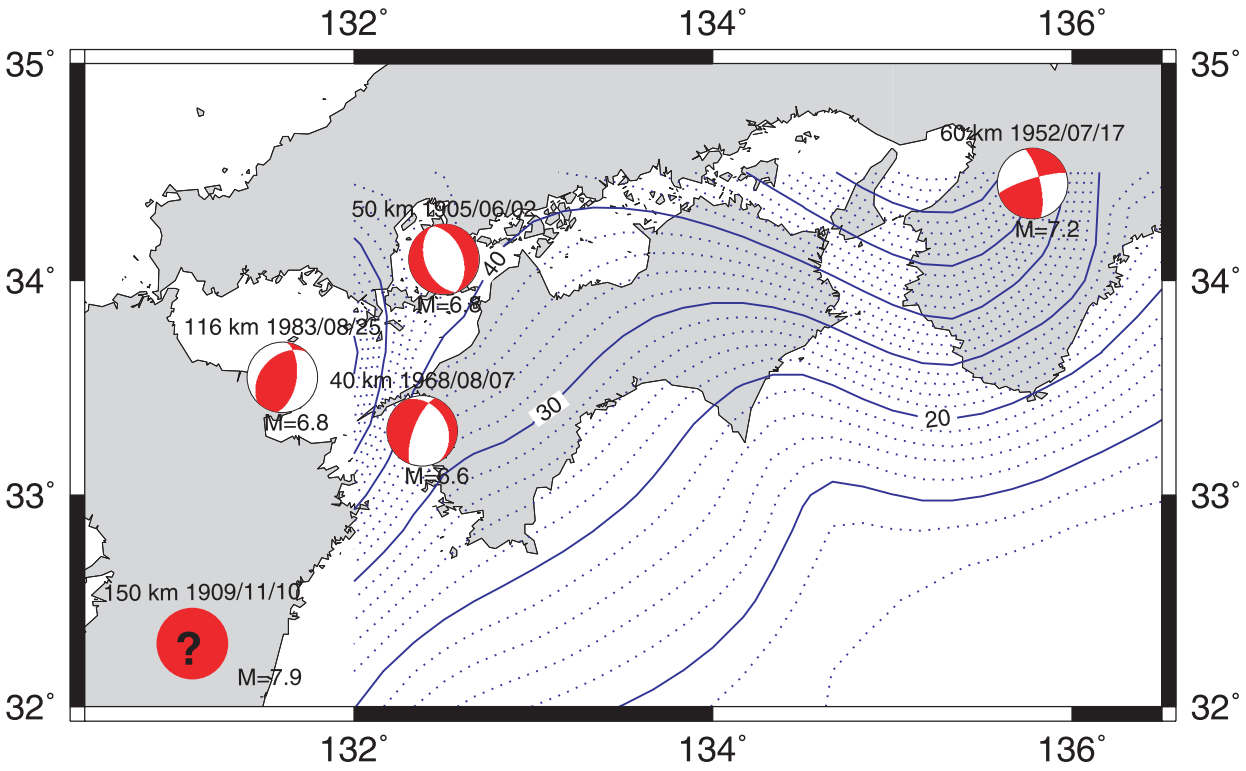

FIGURE 1: A model for the Philippine Sea plate and earthquake source mechanism solutions for large intermediate-depth earthquakes in Southwest Japan.

Large ($M_w \geq 5.5$) intraplate slab earthquakes (1928–2000) of the Prince William Sound region, Alaska

Diane Doser, Monique Velasquez, Wesley Brown and Annette Veilleux
Department of Geological Sciences, University of Texas at El Paso, El Paso, Texas 79968–0555, USA
doser@geo.utep.edu, monique@geo.utep.edu, wesley@geo.utep.edu, veilleux@geo.utep.edu

Earthquake relocations and body waveform modeling studies have been used to examine changes in $M_w \geq 5.5$ seismicity before and after the 1964 great Alaskan earthquake. This portion of our study focuses on the region of the Prince William Sound (PWS) asperity as defined by *Johnson et al*. [1996] (boxes, Figure 1), while ongoing work continues in the Kodiak Island region. In the Prince William Sound region both the Yakutat block and Pacific plate are being subducted beneath North America, with the top of the Yakutat block forming the place interface.

Much of the lower-plate seismicity throughout the study area for the past 70 years appears to cluster immediately downdip of the 1964 asperity. Hypocenters of intraplate slab events in PWS show two persistent zones of seismicity (Figure 2). These zones are shown in cross section in Figure 3 with crustal structure based on the refraction studies of *Brocher et al*. [1994] and *Fuis et al*. [1991]. One zone of earthquakes (Columbia Bay [CB], Figure 1) is located immediately downdip of the 1964 mainshock hypocenter (10–25 km) at 30–40 km depth within the Pacific plate mantle. A second zone (Tazlina [T], Figure 1) occurs 50–70 km from the main shock hypocenter at 50–60 km depth in a region of the Pacific plate mantle where the dip of the Pacific plate begins to steepen [*Brocher et al.*, 1994]. Both zones exhibit normal faulting with northwest–southeast directed *T*-axes (Figure 2). Earthquakes of up to $M_w=6.7$ have occurred within the Tazlina zone prior to the 1964 mainshock and the largest intraslab events following the 1964 mainshock ($M_w=6.5$–6.6) also occurred within this region.

A third region of intraslab earthquakes is located offshore in PWS near Montague Island (MI, Figure 2). Depth control for these earthquakes is poor, but suggests they are occurring either within the lower portion of the Yakutat block or within the crust of the Pacific plate in a region where there is significant flattening in the dip of the Pacific plate [*Brocher et al.*, 1994]. In 1928, a $M_w=7.0$ earthquake occurred in this region and waveform modeling of this event indicates reverse faulting (Figure 2), perhaps due to an upward bend in the Pacific plate.

Within Cook Inlet (Figure 4), intraslab seismicity is complicated by the presence of a double Benioff zone [e.g., *Ratchkovsky et al.*, 1997] and significant contortion of the down-going slab [*Doser et al.*, 1999]. Most large events appear to be occurring within the Pacific plate mantle, although slab geometry is not well constrained due to lack of seismic reflection/refraction studies such as those carried out in the PWS region. Events at 40–60 km depth show normal to normal-oblique faulting (Figure 4) and the largest ($M_w=6.7$–6.8) historic events are no deeper than 60 km. Of particular note is the October 1954 ($M_w=6.8$) earthquake that was associated with a maximum intensity of VIII [*Stover and Coffman*, 1993] in the Anchorage region. Since 1928 only the 1964 mainshock has produced a higher observed intensity in Anchorage.

Below 60 km depth a wider variety of mechanisms is observed. *T*-axes of Cook Inlet earthquakes show northwest to west-northwest oriented extension, regardless of focal depth.

A higher level of seismicity within the subducting plate in the south-central and eastern Kenai Peninsula was observed prior to the 1964 mainshock. Since 1964, no $M_w>6.3$ intraslab events have occurred within Cook Inlet.

These observations suggest that intraplate slab earthquakes represent a significant source of seismic hazard for the Anchorage region. The historic data also suggest that the lower level of moment release within the subducting slab since the 1964 mainshock may not reflect the longer-term average.

References

Brocher, T.M., G.S. Fuis, M.A. Fisher, G. Plafker, M.J. Moses, J.J. Taber, and N.I. Christensen, Mapping the megathrust beneath the northern Gulf of Alaska using wide-angle seismic data, *J. Geophys. Res., 99*, 11,663–11,686, 1994.

Cohen, S.C., and J.T. Freymueller, Deformation of the Kenai Peninsula, Alaska, *J. Geophys. Res., 102*, 20,479–20,488, 1997.

Doser, D.I., A.M. Veilleux, and M. Velasquez, Seismicity of the Prince William Sound region for over thirty years following the 1964 great Alaskan earthquake,

Pure Appl. Geophys., 154, 593–632, 1999.

Fuis, G.S., E.L. Ambos, W.D. Mooney, N.I. Christensen, and E. Geist, Crustal structure of accreted terranes in southern Alaska, Chugach mountains and Copper River basin, from seismic refraction results, J. *Geophys. Res., 96*, 4187–4227, 1991.

Johnson, J.M., K. Satake, S.R. Holdahl, and J. Sauber, The 1964 Prince William Sound earthquake: joint inversion of tsunami and geodetic data, *J. Geophys. Res., 101*, 523–532, 1996.

Ratchkovsky, N.A., J. Pujol, and N.N. Biswas, Relocation of earthquakes in the Cook Inlet area, south-central Alaska, using the joint hypocenter determination method, *Bull. Seismol. Soc. Am., 87*, 620–636, 1997.

Stover, C.W., and J.L. Coffman, Seismicity of the United States, 1568–1989 (revised), *U.S. Geological Survey Prof. Pap. 1527*, 418 pp., 1993.

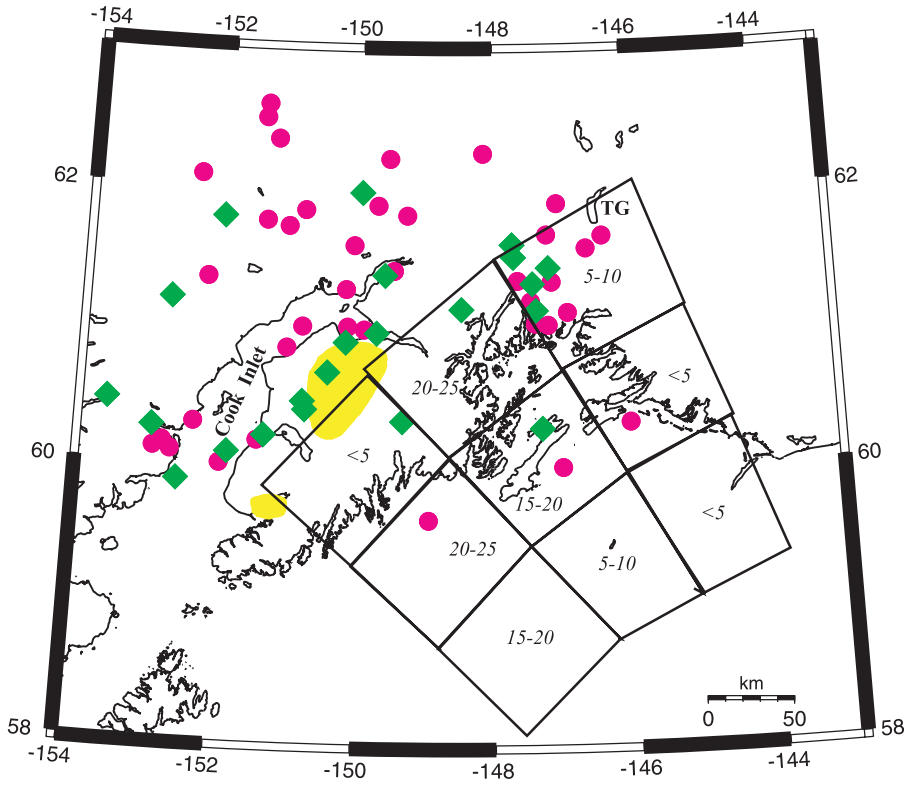

FIGURE 1: Lower plate earthquakes in south-central Alaska. Dots are M_w>5.0 earthquakes following the 1964 mainshock, diamonds are events from 1928–1963. Boxes show slip along plate interface (in meters) during the 1964 mainshock [*Johnson et al.*, 1996]. Yellow patches are regions with post seismic uplift >0.6 m between 1964 and 1995 [*Cohen and Freymueller*, 1997].

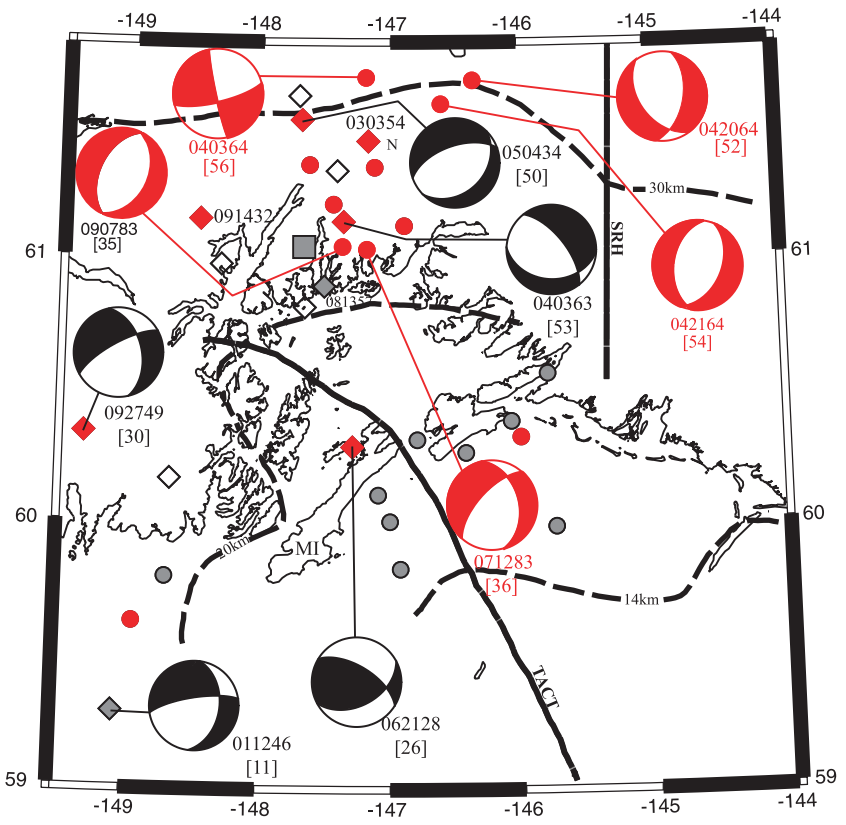

FIGURE 2: Earthquakes in the Prince William Sound area (1928–2000). Dots are post-1964 mainshock, diamonds are pre-1964 mainshock and the square is the 1964 mainshock. Red denotes events below the plate interface. Dashed lines show depth to plate interface. Cross section along South Richardson Highway (SRH) shown in Figure 3. Focal mechanisms are for $M_w \geq 6.0$ events. Numbers in brackets are depths from waveform modeling.

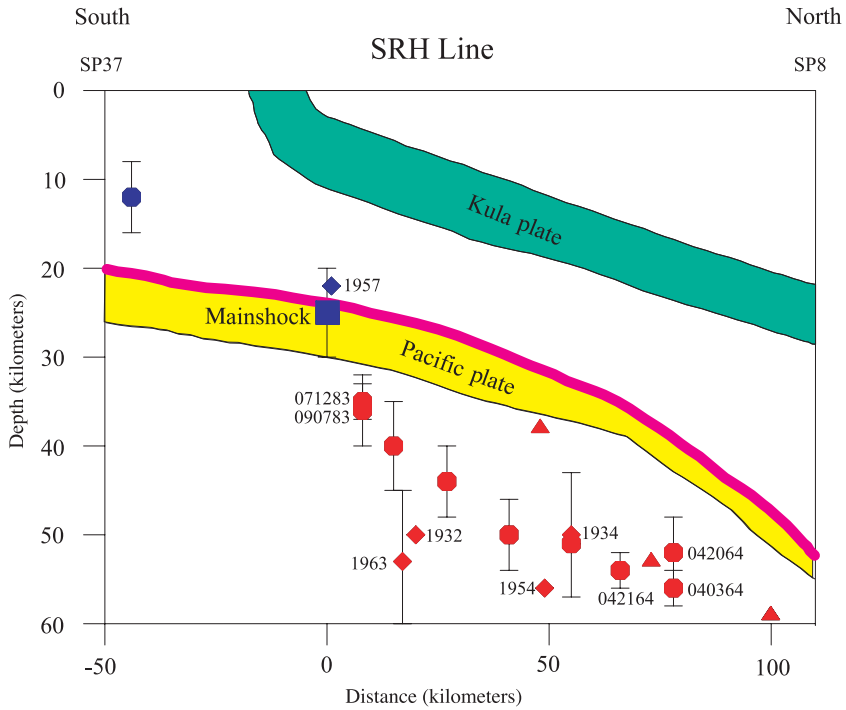

FIGURE 3: Cross section along SRH (Southern Richardson Highway). Structure from *Brocher et al*. [1994] and *Fuis et al.* [1991]. Error bars denote depth uncertainties. Triangles are events from the Harvard Centroid Moment Tensor (CMT) catalog. Pacific plate crust is yellow. Megathrust is bold line.

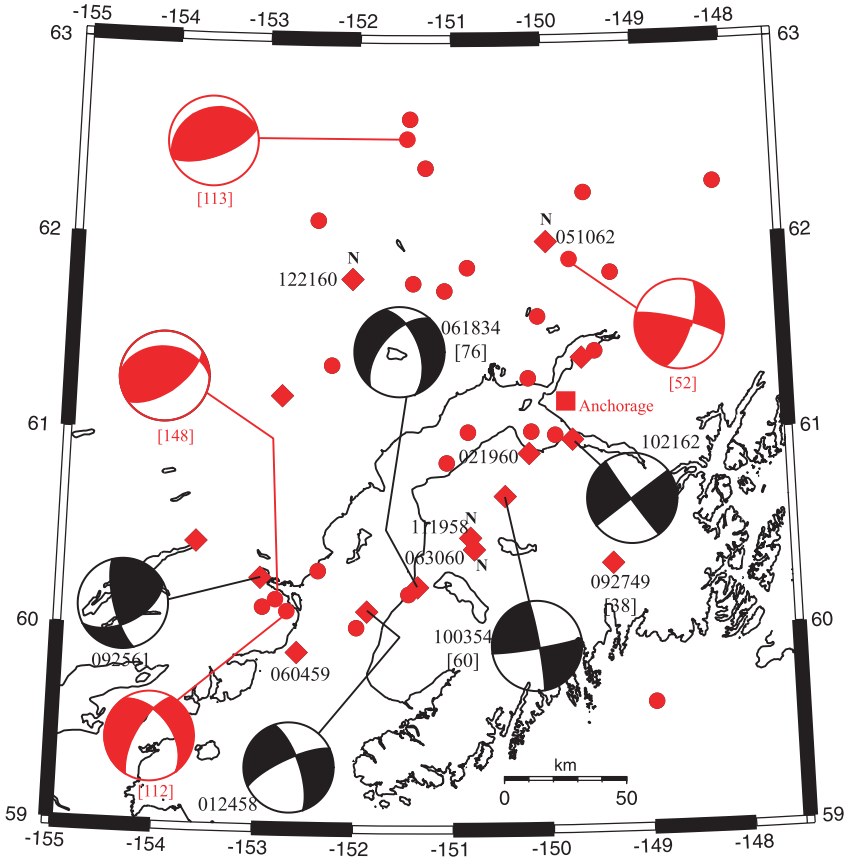

FIGURE 4: Intraslab events of the Cook Inlet region (1928–2000). Symbols are as in Figure 2. Focal mechanisms are shown for $M_w \geq 6.0$ events. Numbers in brackets are focal depths from waveform modeling. Red mechanisms are CMT solutions.

The radiated seismic energy and apparent stress of interplate and intraslab earthquakes at subduction-zone environments: Implications for seismic hazard estimation

George L. Choy[1], John L. Boatwright[2] and Stephen H. Kirby[2]
1 United States Geological Survey, PO Box 25046, Lakewood, Colorado, 80225, USA
2 United States Geological Survey, 345 Middlefield Road, Menlo Park, California, 94025, USA
choy@usgs.gov, boat@usgs.gov, skirby@usgs.gov

ABSTRACT

The radiated seismic energies (E_S) of 980 shallow subduction-zone earthquakes with magnitudes ≥ 5.8 are used to examine global patterns of energy release and apparent stress. In contrast to traditional methods which have relied upon empirical formulas, these energies are computed through direct spectral analysis of broadband seismic waveforms. Energy gives a physically different measure of earthquake size than moment. Moment, being derived from the low-frequency asymptote of the displacement spectra, is a measure of the final static displacement. Thus, moment is related to the long-term tectonic implication of an earthquake. In contrast, energy, being derived from the velocity power spectra, is more a measure of seismic potential for damage to anthropogenic structures. There is considerable scatter in the plot of E_S–M_0 for worldwide earthquakes. For any given M_0, the E_S can vary by as much as an order of magnitude about the mean regression line. The global variation between E_S and M_0, while large, is not random. When subsets of E_S–M_0 are plotted as a function of seismic region, tectonic setting and faulting type, the scatter in data is often substantially reduced. There are two profound implications for the estimation of seismic and tsunamic hazard. First, it is now feasible to characterize the apparent stress for particular regions. Second, a given M_0 does not have a unique E_S. This means that M_0 alone is not sufficient to describe all aspects of an earthquake. In particular, we have found examples of interplate thrust-faulting earthquakes and intraslab normal-faulting earthquakes occurring in the same epicentral region with vastly different macroseismic effects. Despite the gross macroseismic disparities, the M_W's in these examples were identical. However, the M_e's (energy magnitudes) successfully distinguished the earthquakes that were more damaging.

Introduction

There are two compelling reasons for using radiated seismic energy as a complement to moment in estimating seismic and tsunamic hazard. First, energy gives a physically different measure of earthquake size than moment. Energy is derived from the velocity power spectra, while moment is derived from the low-frequency asymptote of the displacement spectra. Thus, moment, being a measure of the final static displacement, is related to the long-term tectonic implication of an earthquake. In contrast, energy, being strongly peaked about the corner frequency of an earthquake, is more a measure of seismic potential for damage to anthropogenic structures. Secondly, significant regional and tectonic variations in energy release are suppressed by empirical formulas. *Choy and Boatwright* [1995] demonstrated that systematic variations in the release of energy and in apparent stress can now be identified that were previously undetectable because of the lack of reliable energy estimates. In this paper, we first review some of the important findings from *Choy and Boatwright* [1995] and then proceed to identify classes of earthquakes with unusually high intensity of energy release relative to moment release. In particular, there is a substantial difference in the energy radiated by normal-faulting intraslab earthquakes and by thrust-faulting interplate earthquakes. Although M_0 (or its derived magnitude M_W) can characterize the area affected by the rupture, E_S (or its derived magnitude M_e) is more capable of describing macroseismic effects. Also, the highest apparent stresses of any earthquake group are associated with strike-slip faulting earthquakes occurring in oceanic environments. Contrary to conventional wisdom, many of these oceanic strike-slip earthquakes have been associated with tsunamis.

Previous methods of computing radiated seismic energy, E_S

The computation of the seismic energy radiated by an earthquake simply requires an integration of radiated energy flux in velocity-squared seismograms. However, most methods of computing energy have historically

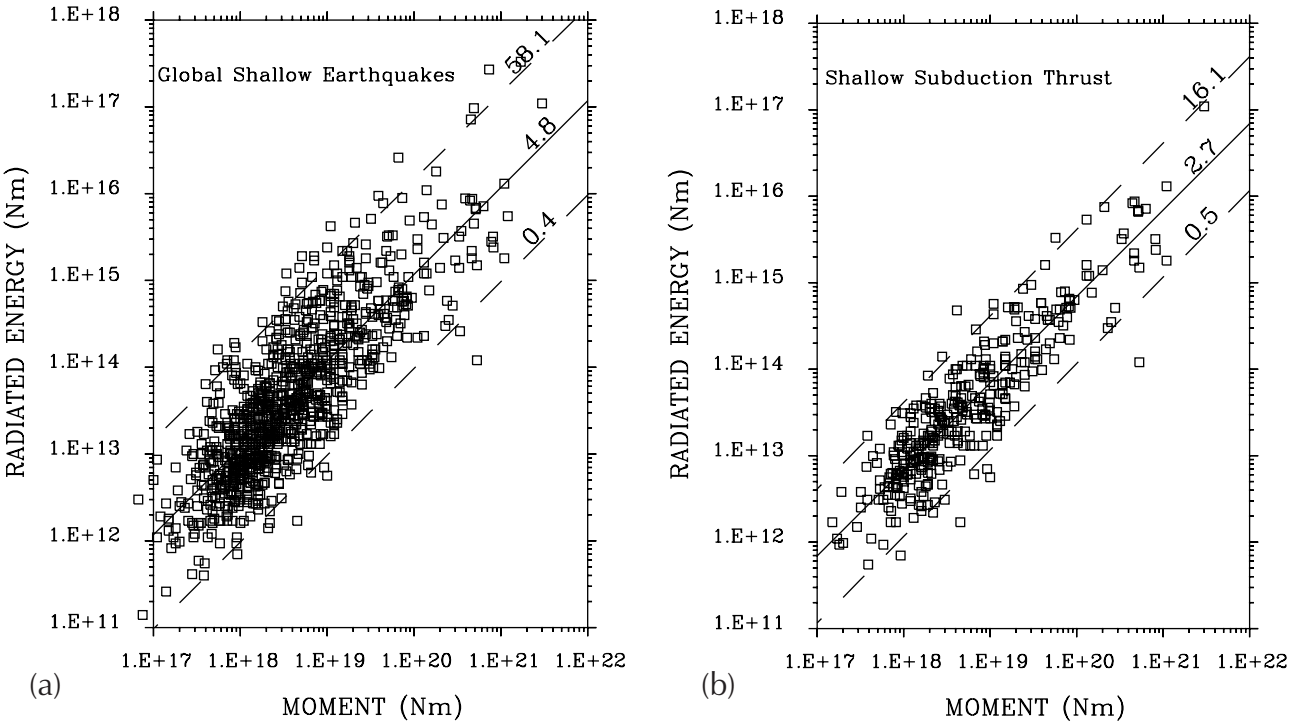

FIGURE 1: a) Radiated energy (E_S) of 980 worldwide shallow-focus earthquakes that occurred between 1988 to 1999 as a function of moment (M_0). The radiated energies are taken from the monthly listings of the PDE (Preliminary Determination of Epicenters) published by the NEIC (National Earthquake Information Center) of the U.S.G.S. The slope of the least-squares linear regression (solid line) yields a global average apparent stress for earthquakes of 4.8 bars. The 95% geometric spread (width of distribution) about the regression line is indicated by the dashed lines. b) E_S–M_0 plot for the subset of 355 shallow-focus earthquakes located near subduction zones with predominantly thrust-faulting focal mechanisms. The geometric spread is significantly smaller for this subset than for the set of world-wide earthquakes.

relied on empirical formulas because routine spectral analysis was impractical with analog data. Two common methods use the Gutenberg–Richter formulas which derive E_S from a magnitude

$$\log E_S = 5.8 + 2.4\, m_b$$
$$\log E_S = 11.8 + 1.5\, M_S$$

(in units of dyne cm). More recently, it has been suggested that

$$E_S \sim 5 \times 10^{-5}\, M_0.$$

Notice that in all these formulas that E_S is never actually computed. Instead it is predicated on another value (m_b, M_S or M_0). No new information is really obtained about the earthquake.

Direct measurement of radiated seismic energy

Fortunately, theoretical and technological impediments to the direct computation of radiated energy have now been removed. The requisite spectral bandwidth is now recorded digitally by a number of seismograph networks and arrays with broadband capability. In addition, corrections for source mechanism and frequency-dependent wave propagation are better understood now than at the time empirical formulas were first developed. We briefly describe the method of *Boatwright and Choy* [1986].

For shallow earthquakes where the source functions of direct and surface-reflected body-wave arrivals may overlap in time, the radiated energy of a *P*-wave group (consisting of *P*, *pP* and *sP*) is related to the energy flux by

$$E_S^P = 4\pi \langle F^P \rangle^2 \left(\frac{R^P}{F^{gP}} \right)^2 \varepsilon_{gP}^*$$

where the *P*-wave energy flux, ε_{gP}^*, is the integral of the square of the ground velocity, corrected for frequency-dependent attenuation; $\langle F^P \rangle^2$ is the mean-square radiation-pattern coefficient for *P* waves; R^P is the *P*-wave geometrical spreading factor; F^{gP} is the generalized radiation pattern coefficient for the *P*-wave group defined as

$$(F^{gP})^2 = (F^P)^2 + (\hat{PP}\, F^{pP})^2 + \frac{2\alpha q}{3\beta} (\hat{SP}\, F^{sP})^2$$

where F^i are the radiation-pattern coefficients for $i=P$,

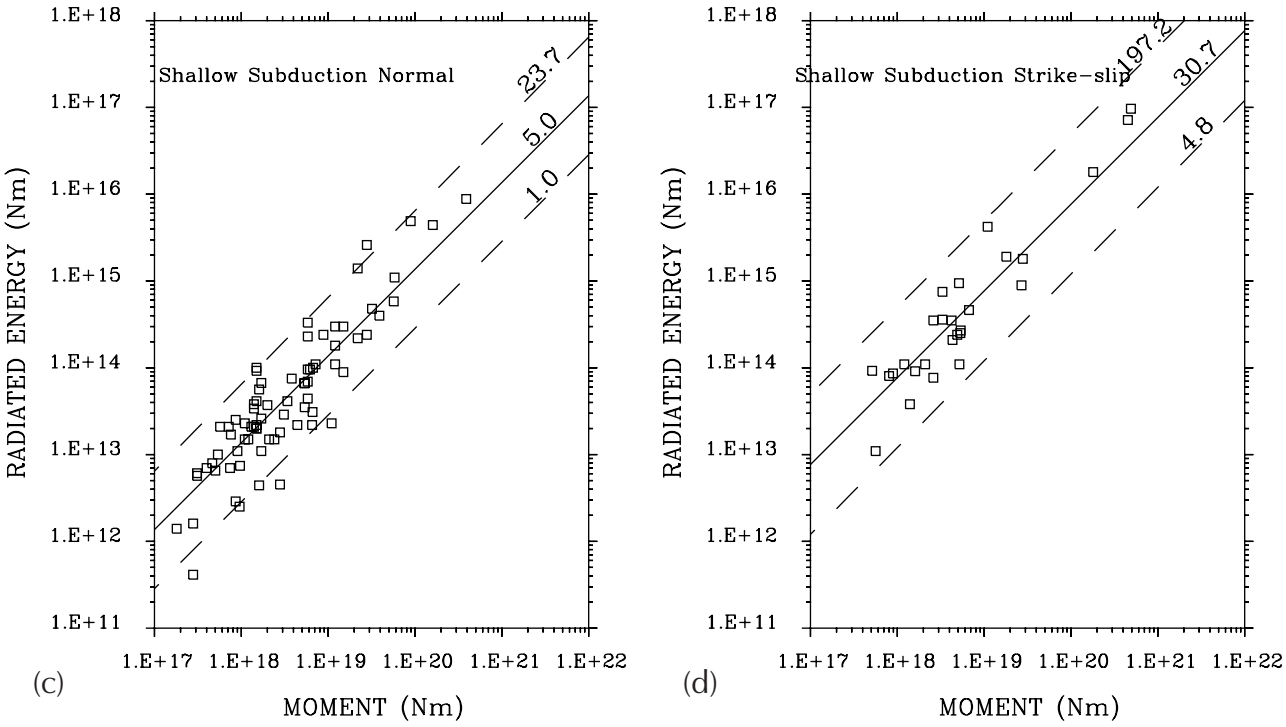

FIGURE 1 (cont'd) : *c) E_S–M_0* for the subset of 76 shallow-focus earthquakes located near subduction zones with predominantly normal-faulting focal mechanisms. The geometric spread is smaller for this subset than for the set of worldwide earthquakes. d) *E_S–M_0* for the subset of 27 shallow-focus earthquakes located near subduction zones with predominantly strike-slip focal mechanisms. The average apparent stress of strike-slip earthquakes is a magnitude larger than that for the earthquakes with dip-slip mechanisms.

pP, and *sP*; $\hat{PP}$ and $\hat{SP}$ are plane-wave reflection coefficients of *pP* and *sP* at the free surface, respectively, and corrected for free-surface amplification at the receiver; and q is ratio of *S*-wave energy to *P*-wave energy. The correction factors explicitly take into account our knowledge that the earthquake is a double-couple, that measurements of the waveforms are affected by interference from depth phases, and that energy is partitioned between *P* and *S* waves. The total radiated energy when using the *P*-wave group is $E_s=(1+q)E_S^P$.

Energy magnitude

From the radiated energies for a set of 378 global shallow earthquakes *Choy and Boatwright* [1995] defined an energy magnitude, M_e,

$$\log E_S = 4.4 + 1.5\, M_e$$

or

$$M_e = 2/3 \log E_S - 2.9$$

where E_S is in units of Newton·meters. Note that magnitude M_e is derived explicitly from energy (whereas in the Gutenberg–Richter formula energy is derived from magnitude).

Although M_e and M_w are magnitudes that describe the size of an earthquake, they are not equivalent. Because they measure different physical properties of an earthquake, there is no *a priori* reason that they should numerically equal for any given seismic event. Indeed, in the following sections we show that earthquakes with the same M_w can cause different macroseismic effects. While the macroseismic effects cannot be distinguished by M_w, they can be quantified by M_e. The energy magnitude, M_e, is an essential complement to moment magnitude, M_w, for assessing seismic potential.

The energy and moment of an earthquake are related by apparent stress, $\tau_a = \mu\, E_s / M_0$, where μ is the average rigidity at the source. Apparent stress also serves as a good indicator of the intensity of seismic energy radiation, E_s, relative to the size of the event as measured by the seismic moment, M_0. A plot of E_s–M_0 for the worldwide population of earthquakes exhibits large scatter (Figure 1a). However, when data are separated into subsets based on faulting mechanism and seismic region, the scatter in the E_s–M_0 plots can be relatively small. The important point is that no single empirical formula can hope to predict E_s from M_0. Indeed, these differences can be exploited to detect patterns of energy and moment that were previously masked by empirical formulas.

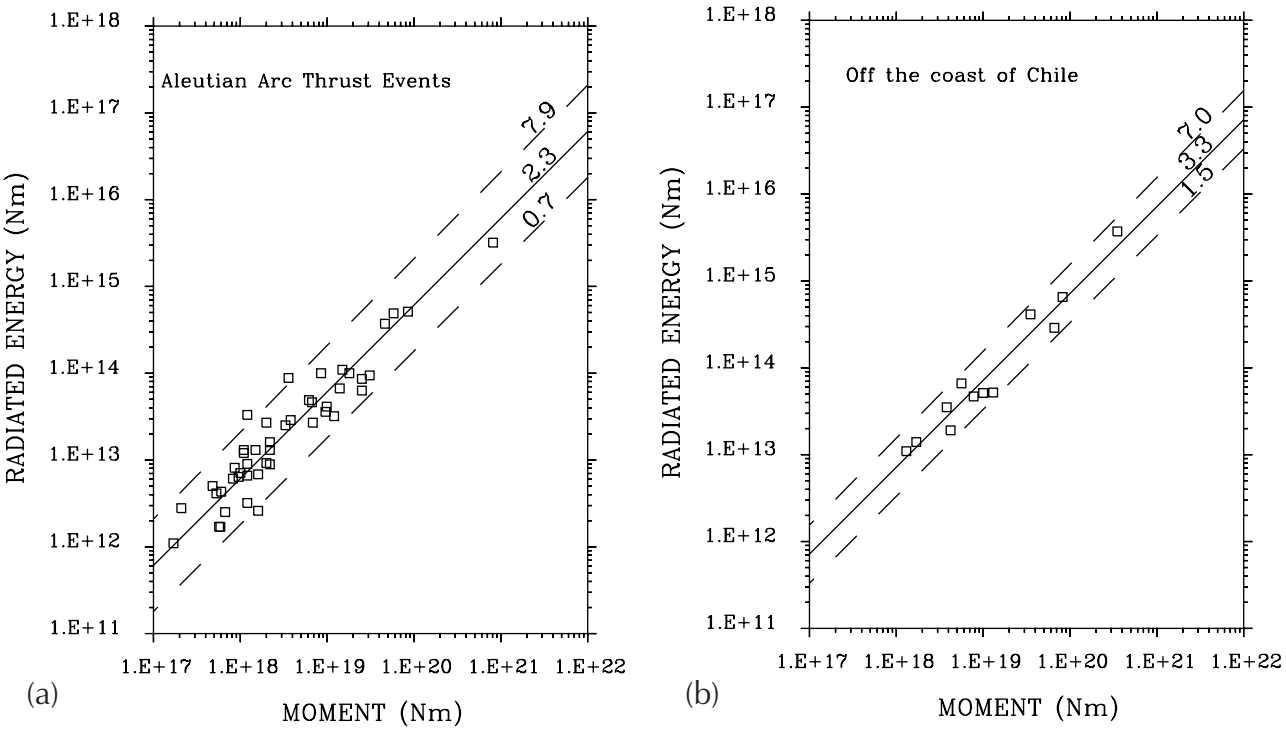

FIGURE 2: a) E_S–M_0 for 46 shallow-focus thrust-faulting earthquakes that occurred between 1988 to 1999 along the Aleutian arc. The characteristic apparent stress for this seismic region is centered narrowly about 2.3 bars. b) E_S–M_0 for 12 shallow-focus thrust-faulting earthquakes that occurred between 1988 to 1994 along the Chile trench. The characteristic apparent stress for this seismic region is centered narrowly about 3.3 bars.

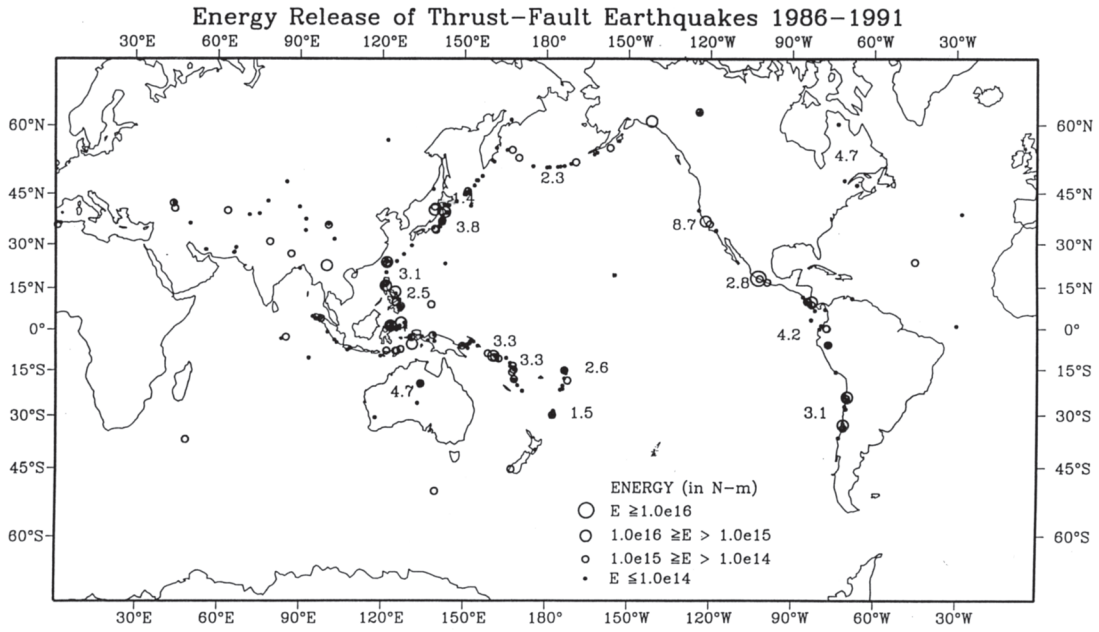

FIGURE 3: Global patterns of energy release for all large ($E_S > 10^{10}$ N • m) shallow thrust-fault earthquakes that occurred between 1988–1991. The characteristic apparent stress, τ_c, is indicated for those seismic regions where the geometric spread about the average stress in the E_S–M_0 plot is less than 15 bars.

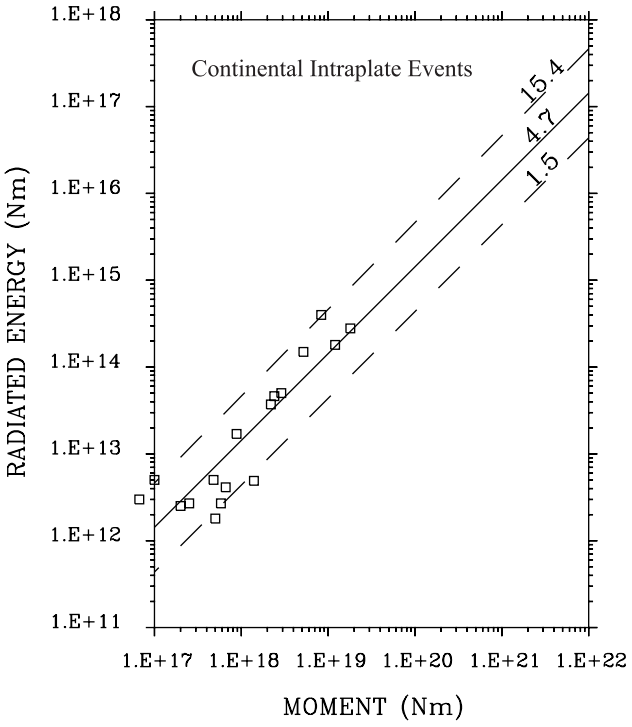

FIGURE 4: E_S–M_0 for 17 continental intraplate earthquakes that occurred between 1988 to 1999. The characteristic apparent stress for earthquakes in this tectonic setting is centered narrowly about 4.7 bars, which is slightly higher than average for all subduction-zone thrust earthquakes.

Systematic variations in energy release and apparent stress

As a function of seismic region and faulting type

The first step in sorting out the scatter in the E_S–M_0 plot is to separate the populations by faulting mechanism. Figure 1a shows the E_S–M_0 plot for the global set of shallow earthquakes with magnitude ≥ 5.8 that occurred between 1988–1999. Figures 1b–1d show E_S–M_0 for subsets consisting of earthquakes whose focal mechanisms are predominantly thrust, normal and strike-slip faulting mechanisms, respectively. Although the scatter is still large, the geometric spread about the average value of each subset does seem to have been reduced. On a global scale, the average apparent stress of strike-slip faulting earthquakes is much greater than that for normal-faulting earthquakes, which in turn is slightly larger than that for thrust-faulting earthquakes.

If we separate the data into subsets by region and mechanism, or by tectonic setting and mechanism, we find the reduction in the geometric spread is more dramatic [*Choy and Boatwright*, 1995]. For most regions of the world, the geometric spread is so narrow for a given faulting type that the average apparent stress can be regarded as the characteristic apparent stress (τ_c) of the region. Two examples are shown here (Figure 2), for thrust-fault earthquakes at the Aleutian arc and the Chile trench. A preliminary global map of the characteristic apparent stress of thrust-faulting earthquakes for seismic regions is shown in Figure 3. A τ_c was computed for a seismic region only if τ_a's from at least five earthquakes were available. A similar mapping of characteristic apparent stress for normal-faulting and strike-slip faulting earthquakes is not yet possible because of the relative paucity of such events. As more statistics on the release of energy are accumulated, spatial and temporal variations in energy release and apparent stress can be refined.

As a function of tectonic setting and faulting type

The geometric spread in the E_S–M_0 plot is also small for subsets based on earthquakes in specific tectonic settings. Figure 4 shows the data for the set of continental intraplate thrust-faulting earthquakes. Note that the average apparent stress for continental intraplate events is greater than the average for subduction-zone thrust-faulting earthquakes.

Normal-faulting intraslab earthquakes

We found two normal-faulting intraslab earthquakes that occurred in the immediate vicinity of interplate thrust-faulting events. For these two earthquakes, we could make a direct comparison of the relative amount of moment and energy associated with the different faulting types and tectonic settings.

The source parameters and macroseismic reports of two events that occurred in Chile are summarized in Table 1. The epicenter of the interplate thrust-faulting event of July 1997 is less than one degree from that of the intraslab normal-faulting event of October 1997. Despite the nearly identical M_S's and M_W's, as well as the spatial and temporal proximity of the epicenters, the intraslab normal-fault event caused extensive damage and loss of life, whereas the effects of the interplate thrust-fault event were minor. M_W is unable to quantify the conspicuous difference in damage reports. On the other hand, the M_e's are commensurate with the disparity in macroseismic effects. The M_e 7.6 of the intraslab earthquake, which caused much greater damage, is almost one and one-half magnitude units larger than the M_e 6.1 of the interplate event.

Another example of the disparity in damage between interplate and intraplate earthquakes can be seen in a suite of earthquakes that occurred in Kodiak, Alaska (Table 2). Again, although the epicenters and M_W's are similar (particularly between the first and third events), the macroseismic effects associated with the normal-faulting intraslab earthquakes are far greater than those of the interplate thrust-faulting earthquake. The differences in macroseismic effects can not be distinguished if one were to rely solely on differences in M_W, but they are

TABLE 1: Near the coast of central Chile.

Date	Latitude (°)	Longitude (E)	Depth (km)	M_e	M_w	m_b	M_s	τ_a (bars)	Faulting type
July 6, 1997[1]	-30.06	-71.87	23.0	6.1	6.9	5.8	6.5	1	interplate-thrust
Oct. 15, 1997[2]	-30.93	-71.22	58.0	7.5	7.1	6.8	6.8	44	intraslab-normal

1. Felt (III) at Coquimbo, La Serena, Ovalle and Vicuna.

2. Five people killed at Pueblo Nuevo, one person killed at Coquimbo, one person killed at La Chimba and another died of a heart attack at Punitaqui. More than 300 people injured, 5000 houses destroyed, 5700 houses severely damaged, another 10,000 houses slightly damaged, numerous power and telephone outages, landslides and rockslides in the epicentral region. Some damage (VII) at La Serena and (VI) at Ovalle. Felt (VI) at Alto del Carmen and Illapel; (V) at Copiapo, Huasco, San Antonio, Santiago and Vallenar; (IV) at Caldera, Chanaral, Rancagua and Tierra Amarilla; (III) at Talca; (II) at Concepcion and Taltal. Felt as far south as Valdivia. Felt (V) in Mendoza and San Juan Provinces, Argentina. Felt in Buenos Aires, Catamarca, Cordoba, Distrito Federal and La Rioja Provinces, Argentina. Also felt in parts of Bolivia and Peru.

TABLE 2: Kodiak Island region of Alaska.

Date	Latitude (°)	Longitude (E)	Depth (km)	M_e	M_w	m_b	M_s	τ_a (bars)	Faulting type
May 7, 1999[1]	56.42	-152.94	20.0	5.8	6.3	5.7	6.1	2	interplate-thrust
Dec. 6, 1999[2]	57.41	-154.49	52.0	7.0	7.0	6.8	-	17	intraslab-normal
Dec. 7, 1999[3]	57.36	-154.10	45.0	6.4	6.5	6.5	6.1	15	intraslab-normal
July 11, 2000[4]	57.60	-154.51	49.0	6.8	6.7	6.3	6.3	25	intraslab-normal

1. No felt reports.

2. Slight damage (VI) at Larsen Bay and Old Harbor. Felt strongly at Akhiok and Kodiak. Felt (III) at Homer and Chignik; (II) at Anchorage, Palmer and Willow. Also felt at Dillingham, Eagle River, Fairbanks, Kasilof, Nelson Lagoon and Nikiski.

3. Felt at Anchorage, Ekwok, Homer, King Salmon, Kodiak and Old Harbor.

4. Some minor damage on Kodiak. Felt throughout southern Alaska and as far north as Fairbanks.

well quantified by the M_e's.

The relative paucity of normal-faulting events precludes a similar comparison for most seismic regions. Nevertheless, radiated energy, apparent stress and M_e are clearly valuable considerations in evaluating seismic hazard.

Tsunamic potential

Choy and Boatwright [1995], using a set of 397 shallow earthquakes distributed worldwide that occurred from 1987 to 1991, ranked earthquakes by energy and by moment. When earthquake size was ranked by energy, the list of the 20 largest events was dominated by strike-slip earthquakes (Table 3). When earthquake size was ranked by seismic moment, the list of the largest events was dominated by thrust-fault earthquakes. Two large strike-slip earthquakes off the western coast of the U.S., for example, are ranked sixth and ninth by energy, but are ranked 36th and 55th by moment. Thus, if a criterion for seismic hazard is earthquake size, then it is important to note that the potential for damage predicted by energy and moment would be different. A second feature in the comparison of rankings is that most of the large (high M_e) strike-slip earthquakes are associated with tsunamis. Although strike-slip earthquakes are not generally thought of as such, they may be capable of generating tsunamis. Thus, M_e may be useful in complementing M_W and M_S in evaluating tsunamic potential.

Estimates of radiated energy for historical earthquakes

For earthquakes that predate the advent of broadband digital instrumentation, E_S can still be estimated if seismograms recorded by broadband instruments can be found and if such records are legible. However, unearthing such records and performing the digitization is both a challenging and daunting task. Fortunately, there may be an alternative. The preliminary results of *Choy and Boatwright* [1995] show that many seismic regions have a characteristic apparent stress, $\tau_c = \mu E_S / M_0$. Solving for E_S and inserting the expression into the definition of M_e,

$$M_e = 2/3\ [\log M_0 + \log (\tau_c / \mu)] - 2.9\ .$$

This equation implies that M_e, as well as E_S, can be estimated for an historical earthquake in a given tectonic setting and a specific faulting type if the M_0 is known. In contrast to E_S, M_0 for historical earthquakes can be derived in numerous ways from geodetic and geologic methods, as well as the spatial distribution of aftershocks.

TABLE 3: Twenty largest earthquakes between 1986–1991 ranked by energy in terms of M_e. The corresponding M_s and M_w are also given. Three significant digits are used in M_e and M_w in order to refine the ranking. T indicates a tsunami was generated; a wave height, if reported, is also given. The type of faulting mechanism (FM) is indicated by TH (thrust), NR (normal) and SS (strike-slip).

Rank	Region	Date	FM	M_e	M_w	M_s
1	Gulf of Alaska (T=85 cm)	1987 11 30	SS	8.42	7.91	7.6
2	Macquarie Islands (T)	1989 05 23	SS	8.12	8.10	8.2
3	Gulf of Alaska (T=10 cm)	1988 03 06	SS	8.12	7.79	7.6
4	Gulf of Alaska (T=10 cm)	1987 11 17	SS	7.74	7.21	6.9
5	Luzon, Philippines	1990 07 16	SS	7.65	7.74	7.8
6	Western Iran	1990 06 20	SS	7.49	7.43	7.7
7	Coast northern California (T=50 cm)	1991 08 17	SS	7.39	7.10	7.1
8	Aroe Islands (T)	1988 07 25	NR	7.35	6.96	6.7
9	Tonga Islands (T=25 cm)	1991 04 06	SS	7.22	6.69	6.7
10	Mariana Islands (T=24 cm)	1990 04 05	NR	7.23	7.47	7.5
11	Tonga Islands	1987 10 06	NR	7.26	7.30	7.3
12	Off coast of Oregon	1991 07 13	SS	7.24	6.88	6.9
13	Costa Rica (T=2 m)	1991 04 22	TH	7.14	7.68	7.6
14	Burma–China border	1988 11 06	SS	7.13	7.05	7.3
15	Banda Sea	1987 06 17	TH	7.03	7.12	--
16	East Papua New Guinea	1987 02 08	SS	7.04	7.36	7.4
17	South of Fiji	1989 08 14	SS	7.00	6.31	5.9
18	Macquarie Islands	1990 09 17	SS	7.00	6.44	6.0
19	Molucca Passage	1989 02 10	TH	6.99	7.15	6.8
20	Coast of north Chile (T=22 cm)	1987 03 05	TH	6.97	7.60	7.3

Conclusions

Radiated seismic energy is a fundamental measure of earthquake size that is different from seismic moment. It can be used to complement seismic moment in evaluating seismic and tsunamic hazard.

- E_S can be directly computed from seismic data. It need not be an empirical quantity.
- Energy is a physically different measure of earthquake size than moment. E_S is a better estimate of the potential for damage than M_0.
- M_e can be used to distinguish between earthquakes with identical M_W but different macroseismic effects.
- The correlation between E_S and M_0 varies systematically with faulting type, seismic region and tectonic environment.
- In particular, the energy radiated by intraslab normal-faulting earthquakes is generally larger than that of interplate thrust-faulting earthquakes. For some normal-faulting intraslab earthquakes, M_e is more effective than M_W in quantifying macroseismic effects.
- Oceanic strike-slip earthquakes can be followed by tsunamis. M_e may be a useful complement to M_W and M_S in evaluating tsunamic potential.
- As statistics about radiated energy and moment are accumulated, and their global variations become more precise, the seismic hazard potential can be estimated from historical as well as contemporary data.

References

Boatwright, J.L., and G.L. Choy, Teleseismic estimates of the energy radiated by shallow earthquakes, *J. Geophys. Res., 91*, 2095–2112, 1986.

Choy, G.L., and J.L. Boatwright, Global patterns of radiated seismic energy and apparent stress, *J. Geophys. Res., 100*, 18,205–18,228, 1995.

TABLE 4: Twenty largest earthquakes between 1986–1991 ranked by moment in terms of M_w. The corresponding M_e and M_s are also given. T indicates a tsunami was generated; a wave height, if reported, is also given. The type of faulting mechanism (FM) is indicated by TH (thrust), NR (normal) and SS (strike-slip).

Rank	Region	Date	FM	M_e	M_w	M_s
1	Macquarie Islands (T)	1989 05 23	SS	8.12	8.10	8.2
2	Gulf of Alaska (T=85 cm)	1987 11 30	SS	8.42	7.91	7.6
3	Gulf of Alaska (T=10 cm)	1988 03 06	SS	8.12	7.79	7.6
4	Luzon, Philippines	1990 07 16	SS	7.65	7.74	7.8
5	Sulawesi	1990 04 18	TH	6.90	7.68	7.4
6	Costa Rica (T=2 m)	1991 04 22	TH	7.14	7.68	7.6
7	South of Fiji	1990 03 13	SS	6.95	7.65	7.4
8	Kuril Islands	1991 12 22	TH	6.61	7.63	7.4
9	Coast of north Chile (T=22 cm)	1987 03 05	TH	6.97	7.60	7.3
10	Solomon Islands	1988 08 10	TH	6.50	7.60	7.4
11	Mindanao, Philippines	1989 12 15	TH	6.64	7.59	7.3
12	Sulawesi	1991 06 20	TH	6.45	7.57	7.0
13	Mariana Islands (T=24 cm)	1990 04 05	NR	7.23	7.47	7.5
14	Macquarie Islands	1987 09 03	NR	6.76	7.43	7.3
15	East coast Honshu (T=56 cm)	1989 11 01	TH	6.85	7.43	7.4
16	Western Iran	1990 06 20	SS	7.49	7.43	7.7
17	New Britain (T=13 cm)	1987 10 16	TH	6.37	7.41	7.4
18	Taiwan	1986 11 14	TH	6.94	7.41	7.8
19	East Papua New Guinea	1987 02 08	SS	7.04	7.36	7.4
20	Costa Rica	1990 03 25	TH	6.36	7.36	7.0

Earthquakes having high apparent stress in oceanic intraplate lithosphere

Art McGarr[1] and George L. Choy[2]
1 United States Geological Survey, 345 Middlefield Road, Menlo Park, California, 94025, USA
2 United States Geological Survey, PO Box 25046, Lakewood, Colorado, 80225, USA
mcgarr@usgs.gov, choy@usgs.gov

Choy and Boatwright [1995] studied shallow earthquakes distributed worldwide and concluded that the highest apparent stresses ($\mu E_s/M_0$, where E_s is the radiated energy, μ is the modulus of rigidity, and M_0 is the seismic moment) are associated with strike-slip earthquakes that occur at oceanic ridge–ridge transform faults and in intraplate environments seaward of island arcs. Our most recent survey of source parameters for earthquakes during the period 1987 through 1998 revealed that the highest apparent stresses found anywhere are associated with events located in the depth range 10–25 km in intraplate oceanic lithosphere. Apparent stresses occasionally exceed 20 MPa for these earthquakes, which share two or more of the following characteristics: 1) their mechanisms are strike-slip; 2) their *P* axes are perpendicular to the nearest transform fault; 3) their *T* axes are perpendicular to the nearest spreading ridge or subduction zone; and 4) they are often located near triple junctions, especially where intraplate deformation is thought to be taking place.

Two of the highest apparent stresses, 27 and 25 MPa, are associated with two large earthquakes in 1987 and 1988 of moment magnitude 7.2 and 7.9 at depths of 18 and 20 km in the Gulf of Alaska. These shocks involved strike-slip faulting along a north–south oriented zone [*Lahr et al.,* 1988]; the sequence also includes a third event of M_w=7.8 having the same mechanism and an apparent stress of 13.5 MPa. This sequence of intraplate earthquakes is considered to indicate fragmentation of the northeast corner of the Pacific plate according to *Lahr et al. [1988].*

Similarly, earthquakes having exceptionally high apparent stresses near the southeast corner of the Gorda plate, where the Mendocino escarpment, the San Andreas fault, and the Cascadia subduction zone form a triple junction, are thought to reflect intraplate deformation along northeast and northwest oriented strike-slip faults (e.g., *Wilson*, [1989]; *Wang et al.*, [1997]). One of the magnitude 6.6 aftershocks of the April, 1992, *M*=7.1 Petrolia earthquake was located about 25 km seaward of the mainshock at a depth of 22 km in the oceanic lithosphere and had an apparent stress of 16 MPa. This event, in contrast to the mainshock and its thrust faulting mechanism, involved right-lateral slip on a northwest-oriented fault plane and a high-level of ground motion onshore [*Oppenheimer et al.,* 1993]. Generally, the southeastern portion of the Gorda plate produces intraplate earthquakes of very high apparent stress quite frequently.

The largest oceanic intraplate earthquake ever recorded, which occurred near the Balleny Islands between Australia and Antarctica, had a moment magnitude of 8.2 [*Wiens et al.,* 1998] and a high apparent stress of 13 MPa. This event, which was located within the Antarctic plate at a depth of about 18 km, indicates strike-slip deformation within the Antarctic plate. Indeed, *Conder and Forsyth* [2000] have ruled out the possibility that this earthquake occurred along the boundary of a microplate that might have existed to accommodate part of the motion between the Antarctic and Australian plates.

The depth distribution of apparent stresses for earthquakes located in oceanic lithosphere shows a steep increase in maximum values 6–10 km below the ocean bottom, peak values in the neighborhood of 25 MPa at 10–20 km depth, followed by a steep decrease at 20–24 km depth. Apparent stresses in excess of 10 MPa are all found in the depth range 10–22 km. Interestingly, this depth distribution of peak apparent stress is qualitatively consistent with estimates of oceanic lithospheric strength inferred from laboratory measurements of rock strength. That is, *Brace and Kohlstedt* [1980], *Kirby and Kronenberg* [1987] and *Kohlstedt et al.* [1995] have all proposed that frictional failure on faults (Byerlee's Law) limits the strength of the uppermost oceanic lithosphere to depths of the order of 20–30 km, below which temperature-dependent creep of olivine results in a steep decline in strength. Thus, the laboratory evidence on lithospheric strength indicates at least the possibility of a peak in the depth range 10–20 km.

To make the comparison between apparent stresses and lithospheric strength more quantitative, we first relate the peak values in apparent stress τ_a to the total shear

stress τ causing fault slip using [*McGarr,* 1999)] $\tau_a/\tau \leq 0.06$ and then we make the common assumption [e.g., *Grasso and Sornette,* 1998] that the applied shear stress is close to the strength limit. Laboratory-based strength estimates, multiplied by 0.06, are in reasonably good agreement quantitatively with our distribution of peak apparent stresses. The curve of *Kohlstedt et al*. [1995] for oceanic lithospheric strength at 20 km depth, for instance, is 350 MPa, which, if multiplied by 0.06, yields a peak apparent stress of 21 MPa. Thus, we conclude that maximum apparent stresses for earthquakes in intraplate oceanic lithosphere are consistent with laboratory-based estimates of strength in the same depth range. If so, then these are the highest apparent stresses to be found anywhere because the uppermost mantle of the oceanic lithosphere is the strongest material within the earth.

We have not attempted to determine the sources of such high levels of shear stress, roughly 350 MPa at depths near 20 km, except to note that typical estimates of "ridge-push" forces, if supported mostly by the strongest part of the oceanic lithosphere, provide deviatoric stresses of the same order as the strength estimates just reviewed. More detail on the causative forces is beyond the scope of our study.

Perhaps the most important conclusion of our study with regard to seismic hazard is that earthquakes in intraplate oceanic lithosphere can produce exceptionally high levels of strong ground motion for their size inasmuch as there is quite a close correspondence between apparent stress and high-frequency ground motion. The large intraplate aftershocks of the 1992 Petrolia earthquake near the southeast corner of the Gorda plate [*Oppenheimer et al.,* 1993] provided a good example of this effect.

References

Brace, W.F., and D.L. Kohlstedt, Limits on lithospheric stress imposed by laboratory experiments, *J. Geophys. Res., 85,* 6248–6252, 1980.

Choy, G.L., and J.L. Boatwright, Global patterns of radiated seismic energy and apparent stress, *J. Geophys. Res., 100,* 18,205–18,228, 1995.

Condor, J.A., and D.W. Forsyth, Do the 1998 Antarctic plate earthquake and its aftershocks delineate a plate boundary?, *Geophys. Res. Lett., 27,* 2309–2312, 2000.

Grasso, J.-R. and D. Sornette, Testing self-organized criticality by induced seismicity, *J. Geophys. Res., 103,* 29,965–29,987, 1998.

Kirby, S.H., and A.K. Kronenberg, Rheology of the lithosphere: selected topics, *Rev. Geophys., 25,* 1219–1244, 1987.

Kohlstedt, D.L., B. Evans, and S.J. Mackwell, Strength of the lithosphere: constraints imposed by laboratory experiments, *J. Geophys. Res., 100,* 17,587–17,602, 1995.

Lahr, J.C., R.A. Page, C.D. Stevens, and D.H. Christensen, Unusual earthquakes in the Gulf of Alaska and fragmentation of the Pacific plate, *Geophys. Res. Lett., 15,* 1483–1486, 1988.

McGarr, A., On relating apparent stress to the stress causing earthquake fault slip, *J. Geophys. Res., 104,* 3003–3011, 1999.

Oppenheimer, D., and 19 coauthors, The Cape Mendocino, California, earthquakes of April 1992: subduction at a triple junction, *Science, 261,* 433–438, 1993.

Wang, K., J. He, and E.E. Davis, Transform push, oblique subduction resistance, and intraplate stress of the Juan de Fuca plate, *J. Geophys. Res., 102,* 661–674, 1997.

Wiens, D.A., M.E. Wysession, and L. Lawver, Recent oceanic intraplate earthquake in Balleny Sea was largest ever detected, *EOS, Trans. AGU, 79,* 353–354, 1998.

Wilson, D.S., Deformation of the so-called Gorda plate, *J. Geophys. Res., 94,* 3065–3075, 1989.

Energy-to-moment ratios for damaging intraslab earthquakes: Preliminary results on a few case studies

Emile A. Okal[1] and Stephen H. Kirby[2]
1 Department of Geological Sciences, Northwestern University, 1847 Sheridan Road, Evanston, Illinois, 60208, USA
2 United States Geological Survey, 345 Middlefield Road, Menlo Park, California, 94025, USA
emile@earth.northwestern.edu, skirby@usgs.gov

ABSTRACT

We use the energy-to-moment ratio, as introduced by Newman and Okal [1998] to examine the source characteristics of normal-faulting intraslab earthquakes, compared to nearby interplate thrust events, based on recent case studies in central Chile and southeastern Mexico. In Chile, we find that the 1997 intraslab event had an exceptionally large E/M_0 ratio, 30 times greater than the nearby interplate shock. This suggests a very fast strain release at the source as the origin of the particularly destructive character of intraslab events. While the difference is less sharp in Mexico, we find a similar trend, which is in agreement with the observation that the locally most damaging earthquakes are indeed the intraslab events. We also document on the 1939 Chilean earthquake the feasibility of extending this approach to historical earthquakes for which high-quality analog records have been archived.

Introduction

Records of instrumental seismicity over the last century show that maximum earthquake size, measured in terms of seismic moment M_0, is achieved by interplate thrust earthquakes at subduction zones, as exemplified by the two largest seismic moments ever measured, the 1960 Chilean and 1964 Alaskan earthquakes (two to five times 10^{30} dyn-cm and 8.2×10^{29} dyn-cm, respectively) [*Kanamori*, 1970; *Kanamori and Cipar*, 1974; *Cifuentes and Silver*, 1989]. In this context, and for the purpose of evaluating seismic risk in a given subduction zone, the largest interplate thrust event expected in the region has generally been used as a benchmark to define greatest possible hazard. For example, in the Pacific Northwest region of the United States, this reference event has been taken as a so-called "mega-thrust" interplate shock [*Heaton and Kanamori*, 1984; *Rogers*, 1988], rupturing the entire plate boundary from Cape Mendocino to the Juan de Fuca Strait, as proposed by *Satake et al*. [1996] for the source of the transpacific tsunami of January 26, 1700.

However, in a recent contribution, *Kirby* [1999] has pointed out that a number of intraplate earthquakes, occurring within the down-going slab, can result in significantly more damage than expected from their reported magnitudes. Examples include the Olympia, Washington event of April 13, 1949 (M_{PAS}=7), which resulted in eight deaths and more than 150 million 1949-dollars of damage and the Chilean earthquake of January 25, 1939 (M_{PAS}=8.3), which killed upwards of 25,000 people, i.e., at least five times as many as the 1960 event, in spite of an estimated moment 200 times smaller. A similar case is that of the Peruvian earthquake of May 31, 1970 which, in addition to casualties directly due to strong motion damage, also triggered a landslide burying the Yangay Valley and resulted in a total of 66,000 deaths. It was determined to be an intraplate event occurring within the descending slab, in a region featuring no great interplate thrust earthquakes [*Plafker et al.*, 1971; *Abe*, 1972]. Such intraslab earthquakes are usually deeper than 40 km, and displaced laterally away from the trench, often beneath populated regions. They frequently, but not always, feature normal faulting.

In comparing the hazards associated with a gigantic interplate thrust earthquake and a smaller intraslab event in the same region, one must bear in mind that the latter may have greater recurrence rate by virtue of its smaller size (expressed either as magnitude or moment). The combination of being closer geographically to populated areas, having a potential for greater damage and a greater probability of occurrence may outweigh the intrinsically smaller nature of the intraplate event and make it, rather than the interplate "megathrust", a potentially greater contributor to seismic risk in the region. This scenario would be particularly relevant in the Pacific Northwest, where the period of recurrence of a 1700-type megathrust event may range from 600 to 1600 years, based on the analysis of sand deposits in the intertidal zone [*Atwater*, 1992], while at least three destructive intraslab earthquakes took place in the past 52 years (Satsop, Washington, 1999; Puget Sound, 1965 [*Langston and Blum*, 1977]; and Olympia, 1949 mentioned above).

There can be *a priori* two explanations for the enhanced damage (in physical terms, higher accelerations)

observed during intraslab earthquakes. One is intrinsic—the strain release at the source would be faster than usual, resulting in a source spectrum richer in higher frequencies. Another model would involve a receiver effect, namely that the areas most affected by the rupture, which are located directly above the source and hence displaced inland with respect to an interplate event sited at the trench, could be set in a geological environment particularly conducive to the local amplification of ground motion. This could be the case, for example, in the sediment-filled Central Valley of Chile, under which the 1939 earthquake took place.

By studying the teleseismic characteristics of damaging intraslab earthquakes, one can hope to eliminate local site effects and discriminate between the two models. We report here on a preliminary analysis of a few case studies in two subduction provinces: the Oaxaca region of southern Mexico and central Chile. We reject site effects as the source of enhanced damage and conclude that the three intraslab earthquakes studied did indeed exhibit a faster than usual seismic source.

Data analysis

In each of the two regions studied, we selected a pair of earthquakes, one underthrusting interplate shock and one intraslab event, of comparable sizes and locations. In particular, the latter constraint ensures that site effects at teleseismic receivers will be comparable for both events in each pair, since seismic rays under the receiver will travel along essentially identical paths.

In Chile, we consider the interplate earthquake of July 6, 1997 (30.06°S, 71.87°W; h=19 km; M_0=1.9 x 10^{26} dyn-cm) and the intraslab event of October 15, 1997 (30.93°S, 71.22°W; h=58 km; M_0=4.9 x 10^{26} dyn-cm). In Mexico, we study the large 1978 Oaxaca interplate event (16.01°N, 96.60°W; h=18 km; M_0=5.3 x 10^{27} dyn-cm) and the more recent normal faulting earthquake of September 30, 1999 (16.06°N, 96.93°W; h=60 km; M_0=1.7 x 10^{27} dyn-cm; [*Singh et al.*, 2000]). Our analysis of these events parallels that by G.L. Choy [pers. comm.] using a generally similar methodology. The source locations listed above are hypocentral parameters given by the USGS. Centroid depths inverted at Harvard are 16 km (interplate) and 47 km (intraslab) in Mexico; in Chile, the intraslab event is given at 70 km, but the depth of the interplate one is unresolved and was constrained at 15 km in the inversion. The distances separating the epicenters in each pair are only 114 km in Chile and 36 km in Mexico (Figures 1 and 2).

We then use the energy-to-moment ratio to characterize the events through their "slowness" parameter

$$\Theta = \log_{10} E/M_0,$$

as introduced by *Newman and Okal* [1998] following the work of *Boatwright and Choy* [1986]. General scaling laws predict Θ=-4.90, in excellent agreement with large worldwide datasets, such as *Newman and Okal's* [1998] and *Choy and Boatwright's* [1995]. Anomalously slow rupture, such as observed during so-called "tsunami earthquakes", leads to values of Θ deficient by as much as 1.5 to 2 units. Our results are summarized on Figure 3. We use energy estimates corrected for available focal mechanisms. For the recent (1997 and 1999) earthquakes, we analyzed between five and six broadband IRIS records at stations providing good azimuthal coverage. For the 1978 Mexican earthquake, we were able to find four short-period vertical records at SRO stations.

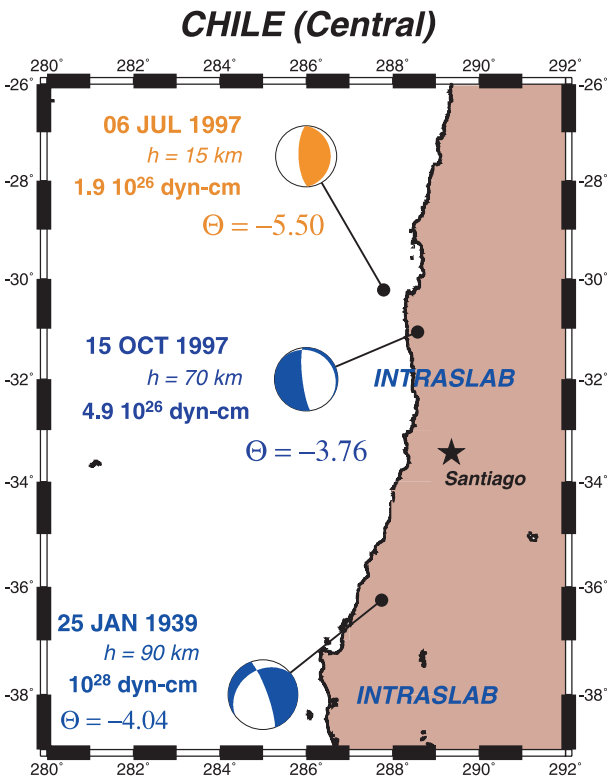

FIGURE 1: Map of central Chile, showing the events analyzed in the present study. Depths plotted are for centroid solutions, either from the Harvard centroid moment tensor (CMT) catalog or as estimated by *Beck et al.* [1998] for the 1939 event. The focal mechanisms are color-keyed to the value of Θ (see Figure 3).

In Chile, we find Θ=-5.50 for the interplate event, which characterizes it as mildly slow. The intraplate earthquake, on the other hand, has Θ=-3.76, making its source one of the fastest analyzed by our technique. We also tested the possibility of using historical earthquakes, by processing the Pasadena–Benioff 1–100 record of the 1939 Chilean event (see Figure 4). This instrument can be regarded as the ultimate prototype of the modern broadband seismometer. We obtain a radiated energy of 8 x 10^{23} ergs (corrected for the focal mechanism given by *Beck et al.* [1998]), leading to Θ=-4.04, for a prob-

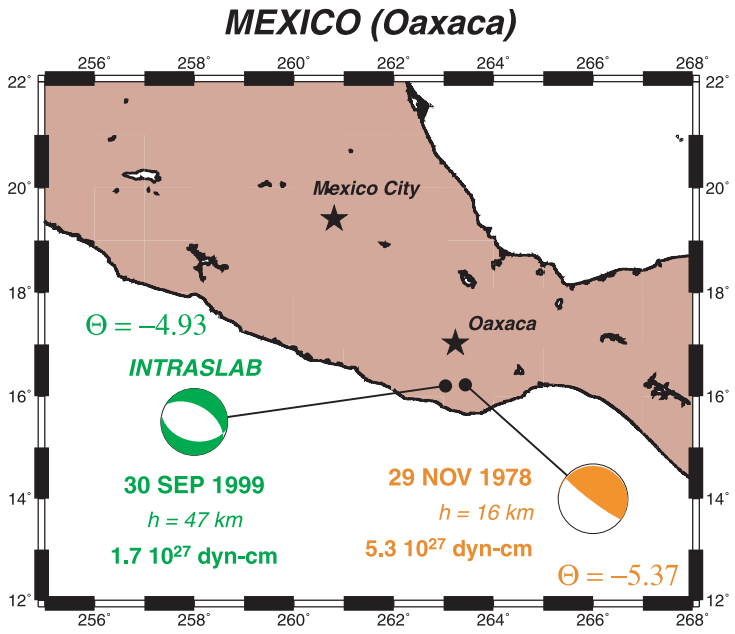

FIGURE 2: Map of southcentral Mexico, showing the events analyzed in the present study. Depths plotted are for centroid solutions, compiled from the CMT catalog. The focal mechanisms are color-keyed to the value of Θ (see Figure 3).

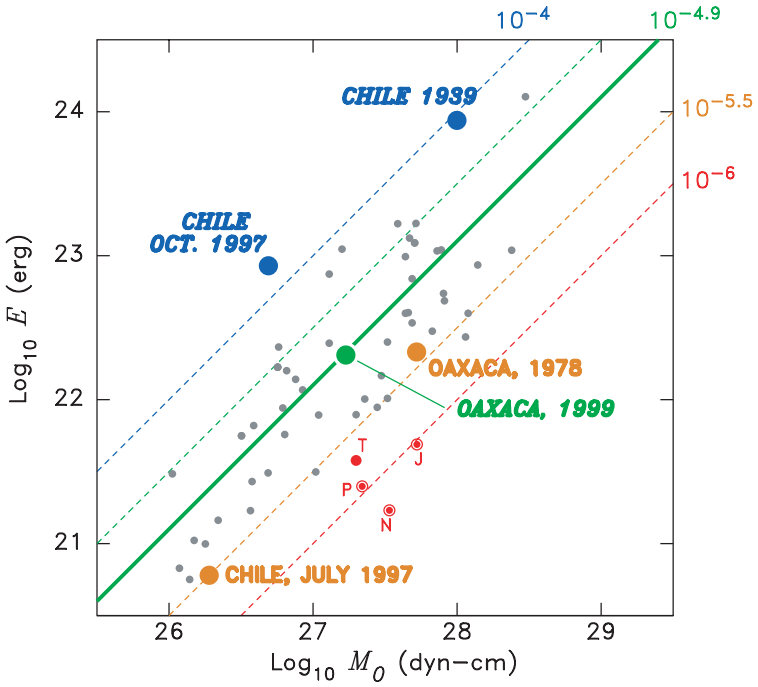

FIGURE 3: Summary of results obtained in this study. This figure plots radiated seismic energy against seismic moment, in logarithmic units (after *Newman and Okal* [1998]). The dashed diagonals are lines of constant Θ, with the thick line (Θ=–4.9) showing the relation predicted by scaling laws; they are color-keyed from fast (blue) to slow (red) sources. The smaller gray symbols are the dataset examined in *Newman and Okal* [1998] with bull's eye symbols referring to the four recent tsunami earthquakes (T: Tonga, 1982; N: Nicaragua, 1992; J: Java, 1994; P: Peru, 1996). The larger symbols show the events studied here. Interplate thrust earthquakes are labeled in roman type, intraslab ones in italics. Note the large disparity in Θ values in Chile and the smaller one in Mexico.

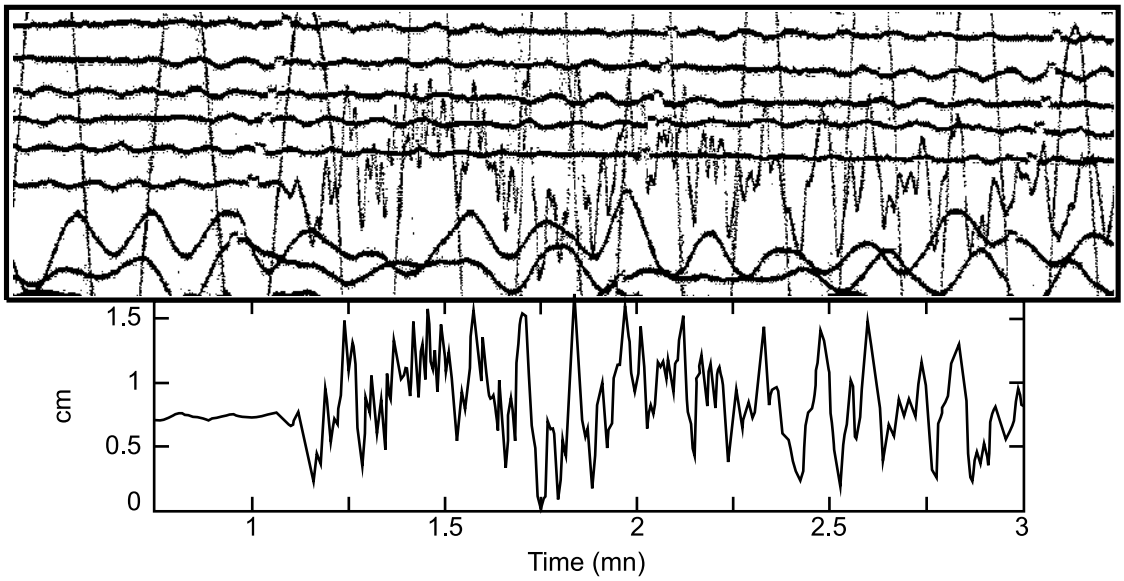

FIGURE 4: Top: Close-up of the *P*-wave arrival of the 1939 Chilean intraslab earthquake, as recorded on the Pasadena–Benioff 1–100 north-south instrument (tick marks are minutes). Bottom: After optical magnification, such records can be successfully digitized at a rate of 10 samples per second and processed through *Newman and Okal's* [1998] algorithm.

able moment of 1 x 10^{28} dyn-cm, as suggested by the G_2 waves recorded on the Pasadena strainmeter. This indicates that the event is definitely fast.

In Mexico, the situation is not as clear-cut, with the deeper event only slightly faster than the interplate shock. The 1999 event has Θ=-4.93, which is essentially the value predicted theoretically on the basis of scaling laws for shallow earthquakes. For the 1978 event, we find Θ=-5.37, giving it a weak trend towards slowness. It is possible that the average character of the 1999 event is due to its relatively shallow centroid depth, as compared to its Chilean counterpart. While the difference in Θ between the two Mexican events is smaller than in Chile and the results are not as conclusive, the trend upholds the observation that the 1999 earthquake was more destructive (with 31 people killed locally) than the 1978 event (one local fatality). Similarly, the great normal-faulting intraslab earthquake of January 15, 1931 was by far the most destructive in Oaxaca province this century [*Ordoñez*, 1931; *Singh et al.*, 1985]. Higher energy-to-moment ratios for shallow normal faulting events (in various configurations including intraslab) were also found by *Choy and Boatwright* [1995] and *G.L. Choy* [pers. comm. to Steve Kirby, 2000].

Conclusion

This very preliminary study, in which we have documented resolvable differences in source slowness between interplate and intraslab earthquakes, suggests the systematic use of the parameter Θ, as introduced by *Newman and Okal* [1998], in the evaluation of the source characteristics of intraslab earthquakes worldwide. It further demonstrates on the case of the 1939 Chilean earthquake the feasibility of extending the technique to historical earthquakes through the use of high-quality analog data. Our work also confirms trends involving these types of earthquakes reported by *Choy and Boatwright* [1995] and *G.L. Choy* [pers. comm. 2000].

In the case of Chile, the comparative analysis of *P* waves from nearby earthquake pairs (one interplate and one intraslab) at teleseismic distances proves that the large accelerations responsible for the destruction during the intraslab event were an inherent characteristic of its source, rather than a local effect due to the structure of the Central Valley of Chile. This is in agreement with similar results reported by *Singh et al*. [this volume] in Mexico.

Postscript

Since this research was presented at the Intraslab Workshop and this report written up, three major intraslab earthquakes took place: on January 13, 2001 in El Salvador; February 28, 2001 in Washington (the "Nisqually" event); and March 24, 2001 near Hiroshima, Japan, all three featuring higher values of Θ [*Okal and Kirby*, 2001].

References

Abe, K., Mechanisms and tectonic implications of the 1966 and 1970 Peru earthquakes, *Phys.Earth Planet. Inter., 5*, 367–379, 1972.

Atwater, B.F., Geologic evidence for earthquakes during the past 2000 years along the Copali River, southern

coastal Washington, *J. Geophys. Res., 97*, 1901–1919, 1992.

Beck, S.L., S. Barrientos, E. Kausel, and M. Reyes, Source characteristics of historic earthquakes along the central Chile subduction zone, *J. So. Amer. Earth Sci., 11*, 115–129, 1998.

Boatwright, J., and G.L. Choy, Teleseismic estimates of the energy radiated by shallow earthquakes, *J. Geophys. Res., 91*, 2095–2112, 1986.

Choy, G.L., and J. Boatwright, Global patterns of radiated seismic energy and apparent stress, *J. Geophys. Res., 100*, 18205–18228, 1995.

Cifuentes, I.L., and P.G. Silver, Low-frequency source characteristics of the great 1960 Chilean earthquake, *J. Geophys. Res., 94*, 643–663, 1989.

Heaton, T.H., and H. Kanamori, Seismic potential associated with subduction in the northwestern United States, *Bull. Seismol. Soc. Amer., 74*, 933–941, 1984.

Kanamori, H., The Alaska earthquake of 1964: Radiation of long-period surface waves and source mechanism, *J. Geophys. Res., 75*, 5029–5040, 1970.

Kanamori, H., and J.J. Cipar, Focal process of the great Chilean earthquake, May 22, 1960, *Phys. Earth Planet. Inter., 9*, 128–136, 1974.

Kirby, S.H., Earthquake hazard appraisal in subduction zones: Intraslab earthquakes are undervalued as hazards relative to interplate thrust events, *Eos, Trans. Amer. Geophys. Un., 80, (46)*, F650, 1999.

Langston, C.A., and D.E. Blum, The April 29, 1965 Puget Sound earthquake and the crustal and upper mantle structure of western Washington, *Bull. Seismol. Soc. Amer., 67*, 693–711, 1977.

Newman, A.V., and E.A. Okal, Teleseismic estimates of radiated seismic energy: the E/M_0 discriminant for tsunami earthquakes, *J. Geophys. Res., 103*, 26885–26898, 1998.

Okal, E.A., and S.H. Kirby, El Salvador, 13 January and SEA-TAC, 28 February: two recent examples of "snappy" intraplate earthquakes, *Eos, Trans. Amer. Geophys. Un., 82*, (20), S263, 2001.

Ordoñez, E., The Oaxaca earthquake, *Bull. Seismol. Soc. Amer., 21*, 47–50, 1931

Plafker, G., G.E. Ericksen, and J. Fernandez C., Geological aspects of the May 31, 1970 Peru earthquake, *Bull. Seismol. Soc. Amer., 61*, 543–578, 1971.

Rogers, G.C., Earthquakes: seismic potential of the Cascadia subduction zone, *Nature, 332*, 17,1988.

Satake, K., K. Shimazaki, Y. Tsuji, and K. Ueda, Time and size of a giant earthquake in Cascadia inferred from Japanese tsunami records of January 1700, *Nature, 379*, 246–249, 1996.

Singh, S.K., G. Suarez, and T. Dominguez, The Oaxaca, Mexico, earthquake of 1931: lithospheric normal faulting in the subducted Cocos plate, *Nature*, *317*, 56–58, 1985.

Singh, S.K., and 11 co-authors, The Oaxaca earthquake of September 30, 1999 (M_w=7.5): a normal-faulting event in the subducted Cocos plate, *Seismol. Res. Letts., 70*, 489–504, 2000.

Singh, S.K., V. Kostoglodov, and J.F. Pacheco, Intraslab earthquakes in the subducting oceanic plates below Mexico, in *The Cascadia Subduction Zone and Related Subduction Systems*, edited by S.H. Kirby, K. Wang, and S.G. Dunlop, pp. 87–92, U.S. Geological Survey Open-File Report 02–328, Geological Survey of Canada Open File 4350, 2002.

Thermal structure and metamorphism of subducting oceanic crust: Insight into Cascadia intraslab earthquakes

Simon M. Peacock[1], Kelin Wang[2] and Aaron M. McMahon[1]
1 Department of Geological Sciences, Arizona State University, Box 871404, Tempe, Arizona, 85287–1404, USA
2 Pacific Geoscience Centre, Geological Survey of Canada, PO Box 6000, Sidney, British Columbia, V8L 4B2, Canada
peacock@asu.edu, wang@pgc.nrcan.gc.ca, Aaron.McMahon@asu.edu

Most of the world's earthquakes, including the largest earthquakes ever recorded, occur in subduction zones where cool oceanic lithosphere descends into the mantle. Subduction-zone earthquakes relieve complex stresses generated by the interaction between the forces that drive and resist subduction, slab flexure, thermal expansion and metamorphic densification reactions [*e.g., Isacks and Barazangi*, 1977; *Spence*, 1987; *Kirby et al.*, 1996]. Recent efforts to integrate thermal-petrologic models of subduction zones with seismological observations suggest that metamorphic reactions cause, or at least control, most subduction-zone earthquakes, particularly intraslab earthquakes that occur at depths >40 km where high confining pressure makes normal frictional sliding difficult. Intermediate-depth, intraslab earthquakes can be very large (e.g., 1963 Banda Sea M_W=8.3) and pose a significant seismic risk. In this century, intermediate-depth earthquakes have killed tens of thousands of people (e.g., 1970 Central Peru, M_W=7.5–8.0, depth=40–66 km; 2001 El Salvador, M_W =7.6, depth=39–57 km) and have caused the most destruction in the Pacific Northwest (1949 Olympia, M=7.1, depth=54 km).

The thermal structure of a subduction zone is determined primarily by the convergence rate and the thermal structure (related to age) of the incoming lithosphere [*e.g., Peacock*, 1996]. Compared to most subduction zones, the Cascadia subduction zone is relatively warm because of the relatively slow convergence rate (~40 mm/yr), the young age (5–10 Ma) of the incoming Juan de Fuca plate, and the thick (3–3.5 km) blanket of insulating sediments which acts to increase temperatures in the underlying oceanic crust. The calculated thermal structure of the Cascadia subduction zone is very similar to other warm subduction zones like southwest Japan (Nankai) and southern Mexico (Figure 1).

Although the Cascadia subduction zone is relatively warm, the subduction of the Juan de Fuca plate beneath North America cools the Cascadia forearc. The low surface heat flux through the Cascadia forearc reflects the downward advection of isotherms by the subducting lithosphere [*Blackwell and Steele*, 1992]. *Hyndman and Wang* [1995] constructed two-dimensional thermal models across the Cascadia forearc. The model which best fits the observed heat flow data requires negligible frictional heating which is consistent with the apparent lack of shear heating in the warm Nankai subduction zone. *Hyndman and Wang's* [1995] thermal models predict thrust temperatures of ~250°C at the deformation front increasing to ~525°C at 40 km depth. The downdip limit of the Cascadia seismogenic zone (where shallow-thrust earthquakes occur) may be controlled by the temperature-induced transition (350–450°C) from stick-slip to stable sliding behavior [*Hyndman and Wang*, 1995].

Intermediate-depth, intraslab earthquakes represent brittle failure within the subducting slab (intraplate) rather than along the plate interface (interplate). Focal mechanisms for intraslab earthquakes commonly show normal faulting with downdip extension although there are many exceptions. Several lines of evidence suggest that most intraslab earthquakes occur within the subducting oceanic crust: 1) seismic tomography studies show that intermediate-depth earthquakes occur near the top of the high seismic-velocity slab [*Zhao et al.,* 1994]; 2) shallow intraslab earthquakes merge with the downdip limit of the interplate earthquakes indicating that intraslab earthquakes occur very near the plate interface within the uppermost few kilometers of the subducting slab [*Kirby et al.,* 1996]; and 3) in well-studied subduction zones, intraslab earthquakes occur within 5–10 km of the plate interface as defined independently by converted seismic phases (e.g., northeast Japan; *Hasegawa et al.*, [1994]) or seismic reflection studies (e.g., Cascadia; *Creager et al.*, [this volume]). Intraslab earthquakes may also occur within the subducting mantle. For example, two recent intraslab earthquakes in southern Mexico occurred 15–30 km beneath the plate interface as defined by interplate thrust events in the same region [*Singh et al.*, this volume]. Intermediate-depth earthquakes in several subduction zones, most notably northeastern Japan [*Hasegawa et al.*, 1994], define two seismic zones separated by 20–40 km. The lower seismic zone clearly occurs within the subducting mantle; such intraslab earth-

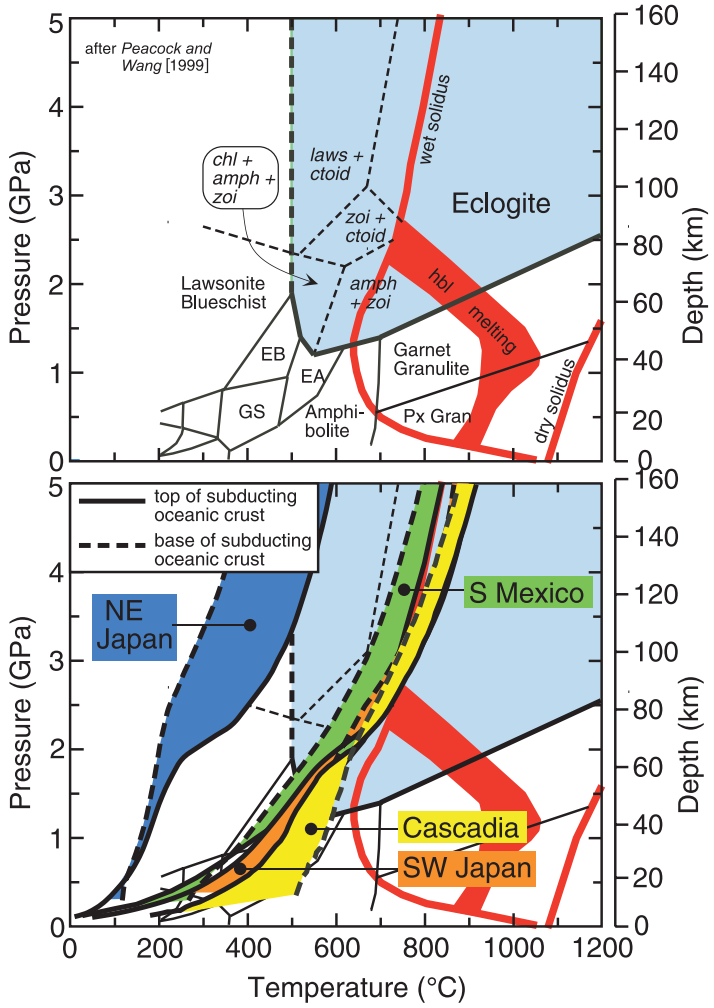

FIGURE 1: Calculated *P-T* paths and metamorphic conditions encountered by oceanic crust subducted beneath Cascadia, southern Mexico, southwest Japan and northeast Japan [*Peacock and Wang*, 1999; *Currie et al.*, 2000; this study]. Metamorphic facies: EA=epidote-amphibolite; EB=epidote blueschist; GS=greenschist; Px Gran=pyroxene granulite. Hydrous minerals stable in the eclogite facies shown in italics [*Poli and Schmidt*, 1995]: amph=amphibole; ctoid=chlorotoid; lawsonite; zoi=clinozoisite. Partial melting reactions in red (see references in *Peacock et al.*, [1994]).

quakes may be triggered by serpentine dehydration reactions [*Peacock*, 2001].

Kirby et al. [1996] proposed a model whereby intermediate-depth earthquakes are triggered by metamorphic dehydration reactions that embrittle the subducting oceanic crust. In this model, the transformation of hydrated oceanic crust (basalt, gabbro) to eclogite releases substantial amounts of H_2O that increases pore pressures and promotes brittle reactivation of pre-existing faults. *Kirby et al.* [1996] noted that the maximum depth of intermediate-depth earthquakes correlates with subduction-zone temperatures; cooler subducting slabs have deeper earthquakes. In order to test this model, *Peacock and Wang* [1999] constructed subduction-zone thermal models that extend to depths >200 km by incorporating flow of the mantle wedge induced by the subducting slab. In a detailed study of the warm southwest Japan and cool northeast Japan subduction zones, we demonstrated that striking differences in intermediate-depth seismicity, as well as differences in seismic-velocity structure and arc magmatism, can be linked to contrasting metamorphic reactions and temperatures in the subducting oceanic crust [*Peacock and Wang*, 1999].

Subducting sediment contains substantial amounts of pore fluids that are expelled at shallow depths <10 km (Figure 2) [*Moore and Vrolijk*, 1992]. Most of the water liberated from subducting slabs at depths >10 km is derived from the variably hydrated basalts and gabbros of the subducting oceanic crust (Figure 2) [e.g., *Peacock*, 1990]. At temperatures of perhaps 200–400°C, substantial amounts of pore water may be expelled from the uppermost basaltic section by porosity collapse. Alterna-

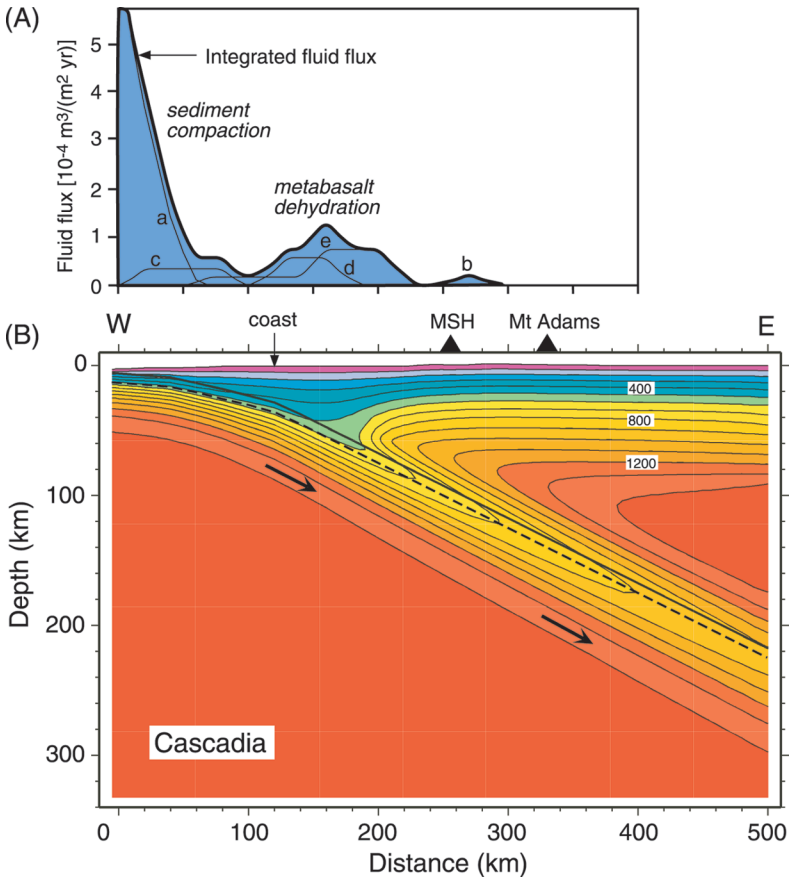

FIGURE 2: Predicted thermal structure and fluid production for Cascadia subduction zone. A) Calculated maximum H_2O flux expelled from the subducting Juan de Fuca plate as a function of distance from the deformation front. Note that calculated fluid fluxes are subject to large uncertainties. Sediment compaction dominates the fluid flux near the deformation front whereas dehydration reactions in subducted metabasalt dominates the fluid flux at ~50 km depth where intraslab earthquakes occur. Important fluid release processes: a= sediment porosity collapse (compaction); b= sediment mica dehydration (800°C); c= basalt porosity collapse (200–400°C); d= basalt garnet-forming dehydration reactions (~500°C); e= basalt high-*T* dehydration reactions (500–700°C). B) Calculated thermal structure for the Cascadia subduction zone at 42°N based on a preliminary finite-element model.

tively, this pore water may react with unaltered basalt to form low-temperature minerals, such as zeolites, which subsequently dehydrate. The progressive metamorphism of metabasalts involves complex, continuous reactions. The most important reactions in subducting oceanic crust involve the transformation to eclogite, a relatively dense, anhydrous rock consisting primarily of garnet and omphacite (Na–Ca clinopyroxene). In a given subduction zone, the depth and nature of eclogite formation and associated dehydration reactions depends on the pressure–temperature (*P–T*) conditions encountered by the subducting oceanic crust. In relatively warm subduction zones like Cascadia, southwest Japan and southern Mexico, the transformation to eclogite occurs at ~50 km depth (Figure 1). In contrast, calculated *P–T* paths for relatively cool subduction zones like northeast Japan pass through the blueschist facies and eclogite may not form until depths >100 km.

Predicting the amount and location of H_2O release from the subducting crust is difficult because of the uncertain amount and distribution of H_2O in the Juan de Fuca plate prior to subduction (Figure 2). Anhydrous portions of the crust will not release any H_2O whereas fully hydrated portions may release as much as 5–10 wt. % H_2O during subduction. Calculated *P–T* paths for the upper basaltic part of the subducting Juan de Fuca crust pass through a complex sequence of metamorphic facies: prehnite–actinolite→ greenschist→ epidote–amphibolite → eclogite facies (Figures 1 and 2). Dehydration of fully hydrated portions of the basaltic crust will occur preferentially at facies boundaries, although there is likely to be some dehydration within facies. Important hydrous minerals which will dehydrate during subduction include prehnite (4.4 wt. % H_2O), chlorite (13 wt. % H_2O), clinozoisite (2 wt. % H_2O) and amphibole (2 wt. % H_2O). Our calculations suggest that Cascadia intraslab earthquakes

occur where metabasalts in the Juan de Fuca plate undergo garnet-forming and higher temperature dehydration reactions (Figure 2). In contrast, the lower gabbroic section of the subducting Juan de Fuca crust at the deformation front lies in the high-temperature amphibolite facies where hornblende (amphibole) may be the only stable hydrous mineral. Both the basaltic and gabbroic sections are predicted to transform to eclogite at 40–50 km depth which correlates with the rapid increase in slab dip. Significant amounts of H_2O is released during transformation to eclogite but small amounts of H_2O-bearing amphibole and clinozoisite may persist to ~80 km depth.

If intermediate-depth seismicity is triggered by metamorphic dehydration reactions in the subducting crust, why does the Oregon sector generally lack intermediate-depth earthquakes? Possible explanations for the lack of seismicity include: 1) the Juan de Fuca crust entering the Oregon part of the subduction zone is essentially anhydrous; 2) H_2O is released by metamorphic dehydration reactions but the hydrogeology in this region (controlled by the overlying Siletz terrane?) prevents fluid pressures from reaching levels necessary to trigger faulting; 3) slab stresses in this region are not sufficient to trigger seismicity (no slab pull?); or 4) the slab in the Oregon sector may be unusually warm due to interaction with the Newberry hot spot.

Acknowledgements

We wish to express our thanks to the Geological Survey of Canada, the United States Geological Survey and the organizers of the Cascadia Intraslab Earthquake workshop for arranging a very stimulating and productive conference in Victoria, British Columbia. This research was supported by NSF grant EAR 98-09602 (SMP).

References

Blackwell, D.D., and J.L. Steele, *Geothermal Map of North America: Decade of North American Geology*, DNAG, Continent-Scale Map-006, Geological Society of America, Boulder, CO, 1992.

Creager, K.C., L.A. Preston, R.S. Crosson, T. Van Wagoner, A.M. Tréhu, and the SHIPS98 working group, Three-dimensional reflection image of the subducting Juan de Fuca Plate, in *The Cascadia Subduction Zone and Related Subduction Systems*, edited by S.H. Kirby, K. Wang, and S.G. Dunlop, pp. 37–42, U.S. Geological Survey Open-File Report 02–328, Geological Survey of Canada Open File 4350, 2002.

Currie, C.A., K. Wang, and R.D. Hyndman, Thermal constraints on megathrust earthquakes of the Mexican subduction zone, *EOS Trans. AGU (Fall meeting suppl.), 81*, F910, 2000.

Hasegawa, A., S. Horiuchi, and N. Umino, Seismic structure of the northeastern Japan convergent plate margin: a synthesis, *J. Geophys. Res., 99*, 22,295–22,311, 1994.

Hyndman, R.D., and K. Wang, The rupture zone of Cascadia great earthquakes from current deformation and the thermal regime, *J. Geophys. Res., 100*, 22,133–22,154, 1995.

Isacks, B.L., and M. Barazangi, Geometry of Benioff zones: lateral segmentation and downwards bending of the subducted lithosphere, in *Island Arcs, Deep Sea Trenches and Back Arc Basins (Maurice Ewing Series Vol. 1)*, edited by M. Talwani and W.C. Pitman, pp. 99–114, American Geophysical Union, Washington, D.C., 1977.

Kirby, S., E.R. Engdahl, and R. Denlinger, Intermediate-depth intraslab earthquakes and arc volcanism as physical expressions of crustal and uppermost mantle metamorphism in subducting slabs, in *Subduction: Top to Bottom, AGU Monograph 96*, edited by G.E. Bebout et al., pp. 195–214, American Geophysical Union, Washington, D.C., 1996.

Moore, J.C., and P. Vrolijk, Fluids in accretionary prisms, *Rev. Geophysics, 30*, 113–135, 1992.

Peacock, S.M., Fluid processes in subduction zones, *Science, 248*, 329–337, 1990.

Peacock, S.M., T. Rushmer, and A.B. Thompson, Partial melting of subducting oceanic crust, *Earth Planet. Sci. Lett., 121*, 227–244, 1994.

Peacock, S.M., Thermal and petrologic structure of subduction zones, in *Subduction: Top to Bottom, AGU Monograph 96*, edited by G.E. Bebout et al., pp. 119–133, American Geophysical Union, Washington, D.C., 1996.

Peacock, S.M., Are double seismic zones caused by serpentine dehydration reactions in subducting oceanic mantle? *Geology, 29*, 299–302, 2001.

Peacock, S.M., and K. Wang, Seismic consequences of warm versus cool subduction metamorphism: examples from southwest and northeast Japan, *Science, 286*, 937–939, 1999.

Poli, S., and M.W. Schmidt, H_2O transport and release in subduction zones: experimental constraints on basaltic and andesitic systems, *J. Geophys. Res., 100*, 22,299–22,314, 1995.

Singh, S.K., V. Kostoglodov, and J.F. Pacheco, Intraslab earthquakes in the subducting oceanic plates below Mexico, in *The Cascadia Subduction Zone and Related Subduction Systems*, edited by S.H. Kirby, K. Wang, and S.G. Dunlop, pp. 87–92, U.S. Geological Survey Open-File Report 02–328, Geological Survey of Canada Open File 4350, 2002.

Spence, W., Slab pull and the seismotectonics of subducting lithosphere, *Rev. Geophys., 25*, 55–69, 1987.

Zhao, D., A. Hasegawa, and H. Kanamori, Deep structure of Japan subduction zone as derived from local, regional and teleseismic events, *J. Geophys. Res., 99*, 22,313–22,329, 1994.

Heat sources in subduction zones: Implications for slab seismicity and arc volcanism

Jason R. McKenna and David D. Blackwell
Department of Geological Sciences, Southern Methodist University, PO Box 750395, Dallas, Texas 75275
jmckenna@post.smu.edu, blackwel@passion.isem.smu.edu

Introduction

The shallow (upper 30–50 km) thermal structure of subduction zones is well-constrained, and with few exceptions, can be modeled utilizing a variety of numerical [e.g., *Hyndman and Wang*, 1993] or even analytical solutions [e.g., *Molnar and England*, 1995]. It is stressed that the intermediate thermal structure of subduction zones remains largely unknown because the mechanism responsible for arc-magma genesis in the depth range of 80–120 km remains subject to debate. Attempts to investigate the source region of intermediate-deep slab seismicity are likewise hampered by the poorly-constrained thermal structure at these depths. Constraints on the conditions on the subducting slab face are therefore necessary to any critical assessment of seismogenic conditions within the interior of the slab.

Most comprehensive thermal models have concluded that additional heat-mass transfer from outside the mantle wedge is necessary to explain the occurrence of arc volcanism and back-arc spreading [*Minear and Toksoz*, 1970; *Tatsumi and Eggins*, 1995]. Early thermal models by *McKenzie and Schlater* [1968], *Oxburgh and Turcotte* [1968; 1970] and *Minear and Toksoz* [1970] tested various heat sources to explain the occurrence of arc volcanism including conductive heating from a stagnant mantle wedge, exothermic phase changes, brittle shear-heating and viscous dissipation. All were ultimately rejected because they failed to satisfy the surface heat-flow over the subduction zone or generate the high-eruption temperature basalts observed in subduction zones (see *Davies and Stevenson* [1992] for a discussion).

However, *Thatcher and England* [1998] have demonstrated that significant ductile shearing localized in the lower crust/upper mantle along the San Andreas fault can explain the observed California Coast Ranges heat-flow anomaly. Because the viscosity of a ductile medium is temperature dependent, ductile shearing is rapidly concentrated in a narrow zone about the slip zone [*Yuen et al.*, 1978] and is virtually independent of slip velocity [*Thatcher and England*, 1998].

Thermal modeling results

The thermal structure of the shallowest 30–50 km of the subduction zone can be modeled satisfactorily using the forearc surface heat-flow profile as the primary constraint [e.g., *Honda*, 1985; *Hyndman and Wang*, 1993]. However, recent work by *McKenna and Blackwell* [2002] has demonstrated that the shallow thermal regime of even young subduction zones is entirely conductive and can be successfully modeled without consideration of the deeper processes that influence the thermal structure of the subduction zone (i.e., arc magmatism and mantle wedge convection).

A thermal model specific to the subduction of the Juan de Fuca plate near 40°N (northern California) has been constructed assuming a subducting plate velocity of 40 mm/yr (the details of which will be presented elsewhere). Qualitatively, the model is comprised of moderately sedimented ~6 Ma Gorda lithosphere subducting beneath the North American backstop (composed of Mesozoic Franciscan complex and Klamath granite) and is overlain by a localized basin of Eel River sediments [e.g., *Smith et al.*, 1993]. This structure was extended eastward to the volcanic arc using crustal structure from *Mooney and Weaver* [1989]. This thermal model is typical of our estimates for the thermal structure in the upper ~40 km of the southern Cascadia subduction zone system. Figure 1 illustrates the resultant temperature–depth curve along the subducting plate top for the initial model. Also presented is a temperature–depth curve representing the Sierra Nevada paleo-subduction zone to emphasize the difference between the cold subduction that occurred in Mesozoic North America (Sierra Nevada) and the much warmer thermal conditions in the present-day Cascadia subduction zone. The most interesting feature of the Cascadia curves is that temperature along the subducting slab face increases rapidly, attaining temperatures in excess of 450°C by the relatively shallow depth of five kilometers. As depth increases, the temperature along the subducting slab face increases only moderately.

The effect of viscous shear-heating on the subduc-

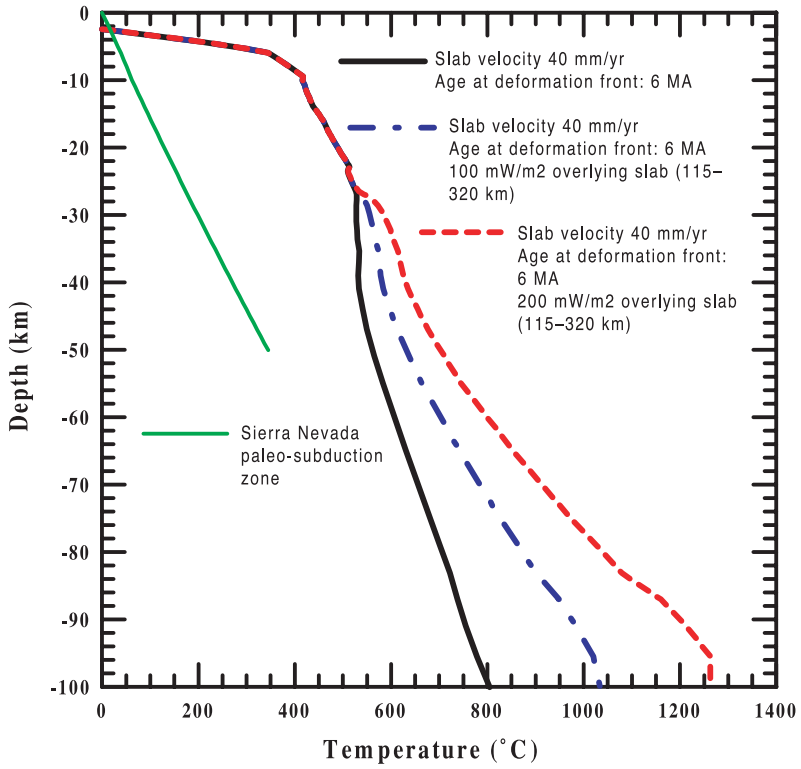

FIGURE 1: Temperature–depth curves along the subducting slab face, northern California. Note the high temperatures encountered along the slab face, even without the additional heat generated by viscous dissipation, when compared to the Sierra Nevada paleo-subduction zone.

tion zone thermal structure is simulated by specifying a heat source within a thin (two kilometers) boundary layer blanketing the slab face for a 200 km horizontal extent (beginning about 115 km landward of the deformation front). The strength of the additional heat source within the boundary layer is between 100 and 200 mW/m^2. We feel that while rather high, these values are not unreasonable estimates for the additional heat generated by viscous dissipation because in the presence of a non-linear (i.e., temperature-dependent) mantle viscosity, even moderate shear velocities can produce large temperature gradients across a thin boundary layer [*Thatcher and England*, 1998]. The resultant temperature–depth curves for the models that include the effects of viscous dissipation are presented in Figure 1. The point at which the heat source is "turned on" is visible as the bifurcation of the initial model curve.

Basalts are volumetrically the dominant lava type in the Cascades [*Blackwell et al.*, 1982; 1990]. Models that satisfy the surface heat-flow profile and still produce the requisite temperature (~1100°C) in the mantle wedge source region are considered successful. Utilizing this criteria, it is clear that only the curve representing the model with an additional heat input of 200 mW/m^2 begins to approach the temperature necessary for arc-basalts.

Figure 2 presents the results of the thermal calculations as pressure–temperature paths along the slab face. It has been suggested that the densification to eclogite via metamorphic dehydration reactions may be responsible for intermediate-depth intraslab seismicity [*Kirby et al.*, 1996; *Peacock et al.*, this volume]. Again, we show the blueschist generating *P–T* conditions in the Sierra Nevada paleo-subduction zone to illustrate the distinct thermal conditions in present-day Cascadia. Here, even the initial model *P–T* path (no additional heat sources) almost reaches the eclogite stability field. Any additional heat introduced downdip through viscous dissipation promotes conditions in which the slab face readily transforms to eclogite by the relatively shallow depth of ~45 km, about 100–150 km west of the volcanic arc. We conclude from this analysis that seismicity below this depth is probably not related to the densification to eclogite, but most likely mechanically generated, and must therefore, be restricted to the cooler interior of the slab.

In addition to facilitating potentially seismogenic *P–T* conditions at shallow depths, the addition of viscous dissipation through a boundary layer overlying the subducting slab can induce local convective upwelling via boundary layer separation. In fluid dynamics, the Reynolds Number describes the stability of some particular flow

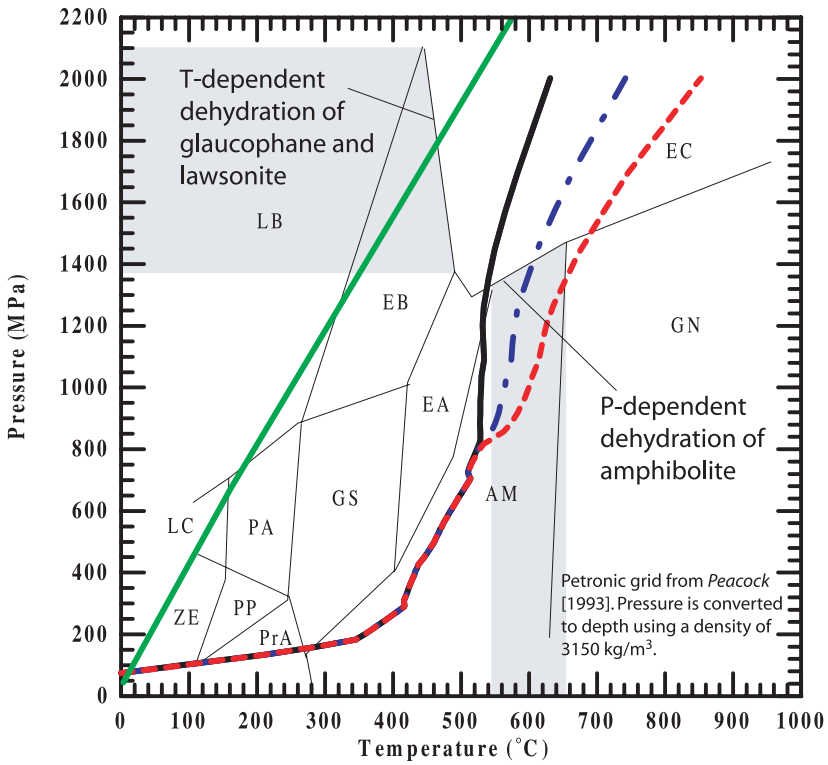

FIGURE 2: Pressure–temperature paths, northern California, curves are the same as in Figure 1. The potentially seismogenic phase transition to eclogite occurs around 45 km depth, and about 100–150 km west of the volcanic arc. If the densification to eclogite is largely completed by this depth, any observed seismicity is likely mechanically generated, and must therefore, be restricted to the cooler interior of the slab.

field and is defined as $Re=UL/\nu$, where U is the free-stream velocity, L is the characteristic length of the flow, and ν is the kinematic viscosity. When $Re<<1$, viscous forces dominate the flow and the velocity is inversely proportional to (dynamic) viscosity. Furthermore, any inertial contributions to the flow may be neglected, greatly reducing the complexity of the analysis. Most, if not all, subduction zones can be characterized by an extremely small Re due to the initial large mantle viscosity, typically, $1x10^{19}$ or $1x10^{20}$ Pa·s in the uppermost mantle. For the northern California subduction zone, $U=40$ mm/yr, $\nu\sim1x10^{19}$ Pa·s, and $L=200$ km, yielding a $Re\sim2x10^{-23}$.

Along the subducting slab, parameters change much faster normal to the slab than along it, so we may expect that a boundary layer of thickness d to be present along the slab. If we define our coordinate system so that the horizontal flow parallels the slab dip, the vertical component of velocity is normal to the slab and should be laminar, so long as: $d<<L$ and $Re<<1$. This is generally true if viscosity is constant. However, if the material properties are temperature-dependent, rapid departures from laminar flow may occur. We have determined the velocity in a boundary layer two kilometers thick parallel to the subducting Gorda slab in northern California. We allowed the viscosity to depend on temperature as follows: $\mu=\mu_o\cdot\exp[Q/RT]$, where $\mu_o=1x10^{19}\cdot\exp[-Q/R(T+1073.15)]$. Q, the activation energy is 522 kJ/m^3, R, the universal gas constant is 8.317 J/K·mol, and T is absolute temperature. Once the velocity field is known within the boundary layer, the point at which the boundary layer separates from the slab is simply where the shear-stress is zero on the slab: $(du/dz)_{slab}=0$.

Figure 3 illustrates the distance at which boundary layer separation occurs for the thermal models incorporating viscous dissipation. The initial thermal model does not attain the vertical velocity gradient reversal necessary for separation within the model geometry. In the model geometry, the position of the volcanic arc corresponds to a distance of 100 km. It is clear that only the models with an additional heat source produce the upwelling beneath the position of the volcanic arc.

Conclusions

1. Reasonable heat source estimates (100–200 mW/m^2) in a thin boundary layer blanketing the subducting slab-face raises the ambient mantle temperature by at least 200–400°C beneath the volcanic arc. Viscous

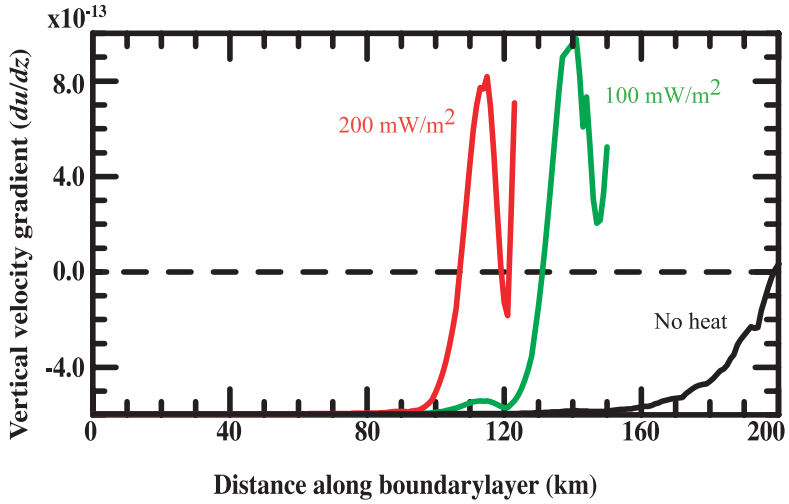

FIGURE 3: Boundary layer separation in the northern California subduction zone resulting from viscous dissipation. When the vertical velocity gradient reverses sign, the thin boundary layer that blankets the subducting slab begins to peel off from the slab, generating convective upwelling. Here, the separation point for 100 mW/m² is about 105 km, while for 200 mW/m², it is closer to 125 km. Both distances are almost directly below the volcanic arc, suggesting that boundary layer separation may contribute mass-flux to the volcanic arc system.

dissipation of heat produced in this layer can produce the minimum source temperature (>1100°C) necessary for the generation of the volumetrically significant basalts observed in the Cascades.

2. High temperatures along the subducting slab predict the seismogenic phase transition to eclogite at relatively shallow depths, even without viscous dissipation, resulting in little intraslab seismicity below ~45 km in the subducting Gorda slab.
3. Because the high slab face temperature restricts seismicity in the upper portion of the slab, the subduction zone thermal structure is a boundary condition on the occurrence of intraslab seismicity that can aid in the interpretation of the subducting slab morphology.
4. The separation of the boundary layer from the slab is a direct result of the strong temperature-dependence of the viscosity and occurs approximately beneath the volcanic arc. This separation should produce local convective upwelling. However, the interaction of the separating boundary layer and any deeper, "corner-flow" remains uncertain. Future work will attempt to model this interaction and quantify the mass-flux off the slab in this region.

References

Blackwell, D.D., R.G. Bowen, D.A. Hull, J. Riccio, and J.L. Steele, Heat flow, arc volcanism, and subduction in northern Oregon, *J. Geophys. Res., 87*, 8735–8754, 1982.

Blackwell, D.D., J.L. Steele, S.H. Kelley, and M.A. Korosec, Heat flow in the state of Washington and thermal conditions in the Cascade Range, *J. Geophys. Res., 95*, 19495–19516, 1990.

Davies, J.H., and D.J. Stevenson, Physical model of source region of subduction zone volcanics, *J. Geophys. Res., 97,* 2037–2070, 1992.

Honda, S., Thermal structure beneath Tohoku, northeast Japan: a case study for understanding the detailed thermal structure of the subduction zone, *Tectonophysics, 112*, 69–102, 1985.

Hyndman, R.D., and K. Wang, Thermal constraints on the zone of major thrust earthquake failure: the Cascadia subduction zone, *J. Geophys. Res., 98*, 2039–2060, 1993.

Kirby, S.H., E.R. Engdahl, and R. Denlinger, Intermediate-depth intraslab earthquakes and arc volcanism as physical expressions of crustal and uppermost mantle metamorphism in subducting slabs, in *Subduction: Top to Bottom*, edited by G.E. Bebout, D. Scholl, S. Kirby, and J.P. Platt, pp. 195–214, American Geophysical Union, Washington D.C., 1996.

McKenna, J.R., and D.D. Blackwell, Shallow thermal conditions in the middle and southern Cascadia subduction zone, *J. Geophys. Res.,* in press, 2002.

McKenzie, D.P., and J.C. Schlater, Heat-flow inside the island arcs of the northwest Pacific, *J. Geophys. Res., 73*, 3173–3179, 1968.

Minear, J.W., and M.N. Toksoz, Thermal regime of a downgoing slab and new global tectonics, *J. Geophys. Res., 75*, 1397–1419, 1970.

Molnar, P. and P. England, Temperatures in zones of steady state underthrusting of young oceanic lithosphere,

Earth Planet. Sci. Lett., 131, 57–70, 1995.

Mooney, W.D., and C.S. Weaver, Regional crustal structure and tectonics of the Pacific coast states: California, Oregon and Washington, in *Geophysical Framework of the Continental United States, Geological Society of America Mem. 172*, edited by L.C. Pakiser, and W.D. Mooney, pp. 493–522, Geological Society of America, 1989.

Oxburgh, E.R., and D.L. Turcotte, Problem of high heat flow and volcanism associated with zones of descending mantle convective flow, *Nature, 218*, 1041–1043, 1968.

Oxburgh, E.R., and D.L. Turcotte, Thermal structure of island arcs, *Geol. Soc. Amer. Bull., 81*, 1665–1688, 1970.

Peacock, S.M., The importance of blueschist–eclogite dehydration reactions in subducting oceanic crust, *Geol. Soc. Am. Bull., 105*, 684–694, 1993.

Peacock, S., K. Wang, and A.M. McMahon, Thermal structure and metamorphism of subducting oceanic crust: insight into Cascadia intraslab earthquakes in *The Cascadia Subduction Zone and Related Subduction Systems*, edited by S.H. Kirby, K. Wang, and S.G. Dunlop, pp. 123–126, U.S. Geological Survey Open-File Report 02–328, Geological Survey of Canada Open File 4350, 2002.

Tatsumi, Y., and S. Eggins, *Subduction Zone Magmatism,* 211 pp., Blackwell, Cambridge, 1995.

Smith, S.W., J.S. Knapp, and R.C. McPherson, Seismicity of the Gorda plate, structure of the continental margin, and an eastward jump of the Mendocino triple junction, *J. Geophys. Res., 98*, 8153–8171, 1993.

Thatcher, W., and P. England, Ductile shear zones beneath strike-slip faults: implications for the thermomechanics of the San Andreas fault zone*, J. Geophys. Res, 103*, 891–905, 1998.

Yuen, D.A., A.L. Fleitout, G. Schubert, and C. Froidevaux, Shear deformation zones along major transform fault, *Geophys. J. R. Astr. Soc., 54*, 93–119, 1978.

Theoretical mineralogy, density, seismic wavespeeds and H_2O content of the Cascadia subduction zone, with implications for intermediate-depth seismicity and earthquake hazard

Bradley R. Hacker[1], Geoffrey A. Abers[2] and Simon M. Peacock[3]
1 Department of Geological Sciences, University of California, Santa Barbara, California, 93106–9630, USA
2 Department of Earth Sciences, Boston University, 675 Commonwealth Avenue, Boston, Massachusetts, 02215, USA
3 Department of Geological Sciences, Arizona State University, Box 871404, Tempe, Arizona, 85287–1404, USA
hacker@geology.ucsb.edu, abers@bu.edu, peacock@asu.edu

ABSTRACT

We calculate physical properties of rocks in subduction zones using a compilation of mineral physical property measurements, a new set of phase diagrams and subduction-zone thermal models, and apply our results to Cascadia. Observed P-wave speeds of the Juan de Fuca plate west of the Cascadia trench are best matched by a greenschist-facies upper crust and metastable, partially hydrated lower crust and mantle. The predicted positions of dehydration reactions in the subducting crust show a spatial link to observed seismicity, suggesting that dehydration may be the cause of the earthquakes and that the predicted location of dehydration reactions in the slab can be used to predict hazardous seismicity the length of Cascadia.

Introduction

Much about subduction zones remains unknown because all our information comes either from indirect geophysical observations or observation of fossil subduction zone rocks. In particular, we would like to understand: the hydration state of the mantle wedge and the incoming slab; where and why slabs devolatilize and how this contributes to arc volcanism; slab buoyancy and shape; seismic wavespeeds and their relation to mineralogy; and intermediate-depth earthquakes and their possible relationship to phase transformations. This study uses a synergistic thermal–petrological–seismological approach to address some of these questions. Our approach comprises six specific steps:

1) Compile and assess physical properties of minerals relevant to subduction zones.
2) Construct phase diagrams apropos to subduction zone rock types and physical conditions.
3) Compute pressures (P) and temperatures (T) for a specific subduction zone.
4) Superimpose calculated phase relations onto the P–T model.
5) Superimpose rock physical properties onto the P–T model.
6) Compare predictions to observations.

1. Compiling mineral properties

We performed an extensive literature search to obtain physical properties of minerals relevant to subduction zones. The necessary physical properties are: formula weight, molar volume, H_2O content, expansivity α, $\partial\alpha/\partial T$, the isothermal bulk modulus K_T, $\partial K_T/\partial P$, the shear modulus μ, $\partial\mu/\partial T$, $\partial\mu/\partial P$, the Grüneisen parameter γ_{th} and the second Grüneisen parameter δ_T. From these we used a second-order finite-strain approximation (which yields negligible error at these pressures for which $P/K_T < 1$) to calculate the adiabatic bulk modulus, shear modulus, density, seismic wavespeeds and Poisson's ratios for each mineral as a function of P and T. Each of these values was examined in some detail to ensure that the calculated values were in agreement with values measured directly on minerals or single-phase mineral aggregates at elevated P and T.

2. Constructing phase diagrams

We chose to simplify the rock compositions under consideration to basalt/gabbro, lherzolite, harzburgite and serpentinite—i.e., the entire overriding plate crust and subducting plate crust was treated as basalt/gabbro, and the remainder was considered ultramafic. We then calculated the P–T stability fields of different minerals and the reactions that bound the various fields. These phase diagrams permit direct assessment of phase proportions, reaction stoichiometries, H_2O content, and, in combination with the rock physical property calculations described above, density, V_P, and V_S of mafic and ultramafic rocks in subduction zones.

To create a phase diagram for mafic rocks, we performed an extensive literature search to identify studies that reported all three of the following: 1) bulk rock compositions; 2) mineral modes; and 3) mineral compositions. From these studies we chose only rocks whose bulk compositions differed from mid-ocean ridge basalts (MORB) by less than ~10%. Assuming that the entire crust is of MORB composition is clearly incorrect for the lower crust, as detailed below. We then compiled the mineral modes and mineral compositions into various metamorphic facies. Next, the *P–T* range over which each mineral assemblage is stable was defined using Thermocalc [*Holland and Powell,* 1998]. Most boundaries are thus defined by discontinuous reactions involving the appearance or disappearance of at least one phase. Obvious outliers were discarded, and a mean mineral mode and set of mineral compositions was computed for each metamorphic facies.

Phase diagrams for lherzolite, harzburgite and serpentinite were constructed principally from Thermocalc [*Holland and Powell,* 1998] using Mg-endmember reactions in the Ca–Fe^{2+}–Mg–Al–Si–H–O system and mineral compositions reported in the literature for naturally metamorphosed ultramafic rocks. Thermocalc's calculations of phase relations at $P > 5$ GPa were modified in light of recent experiments by *Luth* [1995], *Ulmer and Trommsdorff* [1995], *Wunder and Schreyer* [1997], *Bose and Navrotsky* [1998], *Wunder* [1998] and *Pawley* [2000].

3. Computing subduction-zone pressure and temperature

For Cascadia, we used the thermal model of *Wang et al*. [1995] calculated for southern Vancouver Island (Figure 1a). Pressures for the same cross section were calculated using appropriate rock densities.

4. Superimposing phase relations

Onto a subduction-zone cross section depicting *P* and *T* and rock composition, we overlayed the different metamorphic mineral assemblages computed in step 2. Figures 1b and 1c show the results for mafic rocks and harzburgite, respectively. We have assumed that the activity of $H_2O = 1$ (or that $P_{H2O} = P_{lithostatic}$) and that equilibrium obtains. These assumptions cannot be correct everywhere and are addressed partially in a later section.

5. Superimposing rock physical properties

From the mineral physical properties calculated at elevated *P* and *T* in step 1, we derived rock physical properties using a Voigt–Reuss–Hill average weighted by mineral proportions determined in step 2. The results are shown in Figures 1d–1g.

6. Comparing predictions to observations: Cascadia

Beneath Cascadia, the 5–9 Ma Juan de Fuca plate subducts at a rate of 41 mm/yr [*Hyndman and Wang,* 1993], rendering it among the youngest, most slowly subducting, and, consequently, warmest slabs in the world. The slab has a thick sediment blanket and upper plate volcanism is weak to moderate.

Seismicity: the correlation to dehydration

In the vicinity of southern Vancouver Island, seismicity along and near the intraplate subduction thrust occurs in two distinct pulses—one at 30–40 km depth and another around 70 km depth [*Rogers et al.*, 1990] (Figure 1a). It is a primary observation of this study that there is a spatial correlation between this seismicity and the predicted dehydration reactions in the subducting crust (Figure 1b). The upper nest of earthquakes at 30–40 km depth falls within the lower half of the epidote amphibolite field and stops abruptly at the down dip end at the transition to zoisite–amphibole eclogite. This corresponds to a predicted change from 2.1 to 0.7 wt. % crystallographically bound H_2O. The lower nest of earthquakes at ~70 km depth coincides with the transition from zoisite–amphibole eclogite to anhydrous eclogite—a reduction in H_2O content from 0.3 to 0.1 wt. %. In other words, along the south Vancouver Island transect, the bulk of the seismicity occurs at depths coincident with predicted dehydration in the downgoing crust. This same spatial correlation between phase transformations in the crust and intermediate-depth seismicity holds for the Nankai (southern Japan) and Tohoku (northern Japan) subduction zones where thermal conditions are different. We propose, therefore, that calculating the position of dehydration reactions in the slab could be an inexpensive and effective means of predicting future hazardous seismicity; certainly this hypothesis can easily be tested with additional modeling.

The idea that intermediate-depth slab seismicity might be related to dehydration reactions in the upper part of the slab was explored in considerable detail by *Kirby et al*. [1996], *Peacock and Wang* [1999] and *Kirby* [2000]. Our calculations for Cascadia provide a very strong confirmation of this hypothesis. Moreover, the fact that the seismicity correlates well with phase changes predicted from equilibrium considerations implies that at least part of the subducted crust is undergoing mineralogical change in a near-equilibrium fashion. Abundant geologic evidence from localities around the globe demonstrates that fine-grained, H_2O-rich basalts transform to high-pressure mineralogies faster than coarse-grained, H_2O-poor gabbros [*Hacker*, 1996]. Thus, in a subducting slab, we expect phase transformations in the gabbroic layer to lag those in the volcanic layer and produce dehydration at greater depths than predicted by equilibrium considerations. Therefore it is likely that: 1) the observed seismicity is generated principally by dehydration reactions in the volcanic layer of the subducted crust, which trans-

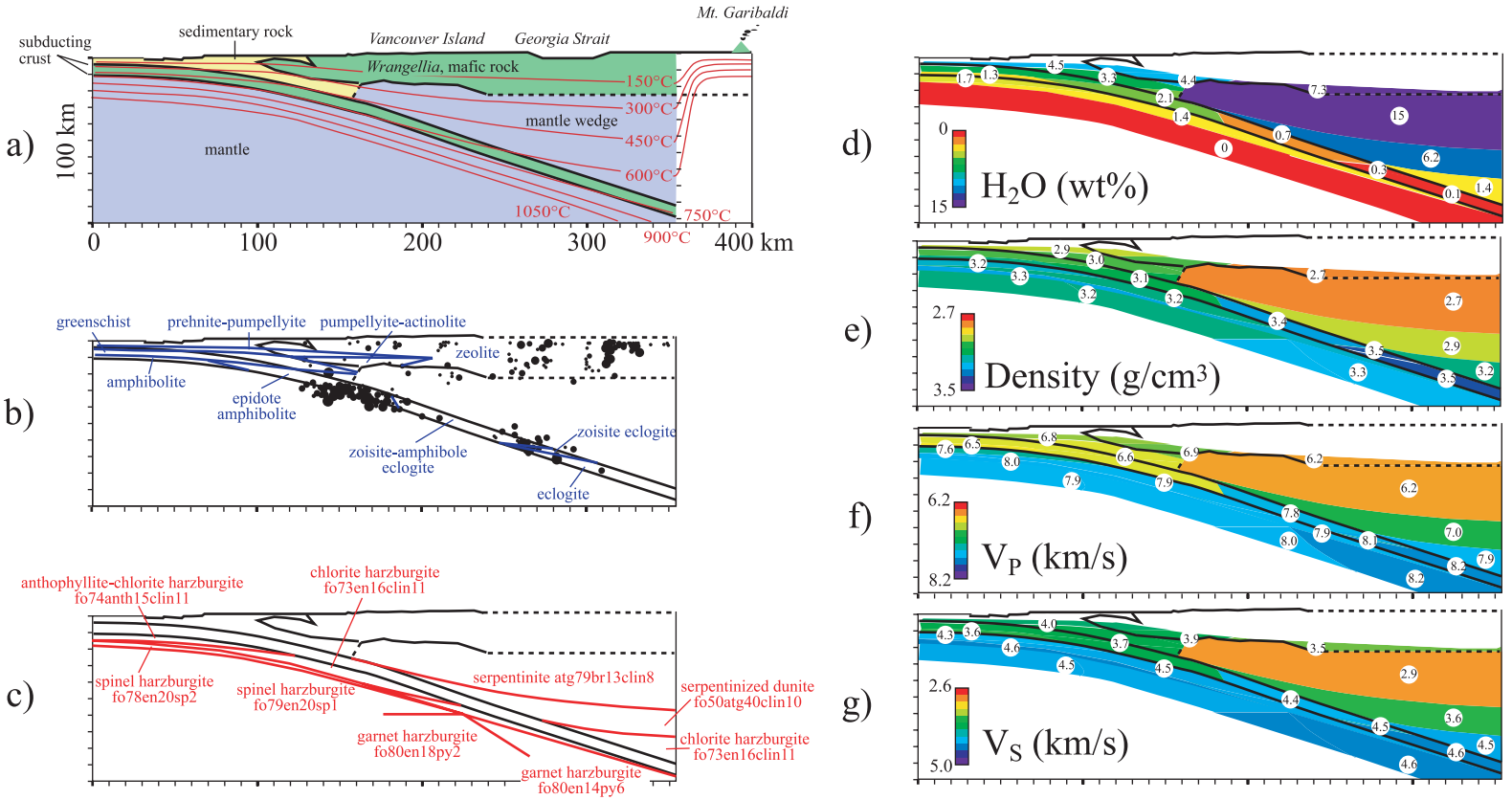

FIGURE 1: Calculated properties of the Cascadia subduction zone along a transect through southern Vancouver Island. a) Geology [*Hyndman and Wang*, 1993] and isotherms [*Wang et al.*, 1995]. b) Calculated phase relations in mafic crust and observed seismicity [*Rogers et al.*, 1990]. c) Calculated phase relations in ultramafic rock. Numbers indicate volume of minerals by percentage: anth, anthophyllite (amphibole); atg, antigorite (serpentine); br, brucite; clin, clinochlore (chlorite); en, enstatite (orthopyroxene); fo, forsterite (olivine); sp, spinel; py, pyrope (garnet). d) Calculated H_2O content. e) Calculated densities. f) Calculated *P*-wavespeeds. g) Calculated *S*-wavespeeds.

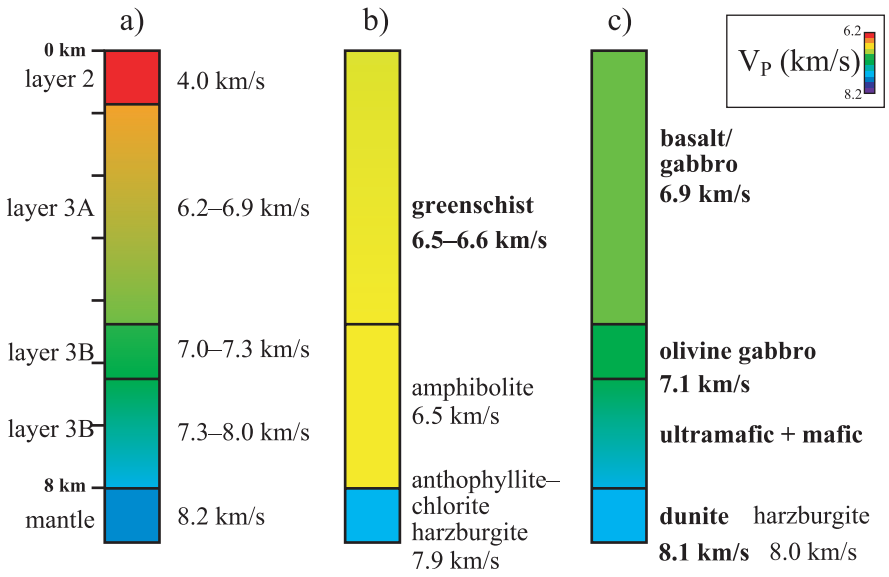

FIGURE 2: Observed and calculated *P*-wavespeeds for the Juan de Fuca plate offshore Vancouver Island. a) Seismic section from *Clowes* [2000]. b) *P*-wavespeeds calculated assuming $a_{H2O}=1$. c) *P*-wavespeeds calculated assuming $a_{H2O}=0$. Calculations in b) and c) are based on pressures and temperatures from most-outboard portion of *Hyndman and Wang's* [1993] thermal model. Best fits to seismic observations are indicated with boldface type.

forms on a near-equilibrium basis to eclogite; and 2) the subducted plutonic layer is nearly anhydrous, generates few earthquakes and transforms to eclogite at greater depth than predicted by equilibrium considerations.

Slab velocities and mineralogy

An ocean-bottom seismometer survey offshore and parallel to Vancouver Island by *Clowes* [this volume] can be compared with our predicted wavespeeds for the Juan de Fuca plate. Clowes' interpretation (Figure 2a) is that the Juan de Fuca plate includes: a one kilometer thick layer 2 with V_P=4.0 km/s; a four kilometer thick layer 3A with V_P=6.2–6.9 km/s; a layer 3B split into a one kilometer layer with V_P=7.0–7.3 km/s above a two kilometer layer with V_P =7.3–8.0 km/s; and an underlying mantle with a *P*-wave speed of 8.2 km/s.

In our equilibrium model (Figure 2b), layers 2 and 3A have a greenschist-facies mineralogy and a *P*-wave speed of 6.6 km/s. Layer 3B is at amphibolite facies and has V_P=6.5 km/s. The immediately underlying mantle is predicted to be an anthophyllite–chlorite-bearing harzburgite with a *P*-wave speed of 7.6 km/s.

Thus, we do not successfully model layer 2, but this may be because we do not consider the effects of porosity and fluids. At greater pressures where fluids are expelled and pores closed, our model may be correct. The faster-than-predicted speeds (>6.6 km/s) in the base of layer 3A imply that the lower part of that layer is not at greenschist facies. Studies of ophiolites imply that the most likely candidate is unaltered basalt/gabbro. If we model layers 3A and 3B as unaltered, metastable basalt/gabbro of MORB composition, we calculate a speed of 6.9 km/s (Figure 1c). Speeds of 7.0–7.3 km/s in the upper one kilometer of layer 3B are also faster than in our model, implying that layer 3B is not amphibolite-facies gabbro. Moreover, the observed speeds are faster than our calculated speeds for metastable gabbro of MORB composition. Such speeds are, however, compatible with calculated speeds for pyroxene gabbro or olivine gabbro. Speeds of 7.3–7.8 km/s in the lower one kilometer of layer 3B can be modeled as a mix of olivine gabbro, wehrlite and clinopyroxenite. Our calculated speed for anthophyllite–chlorite-bearing harzburgite is slow compared to the observed seismic wave speed and the reported V_P implies a mix of anhydrous harzburgite and dunite.

Trying to match the measured seismic *P*-wavespeeds with specific homogeneous rock types is fraught with uncertainty. However, the best match is attained assuming that: 1) layer 3A is greenschist facies at the top and grades downward into an anhydrous, metastable basalt; 2) layer 3B is not MORB-composition gabbro; and 3) the mantle is metastable, anhydrous harzburgite. Alternatively, the velocity gradient observed by *Clowes* [this volume] at the bottom of the crust may reflect lateral and/or vertical resolution limits of the seismic data and a more complex crust-mantle boundary than assumed.

Conclusions

Our model produces calculated physical properties of rocks in subduction zones using a compilation of mineral

physical property measurements, a new set of phase diagrams and subduction-zone thermal models. Comparison of predicted vs. observed *P*-wavespeeds indicates that the lowermost crust and mantle of the Juan de Fuca plate west of the Cascadia trench is not at mineralogical equilibrium with the ambient *P* and *T* and, specifically, is not fully hydrated. A distinctive correlation between the predicted positions of dehydration reactions in the subducting crust and observed seismicity suggests a causal link between the two and that future hazardous seismicity the length of Cascadia can be predicted via our method.

Acknowledgements

Thanks to Steve Kirby and Kelin Wang and their respective institutions for hosting the Victoria Workshop. Steve was also the first to suggest the use of mapping dehydration reactions in the slab as an indicator of future seismicity.

References

Bose, K., and A. Navrotsky, Thermochemistry and phase equilibria of hydrous phases in the system MgO–SiO_2–H_2O; implications for volatile transport to the mantle, *J. Geophys. Res., 103*, 9713–9719, 1998.

Clowes, R.M., Crustal structure of northern Juan de Fuca plate and Cascadia subduction zone—new results, old data, in *The Cascadia Subduction Zone and Related Subduction Systems*, edited by S.H. Kirby, K. Wang, and S.G. Dunlop, pp. 55–58, U.S. Geological Survey Open-File Report 02–328, Geological Survey of Canada Open File 4350, 2002.

Hacker, B.R., Eclogite formation and the rheology, buoyancy, seismicity and H_2O content of oceanic crust, in *Dynamics of Subduction*, edited by G.E. Bebout, D. Scholl, S.H. Kirby, and J.P. Platt, pp. 337–246, American Geophysical Union, Washington, D.C., 1996.

Holland, T.J.B., and R. Powell, An internally consistent thermodynamic data set for phases of petrological interest, *J. Metamorph. Geol.*, *16*, 309–343, 1998.

Hyndman, R.D., and K. Wang, Thermal constraints on the zone of possible major thrust earthquake failure on the Cascadia margin, *J. Geophys. Res.*, *98*, 2039–2060, 1993.

Kirby, S.H., Taking the temperature of slabs, *Nature*, *403*, 31–33, 2000.

Kirby, S.H., E.R. Engdahl, and R. Denlinger, Intermediate-depth intraslab earthquakes and arc volcanism as physical expressions of crustal and uppermost mantle metamorphism in subducting slabs, in *Subduction Top to Bottom, Geophysical Monograph*, edited by G.E. Bebout, D. Scholl, and S. Kirby, pp. 195–214, American Geophysical Union, Washington, D.C., 1996.

Luth, R.W., Is phase A relevant to the Earth's mantle?, *Geochimica et Cosmochimica Acta*, *59*, 679–682, 1995.

Pawley, A., Stability of clinohumite in the system MgO-SiO_2-H_2O, *Contributions to Mineralogy and Petrology*, *138*, 284–291, 2000.

Peacock, S.M., and K. Wang, Seismic consequences of warm versus cool subduction metamorphism: examples from southwest and northeast Japan, *Science*, *286*, 937–939, 1999.

Rogers, G.C., C. Spindler, R.D. Hyndman, and J.L. Varsek, Seismicity along the Vancouver Island Lithoprobe corridor, *Lithoprobe Report*, *11*, 166–169, 1990.

Ulmer, P., and V. Trommsdorff, Serpentine stability related to mantle depths and subduction-related magmatism, *Science*, *268*, 858–861, 1995.

Wang, K., T. Mulder, G.C. Rogers, and R.D. Hyndman, Case for very low coupling stress on the Cascadia subduction fault, *J. Geophys. Res.*, *100*, 12,907–12,918, 1995.

Wunder, B., Equilibrium experiments in the system MgO-SiO_2-H_2O (MSH); stability fields of clinohumite-OH [$Mg_9Si_4O_{16}(OH)_2$], chondrodite-OH ([$Mg_5Si_2O_8(OH)_2$] and phase A ($Mg_7Si_2O_8(OH)_6$), *Contributions to Mineralogy and Petrology*, *132*, 111-–20, 1998.

Wunder, B., and W. Schreyer, Antigorite: high-pressure stability in the system MgO-SiO_2-H_2O (MSH), *Lithos*, *41*, 213–227, 1997.

Slab deformation at the edge of subduction zones: An example from Cascadia

Uri S. ten Brink
United States Geological Survey, 384 Woods Hole Road, Woods Hole, Massachusetts, 02543, USA
TenBrink@usgs.gov

Slab deformation

Understanding the interaction between the subducting plate and the overlying forearc is a key to a successful evaluation of the seismogenic hazard above subduction zones. Here we focus on the interaction, which takes place when subduction ceases. In particular, the cessation of subduction at the southern end of the Cascadia subduction zone offers insights to the processes that operate in a warm subduction zone and the coupling between the plates. We show that the legacy of subduction remains in the thermal structure of California even after subduction ceased.

Plate kinematic interpretations predict a gap in the underlying subducted slab caused by the northward migration of the Pacific–North America (NOAM)–Juan de Fuca (JdF) triple junction (MTJ). Upon cessation of subduction, the weight of the already subducted plate and of the adjacent subducting section continued to pull the slab downward, opening a gap into which sublithospheric material (asthenosphere) upwelled under the former forearc [*Dickinson*, 1997; *Dickinson and Snyder,* 1979a]. Various predictions have been made on the basis of the slab gap hypothesis. The slab gap was envisioned to be the locus of decompression melting in the asthenosphere, resulting in the accretion of a several kilometers thick layer of mafic material to the base of the California crust [*Liu and Furlong*, 1992]. Estimates of hydrocarbon maturation were made based on the thermal regime of a slab gap with asthenoshperic upwelling [*Heasler and Surdam*, 1985]. The Pacific–NOAM plate boundary was envisioned to be subhorizontal at depth and to migrate inland over time as the slab gap annealed [*Furlong et al.*, 1989].

The slab-gap model is based on the configuration of three independently-moving rigid plates, Pacific, NOAM, and JdF, but, in fact, the Pacific plate is the only rigid plate. Non-rigid deformation of the JdF plate, known as the Gorda deformation zone, is manifested by curved magnetic anomalies and pervasive faulting [*Wilson*, 1986]. The NOAM plate in California also does not behave as a single rigid plate. It consists of two blocks, the Sierra Nevada–Great Valley Klamath Mountains block and the Coast Ranges. The latter is essentially a deformation zone between two more competent blocks, the Pacific plate and the Sierra Nevada block [*Walcott*, 1993]. The slab gap model also assumes that the three plates are moving independently. This has not been the case for the JdF plate after the fragmentation of the Farallon plate. Starting 18 Myr ago, the JdF plate has rotated clockwise, seafloor spreading slowed [*Atwater,* 1989], and the JdF plate motion is progressively more aligned with that of NOAM with respect to the Pacific.

We propose an alternative model based on kinematics of non-rigid plate boundaries [*ten Brink et al.*, 1999]. In this model, continuous deformation, rotation and stretching of the JdF plate fill the geometrical gap without large-scale holes and tears. The large and rigid Pacific plate is acting as an indenter into the non-rigid JdF plate. It is moving northwestward in a hot spot reference frame pushing at the JdF plate across the Mendocino fracture zone and causing it to move northward. Although the fracture zone may be weak in shear, north–south oriented normal compressive stresses can be transmitted to the southern part of the JdF plate [*Wang et al.,* 1997]. Landward of the MTJ, however, the subducting Juan de Fuca plate is not pushed by the Pacific plate and is not confined. This allows the plate to spread into the unconfined region.

How much does the subducted plate have to stretch to fill the geometrical gap? Using two different plate kinematic configurations, the estimated size of the gap to be filled is only 27% or 37% of the JdF plate area subducted during the past 4 and 3.2 Myr respectively. If the JdF slab stretches to fill this gap, it will have to thin by a factor of only 1.27 or 1.37. The age of the subducted plate is 6–10 Ma [*Wilson*, 1986]; hence, the thickness of the thermal lithosphere (to a temperature of 1300°C) is 25–30 km. Thinning by a factor of 1.37 reduces the slab's thermal thickness to 18.1–21.7 km, which is equivalent to the thickness of a 4 Ma slab. (Thinning of the subducted slab by a factor of 1.27 reduces the thermal thickness of the lithosphere to 19.7–23.6 km, which is equivalent to the thickness of a 4–5 Ma slab.) Thinning of the mantle at these shallow depths (40–50 km) by this factor is ex-

pected to generate only negligible decompression melting of the upper mantle [*McKenzie and Bickle*, 1988]. Strain may not be uniform, however, so larger amounts of thinning may take place locally as the tomographic images suggest.

Thermal and magmatic consequences

With the slab stretch model in mind, we propose that the thermal evolution of the lithosphere results from thermal re-equilibration following the cessation of subduction and some stretching of the slab. The overlying plate is the forearc region of the subduction zone, which is insulated during subduction by the cold surface of the subducting plate beneath the forearc. When subduction and stretching stop, thermal reequilibration begins, and temperatures at the base of the forearc rise. We approximate this process by calculating the geothermal gradients as a function of time after cessation of subduction (time 0) for subducted slabs with a thermal age of 10 and 4 Ma overlain by 20 and 30 km thick forearc.

There are two important consequences of thermal re-equilibration: 1) melting of the subducted crust; and 2) elevated heat flow in the overlying plate. Minor volcanic activity occurred in the wake of the northward passage of the MTJ, reflected in the younger volcanic outcrops toward the north [*Dickinson*, 1997]. The most recent activity (<2 Ma) is located at Clear Lake. It has been suggested that the volcanism resulted from a slab gap under the forearc [*Dickinson and Snyder*, 1979b; *Johnson and O'Neil*, 1984]. Quantitative estimates of asthenospheric upwelling into the gap, however, predict voluminous magmatic production [*Liu and Furlong*, 1992], far larger than the geologic data suggest. In the slab stretch model, we explain the volcanism as mainly arising from crustal anatexis. Pressure–temperature conditions of the amphibolite solidus (temperatures ≥ 630°C at depths ≥ 25 km) [*Wyllie and Wolf*, 1993] can be attained within the subducted oceanic crust during the first 5 Myr after the cessation of subduction of a hot young (~4 Ma) oceanic lithosphere overlain by 20–30 km thick crust. Magmatism in California is typically short lived and produces small volumes of magma. It occurs mainly in the eastern part of the Coast Ranges [*Johnson and O'Neil*, 1984] where the overlying crustal thickness reaches 20–25 km [*Henstock et al.*, 1997]. A seismic profile across northern California where the MTJ was located <2 Myr ago shows "bright spots" representing melt lenses [*Levander et al.*, 1998] that cluster throughout the fossil oceanic crust. The volcanic rocks are dominantly intermediate to silicic, have relatively high $^{87}Sr/^{86}Sr$ ratios, relatively high $\delta^{18}O$ values (7.5–11.5), and relatively high Th contents [*Johnson and O'Neil*, 1984], suggesting that crustal anatexis played a dominant role in their generation.

Surface heat flow in western California increases rapidly immediately south of the MTJ, reaching a maximum several hundreds of kilometers to the south and then decreasing slightly. Our calculations best fit the data with an overlying crustal thickness of 20 km and an underlying stretched oceanic slab with an equivalent thermal age of 2–4 Ma. The pattern of increasing heat flow south of the MTJ was previously cited as evidence for a slab gap [*Lachenbruch and Sass*, 1980]. Interestingly, however, these authors also pointed out that the heat flow variations are best fit with cooler than astheonospheric temperatures (1000°C) emplaced instantaneously at the base of a 20-km-thick crust. Our proposed geothermal gradient also matches thermobarometric estimates from spinel lhezorlites from Coyote Reservoir [*Jove and Coleman,* 1998].

A broad zone of high heat flow across the entire Coast Ranges averaging 30 mW m^{-2} higher than is typical for continental regions was explained as a result of either: 1) shear heating on horizontal planes due to viscous drag of the upper part of the lithosphere over its substratum [*Lachenbruch and Sass,* 1973]; 2) shear heating on vertical planes in the lithospheric upper mantle along the Pacific–North American diffuse plate boundary [*Molnar,* 1992]; or 3) the effect of the slab gap [*Lachenbruch and Sass,* 1980]. Central California is probably underlain by the stalled Monterey microplate [*Nicholson et al.,* 1994], and therefore a slab gap never existed in central California [*Atwater and Stock,* 1998]. We argue that shear heating is also not required to explain the elevated heat flow. The higher heat flow is simply the consequence of re-equilibration of the geothermal gradient following the cessation of subduction of the Monterey microplate. The stalled Monterey slab underlying the Coast Ranges was probably less than 4 Myr old, assuming a convergence rate of 30–40 km Myr^{-1}. The predicted heat flows for a 2- and 4 Myr old subducted slabs 18 Myr after subduction matches well the observations from this area [*Sass et al.,* 1997]. Note that the Monterey microplate behavior prior to cessation was similar to the JdF plate, namely, clockwise rotation and decreased subduction rate.

References

Atwater, T., Plate tectonic history of the northeast Pacific and western North America, in *The Eastern Pacific Ocean and Hawaii*, edited by E.L. Winterer, D.M. Hussong, and R.W. Decker, pp. 29–72, Geol. Soc. Am., Boulder, Colo., 1989.

Atwater, T., and J. Stock, Pacific–North America plate tectonics of the Neogene southwestern United States: an update, *Int. Geol. Rev., 40,* 375–402, 1998.

Dickinson, W.R., Tectonic implications of Cenozoic volcanism in coastal California, *Geol. Soc. Am. Bull., 109,* 936–954, 1997.

Dickinson, W.R., and W.S. Snyder, Geometry of subducted plates related to San Andreas transform, *J. Geol., 87,* 609–627, 1979a.

Dickinson, W.R., and W.S. Snyder, Geometry of triple junctions related to San Andreas transform, *J. Geophys. Res., 84*, 561–572, 1979b.

Furlong, K.P., W.D. Hugo, and G. Zandt, Geometry and evolution of the San Andreas fault zone in northern California, *J. Geophys. Res., 94,* 3100–3110, 1989.

Heasler, H.P., and R.C. Surdam, Thermal evolution of coastal California with application to hydrocarbon maturation, *AAPG Bull., 69,* 1386–1400, 1985.

Henstock, T.J., A. Levander, and J.A. Hole, Deformation in the lower crust of the San Andreas fault system in northern California, *Science*, *278,* 650–653, 1997.

Johnson, C.M., and J.R. O'Neil, Triple junction magmatism: a geochemical study of Neogene volcanic rocks in western California, *Earth Planet. Sci. Lett.*, *71,* 241–262, 1984.

Jove, C.F., and R.G. Coleman, Extension and mantle upwelling within the San Andreas fault zone, San Francisco Bay area, California, *Tectonics*, *17,* 883–890, 1998.

Lachenbruch, A.H., and J.H. Sass, Thermomechanical aspects of the San Andreas fault system, in *Tectonic Problems of the San Andreas Fault System*, edited by R.L. Kovach, and A. Nur, pp. 192–205, Stanford University Press, Stanford, Calif., 1973.

Lachenbruch, A.H. and J.H. Sass, Heat flow and energetics of the San Andreas fault zone, *J. Geophys. Res.*, *85,* 6977–6989, 1980.

Levander, A., T.J. Henstock, A.S. Meltzer, B.C. Beaudoin, A.M. Trehu, and S.L. Klemperer, Fluids in the lower crust following Mendocino triple junction migration: active basaltic intrusion? *Geology*, *26,* 171–174, 1998.

Liu, M., and K.P. Furlong, Cenozoic volcanism in the California Coast Ranges: numerical solutions, *J. Geophys. Res.*, *97,* 4941–4951, 1992.

McKenzie, D., and M.J. Bickle, The volume and composition of melt generated by extension of the lithosphere, *J. Petrol., 29,* 625–679, 1988.

Molnar, P., Brace–Goetze strength profiles, the partitioning of strike-slip and thrust faulting at zones of oblique convergence, and the stress–heat flow paradox of the San Andreas fault, in *Fault Mechanics and Transport Properties of Rocks,* edited by T.F. Wong and B. Evans, pp. 435–459, Academic, San Diego, Calif., 1992.

Nicholson, C., C.C. Sorlien, T. Atwater, J.C. Crowell, and B.P. Luyendyk, Microplate capture, rotation of the western Transverse Ranges, and initiation of the San Andreas transform as a low-angle fault system, *Geology*, *22,* 491–495, 1994.

Sass, J.H., C.F. Williams, A.H. Lachenbruch, S.P. Galanis, and F.V. Grubb, Thermal regime of the San Andreas fault near Parkfield, California, *J. Geophys. Res.*, *102*, 27,575–27,585, 1997.

ten Brink, U.S., N. Shimizu, and P.C. Molzer, Plate deformation at depth under northern California, slab gap or stretched slab? *Tectonics*, 18, 1084–1098, 1999.

Walcott, D., Neogene tectonics and kinematics of western North America, *Tectonics, 12,* 326–333, 1993.

Wang, K., J. He, and E.E. Davis, Transform push, oblique subduction resistance, and intraplate stress of the Juan de Fuca plate, *J. Geophys. Res., 102,* 661–674, 1997.

Wilson, D.S., A kinematic model for the Gorda deformation zone as a diffuse southern boundary of the Juan de Fuca plate, *J. Geophys. Res., 91,* 10,259–10,269, 1986.

Wyllie, P.J., and M.B. Wolf, Amphibolite dehydration-melting: sorting out the solidus, in *Magmatic Processes and Plate Tectonics,* edited by H. M. Prichard et al., pp. 405–416, Geol. Soc. of London, London, 1993.

Stresses in the Juan de Fuca plate and the role of mantle resistance to horizontal slab motion

Kelin Wang[1], Jiangheng He[1], Earl E. Davis[1] and Chris Goldfinger[2]
1 Pacific Geoscience Centre, Geological Survey of Canada, PO Box 6000, Sidney, British Columbia, V8L 4B2, Canada
2 College of Oceanic and Atmospheric Sciences, Oregon State University, Corvallis, Oregon, 97331, USA
wang@pgc.nrcan.gc.ca, he@pgc.nrcan.gc.ca, davis@pgc.nrcan.gc.ca, gold@oce.orst.edu

The Juan de Fuca plate is a small oceanic plate between the Pacific and North America plates. In the southernmost region, referred to as the Gorda deformation zone, the maximum compressive stress σ_1 constrained by earthquake focal mechanisms is north–south. Off Oregon, and possibly off Washington, northwest trending left-lateral faults cutting the Juan de Fuca plate indicate a σ_1 in a northeast–southwest to east–west direction. The magnitude of differential stress increases from north to south; this is inferred from the plastic yielding and distribution of earthquakes throughout the Gorda deformation zone. To understand how tectonic forces determine the stress field of the Juan de Fuca plate, we have modeled the intraplate stress using both elastic and elastic perfectly-plastic plane-stress finite element models. We conclude that the right-lateral shear motion of the Pacific and North America plates is primarily responsible for the stress pattern of the Juan de Fuca plate. The most important roles are played by a compressional force normal to the Mendocino transform fault, a result of the northward push by the Pacific plate, and a horizontal resistance operating against the northward, or margin-parallel, motion of the slab. Margin-parallel slab resistance results in a large north–south compression in the Gorda deformation zone because the force is integrated over the full length of the Cascadia subduction zone. The Mendocino transform fault serves as a strong buttress that is very weak in shear but capable of transmitting large strike-normal compressive stresses. Internal failure of the Gorda deformation zone potentially places limits on the magnitude of the fault-normal stresses being transmitted and correspondingly on the magnitude of strike-parallel subduction resistance. Transform faults and oblique subduction zones in other parts of the world can be expected to transmit and create stresses in the same manner. Margin-parallel slab resistance is comparable to mantle's updip resistance to slab motion and therefore is comparable to the slab-pull force. It must play a major role in controlling the state of stress in the slab and the occurrence of intraslab earthquakes.

Phase changes, fluids and the co-location of the deep and shallow seismicity beneath Puget Sound and southern Georgia Strait

Garry C. Rogers
Pacific Geoscience Centre, Geological Survey of Canada, PO Box 6000, Sidney, British Columbia, V8L 4B2, Canada
rogers@pgc.nrcan.gc.ca

The majority of contemporary seismicity in the northern half of the Cascadia subduction zone occurs in one location: straddling the international border, adjacent to the change in trend of the North American coastline from north–south to northwest–southeast. This is true in both the subducting oceanic Juan de Fuca plate and in the overlying continental North American plate. Why is the region of crustal seismicity located directly above the subcrustal seismicity and why is the areal extent very similar, even though the two regions are decoupled and have very different stress regimes? The upward migration of fluids offers a potential explanation. In the subducting oceanic crust, the phase change from basalt to eclogite is coincident with the region of seismicity. This phase change creates extensional stress in the subducting oceanic crust and alters the subducting plate buoyancy from positive to negative, adding to the tension near the upper surface. The phase change from hydrous metabasalt to eclogite also releases water. In warm subduction zones such as Cascadia, this phase change takes place over a very narrow range in the down-dip direction. The broad arch in the subducting plate, created by the change in the orientation of the subducting margin, allows margin parallel migration of hot fluids to the highest region: beneath Puget Sound and southern Georgia Strait. The crustal seismicity in the North America plate is characterized by patterns and lineaments, but there is little evidence of fault planes aligning with spatial trends of epicentres. Instead, most crustal seismicity seems to be occurring on random faults, all responding to the same regional stress. Seismicity induced by fluid injection often exhibits this characteristic.

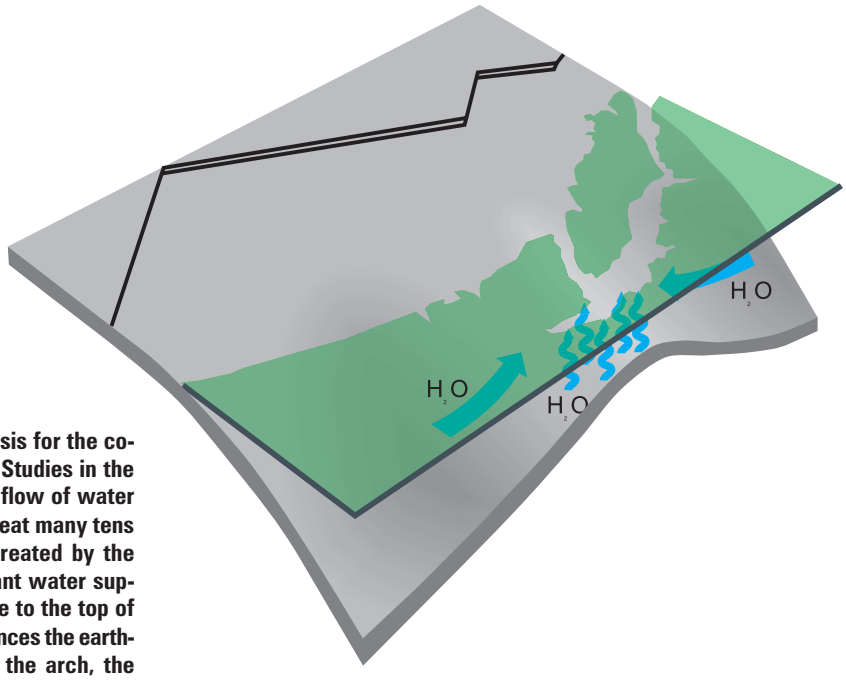

FIGURE 1: This cartoon explains the hypothesis for the co-location of the deep and shallow seismicity. Studies in the oceanic crust offshore have shown that the flow of water in hydrothermal systems can operate over great many tens of kilometers. The tensional environment created by the phase change provides paths for the abundant water supplied by the phase change process to migrate to the top of the arch in the subducting plate, where it enhances the earthquake generating process. From the top of the arch, the water bleeds upwards into the North American plate where it causes a region of increased micro-seismicity.

The role of phase changes in the development of forearc basins

Garry C. Rogers
Pacific Geoscience Centre, Geological Survey of Canada, PO Box 6000, Sidney, British Columbia, V8L 4B2, Canada
rogers@pgc.nrcan.gc.ca

As the oceanic lithosphere is subducted into the mantle, the changing pressure and temperature conditions cause phase changes that result in denser material. The largest density change takes place in the oceanic crust as basalts and gabbros change to eclogite. This causes the thinner crustal portion of the descending lithosphere to contract significantly more than the mantle portion. The net result is a vertical contraction of the subducted crust. In warm subduction zones, this phase change takes place in a very narrow range in the down-dip direction and appears to be reflected as a down-drop in the topography, forming a basin in the forearc region. Evidence for such down-drops can be seen as linear inland seas paralleling the subduction front in the warm subduction regimes of Cascadia, the Nankai region of Japan, and in southern Chile. In Cascadia, the Georgia Strait–Puget Sound–Willamette Valley lowland is directly above the expected location of the basalt to eclogite phase change region. The rapid onset of the basin formation 85 million years ago coincides with a dramatic decrease in the age of oceanic lithosphere being subducted as the Farallon–Kula triple junction migrated along the coast, changing the subduction regime from a cold to a warm one. This phase change process may be an important mechanism for the initiation of forearc basins.

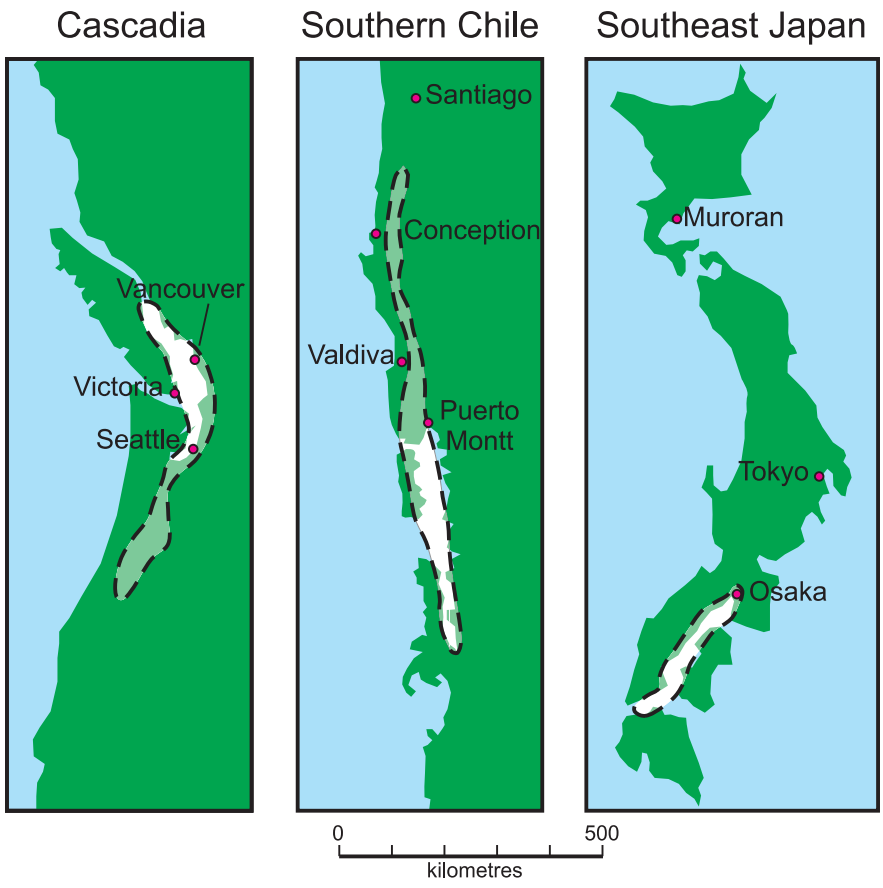

FIGURE 1: Forearc basins above phase-change regions in warm subduction zones can be seen in the forearcs of Cascadia (Georgia Strait/Puget Sound/Willamette Valley), southern Chile (Gulf of Corcovado/Great Longitudinal Valley), and in the southeast region of Japan where the Philippine Sea plate subducts (Seto Inland Sea). The light green/white regions indicate the extent of modern forearc basins.

Knowledge of in-slab earthquakes needed to improve seismic hazard estimates for southwestern British Columbia

John Adams and Stephen Halchuk
Geological Survey of Canada, 7 Observatory Crescent, Ottawa, Ontario, K1A 0Y3, Canada
adams@seismo.nrcan.gc.ca, halchuk@seismo.nrcan.gc.ca

ABSTRACT

In-slab earthquakes (earthquakes within the subducting Juan de Fuca plate) make the major contribution to seismic hazard for the Strait of Georgia region of British Columbia. These earthquakes dominate the hazard, despite their depth, because they have a higher rate and cause stronger shaking than the crustal earthquakes. Key knowledge of in-slab earthquakes needed to improve seismic hazard estimates for southwestern British Columbia includes the constraints on the spatial distribution, rate and maximum size of the earthquakes, the ground motions to be expected, the nature of the earthquake sources and the structure and properties of the lithosphere through which the waves propagate.

Introduction

Seismic hazard for the Strait of Georgia region of British Columbia (including Vancouver, Victoria and a substantial fraction of B.C.'s population) comes from three sources: crustal seismicity in the North American plate, great earthquakes of the Cascadia subduction zone on the interface between the North American and subducting Juan de Fuca plate, and deep earthquakes within the subducting slab ("in-slab" earthquakes). It is, however, dominated by the contribution from in-slab earthquakes. In Canada's fourth generation seismic hazard model (see *Adams et al.*, 1999a, 1999b, 2000), these earthquakes dominate the hazard despite their greater depth, firstly because they occur at a rate up to five-fold higher per unit area than the shallower crustal earthquakes, and secondly, because their predicted shaking is stronger than crustal events of the same size (see below). Thus when attempts are made to improve the estimation of seismic hazard for southwestern B.C., a great deal can be gained by better understanding these earthquakes.

We raise the following series of questions to highlight the knowledge of in-slab earthquakes we believe is needed to improve seismic hazard estimates for southwestern British Columbia. Some of the differences that result from the current level of uncertainty are demonstrated on Figure 1, a comparison of the GSC and USGS deaggregated hazard for Bellingham, Washington. Clear differences are seen in the fraction of the hazard coming from in-slab versus crustal earthquakes, and in the contribution from earthquakes larger than magnitude 7.

What is the spatial distribution likely for future earthquakes within the slab?

The GSC's fourth generation hazard maps use three source zones to model deep earthquake distribution, Georgia Strait (GEO) and Puget Sound (PUG) for one probabilistic model and Georgia Strait/Puget Sound (GSP) for the other, reflecting uncertainty in the future location of damaging deep earthquakes (Figure 2). What is needed are geological or geophysical reasons to constrain the updip, downdip, northern and southern extent of the deep seismicity. Although the two probabilistic models attempt to model the range of possible distributions, the level of hazard is strongly controlled by the active PUG zone. This is especially important for Vancouver, as the northern boundary of PUG lies under the city and generates a steep gradient in hazard across the city (Figure 3). Fairly large changes in hazard for communities in this gradient zone could result from slight adjustments to the source zone boundary, perhaps as the result of new significant earthquake activity outside the currently-defined PUG zone, or a recognition that certain regions within the boundary are (and will continue to be) aseismic. Improved geological/geophysical constraints might identify these regions and so refine the hazard estimates.

What is the rate of activity?

The rate of large earthquakes is a function of the rate of activity for small earthquakes (a-value or alpha for the magnitude-recurrence curve) and the slope of the magnitude-recurrence curve (b-value or beta). Alpha is quite well determined in aggregate, but it is unknown whether it truly varies in space (as it appears to during the historical record), and if so, why it should vary. The GSC uses a source zone approach which assumes uniform rates within each source zone (which may not be valid); the USGS uses spatial smoothing of past activity, which assumes that the locations of future large earthquakes will

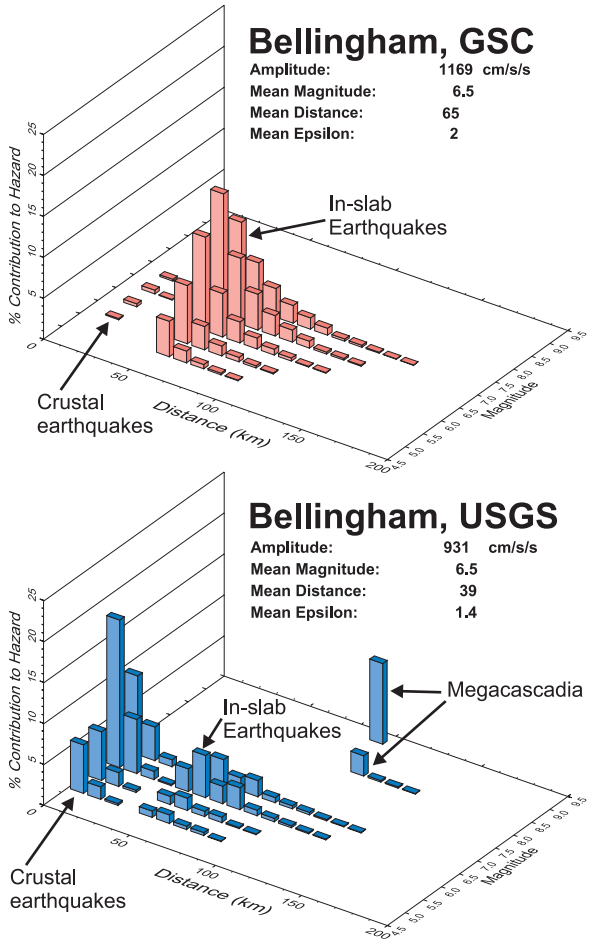

FIGURE 1: Seismic hazard deaggregations of 0.2 second spectral acceleration values at 2%/50 years for Bellingham show the GSC results are dominated by the contribution from in-slab earthquakes, unlike the 1997 USGS results.

precisely mimic the smoothed distribution of the small earthquakes (which may not be valid either).

The slope of the curve (beta) represents the relationship between the number of small and big earthquakes. For PUG, it is distinctively flatter than for most crustal source zones such as the crustal earthquake zone, Cascade Mountains R model (CASR), which overlies it (Figure 4). Two curves are shown for the crustal earthquakes (CASR), one representing the mathematical fit to the observed rates and the other (dashed) accommodating the observed higher rate of $M>6.5$ earthquakes. The value used in the Canadian hazard model is much lower (beta=1.01, b=0.44) than that used by the USGS (beta=1.5, b=0.65) for its deep earthquakes. No sound explanations exist for the different empirical values of beta, though a study of worldwide in-slab earthquakes might confirm the reasonableness of the value chosen, and provide insight into the reasons for such a low value.

Together, the magnitude recurrence parameters explain some of the difference in hazard. Figure 4 shows the activity rates of PUG and the overlying CASR crustal earthquake source. At magnitude 6, the predicted rate of in-slab earthquakes is three to ten times the rate of crustal earthquakes, thus accounting for the larger hazard contribution from the former. On Figure 4, the curve representing the USGS slope is drawn through the magnitude 4 data point on our PUG magnitude recurrence curve. As to be expected, the steeper USGS slope predicts a rate of M>6 earthquakes only one-third the GSC rate, and thus explains some of the hazard difference.

How large can the in-slab earthquakes get?

The largest historical in-slab event occurred in 1949, of moment magnitude about 6.9. Compared with recent earthquakes, almost nothing is known about the rupture parameters of this earthquake, such as its depth extent, fault length or stress drop. Some geophysical constraints such as temperature in the slab are believed to limit the thickness of brittle rock thus restricting fault width; larger earthquakes therefore require greater fault lengths or greater slip (or both). The GSC model currently allows an upper bound magnitude of 7.3 for PUG (with an uncertainty range of 7.1–7.6) as shown on Figure 5, presuming that a future large earthquake could extend deeper into the slab, or have larger displacement, or rupture a longer fault (perhaps through cascading rupture segments as demonstrated during the Lander's earthquake). In 1997, the USGS adopted an upper bound magnitude of 7.0. Because of the high rate for these large earthquakes (due to the small b value), their contribution to the total seismic hazard is not trivial (for the GSC's results, about 14–24% of the seismic hazard, dependent on model, comes from earthquakes larger than the 1949 one). More work in understanding the 1949 and 1965 earthquakes together with the geological/geophysical conditions might allow tighter constraints on the largest possible earthquakes.

How reliable are the current strong ground motion relations?

Both the GSC and USGS use the *Youngs et al.* [1997] relations to compute seismic hazard from the in-slab earthquakes. These relations concluded that in-slab earthquakes produce ground motions 40% larger than ground motions from adjacent subduction interface earthquakes (Figure 6), but this is not completely accepted. On the one hand, the *Youngs et al.* [1997] relations have been criticized as being based on rather sketchy data and upon no long period data at all [*Atkinson and Boore*, this volume]; on the other, the qualitative differences in damage between interface and in-slab earthquakes [e.g., *Okal and Kirby*, this volume] argue that there is almost certainly a quantitative difference in excitation, perhaps even larger than 40%. Considerable work is needed to deter-

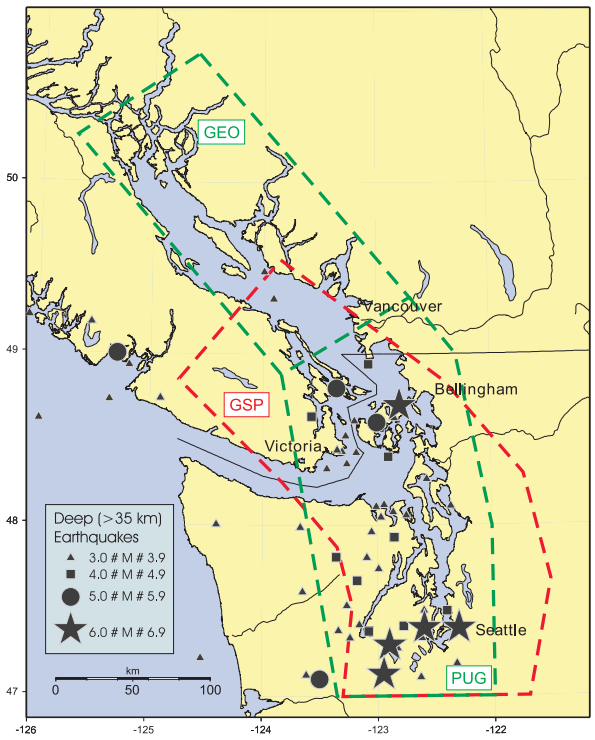

FIGURE 2: Selected in-slab earthquakes (>35 km) in the Puget lowlands/southwestern B.C. and the alternative source zones used to model them for the GSC's fourth generation seismic hazard maps.

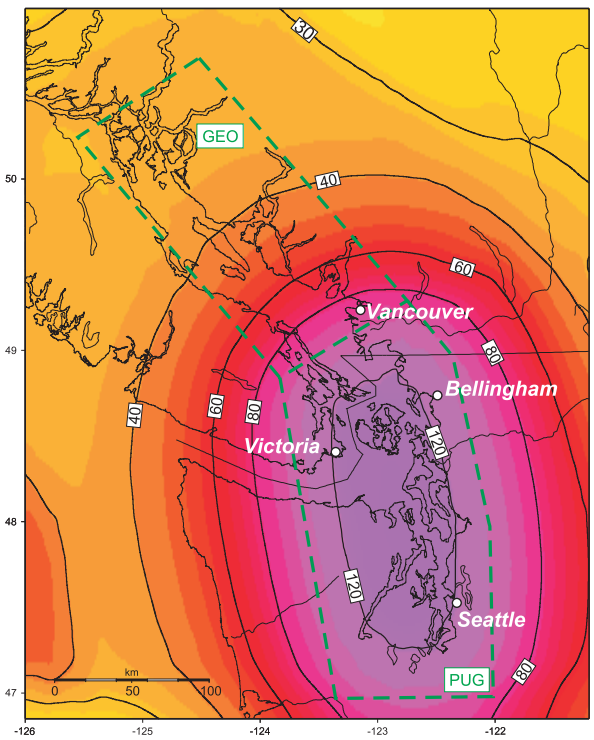

FIGURE 3: Hazard map from the GSC model ('H') using the Puget Sound (PUG) source. Contours, for 0.2 second spectral acceleration and 2%/50 year probability, are in % g. Note how the steep gradient near Vancouver is dependent on the position of the PUG boundary.

mine if the 40% "premium" for in-slab earthquakes is realistic, implausible, or too small, and whether the premium applies to all periods or just to the shorter ones. The comparison of the in-slab and crustal (using the *Boore et al.*, [1997] relations) earthquake motions (Figure 6) indicates that at essentially all the distances significantly contributing to the hazard, the ground motions from a 50-km-deep in-slab earthquake are expected to exceed those from a similar sized 10-km-deep crustal earthquake.

What are the typical seismic sources we have to contend with?

Our knowledge of the seismic source can affect our decision on which strong ground motion relations to use. Most earthquakes will probably have normal faulting mechanisms, but undetermined is the degree to which rupture directivity effects are important, particularly if ruptures tend to rupture upwards from their nucleation point (Figure 7).

If as a first approximation, the in-slab earthquakes are described as Brune sources, what are their stress drops? If as a refinement, they are described as realistic, elasto-dynamic sources, what are the key parameters (e.g. rupture velocity, source elongation, complete or fractional stress drop, source complexity/episodic rupture, fault roughness, etc.) that affect the spectral shapes of the source as radiated towards the overlying urban areas? Do in-slab source acceleration spectra have intermediate (omega^{-1}) slopes, and if so, over what frequency band? *Haddon* [1996] showed that typical M_w=6 eastern earthquake sources have omega^{-1} slopes for about one decade of frequency above a lower corner, and that the high frequency (f>1 Hz) levels exceed those associated with a Brune model for a M_w=6, 100 bar stress drop event by a factor of three, and approach those for a Brune model source a full magnitude larger (see the velocity spectra on Figure 8). The intermediate slopes are consequent on high rupture velocities, rupture directivity effects involving asymmetrical ruptures, episodic ruptures and partial stress drop events. Therefore, given records of small earthquakes, source scaling parameters correctly incorporating these factors are needed to synthesize the ground motions for potentially damaging earthquakes.

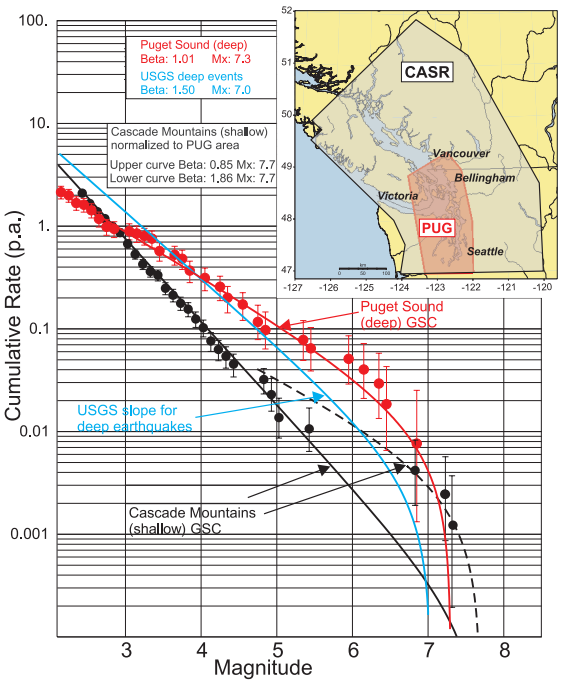

FIGURE 4: Magnitude-recurrence curves and observed activity rates (dots with error bars) for in-slab (red) and crustal (black) earthquakes for the Puget Sound. Both CASR curves have been reduced by a factor of 6.2 to account for the larger area of CASR relative to the PUG (see inset). The scaled USGS relation (blue) for deep earthquakes is also shown.

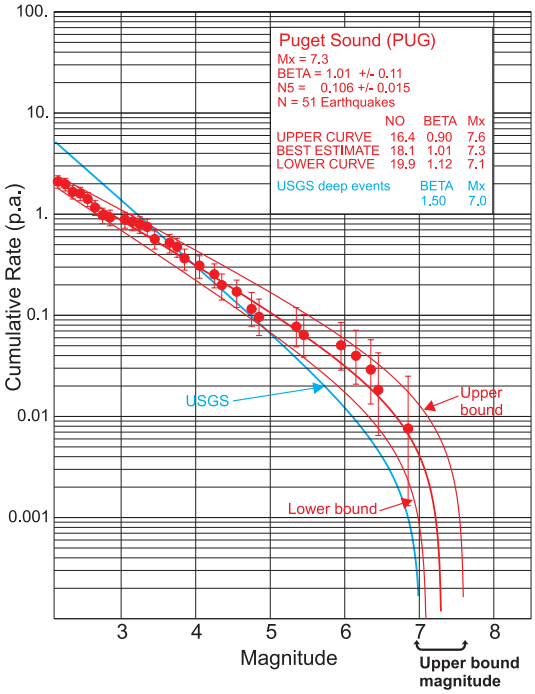

FIGURE 5: Magnitude-recurrence curve for PUG (like Figure 4), showing the upper and lower uncertainty bounds and range of upper bound magnitudes. For comparison, the curve used for the USGS calculations is shown in blue.

What are the crustal/mantle properties (e.g. Q, velocity layering, dipping layers) that affect the radiated energy between the source and the site where hazard is needed?

A reliable interpretation of crustal and mantle properties is needed to assess and adjust the strong ground motion relations and to perform forward modeling to determine the consequences of scenario earthquakes. For example, if crustal conditions differ significantly from Mexico, a source of much in-slab earthquake data, how do we adjust strong ground motion parameters derived from a worldwide dataset?

What earthquake scenario should be adopted for Vancouver and Victoria? How can the use of empirical Green's functions improve hazard estimates?

Deaggregations like Figure 1 indicate the magnitude and distance of the earthquakes contributing to the seismic hazard and are the starting point for design earthquake scenarios. Use of empirical Green's functions can improve hazard estimates (by effectively accounting for all path complexity), but still require much knowledge about the seismic source so that the source scaling can be done appropriately. Hence, future improvements will depend critically on our ability to understand what will happen during the larger earthquakes, and our best insight to that will come from analysis of the past large Puget Sound earthquakes.

Conclusions

Different assumptions were adopted by the USGS in 1997 and the GSC in 1994–1999 and resulted in different estimates of seismic hazard for the U.S. and Canadian territory overlying these in-slab earthquakes. Reconciling these estimates and refining them towards the true hazard will involve better answers to the questions raised above.

References

Adams, J., D.H. Weichert, and S. Halchuk, *Trial seismic hazard maps of Canada 1999: 2%/50 year values for selected Canadian cities*, 107 pp., Geological Survey of Canada Open File 3724, 1999a.

Adams, J., D.H. Weichert, and S. Halchuk, Lowering the probability level—fourth generation seismic hazard results for Canada at the 2% in 50 year probability level, in *Proceedings 8th Canadian Conference on Earthquake Engineering, Vancouver 13–16th June 1999,* pp. 83–88, 1999b.

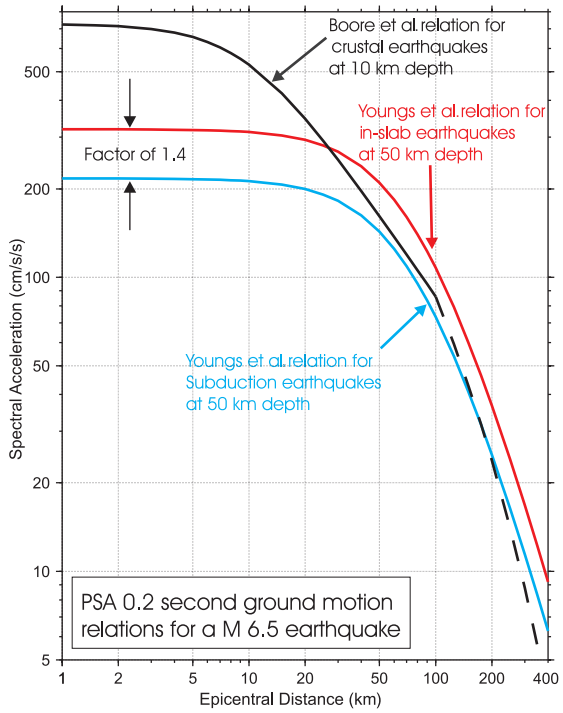

FIGURE 6: A comparison of expected ground motions from adjacent interface and in-slab earthquakes, to those from similar-sized crustal earthquakes (black).

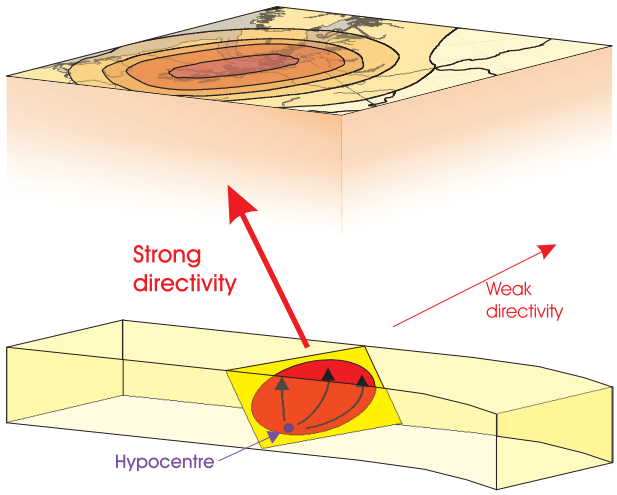

FIGURE 7: Ground motions above a typical in-slab normal faulting earthquake may depend critically on the rupture plane location, rupture plane dip direction and the asymmetry of the rupture relative to the hypocenter, all contributing to directivity effects.

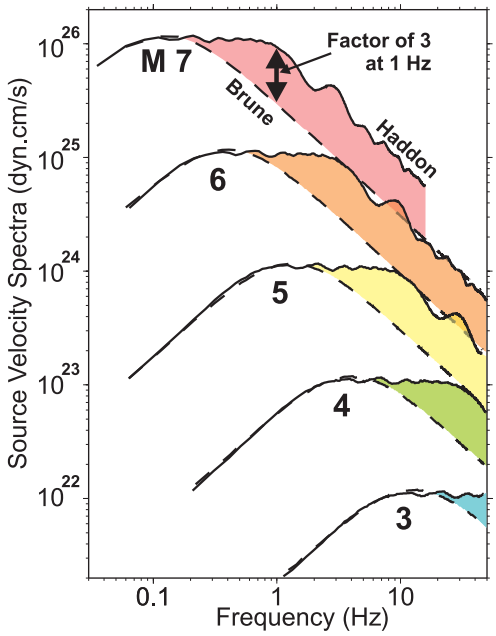

FIGURE 8: According to Haddon, the velocity spectra of typical eastern earthquake sources are flat for about one decade of frequency above their lower corner, and their high frequency (f>1 Hz) levels exceed those associated with the corresponding Brune model event by a factor of three, approaching the shaking of a Brune event one magnitude larger (redrawn from *Haddon,* [1996]).

Adams, J., S. Halchuk, and D.H. Weichert, Lower probability hazard, better performance? Understanding the shape of the hazard curves from Canada's Fourth Generation seismic hazard results, *Paper 1555, 12th World Conference on Earthquake Engineering, Auckland, 30th January–4th February 2000*, 8 pp., 2000.

Atkinson, G.M., and D.M. Boore, Empirical ground motion relations for subduction-zone earthquakes in *The Cascadia Subduction Zone and Related Subduction Systems*, edited by S.H. Kirby, K. Wang, and S.G. Dunlop, pp. 155–158, U.S. Geological Survey Open-File Report 02–328, Geological Survey of Canada Open File 4350, 2002.

Boore, D.M., W.B. Joyner, and T.E. Fumal, Equations for estimating horizontal response spectra and peak acceleration from western North America earthquakes: a summary of recent work, *Seism. Res. Lett., 68,* 128–153, 1997.

Haddon, R.A.W., Earthquake source spectra for Eastern North America, *Bull. Seism. Soc. Amer., 86,* 1300–1313, 1996.

Okal, E., and S.H. Kirby, Energy–to–moment ratios for damaging intraslab earthquakes: preliminary results in *The Cascadia Subduction Zone and Related Subduction Systems*, edited by S.H. Kirby, K. Wang, and S.G. Dunlop, pp. 117–122, U.S. Geological Survey Open-File Report 02–328, Geological Survey of Canada Open File 4350, 2002.

Youngs, R.R., S.-J. Chiou, W.J. Silva, and J.R. Humphrey, Strong ground motion relationships for subduction zone earthquakes, *Seism. Res. Lett., 68*, 58–73, 1997.

Empirical ground motion relations for subduction-zone earthquakes

Gail M. Atkinson and David M. Boore
Department of Earth Sciences, Carleton University, 1125 Colonel By Drive, Ottawa, Ontario, K1S 5B6, Canada
gma@ccs.carleton.ca

Ground motion relations for subduction-zone earthquakes are an important input to seismic hazard analyses for regions affected by the Cascadia subduction zone (Washington, Oregon and British Columbia). There is a significant hazard potential from great thrust events along the subduction interface and from large events within the subducting slab. We have compiled a response spectra database from thousands of strong motion recordings from events of moment magnitude (*M*) 5 to 8.3 occurring in subduction zones around the world, including both interface and in-slab events. The distribution of the database in magnitude and distance (where closest distance to fault surface is used) is shown in Figure 1. We are currently refining the database and performing regression analyses to determine empirical ground motion relations for interface and in-slab events. The large dataset enables better determination of attenuation parameters and magnitude scaling, for both types of events, than has previously been possible. Soil response parameters, including nonlinear effects at strong levels of shaking, can also be determined from the data.

Preliminary regression results suggest that in-slab events attenuate more rapidly with distance than do interface events. For both in-slab and interface events, ground motion amplitudes depend on focal depth, with deeper events showing larger amplitudes. In-slab events cause greater ground motion amplitudes at close distances than do subduction (interface) events but the overall effect is countered by the more rapid attenuation of in-slab motions with distance.

Figure 2 compares the preliminary relation for a subduction thrust (interface) event of $M=7.9$ at a focal depth of about 20 km, to response spectra data in the range from $M=7.5$ to 8.3 (focal depths <35 km), for a frequency of 1 Hz (5% damped pseudo-acceleration [PSA] in cm/s^2, horizontal component). This type of event is a major contributor to the 1 Hz hazard in the Cascadia region. The relation of *Youngs et al*. [1997] is also plotted. The *Youngs et al*. [1997] subduction relations are commonly used for seismic hazard analysis in the region; they were developed in the early 1990s from the much more limited dataset that was available at that time. Figure 2 shows that the AB2000 and Y97 relations are similar for this type of event and that both tend to underestimate the motions in this particular magnitude range. Because the regression relations fit a large range of magnitudes, distances, depths and event types, it is not an unusual circumstance to obtain such a misfit within a specified range of parameters. However, this magnitude range is important and refinements in the regression results to address this mismatch are being pursued.

Figure 3 compares the preliminary relation for an in-slab event of $M=6.8$ at a focal depth of about 60 km for a frequency of 5 *Hz*, to response spectra data in the range from $M=6.5$ to 7.1 (focal depths 40–60 km). This type of event is also important for hazard analysis. The preliminary relation agrees reasonably well with the overall trend of the data but underpredicts the sparse near-fault amplitudes. Again, refinements to better fit this important magnitude-distance range are in progress.

Looking at a broad range of magnitudes and distances, the preliminary results suggest that the subduction ground motion relations of *Youngs et al*. [1997] may tend to overestimate the motions caused by moderate-to-large in-slab events (at all distances) but underestimate the motions from great subduction thrust events at large distances. This finding, if verified by more detailed regression analyses currently in progress, could have significant implications for seismic hazard analysis in the Cascadia region.

References

Youngs, R., S. Chiou, W. Silva, and J. Humphrey, Strong ground motion attenuation relationships for subduction-zone earthquakes, *Seism. Res. L.*, 68, 58–73, 1997.

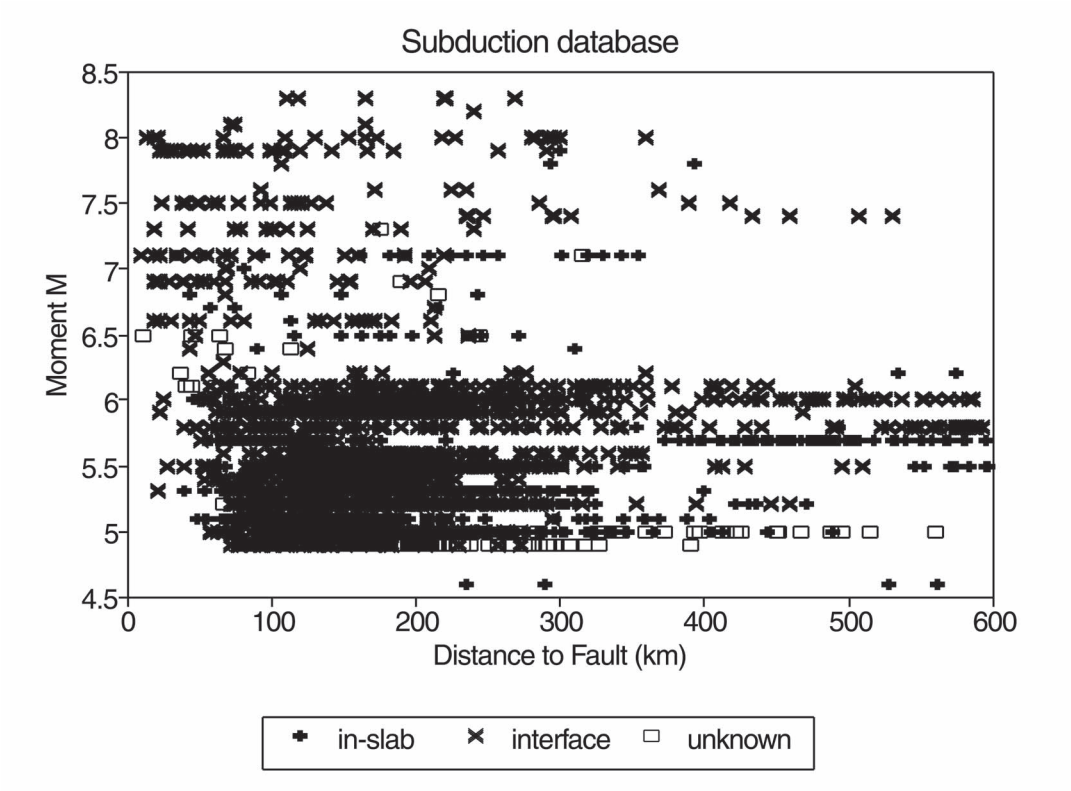

FIGURE 1

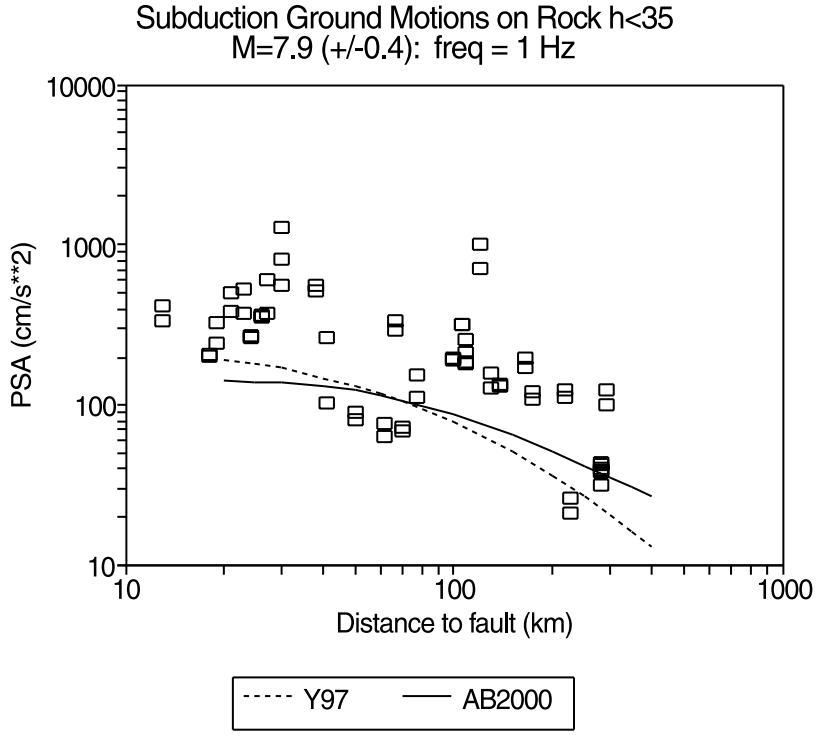

FIGURE 2: AB2000: *Atkinson and Boore*, this paper; Y97: *Youngs et al.*, 1997.

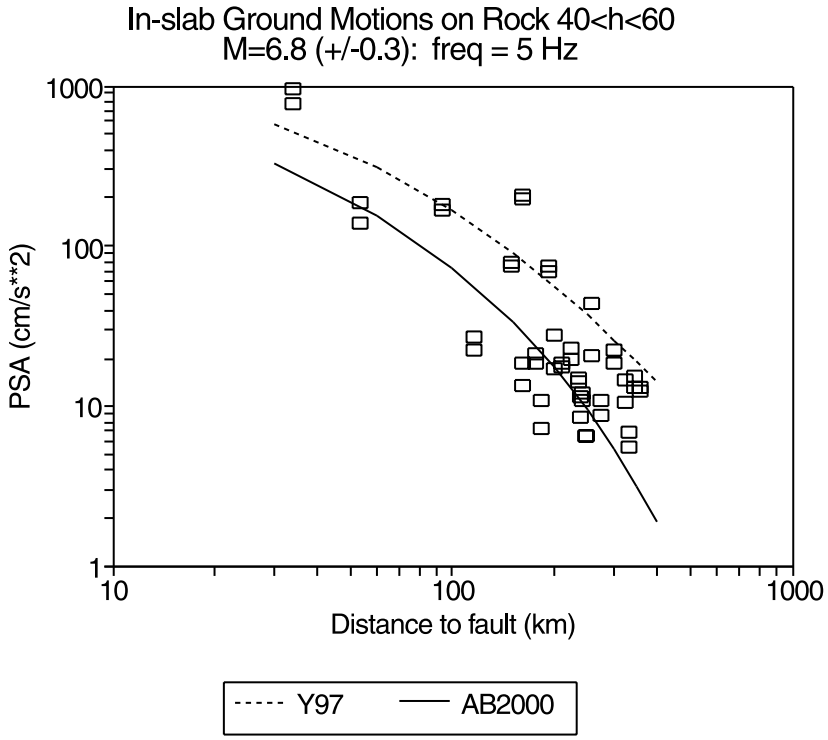

FIGURE 3: AB2000: *Atkinson and Boore*, this paper; Y97: *Youngs et al.*, 1997.

Deep intraslab earthquakes and how they contribute to seismic hazard in the Pacific northwestern U.S.

Mark D. Petersen and Arthur D. Frankel
United States Geological Survey, PO Box 25046, Lakewood, Colorado, 80225, USA
mpetersen@usgs.gov, afrankel@usgs.gov

ABSTRACT

We investigate the impact of two different source and attenuation models for deep intraslab earthquakes to the seismic hazard along the northwestern coast of the United States. Different source models for deep intraslab earthquakes may cause either localized hazard in the lower Puget Sound of Washington and northwestern California, or hazard that is spread out parallel to the Cascadia subduction zone. These source models result in hazard estimates for 2% probability of exceedance in 50 years that differ by as much as 25% near Portland, Oregon. Applying maximum magnitudes (M=7.0–7.4) to the intraslab source model results in differences of less than 10% for the hazard estimates in the Pacific Northwest. Attenuation models [e.g., Youngs et al., 1997; Atkinson and Boore, this volume] that relate the earthquake magnitude and distance to the ground motion, lead to differences of 50% in hazard for one second spectral acceleration near the earthquake sources. The variability in hazard for different source models and attenuation relations indicates the importance of identifying the physical mechanisms that drive the intraslab events and understanding the variability in the ground motions.

Introduction

Seismic hazard along the northwestern coast of the U.S. is dominated by contributions from crustal faults, shallow crustal seismicity, deep intraslab seismicity and great earthquakes along the Cascadia subduction interface [*Frankel et al.*, 1996]. The deep intraslab events contribute significantly to the hazard in the Puget lowlands in the state of Washington, as can be observed from the deaggregation of the seismic hazard (Figure 1) [*Harmsen and Frankel*, 2001]. In fact, the deep intraslab earthquakes contribute 31% and 24% of the hazard at 0.2 and 1 second for the 5% damped spectral acceleration, respectively, for 10% probability of exceedance in 50 years. For the 2% probability of exceedance in 50 years hazard, the contribution from these deep events is not as great in Seattle because the crustal faults become more important.

The hazard questions that arise from observations of deep earthquakes are:

1) Why are the historical deep intraslab events restricted to the Puget lowlands and northwestern California and are not observed beneath the state of Oregon?
2) What is the long-term rate of intraslab earthquakes?
3) What is the maximum size of earthquakes in the subducting crust?
4) What is the variability in ground motions allowed by strong ground motion recordings of intraslab earthquakes?

The answers to these questions are critical in determining the characteristics of earthquake sources that will be used by engineers to design earthquake resistant structures. Therefore, it is imperative that we try to answer these questions since they will impact public safety in this region.

In this article we present two source models that take into account various assumptions about the physical mechanism of strain release in intraslab earthquakes associated with the Cascadia subduction zone. We test these models to understand the sensitivity of the different source model parameters to the hazard. In addition, we evaluate the impact of the maximum magnitude and two different attenuation relations for deep intraslab earthquakes on the seismic hazard in the Pacific Northwest.

Source models for deep intraslab earthquakes

The 1996 national seismic hazard maps [*Frankel et al.*, 1996] and the Oregon Department of Transportation report [*Geomatrix*, 1995] both recognized the importance of deep intraslab earthquakes in the northwestern United States. The national seismic hazard map implemented a source model for the intraslab earthquakes that is based on smoothed seismicity of historical events since 1949. The depths of these earthquakes are poorly constrained, so all of the depths were fixed at 45 km for this hazard analysis. Earthquake sources were smoothed using a Gaussian smoothing operator with a correlation distance of 50 km [*Frankel et al.*, 1996]. This smoothing process assumes that future earthquakes will occur near the locations of historical earthquakes and results in localized hazard beneath the Puget lowlands and northwestern

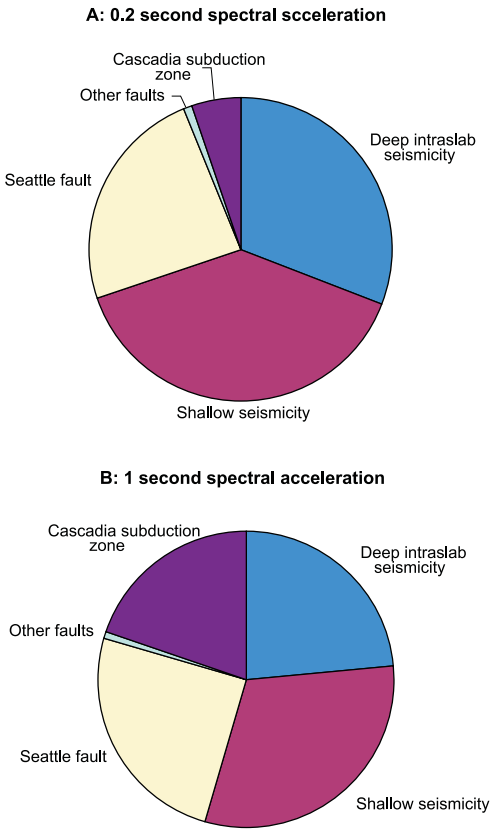

FIGURE 1: Deaggregation of hazard in the 1996 National Seismic Hazard Map for 10% probability of exceedance in 50 years at a site in Seattle, Washington. A) shows the hazard for the 0.2 second spectral acceleration and B) shows the hazard for the 1 second spectral acceleration.

California. The resulting hazard maps are shown in Figures 2a and 2c.

An extreme opposite model is to consider that deep intraslab earthquakes could occur with equal likelihood anywhere along the Cascadia subduction zone. Because we have not observed deep earthquakes beneath Oregon, this model would imply that we have not recorded earthquakes for long enough to recognize deep earthquakes in that region. The hazard resulting from this extended source zone model is lower in areas where we have observed historical intraslab earthquakes and is higher in areas above the slab where we have no evidence of such earthquakes (compare Figures 2a and 2b). For example, if we smooth the earthquakes over a large zone parallel to the Cascadia subduction zone, it raises the overall hazard in parts of western Oregon from about 0.35 g to 0.45 g for 2% probability of exceedance in 50 years. However, this model also decreases the hazard in the places where we have observed historic intraslab earthquakes such as portions of the Puget lowlands (compare Figures 2c and 2d). Therefore, questions arise whether this extended source model is reasonable for public policy hazard maps.

Maximum magnitude

Two deep intraslab earthquakes have caused damage in the Seattle–Tacoma–Olympia region during the past century. These earthquakes occurred in 1949 (M_b=7.1) and in 1965 (M_b=6.5), and indicate the hazard from future deep events in the Pacific Northwest. For calculation of the national seismic hazard maps, a maximum magnitude of M_w=7.0 was assumed (note that this is moment magnitude). The question remains "Is the 1949 earthquake the largest possible intraslab earthquake?" We have tested the sensitivity of the maximum magnitude of the intraslab earthquake to the hazard by varying the maximum magnitude from M_w=7.0 to 7.4. Results of this sensitivity study indicate that increasing the maximum magnitude to M_w=7.4 raises the hazard by 10% when only considering the intraslab earthquakes, and less than 5% in the overall national seismic hazard maps including all sources. Therefore, this parameter by itself does not make a large difference in the current hazard estimates for the Pacific Northwest of the United States.

Attenuation relations

Once the source model is constructed, the ground motion from each earthquake is estimated through an attenuation equation that relates the magnitude and distance to a particular ground motion parameter (e.g., peak horizontal ground acceleration or spectral acceleration). The 1996 hazard model applied only the *Youngs et al.* [1997] attenuation relationship to calculate the ground motion from the intraslab earthquakes, since it was the only one available at that time. Recently another attenuation relationship has been generated by *Atkinson and Boore* [this volume] that uses additional strong ground motion measurements to update the relationship. We applied the *Youngs et al.* [1997] and the *Atkinson and Boore* [this volume] attenuation relations for rock site conditions at one second spectral acceleration to calculate the hazard in the Pacific Northwest. *Atkinson and Boore* [this volume] do not report an uncertainty so we used the uncertainty given in the *Youngs et al.* [1997] relationship that is about a factor of two in size but is dependent on earthquake magnitude. We applied a fixed depth of 45 km for the deep earthquakes. The hazard for one second spectral acceleration at 2% probability of exceedance in 50 years is about 50% lower when using the *Atkinson and Boore* [this volume] relation than when using the *Youngs et al.* [1997] relation (Figure 3).

Discussion and conclusions

The differences between the hazard calculated using the *Atkinson and Boore* [this volume] attenuation relation for one second spectral acceleration differs significantly from the hazard generated using the *Youngs et al.* [1997]

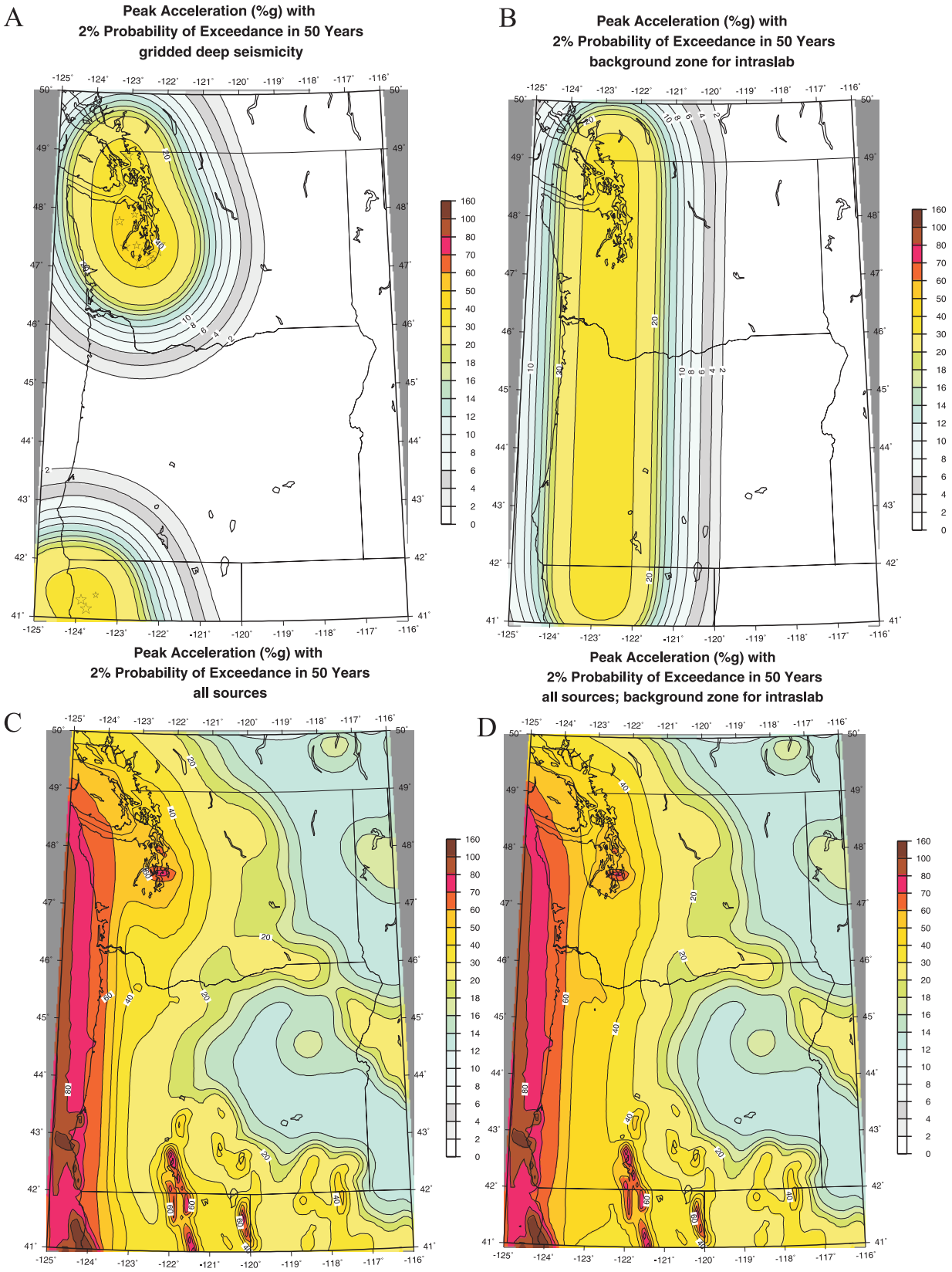

FIGURE 2: Seismic hazard maps produced using: A) 1996 intraslab source model; B) extreme opposite model with extended intraslab source zone; C) full 1996 model with intraslab source model shown in A; and D) 1996 model with intraslab source model shown in B.

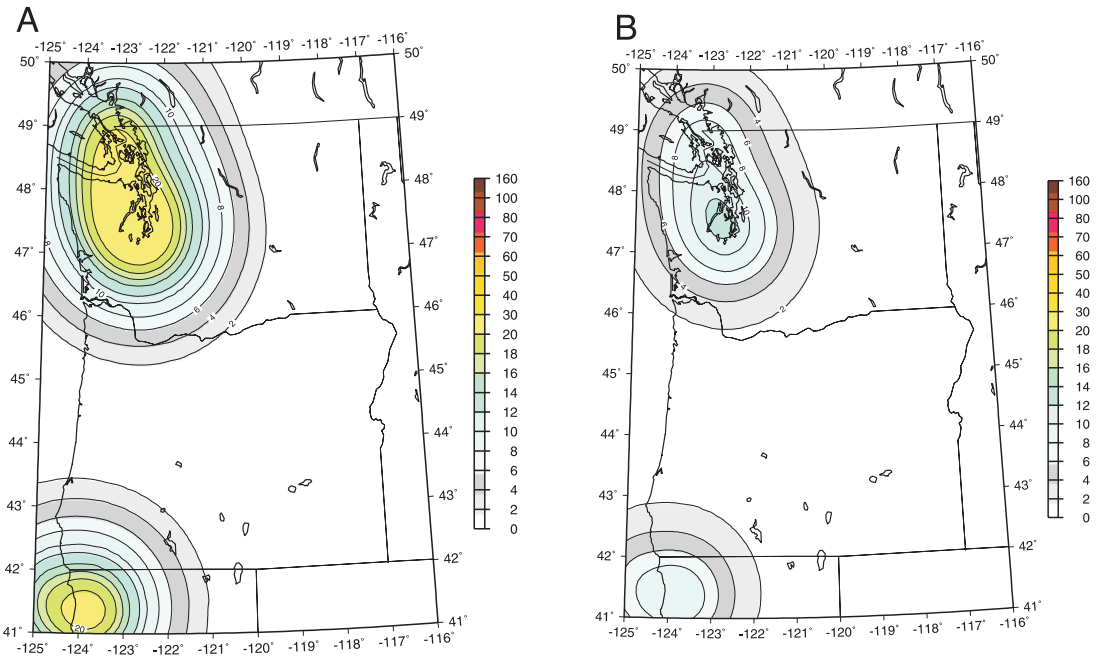

FIGURE 3: Seismic hazard maps for 2% probability of exceedance in 50 years for deep earthquakes in the Pacific Northwest on a uniform rock site condition. Hazard calculated using the one second spectral acceleration of A) *Youngs et al.* [1997] and B) *Atkinson and Boore* [this volume].

equation. The hazard may vary up to 50% or more in many areas near the sources. It is important to determine what level of ground shaking will occur from future deep earthquakes in this area and correctly weight the attenuation relationships in the hazard analysis. This is one of the most important considerations in calculating the hazard for deep earthquakes in this region.

Near Seattle Washington, the hazard is higher when assuming a model that uses the historic seismicity and the hazard is slightly lower when assuming a model that spreads the seismicity along the Cascadia zone. However, near Portland Oregon, the hazard is 25% higher when assuming the model that spreads the seismicity out along the deep Cascadia slab. The latter model gives an upper bound for hazard in Portland and western Oregon from deep earthquakes. We need to focus our scientific efforts on understanding the physical mechanisms of these earthquakes to be able to understand the validity of these models. Questions still remain regarding why the deep earthquakes tend to be correlated with shallow crustal earthquakes and why these deep earthquakes tend to occur near the ends of the subduction zone or where the fault changes strike or dip. The answer to these questions would allow us to constrain our source models for deep intraslab earthquakes and in the resulting hazard maps.

Acknowledgments

We want to thank Steve Harmsen for providing the deaggregation data used to produce Figure 1 and Gail Atkinson for providing a preliminary version of her attenuation relation for deep intraslab earthquakes. We thank Chris Cramer for a thoughtful review.

References

Atkinson, G.M., and D.M. Boore, Empirical ground motion relations for subduction-zone earthquakes in *The Cascadia Subduction Zone and Related Subduction Systems*, edited by S.H. Kirby, K. Wang, and S.G. Dunlop, pp. 155–158, U.S. Geological Survey Open-File Report 02–328, Geological Survey of Canada Open File 4350, 2002.

Harmsen S.C., and A.D. Frankel, Geographic deaggregation of seismic hazard in the United States, *Bull. Seismol. Soc. Am.*, *91*, 13–26, 2001.

Frankel A., C. Mueller, T. Barnhard, D. Perkins, E.V. Leyendecker, N. Dickman, S. Hanson, and M. Hopper, *National Seismic Hazard Maps, June 1996 Documentation, U.S. Geological Survey Open File Report 96–532*, 1996.

Geomatrix Consultants, *Seismic Design Mapping State of Oregon*, prepared for Oregon Department of Transportation Transportation Building Salem, OR 97310, 1995.

Youngs R.R., S.J. Chiou, W.J. Silva, and J.R. Humphrey, Strong ground motion attenuation relationships for subduction zone earthquakes, *Seis. Res. Lett., 68*, 58–73, 1997.

The proposed NEPTUNE seafloor observatory on the Juan de Fuca plate: Applications to studies of intraplate earthquakes

William S.D. Wilcock[1], Kelin Wang[2], Roy D. Hyndman[2], Anne M. Tréhu[3] and Kenneth C. Creager[4]
1 School of Oceanography, University of Washington, Seattle, Washington, 98195, USA
2 Pacific Geoscience Centre, Geological Survey of Canada, PO Box 6000, Sidney, British Columbia, V8L 4B2, Canada
3 College of Oceanic and Atmospheric Sciences, Oregon State University, Corvallis, Oregon, 97330, USA
4 Department of Earth and Space Sciences, University of Washington, Seattle, Washington, 98195–1650, USA
wilcock@ocean.washington.edu, wang@pgc.nrcan.gc.ca, hyndman@pgc.nrcan.gc.ca, trehu@oce.orst.edu, kcc@ess.washington.edu

ABSTRACT

NEPTUNE is a plan to deploy a long-term fiber-optic observatory on the seafloor of the Juan de Fuca plate. The network will support a wide range of scientific observations including a regional broadband seismic network and multidisciplinary experiments to study hydrothermal activity on the Juan de Fuca ridge and its flanks. Such observations will contribute to our understanding of the hydration of oceanic lithosphere and improve seismic images of the Cascadia subduction zone. In the long term, NEPTUNE will contribute to a better understanding of the mechanism of intraslab earthquakes.

Introduction

Oceanography is in the midst of a revolution that is fundamentally changing the means by which scientists observe many processes in and beneath the oceans [*Ryan et al.*, 2000]. Historically, ship-based expeditions have characterized the oceans using data collected onboard and with short deployments of autonomous instruments. As scientific knowledge has advanced, it has become increasingly apparent that many problems cannot be addressed by time-limited visits alone. A new operational paradigm is emerging made possible by advances in computational sophistication, communication and power technologies, robotic systems and sensor design. Ocean research is moving towards a mode of operations in which ship-based studies will be complemented by long-term observations from a network of coastal, regional and global seafloor observatories.

The NEPTUNE project (http://www.neptune.washington.edu) is an ambitious plan to deploy a regional submarine fiber-optic network on the Juan de Fuca plate off the coast of the Pacific Northwest (Figure 1) [*Delaney et al.*, 2000; *Delaney and Chave*, 2000; *NEPTUNE Phase 1 Partners*, 2000]. The network will host scientific instrumentation to study a wide variety of geological, oceanographic and ecological processes. NEPTUNE will link scientists and the public interactively to a wide range of sensors, sensor networks and autonomous mobile platforms in, on and above the seafloor (Figure 2). It will operate both large long-term experiments managed by scientific communities and smaller experiments developed by individual scientists. NEPTUNE will also support extensive educational and outreach activities.

A conceptual design and engineering feasibility study [*NEPTUNE Phase 1 Partners*, 2000] demonstrates that there are no insurmountable technical obstacles. It is envisioned that the NEPTUNE backbone will comprise 3000 km of cable connecting about 30 evenly distributed primary nodes. Secondary branch cables can extend to any location on the plate. At each node a junction box will provide standard power, communication and timing interfaces for scientific instruments. The complete network will carry 10 GB per second of data, deliver up to 100 kW of power and have an operational life span of at least 30 years. The node topology (Figure 1) includes a branch that runs near the base of the continental shelf, extending the length of the subduction zone from the Mendocino transform fault to the Explorer plate, and branches along the Juan de Fuca spreading center and Blanco transform faults. There are two shore landings at Nedonna Beach, Oregon and Victoria, British Columbia.

Seismic studies in NEPTUNE

In the field of marine seismology, the need for seafloor observatories is well documented. Many seismology studies rely on global and regional networks of land-based seismometers that have operated for several decades. Data from these networks have been used to image the earth's interior and they provide a long-term view of seismic

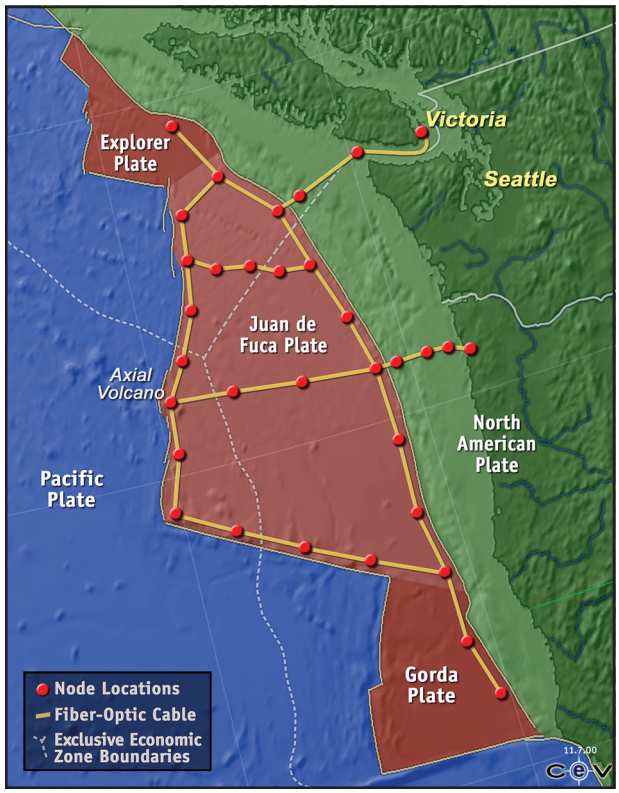

FIGURE 1: Candidate scenario for the NEPTUNE network. A fiber optic cable will connect primary nodes spaced about 100 km apart. Power and communications will be routed through two shore landings.

deformation. However, these networks have two major limitations. First, images of the earth obtained from global networks are severely limited by the lack of instruments on the seafloor. A permanent seafloor seismometer was recently attached to an abandoned telecommunications cable midway between Hawaii and the west coast of the U.S. [*Chave et al.*, 1998], but about 20 additional sites will be required to fill all the oceanic gaps in global networks [*Orcutt and Purdy,* 1995]. Second, most of the Earth's plate boundaries are located offshore and are poorly observed by regional land networks. Several cabled seismometers have recently been deployed off the coast of Japan [e.g., *Suyehiro and Fukao*, 1998], but studies of oceanic plate boundary seismicity are generally limited to teleseismic earthquakes or data collected with short deployments of autonomous ocean bottom seismometers.

NEPTUNE can help address this second limitation. The Juan de Fuca–Gorda–Explorer plate system incorporates a remarkable array of plate tectonic features within a relatively small area, including all the major types of oceanic plate boundary. Although the subduction zone plate boundary is seismically quiet, observations from land and with the Navy's Sound Surveillance System (SOSUS) hydrophone arrays show extensive seismicity in the region (Figure 3). The seismic and geodetic component of the proposed NEPTUNE network will provide an opportunity to study a wide range of geophysical processes including the seismic potential of the Cascadia subduction zone, the mechanisms of plate deformation and interactions, the structure and evolution of the lithosphere/asthenosphere system, and the characteristics of earthquakes and geological processes at plate boundaries [*NEPTUNE Phase 1 Seismology Working Group*, 2000].

NEPTUNE and studies of intraslab earthquakes

In the past century, the most damaging earthquakes in the Pacific Northwest have been intraslab events, earthquakes that occur within the subducted Juan de Fuca plate at depths of 30–70 km. Examples include the magnitude 7.1 Olympia earthquake in 1949 and the magnitude 6.5 SeaTac earthquake in 1965. These earthquakes are believed to be related to metamorphic processes in the slab [*Kirby et al.*, 1996]. The oceanic crust created at the mid-ocean ridges is hydrothermally altered and hydrated. During subduction, the hydrated basalts and gabbros are transformed into the higher density eclogite and this induces deviatoric stresses. The metamorphic transformation also releases a significant amount of water (1–2% by weight) that elevates pore fluid pressure. The combination of the stress and fluid pressure increases may reactivate some pre-existing faults and cause earthquakes.

It has been well documented that the subduction zone thermal regimes have a strong influence on intraslab earthquake processes. *Peacock and Wang* [1999] studied the northeast Japan and southwest Japan subduction zones, typical examples of cool and warm subduction zones, and concluded that the higher temperature in the southwest Japan subduction zone caused the basalt-eclogite transformation and hence intraslab earthquakes to take place at much shallower depths. Other consequences include a shallow termination of a low seismic velocity layer representing the untransformed crust, sparse arc volcanism and possible melting of the slab. The Cascadia subduction zone is a warm subduction zone because of the young age of the subducting Juan de Fuca plate and is very similar to southwest Japan.

NEPTUNE will provide an opportunity to improve our understanding of intraslab earthquakes and will allow us to assess their hazard along the Cascadia margin. Studies of seafloor hydrothermal activity on the Juan de Fuca ridge and its flanks will contribute to our understanding of the degree and depth extent of the hydration of the oceanic lithosphere prior to subduction. Long term monitoring of seafloor seismicity will yield information on the distribution and extent of faults in the subducting slab. In addition to constraining the characteristics of the plate prior to subduction, seafloor seismic observations can be used to study the slab after

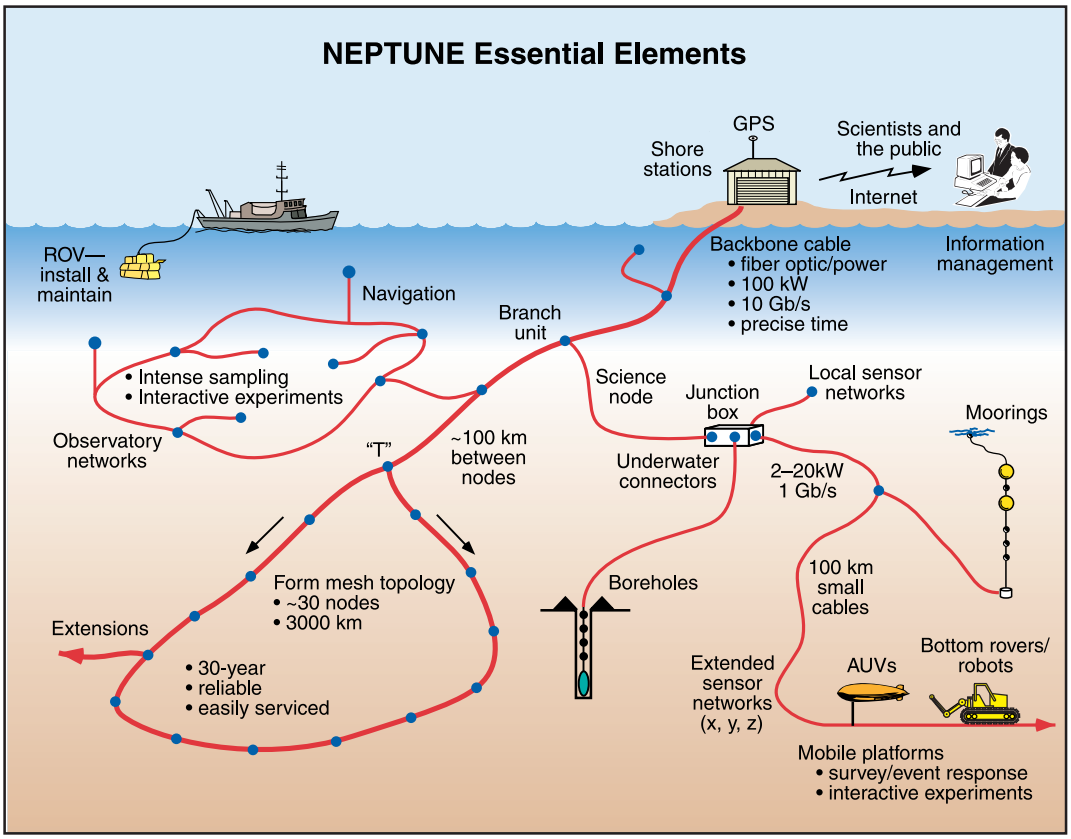

FIGURE 2: Essential elements of NEPTUNE. Land based scientists and the public are linked in real time interactively with sensors, sensor networks and various mobile platforms in, on and above the seafloor, NEPTUNE's fiber optic/power cable and associated technology provide the enabling network infrastructure.

subduction. For this margin, the intraslab stress regime is rather poorly constrained at depths between 10 and 50 km, partly due to the lack of seismic observations offshore. By recording and analyzing seismic waves that are generated by intraslab events and that propagate along the slab, it will be possible to constrain the seismic velocity structure of the slab and thus infer its thermal structure and petrology. Such information is essential if we are to constrain downdip and along-strike variations in the metamorphism and earthquake processes in the slab. In the long term, a better understanding of the mechanism of intraslab earthquakes and the slab thermal and mechanical structure will facilitate a more rigorous hazard study for these earthquakes.

A NEPTUNE seismic network

Figure 4 illustrates a possible design for a NEPTUNE seismic network [*NEPTUNE Phase 1 Seismology Working Group*, 2000]. It is based on a modified version of the candidate node scenario (Figure 1) developed for the conceptual design and feasibility study. It should be emphasized that the final design will require extensive planning to determine community priorities and ensure that the network is optimized for seismic detection and characterization. It is envisioned that a broadband seismometer will be deployed at each primary node. Because the Gorda and Explorer plates are seismically active, the node topology of Figure 1 has been modified to improve coverage in these regions. An additional 30 to 40 broadband instruments will be required to fill large gaps in the network and span the plate boundaries. Strong motion accelerometers and hydrophones will also be deployed throughout the region. Local networks of intermediate band sensors will be required at some nodes for high-resolution observations in regions of particular geological interest.

Future plans

Upon completion of the conceptual design and feasibility study in 2000, NEPTUNE commenced a phase of fundraising and detailed design that will lead to deployment as early as 2005. A consortium of five partners (University of Washington, Jet Propulsion Laboratory, Monterey Bay Aquarium Research Institute, Woods Hole Oceanographic Institution and the Institute of Pacific Ocean Science and Technology [Canada]) are leading the effort to design and

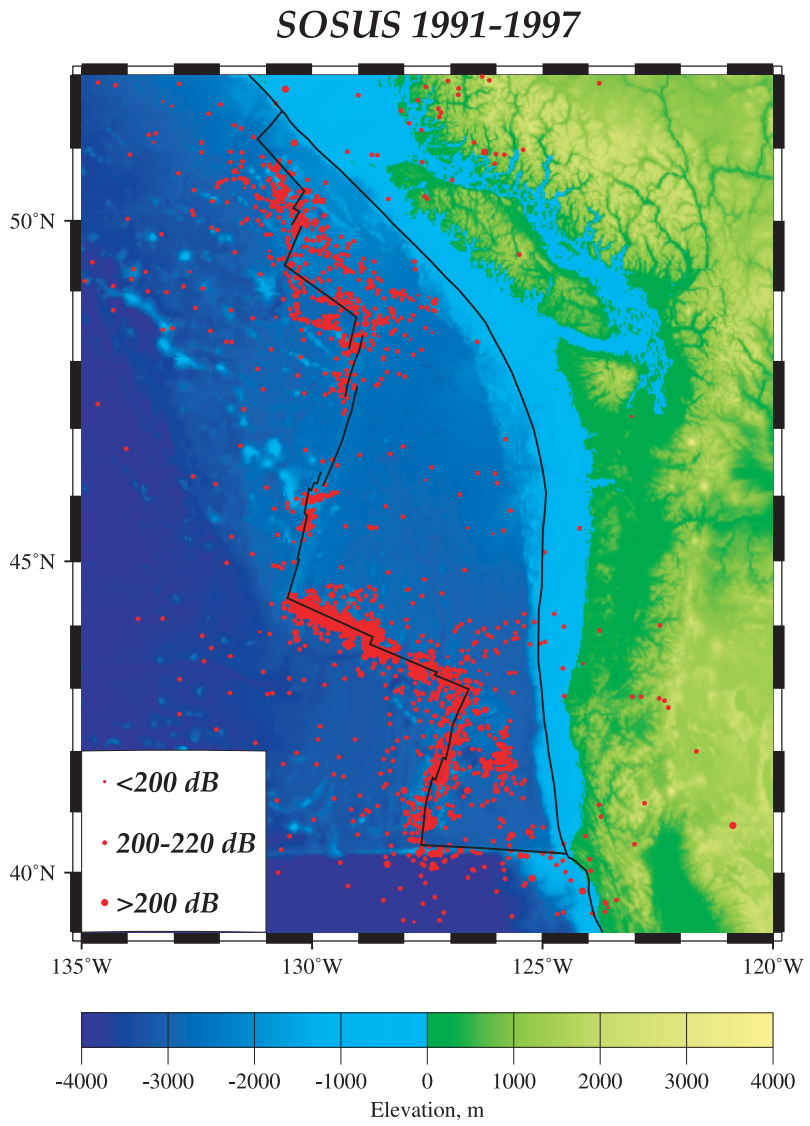

FIGURE 3: Earthquake epicenters for the period August 29, 1991 to December 31, 1997, determined using *T*-phases recorded by underwater hydrophones in the U.S. Navy's Sound Surveillance System (data courtesy of Chris Fox, Pacific Marine Environmental Laboratory, National Oceanic and Atmospheric Administration).

prototype the power, communications and data management systems. Test beds are planned for Monterey Bay and Georgia Basin to evaluate the system performance and to test scientific sensors.

The feasibility study supported a number of small ad hoc scientific working groups but the detailed engineering design must be guided by much more extensive scientific planning. About ten open workshops will be held to develop the motivation and priorities for community experiments. These deliberations will lead to the formation of working groups with members drawn from the whole community. Each working group will be responsible for the design and implementation of an experiment. The workshops on seismology and geodynamics, ridge crest processes and crustal hydrology will be of interest to those studying intraplate earthquakes.

References

Chave, A.D., F.K. Duennebier, R. Butler, R.A. Petitt Jr., F.B. Wooding, A.D. Bowen, D. Harris, and D.R. Yoerger, H_2O: the Hawaii-2 Observatory, *Eos Trans. AGU, 79*, F65, 1998.

Delaney, J.R., and A.D. Chave, NEPTUNE: a fiber-optic 'telescope' to inner space, *Oceanus, 42,* 10–11, 2000.

Delaney, J.R., G.R. Heath, B. Howe, A.D. Chave, and H. Kirkham, NEPTUNE: real-time ocean and earth sciences at the scale of tectonic plate, *Oceanography, 13(2)*, 71–79, 2000.

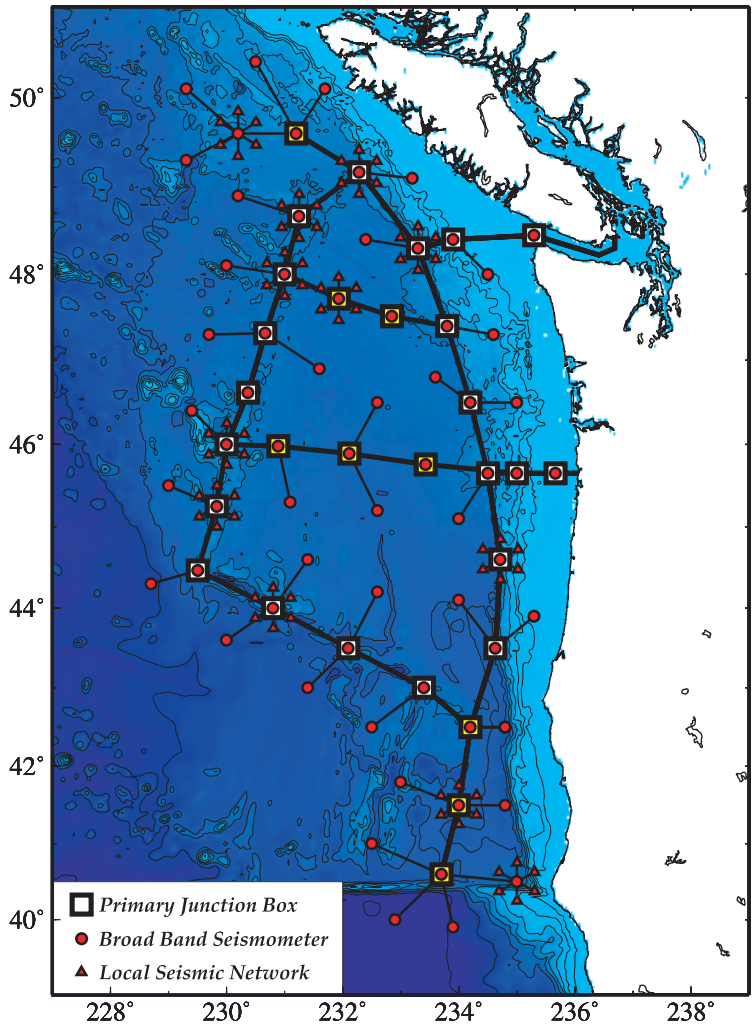

FIGURE 4: Possible NEPTUNE seismic network design based on a modified version of the node topology used for the conceptual design and engineering feasibility study. Yellow symbols are used to depict primary nodes whose location have changed from Figure 1.

Kirby, S., E.R. Engdahl and R. Denlinger, Intermediate-depth intraslab earthquakes and arc volcanism as physical expressions of crustal and uppermost mantle metamorphism in subducting slabs, in *Subduction: Top to Bottom*, edited by E. B. Bebout et al., pp. 195–214, American Geophysical Union, Washington DC, 1996.

NEPTUNE Phase 1 Seismology Working Group, *Opportunities for Seismology and Geodynamics in NEPTUNE*, Online report, http://gore.ocean.washington.edu/neptune, 2000.

NEPTUNE Phase 1 Partners (University of Washington, Woods Hole Oceanographic Institution, Jet Propulsion Laboratory, Pacific Marine Environmental Laboratory), *Real Time, Long-term Ocean and Earth Science Studies at the Scale of a Tectonic Plate—NEPTUNE Feasibility Study* (prepared for National Oceanographic Partnership Program), 106 pp., University of Washington, 2000.

Orcutt, J.A., and G.M. Purdy, *Broadband Seismology in the Oceans—Towards a Five-year Plan*, 105 pp., Joint Oceanographic Institutions Inc., Washington, DC, 1995.

Peacock, S.M., and K. Wang, Seismic consequences of warm versus cool subduction metamorphism: examples from southwest and northeast Japan, *Science, 286*, 937–939, 1999.

Ryan, W.B. F.R.S. Detrick, K. Becker, J. Bellingham, R. Lukas, J. Lupton, L. Mullineaux, and J. Sipress, *Illuminating the Hidden Planet: the Future of Seafloor Observatory Science*, 135 pp., National Academy Press, Washington, D.C., 2000.

Suyehiro, K., and Y. Fukao, Seafloor observatories: Japanese experience, *Eos Trans. AGU, 79*, F62–F63, 1998.

POLARIS: New opportunities in Cascadia

John F. Cassidy[1], Michael G. Bostock[2], Gail Atkinson[3], David W. Eaton[4], Isa Asudeh[5], David B. Snyder[5], John Adams[5], Ian J. Ferguson[6], Alan G. Jones[5] and Colin J. Thomson[7]

1 Pacific Geoscience Centre, Geological Survey of Canada, PO Box 6000, Sidney, British Columbia, V8L 4B2, Canada
2 Earth and Ocean Sciences, The University of British Columbia, 6339 Stores Road, Vancouver, V6T 1Z4, Canada
3 Department of Earth Sciences, Carleton University, 1125 Colonel By Drive, Ottawa, Ontario, K1S 5B6, Canada
4 Department of Earth Sciences, University of Western Ontario, London, Ontario, N6A 5B8, Canada
5 Geological Survey of Canada, 7 Observatory Crescent, Ottawa, Ontario, K1A 0Y3, Canada
6 Department of Geological Sciences, University of Manitoba, Winnipeg, Manitoba, R3T 2N2, Canada
7 Department of Geological Sciences, Queens University, Kingston, Ontario, K7L 3N6, Canada
cassidy@pgc.nrcan.gc.ca, bostock@geop.ubc.ca, gma@ccs.carleton.ca, deaton@uwo.ca, jadams@NRCan.gc.ca, IJ_Ferguson@UManitoba.CA, thomson@geol.queensu.ca

POLARIS (Portable Observatories for Lithospheric Analysis and Research Investigating Seismicity) is a multi-institutional C$10 million project recently funded by the Canadian Foundation for Innovation, provincial governments and universities, and private industry across Canada. This project will provide new, state-of-the-art portable geophysical observatories for research into lithospheric structure, continental dynamics, and earthquake hazards in Canada. POLARIS infrastructure will comprise 90 three-component broadband seismographs and 30 magnetotelluric (MT) mobile field systems and complementary satellite telemetry data acquisition. Over the initial four year installation of this project, the seismograph network will be deployed as three subarrays of 30 instruments each. The MT instruments will be used in shorter-term deployments at each of the three seismic subarrays for lithospheric imaging, and continuous recording at selected elements for deep-mantle imaging. The initial scientific objectives include:

1) three-dimensional detailed mapping of the asthenosphere and upper mantle of the Slave Province in Canada's north to assist the emerging diamond industry;
2) mapping lithospheric structure and earthquake hazards in the heavily populated area of southern Ontario (identifying zones of crustal weakness, obtaining accurate earthquake parameters, and ground motion attenuation studies).
3) mapping the structure and earthquake hazards over the Cascadia subduction zone in southwest British Columbia (subducting oceanic plate, site-response in urban areas, identifying active crustal faults, and seismic attenuation studies).

The latter array will provide new opportunities into research involving slab seismicity, including focal mechanisms, attenuation studies, and detailed structural studies.

Further research initiatives that will be possible include: testing rapid warning systems for ground shaking in the urban areas of Canada; developing new fine-scale imaging techniques using the scattered wavefield; and investigating geomagnetically induced currents that can cause major disruptions to electrical and pipeline infrastructure.